Contributions to model-based predictive energy management in hybrid electric vehicles

Nicoleta Stroe

UNIVERSITÉ D'ORLÉANS

ECOLE DOCTORALE
ENERGIE, MATERIAUX, SCIENCES DE LA TERRE ET DE L'UNIVERS

LABORATOIRE PRISME

THESE présentée par
Nicoleta STROE

soutenue le: **10.11.2017**

pour obtenir le grade de : Docteur de l'Université d'Orléans
Discipline/Spécialité: Energétique

CONTRIBUTIONS TO MODEL-BASED PREDICTIVE ENERGY MANAGEMENT IN HYBRID ELECTRIC VEHICLES

THESE dirigée par

Guillaume COLIN	Maître de conférences, HDR, Université d'Orléans
Sorin OLARU	Professeur CentraleSupélec

Rapporteurs

Carlos OCAMPO-MARTINEZ	Associate Professor, Technical University of Catalunya
Rochdi TRIGUI	Directeur de Recherche, IFSTTAR

Jury

Sebastien DELPRAT	Professeur, Ecole de Valenciennes, Président du jury
Karim BEN-CHERIF	Docteur, Renault, co-encadrant
Yann CHAMAILLARD	Professeur, Université d'Orléans, co-encadrant
Boris ROHAL-ILKOV	Professeur, Slovak University of Technology in Bratislava

Acknowledgments

A PhD thesis, although perceived as an individual work, owes its completion to many people, whether their presence was sustained or only brief, to whom I would like to express my gratitude.

Firstly, I wish to thank my supervisor Associate Professor Guillaume Colin and co-advisor Professor Yann Chamaillard from Orléans for their trust and for giving me the opportunity not only to work on an interesting topic, but also to discover the automotive field.

I thank my supervisor Professor Sorin Olaru from CentraleSupélec for his support on the control part and for his availability.

I am indebted to my co-advisor from Renault, Karim Ben-Cherif for his precious advice and for constantly showing a vivid interest for this thesis despite his busy schedule and his transfer to Japan.

I am deeply thankful to all the members who agreed to be part of the committee: Professor Sebastien Delprat and Professor Boris Rohal-Ilkov, with special thanks to Associate Professor Carlos Ocampo-Martinez and Professor Rochdi Trigui, who carefully reviewed my manuscript.

I would also like to thank Jean-Marc Welsch for the warm welcome in his team after Karim's departure and of course, to all my colleagues from Renault, too numerous to be mentioned here, for their encouragements and humor, which made these three years unforgettable. Special thanks to the new team I joined, whose support and understanding helped me finish the manuscript.

I keep pleasant memories from the time spent in Orléans, in the PRISME Laboratory. I had the chance to discover a very united team, which I thank again for the precious support during my defense day. Many thanks also to the Control Department from CentraleSupélec for their trust and for allowing this beautiful french journey to start in April 2012.

And last, but definitely not least, my deepest gratitude goes to my sister, without whom I don't know how I would have finished this PhD study.

Contents

List of Figures XII

Nomenclature XIII

General introduction 1

1 Motivation . . . 1
2 Motivation (en français) . . . 4
3 Organization of the manuscript . . . 7
4 List of publications and oral presentations . . . 9

1 Hybrid electric vehicles: an overview of architecture, modeling and energy management 11

1 System description . . . 11
1.1 Main components . . . 12
1.2 Architecture types . . . 14
2 Market trend, legislation and performance evaluation . . . 16
3 Quasi-static modeling . . . 19
3.1 Vehicle longitudinal dynamics . . . 20
3.2 Powertrain . . . 21
3.2.1 Gearbox . . . 21
3.2.2 Internal combustion engine . . . 22
3.2.3 Electric motor . . . 22
3.3 Energy storage elements . . . 23
4 Energy management . . . 25
5 Conclusions . . . 27

2 Generic powertrain control-oriented model 29

1 State-of-the-art . . . 31
2 Model synthesis . . . 32
2.1 Powertrain configuration . . . 33
2.2 Torque and rotational speed generic expressions . . . 34
2.3 Validation on different hybrid architectures . . . 36
2.3.1 Unified modeling . . . 36
2.3.2 Parallel architecture . . . 37
2.3.3 Series architecture . . . 39
2.3.4 Series-parallel architecture . . . 40
2.4 Fuel consumption approximation . . . 42
3 Conclusions . . . 47

3 Predictive energy management **49**
1 State-of-the-art . . . 51
2 Model predictive control-based torque split . . . 55
2.1 MPC: an overview . . . 55
2.2 Prediction model . . . 57
2.3 Optimization criterion . . . 59
2.4 Linear Time-Varying MPC framework . . . 61
2.4.1 Standard formulation . . . 61
2.4.2 Application to the torque split problem . . . 64
2.4.3 Constraints formulation and SOC balance problem . . . 65
3 Analysis of the control law . . . 67
3.1 Tuning . . . 67
3.2 Influence of PWL approximation for fuel consumption . . . 70
4 Stop-start inclusion: a model-based activation . . . 73
5 Coasting functionality . . . 77
5.1 Motivation: basic case study . . . 77
5.2 Problem formulation and proposed solution . . . 86
6 Conclusions . . . 92

4 Model-in-the-Loop validation **95**
1 Simulation framework . . . 96

2 Case-study: hybrid dual-clutch transmission 97
3 Simulation results 100
3.1 Influence of the tuning horizon 101
3.2 Influence of the MPC horizon and of S&S 102
3.3 Comparison with offline method PMP 109
4 Robustness analysis 115
5 Slope influence 119
6 Conclusions 121

Conclusions and perspectives **123**

Conclusions et perspectives (en français) **127**

Bibliography **130**

List of Figures

1.1 Hybrid electric vehicle representation [1] . . . 12
1.2 Specific energy density and volumetric energy density for different battery technologies [2] . . . 14
1.3 Block representation of HEV architectures; CONV - convertor, BAT - battery, Trans - transmission; black lines: mechanical links, green lines: electrical links [3] . . . 15
1.4 Planetary gearset (PGS) representation . . . 16
1.5 Examples of PGS-based hybrid architectures . . . 16
1.6 Evolution in time of CO_2 reduction requirements for passenger car standards, in different countries [4] . . . 17
1.7 Speed profile for NEDC, FTP-75, WLTC and Traffic Jam . . . 19
1.8 Speed profile for Artemis urban, road and highway . . . 20
1.9 Backward simulation; v - vehicle speed setpoint, a - acceleration, T_w - wheel torque, ω_w - wheel rotational speed . . . 20
1.10 Gearbox quasi-static representation; i - input, o - output . . . 21
1.11 Iso-specific fuel consumption map for a spark-ignition engine . . . 22
1.12 Iso-efficiency map for an electric machine, with its torque limits . . . 23
1.13 Equivalent internal resistance circuit for batteries; OCV - open circuit voltage; R - internal resistance . . . 24
1.14 Open circuit voltage and internal resistance evolution with respect to SOC for a typical Li-ion battery . . . 24

2.1 Input-output representation of a planetary gear set, [3] . . . 32
2.2 Generic representation of a hybrid powertrain; front and rear drive. *GB* - gearbox . . . 33
2.3 Generic representation of a hybrid powertrain, compact form; R_f - axle ratio . . . 33
2.4 Configuration (1) and (2): schematic representation . . . 34
2.5 Configuration (3): hybrid DCT with EM connected to the primary shaft . . . 34
2.6 DCT-based hybrid: Charge during driving, torque split and parallel mode . . . 36
2.7 DCT-based hybrid, charge at standstill . . . 36
2.8 Nissan one motor, two-clutch system; parallel architecture . . . 38
2.9 Nissan one motor, two-clutch system, schematic representation . . . 38
2.10 Series hybrid architecture; CONV - power converter, Trans - transmission; BAT - battery 39
2.11 Nissan e-Power Range Extender architecture . . . 39
2.12 General Motors Range Extender (GM RE) hybrid powertrain with the 2ET50 transaxle [5] 40
2.13 Three representative PGS-based hybrid architectures [5]; *diff* - differential . . . 41

2.14 Fuel rate evolution with respect to engine torque, for different values of speed; turbocharged, 1.2 SI engine . . . 44
2.15 Fuel rate evolution with respect to engine torque, for different values of speed; turbocharged CI engine . . . 44
2.16 Torque dependence of polynomial parameters for (2.24c), SI engine case-study; real values and PWL approximation . . . 46
2.17 PWL approximation with respect to torque for the fuel rate of the SI engine . . . 47

3.1 Schematic representation of PMP implementation, with the equivalence factor λ kept constant *a priori* during the entire drive cycle; if at the end of the drive cycle the SOC is different from the target, then an adjustment of the λ value is necessary; $U_{admissible}$ is a vector with admissible inputs for which the Hamiltonian H is evaluated . . . 53
3.2 Schematic representation of ECMS implementation, with the equivalence factor λ adapted with respect to SOC; $U_{admissible}$ is a vector with admissible inputs for which the Hamiltonian (3.7) is evaluated. The output of the ECMS is the torque of the ICE. . . . 54
3.3 MPC principle; k is the current time index, N_c the control horizon and N_p the prediction horizon . . . 56
3.4 Principle of SOC LTV model validation . . . 59
3.5 SOC LTV model vs SOC nonlinear model, for a prediction of 5s . . . 59
3.6 Graphic representation of fuel and electrochemical power evolution w.r.t. the control variable; α and β are the coefficients that define the fuel consumption approximation; B_k and D_k define the SOC linearized model . . . 62
3.7 SOC limits for 2 cases: total distance known and reset distance fixed at 10 km, respectively 66
3.8 SOC limits relaxation for $\alpha = 0.85$ . . . 67
3.9 Control structure with a high-level tuning block . . . 69
3.10 Jerk periodogram for LA92 cycle; low frequencies correspond to traffic-related aggressiveness (unavoidable situations) and high frequencies indicate the driver characteristics [6] . . . 70
3.11 Ratio (3.48) of the frequency content for different prediction horizon values and drive cycles . . . 71
3.12 Tuning parameters (SOC_{sp} and N_λ) adaptation w.r.t. slope . . . 71
3.13 A case study with variable slope profile. Top figure: the speed profile and the slope; middle: the wheel power; bottom: ratio (3.48) of the frequency content . . . 72
3.14 Control structure with S & S included . . . 75
3.15 Schematic representation of the S & S strategy . . . 76
3.16 Speed profile of a basic case study with flat road (zoom). Comparison between coasting with recovery (blue) and baseline coasting (red) . . . 78
3.17 Extension of the control structure from Fig. 3.14 with coasting functionality . . . 79
3.18 Coasting initiation: details about influence on the wheel torque prediction and impact on the λ feed-forward component . . . 79
3.19 Simulation results for a basic case study with flat road: coasting with recovery (e-Coasting), coasting and baseline . . . 80
3.20 Speed profile of a basic low-speed case study with flat road. Comparison between coasting with recovery (blue) and baseline coasting (red) . . . 81
3.21 Simulation results for a basic low-speed case study with flat road: coasting with recovery (e-Coasting), coasting and baseline . . . 82

3.22 Basic case study, with coasting and e-coasting deactivated at the same time; speed profile 83
3.23 Basic case study, with coasting and e-coasting deactivated at the same time; simulation results . . . 84
3.24 Simulation results for case study Fig. 3.16 with constant feedforward tuning factor λ_{k0} . 84
3.25 Simulation results for case study Fig. 3.20 with constant feedforward tuning factor λ_{k0} . 85
3.26 Simulation results for case study Fig. 3.22 with constant feedforward tuning factor λ_{k0} . 85
3.27 Comparison between the speed profiles given by J_1 and J_2; speed profile - WLTC 88
3.28 Comparison between the speed profiles given by the 2 cost functions; speed profile - Artemis highway . . . 88
3.29 Example of coasting trajectories for different starting points . . . 90
3.30 Cost function J_1 for case study from Fig. 3.29 . . . 90
3.31 Cost function J_2 for case study from Fig. 3.29 . . . 91

4.1 Simulation framework: basic representation with the 3 main components: the plant (vehicle), driver and powertrain management and the controller (energy management); *GB* - gearbox, *pwt* - powertrain . . . 96
4.2 Validation framework - block representation; sp - setpoint, req - request, ind - indicated, acc - accelerator; green signals: output from the high-fidelity model; red: energy management controller, with a possible extension to coasting (dashed block); black: driver and powertrain management blocks (Driver model, Driveline supervision & management, ICE supervisor & coordinator); bold black signals: exogenous inputs (vehicle speed and slope) . . . 98
4.3 Case-study: hybrid DCT, with EM connected to the primary shaft . . . 99
4.4 Speed profiles for the considered drive cycles . . . 100
4.5 Standard deviation σ of the feedforward component λ_0 for different tuning horizons N_λ . 101
4.6 Ratio between standard deviation σ and average avg of the feedforward component λ_0 for different tuning horizons N_λ . . . 102
4.7 Evolution of the feedforward component λ_0 for different tuning horizons N_λ and drive cycles . . . 103
4.8 Evolution of the normalized consumption w.r.t. N_λ for different drive cycles . . . 103
4.9 SOC trajectories for different tuning horizons N_λ; 4 drive cycles . . . 104
4.10 Comparison between $N_{mpc} = 1$s and $N_{mpc} = 5$s; NEDC . . . 106
4.11 Comparison between $N_{mpc} = 1$s and $N_{mpc} = 5$s; Artemis urban . . . 106
4.12 Comparison between $N_{mpc} = 1$s and $N_{mpc} = 5$s; FTP-75 . . . 107
4.13 Comparison between $N_{mpc} = 1$s and $N_{mpc} = 5$s; Traffic jam . . . 107
4.14 Comparison between MPC with and without S&S, $N_{mpc} = 1$s; NEDC, zoom . . . 108
4.15 Comparison between MPC with and without S&S, $N_{mpc} = 1$s; Artemis urban, zoom . . . 108
4.16 Traffic jam; influence of penalties on torque variations, as in (3.57) . . . 109
4.17 PMP vs MPC with $N_{mpc} = 5$s; NEDC . . . 111
4.18 PMP vs MPC with $N_{mpc} = 5$s; Artemis urban . . . 112
4.19 PMP vs MPC with $N_{mpc} = 5$s; FTP-75 . . . 113
4.20 PMP vs MPC with $N_{mpc} = 5$s; Traffic jam . . . 114
4.21 SOC trajectories for 2 different N_λ values, used in the robustness analysis scenarios; black curves represent SOC distance-varying limits . . . 116
4.22 Trajectories for Artemis urban, $N_\lambda = 10$s, different robustness scenarios . . . 117

4.23 Comparison between real values and measurements (engine torque and SOC); Artemis urban, $N_\lambda = 10$s 117
4.24 Evolution of the normalized consumption as a function of N_λ for a battery with a double capacity than the baseline case 118
4.25 Speed profiles (blue) and slope (red) of basic case-studies 119
4.26 Case-study (1), SOC distance-varying limits, constant SOC_{sp} 120
4.27 Case-study (1), SOC trajectories for different N_λ values; constant and variable SOC_{sp}, respectively; constant SOC_{min} 121

Nomenclature

Acronyms

ARTEMIS	Assessment and Reliability of Transport Emission Models and Inventory Systems
BEV	Battery Electric Vehicle
CI	Compression Ignition
CVT	Continuously Variable Transmission
DCT	Dual-Clutch Transmission
DP	Dynamic Programming
ECMS	Equivalent Consumption Minimization Strategy
EM	Electric Machine
EV	Electric Vehicle
FCV	Fuel Cell Vehicle
GB	Gearbox
GIS	Geographic Information System
HEV	Hybrid Electric Vehicle
ICE	Internal Combustion Engine
LP	Linear Programming
LTV	Linear Time-Varying
Li-ion	Lithium-ion
MPC	Model Predictive Control
NEDC	New European Driving Cycle
NiMH	Nickel-Metal Hydride
PGS	Planetary Gear Set
PHEV	Plug-in Hybrid Electric Vehicle
PMP	Pontryagin's Minimum Principle
PSD	Power Split Device
QP	Quadratic Programming
RE	Range Extender
RMSE	Root Mean Square Error
S&S	Stop&Start
SFC	Specific Fuel Consumption
SI	Spark Ignition
WLTC	Worldwide harmonized Light vehicles Test Cycles

Subscripts and superscripts

Symbol	Description
bat	battery
crk	crankshaft
pos	position
prim	gearbox primary shaft
sec	gearbox secondary shaft
w	wheel

Symbols

Symbol	Unit	Description
A_f	[m^2]	vehicle frontal area
C_1	[-]	odd clutch
C_2	[-]	even clutch
c_d	[-]	aerodynamic drag coefficient
c_{r1}	[(m/s)$^{-1}$]	rolling friction coefficient
H_{LV}	[J/kg]	lower heating value
I_{bat}	[A]	battery current
I_d	[kgm^2]	driveline inertia
I_w	[kgm^2]	inertia of one isolated wheel
$\dot{m}_f$	[g/s]	fuel rate
m_v	[kg]	vehicle mass
N_2	[-]	$\min(R_2, 1)$: used in a case of a DCT, with one EM at the primary shaft
N_{mpc}	[-]	MPC prediction horizon
N_λ	[-]	prediction horizon used for tuning
OCV	[V]	open circuit voltage
P_f	[W]	fuel power
P_e	[W]	electrochemical power
Q_{max}	[C]	battery capacity
R_1	[-]	odd shaft gear ratio
R_2	[-]	even shaft gear ratio
rat_{EM}^{pos}	[-]	ratio between the EM and the corresponding shaft pos where it is connected
r_{ICE}^{pos}	[-]	ratio from the engine torque to the position pos
$r_{EM}^{w/pos}$	[-]	ratio from the EM placed at pos level to the wheel
R_f	[-]	axle ratio
R_w	[m]	wheel radius
SOC	[%]	battery state-of-charge
SOH	[%]	battery state-of-health
T_{em}	[Nm]	electric machine torque
T_f	[Nm]	final drive torque

T_{ice}	[Nm]	engine torque
$T_{m/g}$	[Nm]	motor/generator torque
T_w	[Nm]	wheel torque
U_{bat}	[V]	battery voltage
v	[km/h]	vehicle speed
λ	[-]	MPC tuning factor
ω_{em}	[rpm]	electric machine rotational speed
ω_{ice}	[rpm]	engine rotational speed
ω_{idle}	[rpm]	engine idle speed

General introduction

1 Motivation

In the last years, stringent emission regulations, as well as fossil fuels resources reduction have triggered a determined orientation toward alternative transportation technologies. The techniques of improvement span several fields, such as alternative fuels (compressed natural gas, hydrogen, bio-diesel), new engine types such as homogeneous charge compression ignition (HCCI) or alternative vehicles such as hybrid and all-electric vehicles. Several types of hybridization can be distinguished: fly-wheel, pneumatic, hydraulic and electric, the latter being the most encountered. The market development of hybrid electric vehicles depends on two main factors: financial benefit (cost of manufacture vs. customer value) and environmental impact (electric energy production, components recycling), which are strongly dependent on the local policies and continuously subject to changes.

Three main optimization layers for hybrid electric vehicles can be identified: architecture choice, sizing and control algorithms [7]. The former handles the position, number and type of electric machines, type of storage element, engine and transmission. Sizing concerns the engine displacement, the maximum rated power of the electric machine and consequently, the battery capacity. The choices at these two levels are mainly dictated by cost, performance requirements and packaging limitations i.e. occupied volume. The latter spans different aspects, from high-level controller (speed regulator, lateral control) to low-level such as throttle, lambda or knock control. All of them can be seen as optimization-based decisions and the interplay between these layers suggest a hierarchical dependence in between the design choices.

For a fixed architecture with given dimensions for its elements, one of the most challenging aspects from a control perspective is the power distribution between the two power sources, problem referred to as the energy management, which lays within upper-level control algorithms, as it usually provides only the setpoints for the components. For a conventional vehicle, the powertrain setpoints of torque and speed are directly determined from the driver's request, in the case of a manual transmission or in conjunction with a gearbox controller, if otherwise. For a hybrid electric vehicle (HEV), the question that arises is how to exploit the additional degree of freedom - the electric path - such that the vehicle performance is improved. For some specific cases, this answer is straightforward:

- if the vehicle is braking, instead of dissipating the kinetic energy as heat, it can be recovered by the electric machine to replenish the energy storage element (usually a battery) and use this energy later, during electric traction
- if the engine cannot provide the required torque on its own, the motor can assist it and therefore, allow a more dynamic driving
- if an engine start is requested, the electric machine, depending on its position, can ensure a fast

restart, without the need, for example, of a belt-integrated starter generator (BSG)

In general though, the contribution of each element (the engine and the motor) needs to be calculated, if both of them can participate to traction. First, an objective needs to be defined and the most encountered is the reduction of fuel consumption. A basic strategy would be to use the electric motor at low speeds and torques and the hybrid mode such that the overall efficiency is maximized, within a rule-based approach [8], [9]. Although it presents the advantage of simplicity in design and implementation, this strategy suffers from an important lack of portability, since it is strongly application-oriented. Moreover, the use of the powertrain efficiency as a performance objective is not necessarily an indicator of the fuel gain improvement. Therefore, it is more appropriate to explicitly consider the fuel consumption, which can be done either by evaluating a static map or by an approximation model.

In addition to the fuel consumption reduction, which remains the main goal, other objectives can also be envisioned: drivability (related mostly to gearshifts [10]), pollutant emissions minimization [11], [12] and battery lifetime extension [13], [14]. Multi-objective optimization problems are difficult to be handled in a heuristic framework, which enforces the choice of model-based approaches.

The design of energy management strategies targets an on-line implementation, which can only ensure suboptimal results. A complete evaluation of their performance is usually done relative to the global optimum, obtained with an offline strategy and which is an indicator of the potential of an HEV for a given scenario. In this case, the drive cycle is considered entirely known in advance and the most popular algorithm used to solve this problem is dynamic programming [15]. Complete information about the speed profile and road grade is unrealistic and therefore, its usage is restricted to offline methods, but future information about the traffic can be available for a limited horizon, with a certain accuracy, which encourages the use of predictive control strategies [16], [17], [18], [19].

Among these strategies, model predictive control (MPC) emerges as a solution with a high potential. It shows an increased presence in the automotive industry, with applications spanning several fields, such as engine control [20], lateral vehicle dynamics [21], cruise control [22] or autonomous vehicle [23]. MPC is a model-based constrained optimization strategy, which calculates a sequence of commands that minimizes a cost function over a finite horizon, but where only the first command is applied. It combines therefore the open-loop optimal control with the feedback from the system. Its capacity of handling constraints and predictive data makes it an attractive alternative to the currently most popular energy management strategy, *Equivalent Consumption Minimization Strategy* (ECMS) [24], [25], [26].

MPC can be found under various forms, depending on the nature of the prediction model (linear, linear time-varying and nonlinear) and of the cost function (usually linear or quadratic). Standard MPC formulations such as quadratic programming are generally preferred, due to the existence of dedicated efficient solvers and this formulation will be also retained in the present thesis.

Modeling is the first step in the MPC design and for the energy management problem a powertrain control-oriented model is needed, which has been addressed in the literature, mostly for specific case studies. Considering the diversity of hybrid powertrain architectures, a unified model would be an useful tool and current state-of-the-art witnessed attempts toward this direction [27], [28]. A feature that would complete the existing work is the introduction of a dual-clutch transmission-based HEV.

The cost function is another fundamental element in the MPC design and in general, a criterion expressed as a trade-off between tracking error and command effort reduction is employed. For the energy management problem, the cost function definition is not straightforward. The objective is to reduce the

fuel consumption by exploiting an additional source of energy, which cannot be replenished from the grid in the case of an HEV without a plug-in. The performance evaluation needs to take into account the consumption of two types of energy sources, placing the problem into an energetic framework. Therefore, two main aspects that need to be solved can be identified at this level: the mathematical expression for the energetic problem and its processing for a standard formulation.

The cost function tuning has a major impact on the control performance and for the considered problem, it is a particular challenge, due to its high dependence on the drive cycle. The interest is to find a mechanism that facilitates the tuning factor adaptation with respect to the speed and road grade profile. The access to traffic preview data can be exploited in order to extract information about the drive cycle characteristics and frequency analysis is a potential tool [29], [6].

It is not uncommon to handle the gearshift strategy outside the energy management, which reduces the considered problem to torque distribution. Engine stop-start can bring an important fuel gain for an HEV, especially in urban driving and therefore, it is often addressed by the energy management, either separately from [30] or in conjunction with the torque split [31]. For a standard MPC-based formulation, this would imply the introduction of a discrete control variable, leading to a mixed-integer linear/quadratic problem, which needs a more computationally expensive solver. For a greater flexibility, sometimes it is preferred to propose a formulation that handles at a first stage only the main objective (here, the torque split), but where extensions (engine stop-start or drivability) are allowed without major changes.

The speed profile is often imposed by the drive cycle and its tracking is handled at an upper level, by a driver model, but in some cases, it represents an additional degree of freedom used for fuel gain improvement [32], [33]. The driver behavior has also an important impact on the fuel consumption and therefore, speed profile adjustments may be introduced in the energy management framework. A functionality with this potential is coasting or *free-wheeling*, where the vehicle movement is determined only by resistive forces, the gas and brake pedal not being pressed. The potential of coasting in fuel gain has been the object of a rather limited number of papers, as far as the authors' knowledge is concerned, and it addressed mainly the constant speed phases on highway. Moreover, the focus was on conventional vehicles and to a less extent for hybrid electric passenger cars. An analytical approach that extends the problem to time-varying speed sections would provide a generalized tool for the performance evaluation and hence, completing the existing analysis.

2 Motivation (en français)

Dans les dernières années, le durcissement des normes d'émissions, ainsi que la réduction de ressources de carburants ont déclenché une orientation déterminante vers des technologies de transportation alternative. Les méthodes d'amélioration couvrent différents domaines, comme les carburants alternatifs (gaz naturel comprimé, hydrogène, bio-diesel), de nouveaux types de moteurs, comme HCCI (homogenous charge compression ignition) ou des véhicules alternatives, comme les véhicules hybrides ou électriques. Plusieurs types d'hybridation peuvent être distingués : volant d'inertie, pneumatique, hydraulique et électrique, le dernier étant le plus rencontré. Le développement du marché des véhicules électrique - hybrides dépend de deux facteurs principaux : le bénéfice financier (le coût de production vs. Customer value) et l'impact environnemental (production de l'énergie électrique, le recyclage des composantes), qui dépendent fortement des politiques locales et qui sont continuellement soumises aux changements.

Il y a trois niveaux d'optimisation qui peuvent être distingués : le choix de l'architecture, le dimensionnement et les algorithmes du contrôle [7]. Le premier gère la position, le nombre et le type de machine électrique, le type d'élément de stockage, le moteur et la transmission. Le dimensionnement concerne la cylindrée du moteur, la puissance maximale de la machine électrique et par conséquent, la capacité de la batterie. Ces choix sont notamment dictés par le coût, les critères de performance et les limitations liées au packaging (le volume occupé). Le dernier niveau d'optimisation couvre différents aspects, du contrôleur haut-niveau (le régulateur de vitesse, contrôle latéral) au bas-niveau, comme la commande du papillon, de la richesse ou du cliquetis. Tous peuvent être regardés comme des décisions *optimisation-based* et l'interdépendance entre ces couches suggère une dépendance hiérarchique entre les décisions du design.

Pour une architecture avec un dimensionnement fixé, un des aspects les plus compliqués d'une perspective orientée contrôle est la distribution de puissance entre les deux sources, problème appelé gestion d'énergie, qui se retrouve au niveau des algorithmes de contrôle, parce qu'elle ne fournit généralement que les références pour les couples des composantes. Pour un véhicule conventionnel, les références de couple et vitesse pour le groupe motopropulseur (GMP) sont directement déterminées de la demande conducteur, dans le cas d'une transmission manuelle ou en conjonction avec un contrôleur de boîte de vitesse, dans le cas contraire. Pour un véhicule électrique hybride (HEV), la question qui surgit est comment exploiter le degré de liberté supplémentaire - la voie électrique - afin que la performance véhicule soit améliorée. Pour certains cas spécifiques, la réponse est immédiate :

Si le véhicule freine, au lieu de dissiper l'énergie cinétique comme chaleur, elle peut être récupérée par la machine électrique pour charger l'élément de stockage (en général une batterie) et utiliser son énergie plus tard, pendant la traction électrique

- Si le moteur ne peut pas fournir tout seul le couple demandé, la machine peut l'assister et par conséquent, permettre une conduite plus dynamique

- Si un démarrage moteur est demandé, la machine peut, selon sa position, assurer un démarrage rapide, sans l'utilisation d'un BSG par exemple

Cependant, la contribution de chaque élément (le moteur et la machine) doit en général être calculée, si les deux peuvent participer à la traction. Premièrement, un objectif doit être défini, le plus répandu étant la réduction de la consommation carburant. Une stratégie élémentaire serait d'utiliser la machine pour les faibles vitesses et couples et le mode hybride de manière à ce que le rendement global est maximisé, dans le cadre d'une stratégie heuristique [8], [9]. Malgré sa simplicité, cette stratégie présente un manque important de portabilité. De plus, le rendement du GMP en tant qu'objectif d'optimisation n'indique pas nécessairement l'amélioration du gain en consommation. Il est donc plus approprié d'explicitement considérer la consommation de carburant, qui peut se faire soit par l'évaluation

d'une cartographie, soit par un modèle d'approximation.

Outre la réduction de la consommation, qui demeure le but principal, d'autres objectifs peuvent également être envisagés : l'agrément (lié essentiellement aux changements de rapports [10]), les émissions de polluants [11], [12] et la durabilité de la batterie [13], [14]. Les problèmes d'optimisation multi-objectifs sont difficilement gérés dans un cadre heuristique, ce qui renforce le choix des approches basées sur des modèles. La conception des stratégies de gestion d'énergie cible une implémentation en-ligne, qui ne peut assurer que des résultats sous-optimaux. Une évaluation complète de leur performance est généralement réalisée relatif à l'optimum global, obtenu offline et qui est un indicateur du potentiel d'un HEV pour un scénario donné. Dans ce cas, le cycle de conduite est supposé connu à l'avance et l'algorithme le plus populaire utilisé à résoudre ce problème est la programmation dynamique [15]. L'accès aux informations complètes sur le profil de vitesse et la pente n'est pas réaliste et donc, son utilisation est restreinte aux méthodes offline, mais des informations futures sur le trafic peuvent être disponibles pour un horizon limité, avec une certaine précision, ce qui encourage l'utilisation des stratégies de contrôle prédictif [16], [17], [18], [19].

Parmi ces stratégies, model predictive control (MPC) émerge comme une solution avec un potentiel considérable. Il est de plus en plus présent dans l'industrie de l'automobile, avec des applications qui couvrent différents domaines, comme le contrôle moteur [20], la dynamique latérale du véhicule [21], cruise control [22] où véhicule autonome [23]. MPC est une stratégie d'optimisation à base de modèle, sous contrainte, qui calcule une séquence de commandes qui minimisent une fonction coût sur un horizon fini, mais où seulement la première commande s'applique. Il combine donc le contrôle optimale boucle ouverte avec le retour du système. Sa capacité de gérer les contraintes et les données prédictives le rend une alternative attractive à la plus populaire stratégie de gestion d'énergie du présent *Equivalent Consumption Minimization Strategy* (ECMS) [24], [25], [26].

MPC peut être trouvé sous des formes différentes, en fonction de la nature du modèle de prédiction (linéaire, linéaire variant dans le temps et nonlinéaire) et de la fonction coût (habituellement linéaire ou quadratique). Les formulations standard du MPC comme la programmation quadratique sont généralement préférées, grâce à l'existence des solveurs dédiés efficaces et cette formulation sera également retenue dans cette thèse.

La modélisation est la première étape du design MPC et pour le problème de gestion d'énergie un modèle orienté-contrôle pour le GMP est nécessaire, qui a déjà été adressé dans la littérature, généralement pour des études de cas spécifiques. Compte tenu de la diversité des architectures hybrides, un modèle unifié apparaît comme utile et l'état de l'art courant témoigne des essais dans cette direction [27], [28]. Une caractéristique qui compléterait le travail existant est l'introduction des HEV basés sur une transmission double-embrayage.

La fonction coût est un autre élément fondamental dans le design du MPC et en général, on emploie un critère exprimé comme un compromis entre la réduction de l'erreur de suivie de l'effort de commande. Pour le problème de gestion d'énergie, la définition de la fonction coût n'est pas immédiate. L'objectif est de réduire la consommation de carburant en exploitant une source supplémentaire d'énergie, qui ne peut pas être rechargé de l'extérieur, dans le cas d'un HEV sans plug-in. L'évaluation de la performance doit prendre en compte la consommation de deux types de source d'énergie, plaçant le problème dans un cadre énergétique. Par conséquent, on peut identifier deux aspects principaux qui doivent être résolus à ce niveau: l'expression mathématique pour le problème énergétique et son traitement pour une formulation standard.

La calibration de la fonction coût a un impact majeur sur la performance du contrôle et pour le problème considéré c'est particulièrement un défi, en raison de sa dépendance élevée du cycle de conduite. Le but est de trouver un mécanisme qui facilite l'adaptation du terme de calibration en fonction du profile de vitesse et de la pente. L'accès aux données prédictives peut être exploité pour extraire des informations sur les caractéristiques du cycle et une analyse fréquentielle est un outil possible [29], [6].

Ce n'est pas inhabituel de traiter la stratégie du changement des rapports en dehors de la gestion d'énergie, ce qui réduit le problème à la distribution du couple. Le stop-start du moteur peut apporter un important gain en consommation pour un HEV, particulièrement pour la conduite urbaine et par conséquent, il est souvent adressé dans la gestion d'énergie, soit séparément [30], soit en conjonction avec la distribution du couple [31]. Pour une formulation MPC classique, ça impliquerait l'introduction d'une variable discrète du contrôle, conduisant vers une optimisation linéaire/quadratique *mixed-integer*, qui nécessite des solveurs plus complexes. Pour une plus grande flexibilité, parfois c'est préférable de proposer une formulation qui gère dans une première étape uniquement l'objective principale (pour le cas considéré, la distribution du couple), mais qui permet des extensions (stop-start moteur ou agrément) sans changements majeurs.

La vitesse véhicule est souvent imposée par le cycle de conduite et son suivi est géré à un niveau supérieur, par un modèle conducteur, mais dans certains cas, il représente un dégrée de liberté supplémentaire pour l'amélioration du gain en consommation [32], [33]. Le comportement du conducteur a également un impact important sur la consommation et des ajustements du profil de vitesse peuvent donc être introduits dans le cadre de la gestion d'énergie. Une fonctionnalité avec ce potentiel est le *coasting* ou *free-wheeling*, où le mouvement du véhicule est donné seulement par les forces résistives, les pédales d'accélération et de frein n'étant pas appuyées. Le potentiel du coasting pour le gain en consommation a été l'objet de certains travaux publiés, mais plutôt peu nombreux, de la connaissance des auteurs, et ils ont principalement traité les phases de vitesse constante sur l'autoroute. De plus, les études de cas étaient concentrés sur les véhicules conventionnels et moins sur les véhicules hybrides. Une approche analytique qui étend le problème pour les phases de vitesse variante dans le temps serait un outile généralisé pour l'évaluation de la performance et par conséquent, compléterait l'analyse qui existe actuellement.

3 Organization of the manuscript

The manuscript is organized in 4 chapters, that will be briefly introduced next. The first chapter defines the framework, from both technological and control design methodology, whereas chapter 2 and 3 are dedicated to the contributions at the specific modeling and control level, respectively. Finally, chapter 4 validates the proposed strategy based on a Model-in-the-Loop simulation. Conclusions and perspectives will complete the manuscript.

Chapter 1 presents an overview of hybrid electric vehicles, with a focus on the main aspects related to model-based control: architecture types, performance evaluation (drive cycles for homologation, pollution norms), quasi-static modeling of main components (engine, gearbox, electric machine), dynamics of energy storage elements and the framework of the energy management. For the latter topic an overview is presented, the details being provided in chapter 3, together with a series of contributions.

Chapter 2 is dedicated to the generic control-oriented model for a hybrid powertrain. Firstly, current attempts toward a general modeling are presented and next, the assumptions under which the proposed model is valid are introduced and analyzed. The purpose of this model is to cover a certain class of hybrid architectures that will allow the formulation of a generic model-based control strategy, regardless of the electric machine position and transmission type. The wheel level offers complete information about the hybrid powertrain and for a comprehensive description, intermediate levels are also considered. The model is defined by two main components:

- static relations, given by torque expressions at different powertrain levels and speed of components
- dynamics related to the battery state-of-charge

The model is detailed for parallel and series architectures, with a special emphasis on dual-clutch transmission powertrain which allow special use cases, as a result of the presence of two clutches. A linear-based approach is chosen in this work and therefore, the construction of our results will be considered after building the linearization of the battery dynamics model and proposing several rules for its online use as a prediction model. The goal of this work is to improve the fuel gain obtained with a hybrid electric vehicle. The fuel rate is usually given as nonlinear map in function of engine torque and rotational speed, but for a model-based approach, an analytic expression is needed. Hence, fuel consumption approximation is also handled in this chapter.

Chapter 3 handles the energy management problem, which is the main topic of this thesis. The first part continues the introduction from the first chapter with a detailed state-of-the-art of the control strategies for this problem. The focus is on predictive methods, which will be used in the present work, too. Fundamental notions about MPC are next presented, having as main goal the methodological aspects and their particular structural properties in relationship with the energy management. The stability *per se* not being an issue for this kind of application (nor the recursive feasibility) we will not dwell on the particular notions needed to reinforce convergence and their theoretical aspects, but concentrating our efforts in the optimization of the cycles and on the particular implications of the battery management and the driving patterns. The goal is not to bring a contribution at the theoretical level but to formulate the problem of the energy management in the MPC framework. This implies several steps: control-oriented model (already handled in chapter 2), cost function definition, tuning and constraints formulation. The focus will be at first on torque distribution, but it will be shown afterwards that the problem can be extended

to include engine stop, too. The novelty of the strategy is that this functionality is introduced without the use of an additional discrete control variable, nor by separation into a two-layer optimization. The stop-start decision is taken *a-posteriori*, based on the sequence of commands provided by the MPC. An improvement in the fuel gain can therefore be obtained without essentially changing the problem formulation. This simplification is noticeable not only at the formulation level, but also at implementation: the solver does not need to be changed in order to cope with binary decision variables (ON/OFF command for the engine).

Another contribution is related to the tuning procedure: the cost function describes a trade-off between fuel and battery consumption, ensured by the use of a weighting term, whose choice is extremely important for the strategy performance. Its dependence on the drive cycle makes its tuning a challenging problem. The method proposed here takes into account the foreseen torque demand and the upper and lower bounds of the two power sources. Based on these information, a ratio of variations between lower and upper limits can be calculated and the tuning term is defined as an average over an horizon.

The chapter is finalized with the analysis and design of coasting. Here, unlike the previous work, an analytical approach is proposed that decides the coasting initiation, duration and quantifies the acceptance of solution in terms of time-wise speed deviation.

Chapter 4 is dedicated to the Model-in-the-Loop validation of the proposed strategy. The case study is a dual-clutch transmission hybrid with an electric machine connected to the even primary shaft. The simulations are performed in Matlab/Simulink, with co-simulation in AMEsim, where the vehicle high-fidelity model was designed. The performance is evaluated for different drive cycles and compared with Pontryagin's Minimum Principle method, which provides close-to-optimal results. The tuning mechanism introduced in the previous chapter is validated for the considered drive cycles and the MPC anticipation is proven useful especially due to stop-start functionality. In order to test the robustness of the strategy, a sensitivity analysis is performed with respect to engine torque and battery state-of-charge measurements, as well as to battery size. The evaluation is completed with an analysis of the slope influence, which is only considered for basic case studies, in the absence of slope information for standard drive cycles.

4 List of publications and oral presentations

Accepted conference papers

- N. Stroe, G. Colin, K. Ben-Cherif, S. Olaru, and Y. Chamaillard: Towards a generic control-oriented model for HEV predictive energy management, *8th IFAC International Symposium in Advances in Automotive Control*, 2016
- N. Stroe, S. Olaru, G. Colin, K. Ben-Cherif, and Y. Chamaillard: Time-varying MPC-based energy management for HEV including engine stop & start, *20th Int. Conf. on System Theory, Control and Computing Joint Conf. SINTES 20, SACCS 16, SIMSIS 20*, 2016.
- N. Stroe, S. Olaru, G. Colin, K. Ben-Cherif, and Y. Chamaillard: A two layer predictive control for hybrid electric vehicles energy management, *20th IFAC World Congres*, 2017.

Oral presentations

- MPC in powertrain control, *TEMPO Research Review and Automotive Embedded Control Workshop*, February 2015, Paris
- Modeling for control in hybrid electric vehicles: a generic control-oriented model and a MPC - based energy management strategy, *Groupe du Travail Automatique et Automobile*, November 2015, Bordeaux
- Time-varying MPC-based energy management for HEV with engine stop & start, *4th European Conference on Computational Optimization*, September 2016, Leuven, Belgium
- Generic predictive control framework for energy management of hybrid electric vehicles, *Journée de Jeunes Chercheurs*, December 2016, Orléans

Awards

- Best Paper Award at *Journée de Jeunes Chercheurs* 2016, Orléans, for the paper: Generic predictive control framework for energy management of hybrid electric vehicles

Submitted journal papers

- N. Stroe, S. Olaru, G. Colin, K. Ben-Cherif, and Y. Chamaillard: Predictive Control Framework for HEV: Energy Management and Free-Wheeling Analysis, *IEEE Transactions on Intelligent Transportation Systems*

Chapter 1

Hybrid electric vehicles: an overview of architecture, modeling and energy management

This chapter is a synthesis of elementary notions and concepts related to hybrid electric vehicles that will facilitate the comprehension of the goals of the present thesis. A brief description and modeling are given for the main components of a hybrid powertrain. An introduction to the energy management problem is also included.

Ce chapitre est une synthèse des notions et concepts élémentaires liés aux véhicules hybrides, qui vont faciliter la compréhension des objectifs de cette thèse. Une courte description, ainsi que la modélisation sont présentées pour les principales composantes d'un groupe moto-propulseur hybride. Une introduction de la gestion d'énergie est également inclue.

1 System description

Definitions of hybrid electric vehicles (HEV) are not always unitary, but it is commonly stated that they are characterized by an internal combustion engine (ICE) and one or more electric machines (EM), powered by a battery or ultra-capacitor [34], see Fig. 1.1 for an example. Vehicles powered by a battery and a fuel cell are referred to as fuel cell electric vehicle (FCEV).

The functionalities rendered possible by hybridization are the following, numbered from 1 to 4:

1. stop-start (S&S): automatically stop the engine when the vehicle is at standstill and restart it when the gas pedal is pressed

2. regenerative braking: to slow down the vehicle, instead of dissipating the energy as heat, it is recovered by the EM, which functions as a generator, to replenish the storage element (battery or ultra-capacitor)

3. torque assist: in some cases, especially for aggressive drivers, the engine cannot provide the requested torque and therefore, the EM contribution is used to satisfy the driver request

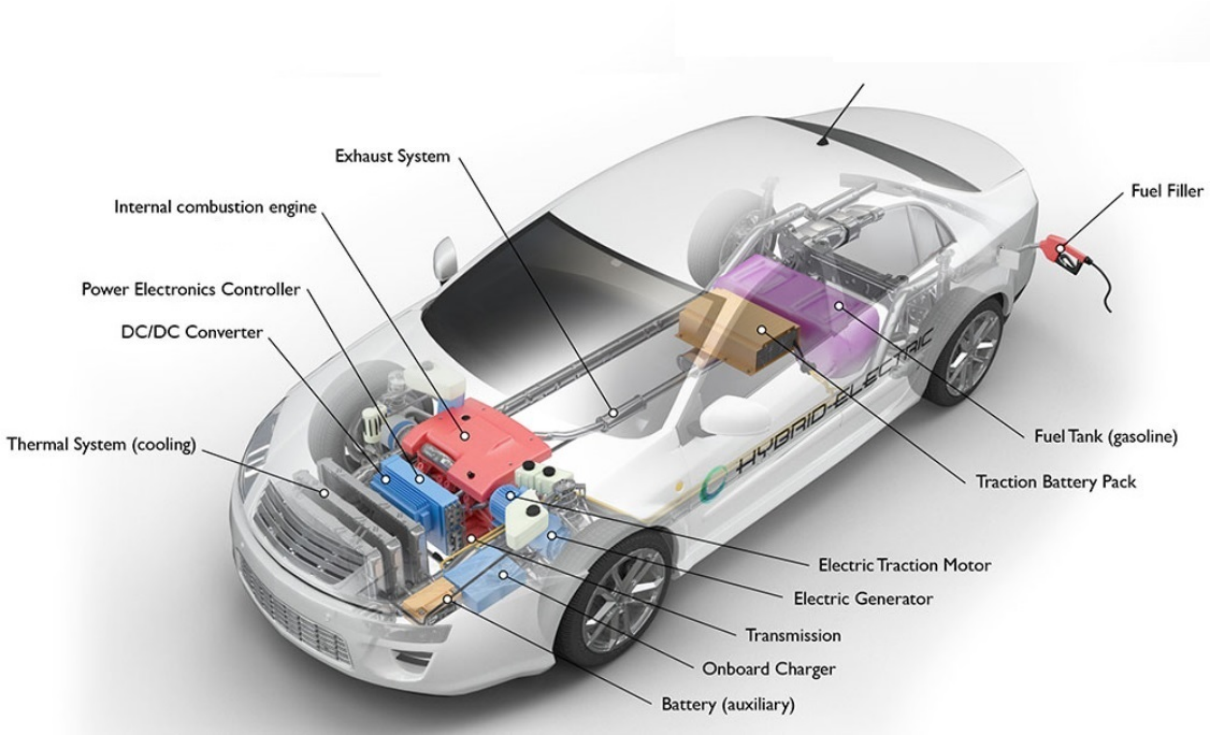

Fig. 1.1 – Hybrid electric vehicle representation [1]

4. electric drive: the entire power demand is ensured by the electric path. This is only possible for architectures that allow the engine and the traction motor to be decoupled

HEV classification in micro, mild, full and plug-in hybrid, is usually done in relation to these functionalities, that imply certain power and voltage requirements, as detailed in Table 1.1. The hybridization factor (HF), defined as

$$HF = \frac{P_{EM}}{P_{ICE} + P_{EM}}$$

can also be used as an indicator of hybridization category [35]. It can vary between 0 (conventional vehicle) and 1 (all-electric vehicle). An intermediate category of *medium hybrid* can also be defined, as in [36], for a voltage level of $\sim$144V. In [37] a distinction is made between S&S-only architecture (referred to as micro hybrid) and soft or micro-mild, which exhibits in addition a modest energy recovery possibility. Therefore, another classification is possible, as presented in Table 1.2, with information regarding the type of electric machine connection and the potential fuel consumption gain.

1.1 Main components

As already mentioned, in addition to the elements of a conventional vehicle, HEV contain one or more electric machines, an energy storage element and power electronic components. The engine can be spark ignited (SI) or compression ignited (CI), naturally aspired or turbocharged. The electric motors present in an HEV can be of different types, their selection depending on cost, design constraints (weight, size) and performance objectives: brushless direct current, switch reluctance or asynchronous machines.

Table 1.1 – HEV classification and characterization, according to [38]

Hybrid / Characteristics	Micro	Mild	Full	Plug-in
Functionalities	(1)+(2) (minimal)	(1)+(2)+(3)	(1)+ (2)+ (3)+(4)	(1)+ (2)+ (3)+(4)+plug-in
Electric power (kW)	3	10-30	60	60
System voltage (V)	14	48-200	300-600	300-600
HF	< 0.1	< 0.25	$(0.25; 0.5)$	> 0.5

Table 1.2 – HEV classification and characterization, according to [37]

Hybrid / Characteristics	Micro	Soft	Mild	Full	Plug-in
Electric power (kW)	2-4	4-6	10-20	20-60	40-110
System voltage (V)	14	42	100-150	200-300	200-370
Electric machine connection	belt	belt or integrated	belt or integrated	integrated	integrated
Consumption gain [%]	5-7	7-12	15-25	25-40	40-60

The energy storage component is among the most important elements in a hybrid powertrain. A possible option is the ultra-capacitor, whose main advantage is the high charge and discharge rate, but it exhibits an important self-discharge rate and a low energy density. Batteries are the usual choice and the main requirements related to their performance are a high energy density and a long calendar life. Different types of batteries can be encountered for vehicle applications: valve-regulated lead acid (VRLA), nickel-cadmium (NiCd), nickel-zinc (NiZn), nickel-metal hydride (NiMH), lithium metal-polymer (LiM-polymer) and lithium-ion (Li-ion) [39]; a comparison between them in terms of specific energy density and volumetric energy density is depicted in Fig. 1.2. Due to their extensive usage, a brief presentation of NiMH and Li-ion batteries is next introduced. However, the model and the control strategy that will be introduced in the next chapters do not depend on the battery type.

NiMH batteries are the most popular energy storage elements for HEV. It was only in 2010 that Li-ion batteries entered the HEV market, with Mercedes S400 hybrid. However, their wide operating range 10%-100% [39], as well as the high energy density and fast charging ability [40] makes them an attractive choice for plug-in HEV (PHEV), such as Toyota Prius Plug-in, GM Chevrolet Volt, Hyundai Sonata.

The main drawbacks for NiMH battery are the elevated self-discharge (for higher voltage systems is at 30% per month, at 20°C) and the poor performance at low temperature [39]. Conversely, Li-ion batteries exhibit at least 20% lower self-discharge, a reduced weight (gain of $\sim$30% for the same energy) [39] and also a temperature range from -20°C to 60°C.

In [39], chapter 10, a comparison between NiMH and Li-ion batteries is presented, as a result of the test drives performed by Nissan on two HEVs with identical characteristics, except the battery pack. It was observed that the average delivered power was almost the same, but with a higher energy efficiency for Li-ion (95% vs 83%) and also, a lower temperature for it (49°C vs 52°C). The SOC variation was slightly larger for Li-ion ([30%-85%] vs [40%-80%]), but the most notable difference was related to the activation of the battery management system to limit the battery discharge power, where Li-ion showed

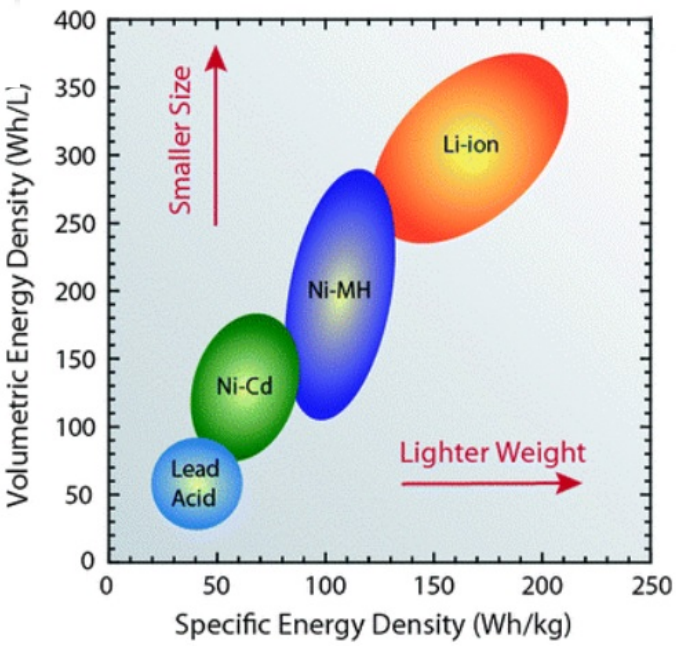

Fig. 1.2 – Specific energy density and volumetric energy density for different battery technologies [2]

a far better performance: 2.2% vs 44% (the numbers represent the percentage of time when the system had to be activated).

Another comparison between these two technologies can be found in [41], for Toyota HEV (NiMH) and GM HEV (Li-ion). The latter definitely outperforms the former in the case of specific energy: 56 vs 46 [Wh/kg] and specific output power 3000 vs 1300 [W/kg]. However, Li-ion batteries need a more complex cooling system in order to extend their lifetime, which introduces an additional weight in the system. After taking it into account, the NiMH battery may have a greater system-level specific energy. Another drawback of Li-ion batteries is that they need a battery management system at the cell level, rather than system level, as is the case for NiMH. It is also stated that for regenerative braking, a scaling factor (around 3) is applied to the specific output power for Li-ion, in order to avoid overheating, which reduces the differences between the performance of the two battery types.

1.2 Architecture types

There are 3 main architecture types that can be identified for an HEV, as depicted in Fig. 1.3, in a schematic manner: parallel, series and series-parallel. Examples from the market with their associated degree of hybridization are summarized in Table 1.3.

In parallel architectures, both the combustion engine and the electric machine can be used independently or together for traction. The ICE and EM speed are directly determined from the vehicle speed, the axle ratio and the gear engaged. Usually there is only one EM, but it is possible to imagine different configurations. The EMs can be found at different levels, their position being mostly dictated by packaging constraints (the occupied volume) and the hybridization degree.

The advantages of this architecture come from a good energetic efficiency, limited modifications with respect to a conventional architecture, a limited number of components, whereas the disadvantages concern reduced possibilities of downsizing, complex mechanical coupling and components placement,

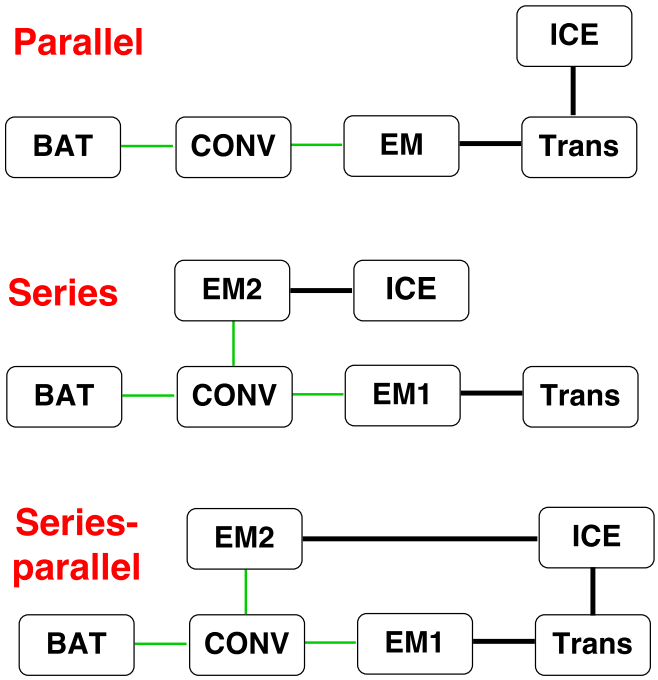

Fig. 1.3 – Block representation of HEV architectures; CONV - convertor, BAT - battery, Trans - transmission; black lines: mechanical links, green lines: electrical links [3]

Table 1.3 – Examples of HEV, classified w.r.t. architecture and degree of hybridization

Configuration / Hybridization level	Parallel	Series	Series-parallel
Micro	Citroen C3	-	-
Mild	Honda Civic	-	-
Full	Kia Optima Hybrid	Nissan e-Power	Ford Fusion Hybrid
Plug-in	Hyundai Sonata Plug-in	GM Chevy Volt	Prius Plug-in

engine dynamical transient behavior not entirely eliminated [37].

Series architectures on the other hand, contain at least two electric machines: one that is used for traction (EM1) and another that acts as a generator (EM2). The engine mechanical output is converted into electricity by the generator, which can be used directly by the traction motor or to charge the battery. The successive energy conversions, mechanical-electrical-mechanical, explains the choice of the architecture name. There is no mechanical link between the engine and the wheels, which presents the advantage of choosing the engine operating point, but also the reduction of the engine dynamics, as well as an important downsizing. The placement of components is easier than for a parallel configuration and the main applications are for heavy duty and public transportation.

The drawbacks are related to the reduced energetic efficiency (as a result of the double electric path), elevated cost and weight due to the presence of two electric machines, the need of important modifications with respect to a conventional architecture, as well as the absence of a pure ICE mode [37].

For series-parallel architectures two categories can be distinguished:

- architectures with multiple clutches that allow the switch between series and parallel mode, justifying thus the combined name of *series-parallel*. They contain at least two EMs and they integrate advantages from both configurations
- architectures based on planetary gear sets (PGS), which allow a continuous power distribution between the components, leading to the name of *power split* architectures. The speed of an EM is an additional degree of freedom and they allow different interconnections between the components.

A planetary gear set (PGS) is a mechanical transmission element that possesses two degrees of freedom: it couples 3 shafts with different rotational speeds, with the speed of one shaft being determined from the others. A particular case of PGS is the axle differential, located between the two driving wheels of a vehicle [37]. Its components are called *ring (R), carrier (C)* and *sun (S)*, as depicted in Fig. 1.4. The components of a hybrid powertrain can be connected in different manners to a PGS and multiple clutches can also be present in order to have several functioning modes, the switch being performed, for instance, with respect to the power request level. Among the most popular PGS-based architectures are Toyota Prius (1 PGS) and Lexus (2 PGS), whose schematic representations are depicted in Fig. 1.5.

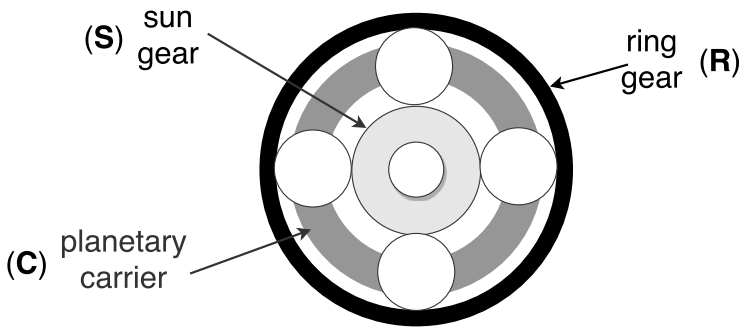

Fig. 1.4 – Planetary gearset (PGS) representation

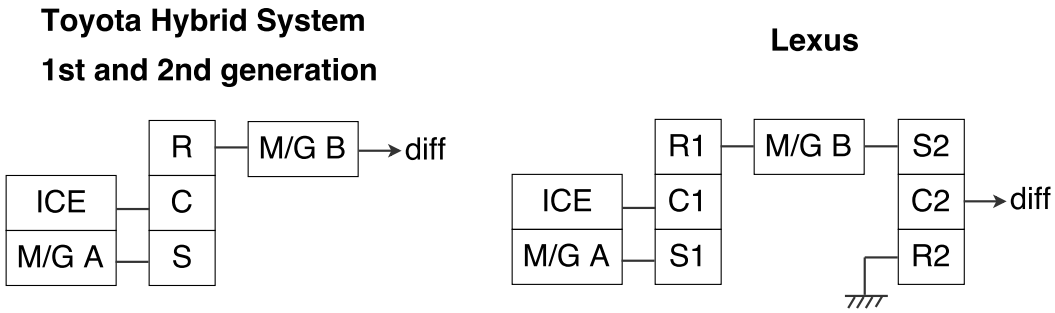

Fig. 1.5 – Examples of PGS-based hybrid architectures

2 Market trend, legislation and performance evaluation

Oil price increase and climate changes led to an adaptation of the automotive market trend, which gradually started to encourage the orientation toward alternative transportation systems. This is also

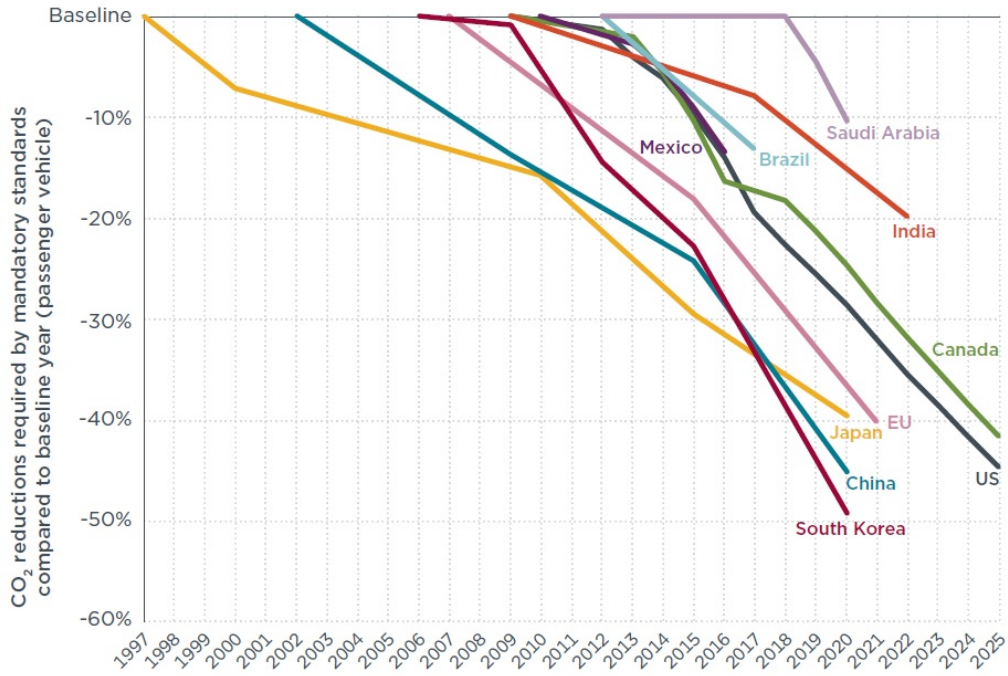

Fig. 1.6 – Evolution in time of CO_2 reduction requirements for passenger car standards, in different countries [4]

supported by a new legislation that enforces a CO_2 reduction target, more stringent with every year, but with a rate of change dependent on the country, as shown in Fig. 1.6. As far as the pollutant emissions (HC, CO, NO_x) are concerned, the situation is similar. The US passed a legislation on vehicle emissions in the 1960s, mostly due to the increased level of smog and in 1975, as a response to the rising oil price, norms on vehicle economy (Corporate Average Fuel Economy, CAFE) were adopted [42]. In Europe, the first norms emerged almost 20 years later, in 1992 with Euro 1, subject to changes over the years that eventually lead to Euro 6 in 2014, currently in use; a synthesis of this evolution is given in Table 1.4, for compression ignition and positive ignition engines. Because of their harmful effects on health, NO_x and particulate matter (otherwise known as *soot*) witnessed the most restrictive evolution: a tenfold reduction of their admissible thresholds in 14 years, from 2000 to 2014, for Diesel engines and threefold for gasoline engines (for NO_x emissions), whilst the norms on particulate matter are only enforced since 2009. It should be noted that for the PM, in addition to the standards expressed in [g/km], norms quantified in number of particles are also enforced.

Table 1.4 – Emissions norms in Europe (g/km) for passenger cars; PM - particulate matter [42]

Stage	Year	Compression ignition (Diesel)			Positive ignition (gasoline, natural gas etc)			
		CO	NO_x	PM	CO	HC	NO_x	PM
Euro 1	1992	1	-	0.14	2.2	-	-	-
Euro 2	1996	0.64	-	0.1	2.3	0.2	-	-
Euro 3	2000	0.5	0.5	0.05	1	0.1	0.15	-
Euro 4	2005	0.5	0.25	0.025	1	0.1	0.08	-
Euro 5	2009	0.5	0.18	0.005	1	0.1	0.06	0.005
Euro 6	2014	0.5	0.08	0.005	1	0.1	0.06	0.005

To evaluate the conformity with the norms, driving scenarios that represent different types of driving conditions (urban, road, highway, jam) or driving styles (standard, eco, dynamic) need to be defined for each class of vehicles (passengers cars, trucks). They are referred to as standard drive cycles, but the standardization is only local, due to the differences related to legislation, as well as driving style. For Europe, the standard is NEDC (New European Driving Cycle), depicted in Fig. 1.7, with a urban sequence of 200s repeated 4 times and an extra-urban part, with a maximum speed of 120 km/h. The cycle being often considered unrepresentative, alternative profiles that reproduce the urban, road and highway trips, as well as congested urban traffic, were later proposed: the Artemis drive cycles [43], presented in Fig. 1.8 and Traffic Jam, in Fig. 1.7, bottom. For the US, the standard drive cycle is FTP-75 (Federal Test Procedure, Fig. 1.7), which is mainly defined by urban driving and it presents a 6-minute standstill phase, used for thermal analysis.

More recently, an attempt to converge toward a unified standard is through WLTC (Worldwide harmonized Light vehicles Test Cycles, Fig. 1.7), which contains 4 main speed phases: low, medium, high and extra-high. Its advantages over NEDC come mainly from stronger speed variations and lower repetitiveness, making it more realistic. However, NEDC remains currently the standard drive cycle in Europe.

The potential of an HEV is especially visible in urban driving, characterized by low power demands and frequent stops and where the electric path can therefore bring an important contribution. For highway profiles, the hybridization can be useful for boost, but the fuel reduction is insignificant. Therefore, drive cycles such as Artemis road and highway are not very profitable for an HEV fuel gain evaluation.

It must be noted that in addition to the norms, there are also performance indicators related to NVH (Noise, Vibration and Harmonics) and drivability, (e.g. take-off, acceleration feeling from 0 to 100 km/h) or to the total cost of ownership (cost of acquisition and of maintenance), which are not standardized.

The previous analysis does not include the upstream process of fuel production, transportation and distribution, nor the production of electricity, its purpose being to evaluate only the vehicle performance. This framework is referred to as tank-to-wheel analysis and it considers only the fuel combustion, evaporation, tire and brake wear [39], as well as the battery consumption, for an HEV. The environmental impact of alternative vehicles cannot be nonetheless neglected and the inclusion of the production and transportation of the energy would complete their performance evaluation. In this case, the framework is referred to as well-to-wheel.

Its dependence on the power generation regulations of each country led to geo-politically oriented studies: a detailed report for European Union on well-to-wheel analysis for conventional and alternative fuels, in conjunction with primary energy sources (natural gas, biomass, wind) can be found in [44]; for

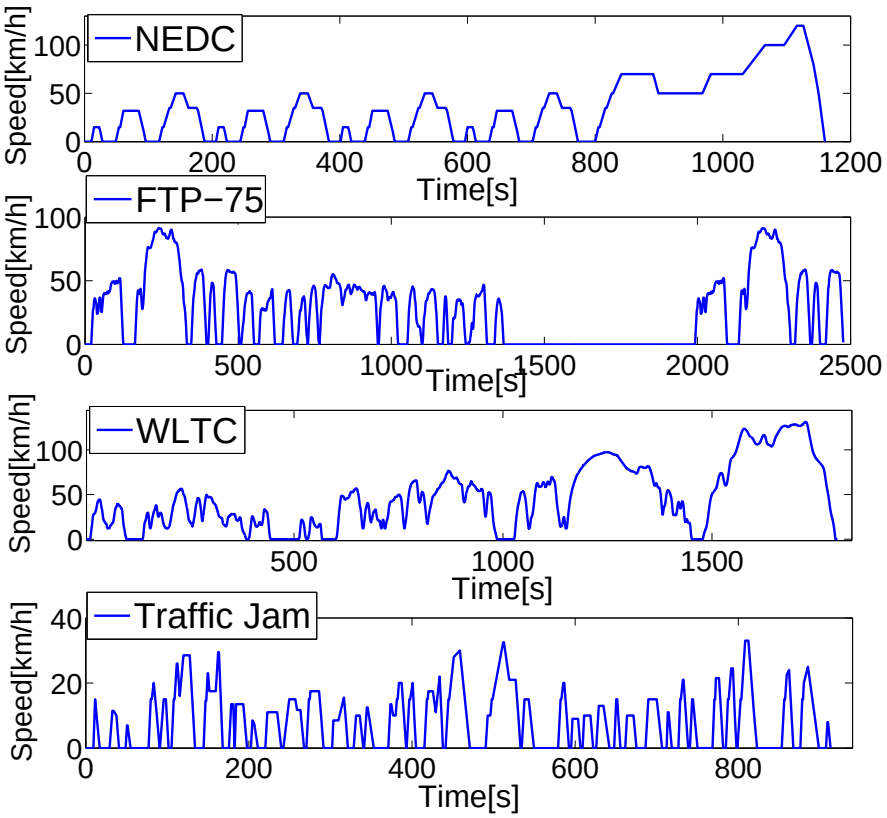

Fig. 1.7 – Speed profile for NEDC, FTP-75, WLTC and Traffic Jam

the US, Argonne National Laboratory conducted a research project on different vehicle technologies (SI, CI engines, BEV and FCV), fuels (gasoline, ethanol, hydrogen) and feedstocks (corn, biomass, natural gas, electricity) [45]; for China, in [46] an evaluation for pure electric and hybrid electric vehicles, with detailed emission factors was presented; for Japan, [47] analyses the CO_2 impact of pure electric vehicles (EV), HEV and PHEV in order to foresee the market share of these vehicle types.

For a PHEV, a fair analysis would be in a well-to-wheel framework, in order to correctly address the battery charging from the grid. However, for vehicle-oriented control applications, the focus is only on tank-to-wheel evaluation, for conventional, as well as for hybrid vehicles.

3 Quasi-static modeling

The powertrain modeling for simulation distinguishes two approaches: forward and backward. The first approach respects the physical causality of the power flow (from engine to vehicle speed), whereas the second starts from the target drive cycle (vehicle speed and road slope, when available) and it calculates the references for the propulsion system. A comparison between the two can be found in [48]. The backward approach is retained in control-oriented applications, i.e. it is assumed that there is an imposed drive cycle and a control law for the components needs to be designed in order to ensure the speed tracking. A schematic representation is given by Fig. 1.9.

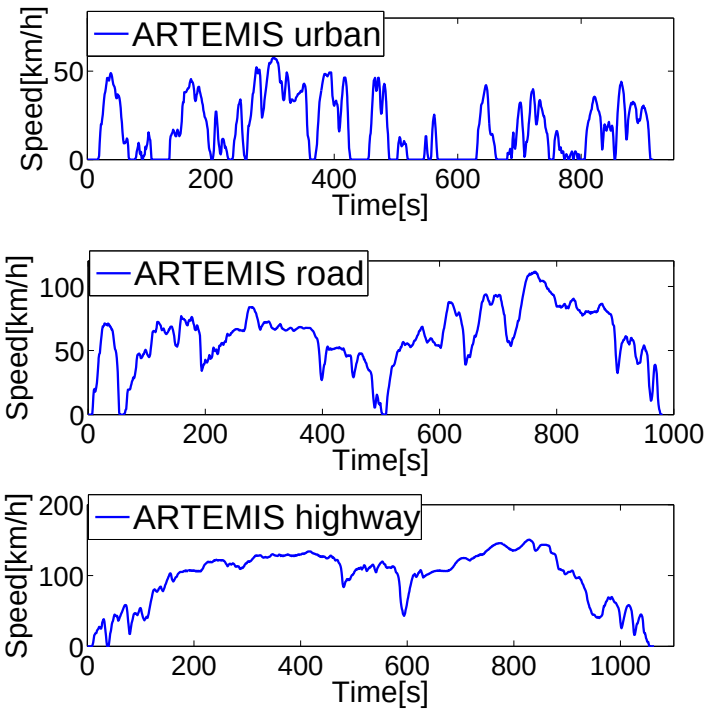

Fig. 1.8 – Speed profile for Artemis urban, road and highway

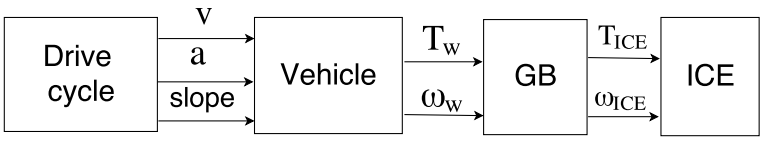

Fig. 1.9 – Backward simulation; v - vehicle speed setpoint, a - acceleration, T_w - wheel torque, ω_w - wheel rotational speed

3.1 Vehicle longitudinal dynamics

Vehicle propulsion implies a torque supply that overcomes the resistive forces given by aerodynamic drag F_{aero}, rolling friction losses F_{roll}, force induced by gravity F_g and inertia F_i. In a backward approach, at each instant, given the vehicle reference speed v, the road slope and vehicle parameters, the traction force can be calculated as follows:

$$
\begin{aligned}
F_t &= F_{aero} + F_{roll} + F_g + F_i \\
F_{aero} &= \frac{1}{2}\rho_{air} A_f c_d v^2 \\
F_{roll} &= (c_{r1} v + c_{r0}) m_v g cos(\alpha) \\
F_g &= m_v g sin(\alpha) \\
F_i &= m_v \dot{v}
\end{aligned}
\tag{1.1}
$$

The wheel torque demand can be thus determined, where R_w is the wheel radius:

$$T_w = F_t R_w \tag{1.2}$$

where ρ_{air} is the air density, m_v - vehicle mass, A_f - vehicle frontal area, c_d - aerodynamic drag coefficient, c_{r0}, c_{r1} - rolling friction coefficients and α is the road grade.

3.2 Powertrain

3.2.1 Gearbox

If losses are neglected, the dependence between the input and output for a discrete gearbox (see Fig. 1.10) is expressed as:

$$\omega_i = R_{GB}\omega_o, \quad T_i = \frac{T_o}{R_{GB}} \tag{1.3}$$

where R_{GB} is the ratio of the engaged gear. This variable can also have continuous values, as in continuously variable transmissions (CVT). For this type of transmission the losses are not negligible and therefore, the above torque expression is written as:

$$T_i = \frac{T_o}{R_{GB}} \eta_{GB}^{-sign(T_o)} \tag{1.4}$$

where η_{GB} is the gearbox efficiency.

Fig. 1.10 – Gearbox quasi-static representation; i - input, o - output

For a PGS (see Fig. 1.4) the relation between the speeds of the 3 elements (ring, carrier, sun) is expressed as:

$$\omega_S N_S + \omega_R N_R = \omega_C (N_R + N_S) \tag{1.5}$$

where N_S, N_R are the number of teeth of the sun and the ring, respectively.

3.2.2 Internal combustion engine

The engine is characterized by fast dynamics, which cannot be captured by a supervisory controller that handles only the torque and the speed setpoints. Therefore, at this level, a static model is representative enough for an engine, regardless of its characteristics (SI, CI, with direct or port injection, naturally aspired or turbocharged, with exhaust gas recirculation etc). An ICE is usually described by its fuel rate evolution $\dot{m}_f$, which is generally expressed as a nonlinear map, dependent on the torque T_{ICE} and speed ω_{ICE} and whose usual unit is $\left[\frac{g}{s}\right]$:

$$\dot{m}_f = f(T_{ICE}, \omega_{ICE}) \tag{1.6}$$

Another useful quantity for an upper-level description of an engine is the *specific fuel consumption* (SFC), which evaluates the engine performance and it is defined as the ratio between the fuel rate and the power output P [49]:

$$SFC = \frac{\dot{m}_f}{P} \tag{1.7}$$

The most common unit is $\left[\frac{g}{kWh}\right]$; low values are an indicator of a good efficiency and they are different for SI or CI. The iso-SFC map for a SI engine are depicted in Fig. 1.11, along with the maximum engine torque T_{ICE}^{max} curve, which is usually given as a nonlinear map in engine speed (the minimum torque is considered zero):

$$T_{ICE} \in [0; T_{ICE}^{max}(\omega_{ICE})]$$

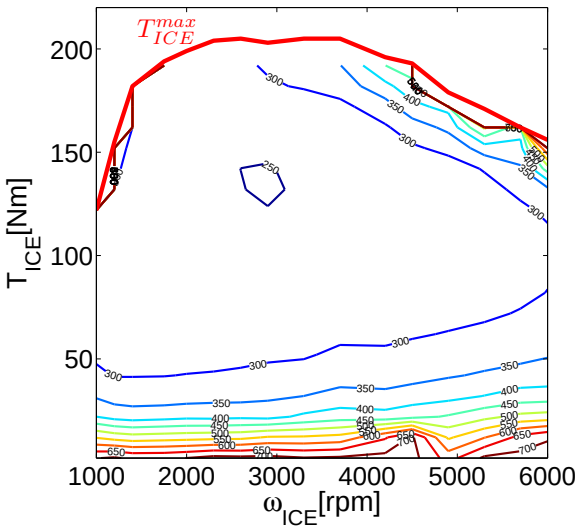

Fig. 1.11 – Iso-specific fuel consumption map for a spark-ignition engine

3.2.3 Electric motor

The electric machine has two functional modes: motor, defined by a positive torque and generator, with a negative torque, both with a upper and lower bound, respectively, dependent on the EM speed:

$$T_{EM} \in \left[T_{EM}^{min}\left(\omega_{EM}\right), T_{EM}^{max}\left(\omega_{EM}\right)\right]$$

An example of this dependence for an EM can be seen in Fig. 1.12, along with the iso-efficiency map.

The output power is either given as a static map, as a function of torque T_{EM} and speed ω_{EM}, or directly expressed from torque and speed, with losses given as a map:

$$P_{EM} = \frac{\pi}{30}\omega_{EM}T_{EM} + loss\left(\omega_{EM}, T_{EM}\right) \tag{1.8}$$

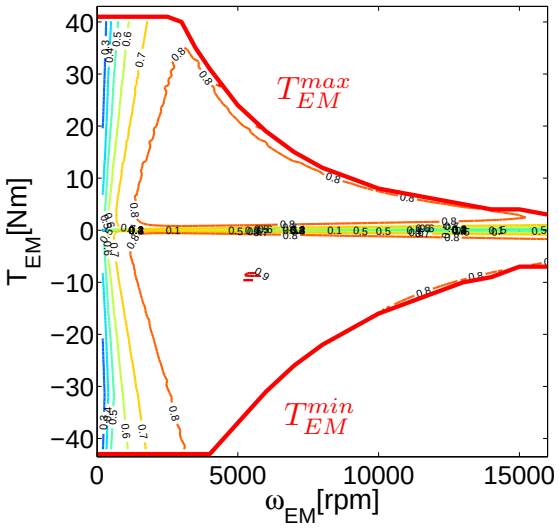

Fig. 1.12 – Iso-efficiency map for an electric machine, with its torque limits

3.3 Energy storage elements

Batteries are the most encountered energy storage elements for HEV and therefore, in what follows, the modeling will be exclusively addressed for them. For ultra-capacitors, a basic physical model can be found in [3].

For supervisory control application, a simple equivalent circuit with internal resistance is usually used for batteries [3], as depicted in Fig. 1.13. More complicated equivalent circuit models that capture the thermodynamical behavior can be found in [41] or [50]. The open circuit voltage OCV and the internal resistance R depend on SOC, their evolution with respect to SOC being depicted in Fig. 1.14 for a Li-ion battery. Note that R has a different evolution for charge and discharge.

The most important variable that describe the battery dynamics is the state-of-charge, defined as:

$$SOC(t) = SOC(t_0) - \frac{1}{Q_{max}}\int_{t_0}^{t} I_{bat}(\tau)d\tau \tag{1.9}$$

The battery current can be deduced from Kirchhoff's law applied to the equivalent circuit from Fig. 1.13: $OCV - I_{bat}R = U_{bat}$. By multiplying it with I_{bat} and given that $I_{bat}U_{bat} = P_{bat}$ is the power

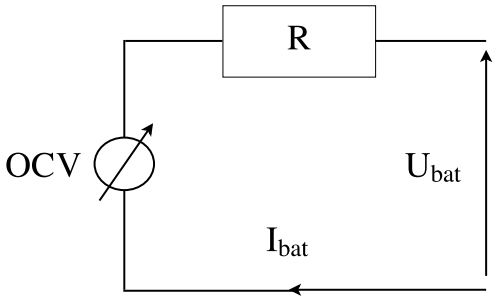

Fig. 1.13 – Equivalent internal resistance circuit for batteries; OCV - open circuit voltage; R - internal resistance

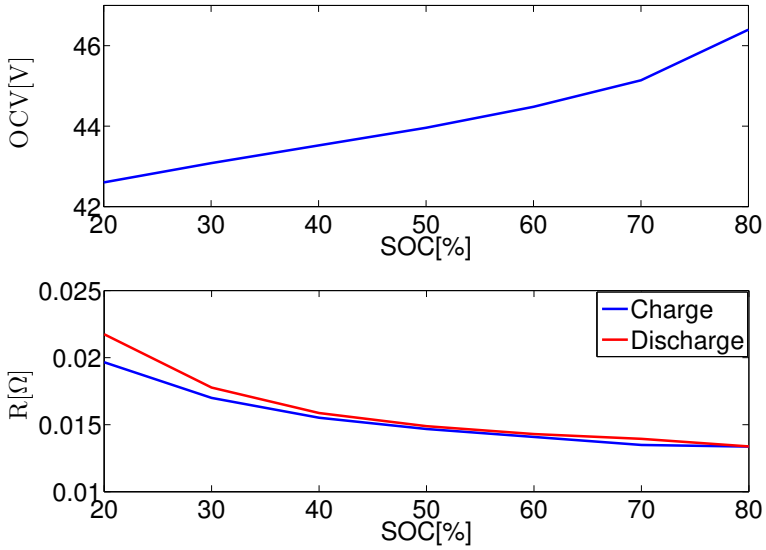

Fig. 1.14 – Open circuit voltage and internal resistance evolution with respect to SOC for a typical Li-ion battery

exchanged between the battery and the electric machine, this yields to the solution of a second order equation:

$$I_{bat} = \frac{OCV - \sqrt{OCV^2 - 4RP_{bat}}}{2R} \tag{1.10}$$

where $P_{bat} = \frac{\pi}{30}\omega_{EM}T_{EM} + loss\left(\omega_{EM}, T_{EM}\right)$. It should be noted that only one solution was retained, since the battery current can be positive (discharge, $P_{bat} > 0$) or negative (discharge, $P_{bat} < 0$), the other solution of this second order equation being always positive.

The variation of SOC can therefore be expressed as:

$$\dot{SOC} = -\frac{OCV\left(SOC\right) - \sqrt{OCV\left(SOC\right)^2 - 4R\left(SOC\right)P_{bat}}}{2R\left(SOC\right)Q_{max}} \tag{1.11}$$

where the SOC dependence of OCV and R was explicitly marked.

In addition to SOC, another variable that characterizes the battery, is the state-of-health (SOH), which quantifies the battery wear-out. There are three main types of SOH models [13]: electrochemical, event-based and energy-throughput-based models. The latter is suitable for real-time control problems due to its simplicity and it takes into account the number of cycles of charge/discharge:

$$\dot{SOH}(t) = -\frac{|I_{bat}(t)|}{2NQ_{max}} \tag{1.12}$$

where N is the number of total number of cycles until the end-of-life, which is defined as the loss of 20% of the rated capacity.

4 Energy management

For a hybrid vehicle, three main optimization layers can be identified in the literature:

1. Architecture optimization: it concerns the components position and their interconnection [51], [52]
2. Optimal sizing: engine displacement, electric machine power, battery capacity. This can be individually handled, at an upper layer, [53] or with energy management co-optimization [54], [55]
3. Optimization-based control algorithms, which include the energy management

The presence of an additional energy source introduces a new degree of freedom within the control design algorithms for a hybrid architecture. One of the challenges that arise is the management of this source such that the vehicle performance is improved. The power distribution between the two sources is referred to as energy management and it will represent the major topic of this thesis. In most of the cases, this problem is formulated for a fixed architecture and sizing, but as mentioned above, an energy management and sizing co-optimization can also be encountered.

The scientific literature is abundant in publications that handle the energy management and its field extended, especially in recent years, by covering adjacent problems. Several criteria can be employed to classify the current research work. The uppermost criterion is related to the hybridization type, followed by vehicle type (passenger, trucks, buses or even race cars) and configuration type, which includes the 3 types presented in the beginning of this section, with a distinguished category for the plug-in case, as it is summarized in Table 1.5:

Table 1.5 – Classification of energy management applications w.r.t. overview criteria: hybridization, configuration and vehicle type

Hybridization type	**Vehicle type**	**Configuration (HEV)**
electric: most common	passenger car: most common	parallel [25], [56], [15], [57]
hydraulic [58]	truck [59], [60], [61]	series [62], [63], [64]
pneumatic [65], [66]	bus [67], [68], [69], [70], [71]	series-parallel [72], [73], [74], [75]
fuel cell [76], [77]	race car [78], [79], [80]	PHEV [81], [82], [83]

If the engine speed is not included in the optimization, the problem is reduced to torque distribution and this is the particular framework for parallel hybrid architectures. Series architectures and those based on PGS include by default the engine speed as an optimization variable, as showed in the first subsection.

For an HEV, the energy management targets especially the reduction of CO_2 emissions, which is primarily handled by the torque distribution, with a possible extension to gearshift optimization, as in [84], [30] or even velocity profile co-optimization, as in [32], [33], [85], [22]. Vehicle speed can therefore represent a new degree of freedom in the optimization, in addition to the engine torque and speed.

Fuel consumption reduction is the primary objective, but it is not unique, multi-objective optimizations being equally used to address:

- drivability: the objective can be to simultaneously minimize the fuel consumption and the number of gearshifts and engine events (stop-start) [10], [86]; drivability problem handles the power fluctuations absorption [87]

- reduction of pollutant emissions: the state space is extended with the catalytic converter temperature [11]; the objective is expressed as a trade-off between the fuel consumption and the emissions [12], [88]

- duration improvement (battery health): battery state-of-health is explicitly considered and defined with respect to number of cycles of discharge and charge [13]; battery cell temperature is introduced as an additional state [14]

- driver's thermal comfort: depending on the climate conditions, the impact of cabin heating on fuel consumption cannot be neglected [89]

In some cases, maximizing the efficiency is the main objective, as in [90], where an extremum seeking method was used for a parallel architecture or as in [63], where a model predictive control-based energy management was applied to a series architecture. For the latter, this approach is mainly due to the particularities of the configuration: choice of the engine operating point regardless of the vehicle speed and poor efficiency of the double electrical path. However, an efficiency-oriented objective does not necessarily yield optimal fuel gain results.

The type of algorithm used by the strategy determines different possible classifications. One of the most encountered distinctions is between rule-based and model-based strategies. The former are based on a heuristic description of the system and their simplicity makes them an attractive option for real-time algorithms. They can be implemented as a set of *if - then - else* rules (as a finite state machine, for instance) and they further distinguish the following modes:

- electric traction for low speeds (if the battery allows it)

- regenerative braking

- electric assistance when the power demand cannot be provided by the engine

- exclusive ICE traction for low battery levels or low electric efficiency

- hybrid mode with best combined efficiency [8], [9].

For some specific architectures, such as torque-assist hybrids, where the EM and ICE are always coupled, a simplified rule-based strategy is proposed; the EM interferes only for launch from standstill, braking energy recovery and boost [91].

The main drawback of this method is the lack of portability, the set of rules being only valid for a certain application. Moreover, the threshold values used to switch between the modes strongly depend on the powertrain configuration and on drive cycle characteristics, which makes their tuning a complicated

process. An improvement can be obtained by using an alternative heuristic method, a Fuzzy Logic Controller (FLC) [92], [93]. A detailed description of this method, with its variations (predictive and adaptive) can be found in [94].

The model-based methods can provide the global optimum, but with a limited use to an offline application, or the local optimum, with a possible real-time implementation. The former is only used as a reference in order to evaluate the performance of real-time strategies. Since the focus of this work is model-based control, more details about these methods will be provided in Chapter 3.

Sometimes, heuristic strategies are used in conjunction with optimization-based methods, i.e. the former are defined such as they reflect the behavior of the latter [95] or the results of the optimization strategy is exploited in defining the aforementioned threshold values for mode switching [96]. More recently, meta-heuristic methods can also be encountered [97] or game theory [98], where the two power sources are seen as non-cooperative players. These strategies are however more popular when the optimization of the components size is included, the problem becoming a multi-objective optimization [99], [100].

Another common distinction is made between causal and non-causal methods. As the name indicates, a causal strategy relies only on current information, such as the instantaneous power demand and the current vehicle speed and, if necessary, past information, whereas a non-causal method uses predictive information, obtained in different ways:

- directly from navigation system [18] (speed limits, traffic signs and density) or GPS [19]
- constructed from the position of the lead vehicle [22] without the possibility of overtaking [17] or with this possibility [32]
- generated by a prediction model (Markov chain [101], neural networks, exponentially varying predictors; a comparison between these 3 techniques can be found in [102])
- combinations: road grade and speed limits modeled as a Markov chain, but traveling direction given by GPS and road profile by GIS [103]

The work done in the present thesis considers passenger cars, for a fixed architecture, with a focus on parallel configuration and the main goal is the fuel consumption reduction. A predictive model-based strategy is chosen, with real-time implementation potential. Traffic prediction is not explicitly handled, the preview information is considered available from navigation data.

5 Conclusions

This chapter presented a basic description of HEV i.e. main components and architecture types, as well as notions about the performance evaluation. The quasi-static modeling was also addressed, which is necessary to the understanding of the control-oriented model that will be next introduced. For the energy management problem, only an overview presentation was provided, which allowed the distinction of different optimization layers, control objectives, degrees of freedom and control algorithms. More details about predictive energy management will be included in Chapter 3.

Ce chapitre a présenté une description basique des véhicules hybrides i.e. les éléments principaux et les types d'architecture, ainsi que des notions sur l'évaluation de la performance. La modélisation quasi-statique a également été traitée, étant nécessaire pour la compréhension du modèle orienté contrôle qui sera présenté par la suite. Pour le problème de la gestion d'énergie, seulement une présentation générale a été fournie, qui a permis la distinction entre les différents couches d'optimisation, les objectives du contrôle, les dégrées de liberté et les algorithmes du contrôle. Plusieurs détails sur la gestion d'énergie prédictive seront inclus dans le troisième chapitre.

Chapter 2

Generic powertrain control-oriented model

Model-based control strategies have the advantage of handling multiple configurations for a given system, by means of parametrization. For an HEV, the energy management controller is often restricted to a specific architecture, i.e. for a certain transmission type and electric machine(s) position. The most encountered distinction is made with respect to the three hybrid architectures: series, parallel and series-parallel. This is mainly due to the differences concerning the degrees of freedom, but also to the physical features of each architecture that favor certain control strategies. Although a unified energy management approach can be hardly envisioned, a generic powertrain control-oriented model would offer a compact description that could be easily exploited by a model-based controller and its construction is the main objective of the present chapter.

The uppermost level provides an overview of the system's structure, whereas intermediate levels complete the description based on physical relationships. For a hybrid powertrain, the wheel torque includes information about the transmission, engine type and the electric machines positions, but also about exogenous inputs, such as slope. In our approach, under mild assumptions, general static expressions for the torque at different levels (wheel, gearbox, crankshaft) and for the speed of components are introduced. The proposed model is detailed for a parallel architecture, with the inclusion of the dual clutch transmission case, which is often neglected in the literature. The presence of two clutches in the powertrain model allows extensions for series and series-parallel architectures, except the cases with multi-mode configurations. These systems contain more than 2 clutches that allow different interconnections and therefore more flexibility. For their modeling, additional degrees of freedom are necessary and here, the adjustments are presented only for a range of encountered case-studies.

The fuel rate is usually provided as a lookup table of engine speed and torque, while for a model-based approach, an analytical expression is needed. A physical model being unnecessarily complex for a supervisory control, an approximation of the fuel map is instead used. In the literature, various consumption models can be encountered and Willans line emerges as a unified approach. However, it fails to cover all the operating range, especially for turbocharged SI engines. Here, a PWL approximation in torque is proposed, that can be applied to all engine types, for an appropriated partitioning.

Les stratégies de contrôle basées sur des modèles présentent l'avantage de gérer de configurations multiples pour un système donné, à travers une paramétrisation. Pour un véhicule hybride, la gestion d'énergie est souvent réduite à une architecture spécifique, pour un certain type de transmission et pour une position de la machine électrique. La plus répandue distinction se fait par rapport aux trois architectures hybrides: série, parallèle et série-parallèle. Ceci est notamment dû aux différences concernant les dégrées de liberté, mais aussi aux caractéristiques physiques de chaque architecture qui favorisent certaines stratégies de contrôle. Une approche unifiée pour la gestion d'énergie serait difficilement envisageable, mais un modèle générique, orienté contrôle pour le groupe moto-propulseur (GMP) offrirait une description compacte, qui pourrait facilement être exploitée par un contrôleur model-based *et sa construction sera l'objectif principal de ce chapitre.*

Le niveau supérieur offre une vision générale sur la structure du système, alors que des niveaux intermédiaires complètent la description basée sur des relations physiques. Pour un GMP hybride, le couple à la roue inclut des informations sur la transmission, le type du moteur et les positions des machines électriques, ainsi que sur des entrées exogènes, comme la pente. Dans notre approche, sous certaines hypothèses, des relations statiques générales pour le couple à des différents niveaux (roue, boîte, vilebrequin) et pour la vitesses des composantes sont introduites. Le modèle proposé est détaillé pour une architecture parallèle, avec l'inclusion de la transmission double embrayage, souvent négligée dans la littérature. La présence de deux embrayages dans la modèle permet des extensions pour les architectures série et série-parallèle, à l'exception des configurations multi-modes. Ces systèmes contiennent plus de deux embrayages qui permettent de différentes interconnections et par conséquent, plus de flexibilité. Pour leur modélisation, des dégrées de liberté supplémentaires sont nécessaires et dans ces travaux, des ajustements sont introduites seulement pour des études de cas présentes sur le marché.

La consommation de carburant est généralement fournie comme une cartographie en couple moteur et régime, mais pour une approche à la base de modèle une expression analytique est nécessaire. Un modèle physique étant inutilement complexe pour un contrôle au niveau superviseur, une approximation de la cartographie de consommation est en revanche utilisée. Dans la littérature, on peut rencontrer différents modèles de consommation et la courbe de Willans émerge comme une approche unifiée. Cependant, elle ne couvre pas toute la plage de fonctionnement, en particulier pour les moteurs essence turbo-chargés. Dans cette thèse, une approximation linéaire par morceaux en couple est proposée, qui peut être appliquée sur tous les types de moteurs, pour une partition appropriée.

1 State-of-the-art

As mentioned in the introduction, the energy management of HEV handles the power distribution between two propulsion elements. When the rotational speed is pre-imposed, either by the drive cycle standards, or calculated at a supervisory level, the problem is reduced to torque split. Therefore, at each sampling time, the wheel torque demand is calculated from the target speed, resistive forces and slope, and then, a controller decides the distribution of torque between the engine and the electric machine. The level where the repartition occurs is defined by the position of the electric machine (crankshaft, gearbox or wheel) and hence, from a control perspective it is useful to propose a model that covers a large class of configurations.

The first attempt toward a generalized model for an HEV powertrain is encountered in [27], where an approach based on energy flow was proposed. The components are classified into energy converters, energy transformers and energy storage elements. Scalability and composability are the main targeted properties of the model. The former allows an unique representation of elements that belong to the same class (ICE and EM, for instance), such that only a scaling or displacement factor needs to be defined for each element. The second property facilitates the generation of different systems, under acceptable topological rules. The generation of topologies can also be encountered in a recent publication [51], where a platform-based design under functional and cost constraints is used.

In [28] a more detailed energy-based approach was introduced: energetic macroscopic representation (EMR), that can represent different vehicle types: conventional, electric and hybrid. Unlike the aforementioned publication, the interconnection of the components is explicitly handled here. The engine and the electric machines are not characterized only by their losses and their admissible lower and upper torque, but also by their dynamic torque-speed relation. For a hybrid vehicle, the three architecture types are handled: series, parallel and series-parallel. Since the type of transmission and the position of the electric machine are not explicitly considered for a parallel configuration, the present study aims to extend this work by including them in the modeling.

Power-split architectures have witnessed a more elaborate modeling and topology-oriented work, as a result of their complexity, as witnessed by Toyota Prius success. Among the first publications which addressed this topic is [104], where an algorithm of automatic generation of mathematical models for power-split HEV with 2 planetary gear sets was proposed, with a possible utilization for sizing based on optimization. A later attempt was [105], where the bond graph method [1] was used for steady-state modeling of the most common power-split architectures, single and two-mode, likewise. The same approach was later extended to include shaft inertias and a clutch friction model [107].

Multi-mode configurations enjoyed a more detailed analysis in [108], where the possibility of clutches installation and their impact on fuel consumption was addressed. The case studies were fictitious architectures based on Toyota Prius and Chevrolet Volt, obtained by adding or removing clutches. The architectures considered here contain only one planetary gear set, but in [109] the multi-mode, multi-planetary gear set configurations were handled. More recent publications [52], [110] combine modeling and design optimization of multi-mode configurations, the two main objectives being fuel economy and acceleration performance.

In this chapter, a static model for torque and speed will be introduced, that can appropriately address the functioning of a dual-clutch transmission, which is often neglected in the literature. First, a parallel architecture is considered and subsequently it will be shown that the model allows extensions. In Chapter 4 of [3] the architectures based on planetary gear sets were treated and a very compact model was

[1] Bond graph is a graphical language that allows an energetic representation of dynamical systems [106]

proposed in the form:

$$\begin{bmatrix} T_f \\ T_g \end{bmatrix} = M^T \begin{bmatrix} T_{ice} \\ T_m \end{bmatrix}, \begin{bmatrix} \omega_{ice} \\ \omega_m \end{bmatrix} = M \begin{bmatrix} \omega_f \\ \omega_g \end{bmatrix}, \tag{2.1}$$

where *f, g, m* stand for *final driveline, generator* and *motor*, respectively. In what follows, it will be shown that our proposed model integrates and extends 2.1.

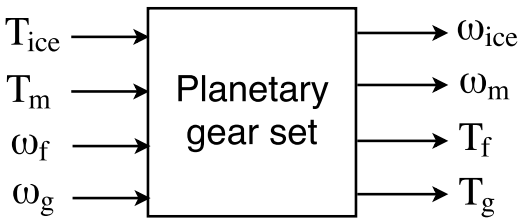

Fig. 2.1 – Input-output representation of a planetary gear set, [3]

2 Model synthesis

The proposed model aims to cover a large class of HEV architectures under the following viewpoints:

i. potential EM connected to the crankshaft (crk), primary shaft ($prim$), secondary shaft (sec) and to the wheel (w), as depicted in Fig. 2.3

ii. one electric storage element (battery, supercapacitor)

iii. one gear-shaft EM (an EM to the either odd or even shaft, but not both - for a dual-clutch transmission). The notation conventions will assign the shaft index *2* to the EM connected to the primary. If the EM is connected to the odd shaft, the indexes will be switched.

iv. gear and clutch dynamics are not considered

v. gear efficiency is considered only in the case of a CVT

Fig. 2.2 depicts a generic hybrid powertrain, with all possible connections of the EM, front and rear drive included. The EMs can be found alone or in combinations, usually by two: *crk* and *w*, *crk* and *prim/sec*. Their position is mostly dictated by design constraints (the occupied volume) and hybridization level; for instance, a full hybrid has an EM connected at the secondary shaft or wheel, whereas mild hybrids use smaller EMs that can be placed at crankshaft level or primary shaft. Moreover, to improve the performance (available power and drivability) or to respond to design constraints such as packaging, the EMs can be simultaneously found on the front and rear drive axle (e.g. Mitsubishi Outlander PHEV).

From an energy management perspective, the compact representation in Fig. 2.3 should be preferred, where the front drive includes all the EMs. A discrimination between front and rear drive is important for vehicle stability, this aspect being usually handled aside the energy management. Therefore, in what follows, the proposed model adopts the architecture from Fig. 2.3 and aims to span all its degrees of freedom within a generic parametrization.

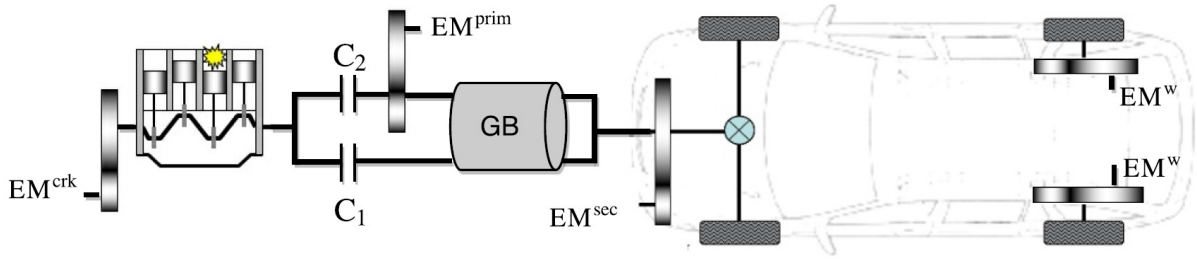

Fig. 2.2 – Generic representation of a hybrid powertrain; front and rear drive. *GB* - gearbox

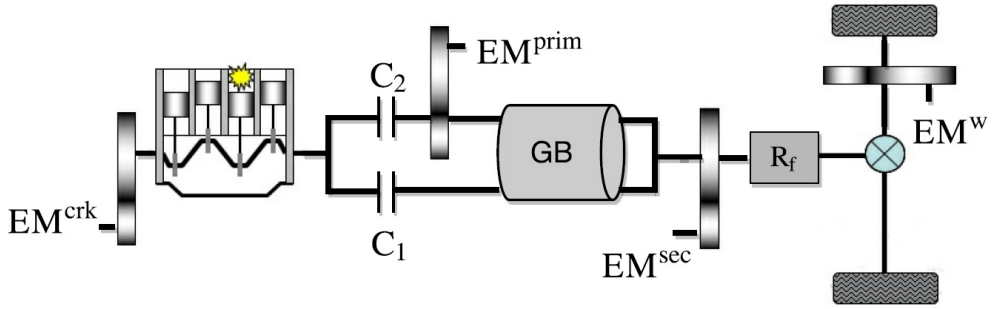

Fig. 2.3 – Generic representation of a hybrid powertrain, compact form; R_f - axle ratio

2.1 Powertrain configuration

From Fig. 2.3 three types of configuration with respect to clutch can be extracted:

1. one-clutch (independent of the EM position), as in Fig. 2.4, top
2. no clutch (independent of the EM position), as in Fig. 2.4, bottom
3. dual-clutch (particular case for EM connected to the primary shaft, as in Fig. 2.5)

A description of these configurations is given in Table 2.1. Let rat_{EM}^{pos} be the ratio between the EM and the shaft position (pos).This variable takes values in a subset $\overline{pos} \subseteq \{crk, prim, sec, w\}$ describing the positions of the EMs for a given hybrid architecture. Therefore, the absence of an EM to a certain shaft $pos \notin \overline{pos}$ is translated in mathematical terms by $rat_{EM}^{pos} = 0$.

Table 2.1 – Architectures description, EM connected to $\overline{pos}$; 0 - open clutch; 1 - closed clutch

Configuration	Description
1	$C_1 = 0, C_2 \in \{0, 1\}$
2	$C_1 = 0, C_2 = 1$
3	$C_1, C_2 \in \{0, 1\}, prim \in \overline{pos}$

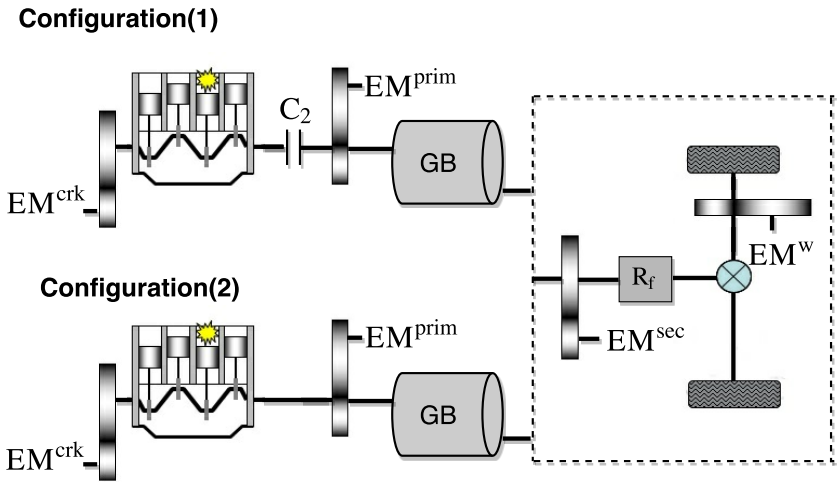

Fig. 2.4 – Configuration (1) and (2): schematic representation

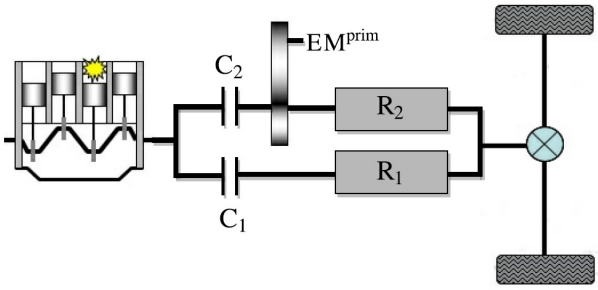

Fig. 2.5 – Configuration (3): hybrid DCT with EM connected to the primary shaft

2.2 Torque and rotational speed generic expressions

From an energy management point of view, the torque expression at the wheel level includes the complete information about a HEV architecture (EM position and gearbox). For a detailed characterization, the model has to describe the relationship between the components torque and the torque delivered at the 4 shafts (*crk, prim, sec, w*) and also the rotational speeds of the components, as functions of the vehicle speed *v* and the engine idle speed ω_{ICE}^{ctrl}. The expressions (2.2)-(2.12) are written for a parallel architecture with a dual-clutch transmission, defined by 2 shafts that contain the odd and even gear numbers, respectively, whose ratios are denoted as R_1 and R_2. As shown in Table 2.1, this configuration can be reduced to one clutch and no clutch transmissions with a proper parameterization. In the following sections it will be shown that the proposed model can also define series and series-parallel architectures, under certain assumptions.

$$T_w = r^w_{ICE} T_{ICE} + \sum_{pos} r^{w/pos}_{EM} T^{pos}_{EM} \text{ with } pos \in \{crk, prim, sec, w\} \tag{2.2}$$

$$\begin{bmatrix} T_{crk} \\ T_{prim} \\ T_{sec} \\ T_w \end{bmatrix} = A_T \begin{bmatrix} T_{ICE} \\ T^{crk}_{EM} \\ T^{prim}_{EM} \\ T^{sec}_{EM} \\ T^{w}_{EM} \end{bmatrix}, \begin{bmatrix} \omega_{ICE} \\ \omega^{crk}_{EM} \\ \omega^{prim}_{EM} \\ \omega^{sec}_{EM} \\ \omega^{w}_{EM} \end{bmatrix} = A_\omega \begin{bmatrix} v\frac{1}{R_w} \\ \omega^{ctrl}_{ICE} \end{bmatrix} \tag{2.3}$$

$$A_T = \begin{bmatrix} 1 & rat^{crk}_{EM} & 0 & 0 & 0 \\ r^{prim}_{ICE} & r^{prim/crk}_{EM} & rat^{prim}_{EM} & 0 & 0 \\ r^{sec}_{ICE} & r^{sec/crk}_{EM} & r^{sec/prim}_{EM} & rat^{sec}_{EM} & 0 \\ r^{w}_{ICE} & r^{w/crk}_{EM} & r^{w/prim}_{EM} & r^{w/sec}_{EM} & rat^{w}_{EM} \end{bmatrix} \tag{2.4}$$

$$A_\omega = \begin{bmatrix} r^w_{ICE} & 1 - C_1 - N_2 C_2 \\ r^{w/crk}_{EM} & rat^{crk}_{EM}\left(1 - C_1 - N_2 C_2\right) \\ r^{w/prim}_{EM} & rat^{prim}_{EM} C_2 \left(1 - C_1\right)\left(1 - N_2\right) \\ r^{w/sec}_{EM} & 0 \\ rat^{w}_{EM} & 0 \end{bmatrix} \tag{2.5}$$

$$r^{prim}_{ICE} = C_1 + C_2 - C_1 C_2 \tag{2.6}$$

$$r^{sec}_{ICE} = R_1 C_1 + R_2 C_2 \tag{2.7}$$

$$r^{w}_{ICE} = R_{f(R_1)} R_1 C_1 + R_{f(R_2)} R_2 C_2 \tag{2.8}$$

$$r^{pos/crk}_{EM} = r^{pos}_{ICE} rat^{crk}_{EM}, \quad pos \in \{prim, sec, w\} \tag{2.9}$$

$$r^{sec/prim}_{EM} = \left(R_1 C_1 C_2 + R_2\right) rat^{prim}_{EM} \tag{2.10}$$

$$r^{w/prim}_{EM} = R_{f(R_1 C_1 C_2 + R_2)} r^{sec/prim}_{EM} \tag{2.11}$$

$$r^{w/sec}_{EM} = R_{f(sec)} rat^{sec}_{EM}, \quad r^{w/w}_{EM} = rat^{w}_{EM} \tag{2.12}$$

where $N_2 = \min(R_2, 1)$, $R_{f(R_1)}$ denotes the axle ratio associated to gear with ratio R_1. Usually, the axle ratio is constant, but for dual-clutch transmissions two values might be admissible. It should be noted that for a CVT, the above formulation no longer presents a symmetry between speed and torque expressions due to the presence of gearbox losses, as defined in (1.4). For simplicity, the following analysis will consider exclusively the case where the gearbox losses are negligible.

The terms in matrices A_T and A_ω include products between the 2 clutches in order to appropriately integrate special use-cases of a DCT-based hybrid, where both clutches can be simultaneously closed. For instance, (2.6) defines the ratio between the torque at primary and at crankshaft r^{prim}_{ICE} and it is the arithmetical expression for the logical OR operation. The binary variable N_2 is introduced in order to correctly define the case when the even shaft is on neutral, while the clutch is closed, as in Fig. 2.6 and 2.7. Relation (2.10) finds a detailed characterization in Table 2.2, which is well defined for $rat^{prim}_{EM} \neq 0$. For a DCT, if both clutches are closed (Fig. 2.6, right) the EM will run at the same speed as the ICE, the operating point being defined by the vehicle speed and the gear engaged on the odd shaft (R_1).

The condition that ensures the engine is disconnected from the drive (its speed being therefore defined by ω^{ctrl}_{ICE}) is $C_1 + N_2 C_2 = 0$. This covers the cases where both clutches are open and also the charge at standstill mode ($C_1 = 0, C_2 = 1, N_2 = 0$). The latter is defined for an architecture with one EM to

Table 2.2 – EM to primary shaft, (2.10) description; configurations from Fig. 2.4 and 2.5

C_1	C_2	$r_{EM}^{sec/prim}/rat_{EM}^{prim}$	Configuration
0	0	R_2	1, 3
0	1	R_2	1, 2, 3
1	0	R_2	3
1	1	R_1	3

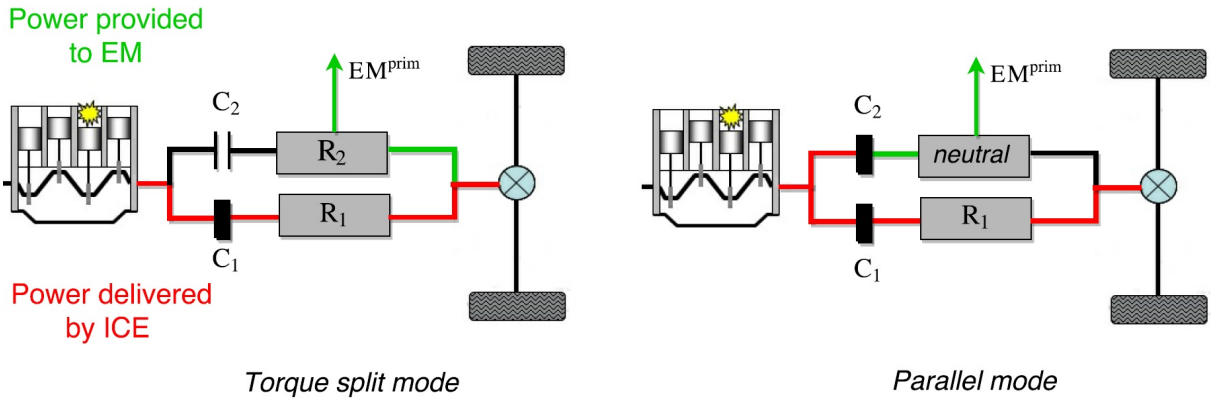

Fig. 2.6 – DCT-based hybrid: Charge during driving, torque split and parallel mode

the primary shaft and involves decoupling the engine from the wheel ($N_2 = 0$) and closing the clutch between the engine and the EM^{prim} ($C_2 = 1$), as in Fig. 2.7. In the case of a DCT, C_1 will be set to zero, according to assumption (iii) in section 2. Thus, the EM rotational speed will be equal to ω_{ICE}^{ctrl} and this is defined in the ω_{EM}^{prim} expression by the term $C_2\,(1 - C_1)\,(1 - N_2)$.

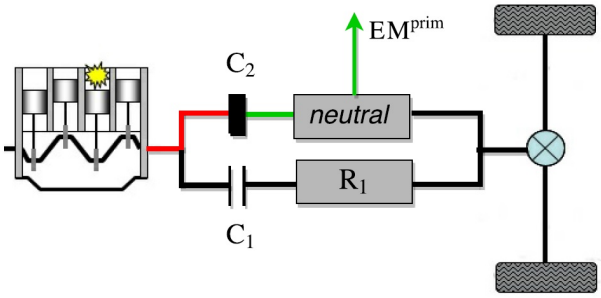

Fig. 2.7 – DCT-based hybrid, charge at standstill

2.3 Validation on different hybrid architectures

2.3.1 Unified modeling

For a parallel architecture the component torques are independent and the rotational speeds are directly determined from the vehicle speed (exception for special cases of disconnection from the drive-

line). For a series-parallel architecture, the torque of one EM is calculated from the torques of the other components torque, but its speed is an additional degree of freedom, as in (2.1). Let:

$$M^T = \begin{bmatrix} r_{ICE}^w & r_{EM}^{w/crk} & r_{EM}^{w/prim} & r_{EM}^{w/sec} & r_{EM}^w \\ r_{ICE}^g & r_{crk}^g & r_{prim}^g & r_{sec}^g & r_w^g \end{bmatrix}$$

$$T_{EM} = \begin{bmatrix} T_{EM}^{crk} & T_{EM}^{prim} & T_{EM}^{sec} & T_{EM}^w \end{bmatrix}^T$$

$$\omega_{EM} = \begin{bmatrix} \omega_{EM}^{crk} & \omega_{EM}^{prim} & \omega_{EM}^{sec} & \omega_{EM}^w \end{bmatrix}^T$$

With these notations, (2.3) can be reduced to a relation similar to (2.1):

$$\begin{bmatrix} T_w \\ T_g \end{bmatrix} = M^T \begin{bmatrix} T_{ICE} \\ T_{EM} \end{bmatrix}; \begin{bmatrix} \omega_{ICE} \\ \omega_{EM} \end{bmatrix} = M \begin{bmatrix} \frac{v}{R_w} \\ \omega_g \end{bmatrix} \tag{2.13}$$

This compact expression eliminates the shaft torque at intermediate levels and introduces the torque of an electric machine, needed for series and series-parallel architectures. It can be observed that for $\omega_g = \omega_{ICE}^{ctrl}$, the model describes a parallel hybrid architecture at the wheel level (T_g is not used).

An overview description of this model is given in Table 2.3 for the three hybrid architecture types. For a parallel architecture the clutches values depend on the transmission type, as will be next introduced. For the series case, the absence of a mechanical link between the engine and the wheels leads to $C_1 = C_2 = 0$. The EM that acts as a generator g, is assimilated to EM^{crk} and the ratio between the engine and the generator r_{ICE}^g is either a non-null constant or zero, if a clutch is present between the two components. The traction EM is EM^{prim}, which leaves the secondary shaft and the wheel without an EM, i.e. $r_{sec}^g = r_w^g = 0$. The series-parallel architectures have more complicated configurations and the table provides only a very brief characterization. Systems based on planetary gear sets do not contain clutches, except for the cases with multi-mode configurations, as will be detailed in the next subsection. Therefore, C_1, C_2 are not constrained and their values span all the configurations.

Table 2.3 – Application of model (2.13) for HEV architectures

Parallel	Series	Series-parallel
$C_1, C_2 \in \{0, 1\}$	$C_1 = C_2 = 0 \rightarrow r_{ICE}^w = 0$	$C_1, C_2 \in \{0, 1\}$
$\omega_g = \omega_{ICE}^{ctrl}$	$g = crk, \quad r_{crk}^g = 1$	$g = crk$
T_g not used	$r_{ICE}^g \in \{0, const\}$	$r_{ICE}^w \neq 0$
$M(:, 2) = A_\omega(:, 2)$	$r_{sec}^g = r_w^g = 0$	$r_{ICE}^g \neq 0$

2.3.2 Parallel architecture

For a parallel hybrid, the model can be simplified if the powertrain configuration is fixed. The static relations (2.3) are expressed for a DCT-based hybrid and they can be reduced to cases with one-clutch transmissions, if parameterized accordingly. No clutch transmissions are based on planetary gear sets, as in Fig. 1.5 and they correspond to power-split architectures, which will be next handled.

One clutch transmission configurations are characterized by the set of relations below, where only one electric machine connected to primary shaft is considered, for a straightforward visualization:

$$\begin{cases} C_1 = 0, C_2 \in \{0,1\} \\ R_2 - \text{all gear ratios} \\ \begin{bmatrix} T_{crk} \\ T_{prim} \\ T_{sec} \\ T_w \end{bmatrix} = \begin{bmatrix} 1 & 0 \\ C_2 & rat_{EM}^{prim} \\ R_2C_2 & R_2 rat_{EM}^{prim} \\ R_f R_2 C_2 & R_f R_2 rat_{EM}^{prim} \end{bmatrix} \begin{bmatrix} T_{ICE} \\ T_{EM}^{prim} \end{bmatrix} \\ \begin{bmatrix} \omega_{ICE} \\ \omega_{EM}^{prim} \end{bmatrix} = \begin{bmatrix} R_f R_2 C_2 & 1 - N_2 C_2 \\ R_f R_2 r_{EM}^{prim} & rat_{EM}^{prim} C_2 (1 - N_2) \end{bmatrix} \begin{bmatrix} \frac{v}{R_w} \\ \omega_{ICE}^{ctrl} \end{bmatrix} \end{cases} \tag{2.14}$$

Nissan's one-motor, two-clutch system depicted in Fig. 2.8 and 2.9 is a parallel architecture that contains two clutches: one wet multi-plate clutch between the EM and the gearbox (C_1) and one dry single-plate clutch between the ICE and the EM (C_2). The latter allows the engine to be disconnected from the driveline, whereas the former acts like a starting element, replacing the torque converter and it ensures an improvement in the drivability, by stabilizing the torque during engine start operation. Clutch C_1 plays therefore an important role during transient phases, when it is slipping, which is not covered by the proposed model, see assumption (iv). Hence, in spite of the presence of two clutches, this configuration does not correspond to a dual-clutch transmission case, but rather to a single-clutch, by assimilating C_1 into the gearbox. If $C_1 = 1$, then R_2 from the model above takes the value of the selected gear; if $C_1 = 0$, then $R_2 = 0$. Therefore, C_1 from this configuration is rather the binary value $N_2 = \min(R_2, 1)$ that defines whether the shaft is decoupled or not.

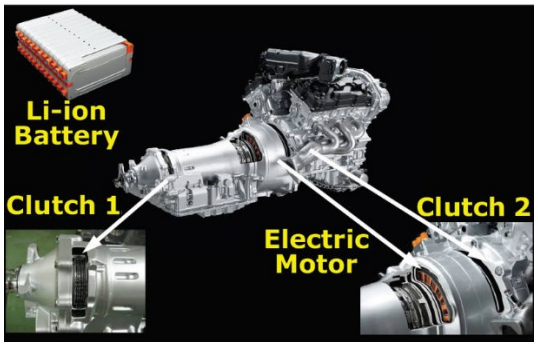

Fig. 2.8 – Nissan one motor, two-clutch system; parallel architecture

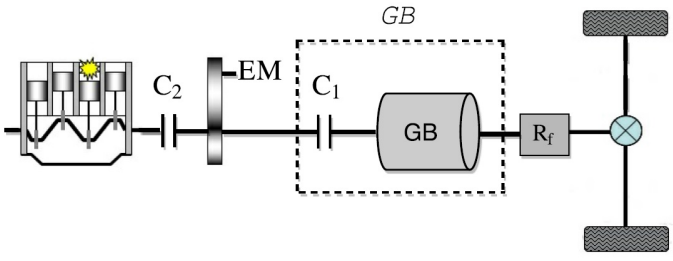

Fig. 2.9 – Nissan one motor, two-clutch system, schematic representation

2.3.3 Series architecture

The proposed model can also describe the series architecture, depicted in 2.10. In this case, the engine is decoupled from the drivetrain and there are two EM: one for traction (B), and another that acts as a generator (A), to convert the engine mechanical output into electricity. From Fig. 2.3 this implies that the traction motor is EM^{prim} and the generator- EM^{crk}.

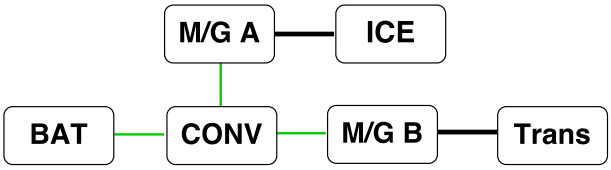

Fig. 2.10 – Series hybrid architecture; CONV - power converter, Trans - transmission; BAT - battery

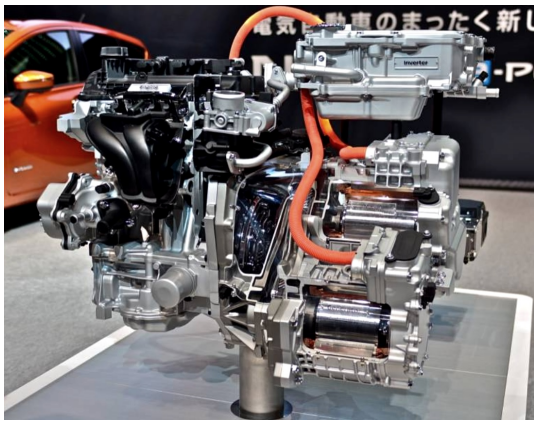

Fig. 2.11 – Nissan e-Power Range Extender architecture

Therefore, (2.16) can be detailed as below:

$$\begin{cases} C_1 = C_2 = 0 \\ r^g_{ICE} \in \{0, const\} \\ R_2 - \text{all gear ratios} \\ \begin{bmatrix} \omega_{ICE} \\ \omega_{M/GB} \end{bmatrix} = \begin{bmatrix} 0 & r^g_{ICE} \\ R_2 rat^{prim}_{EM} & rat^{prim}_{EM}(1-N_2) \end{bmatrix} \begin{bmatrix} R_f \frac{v}{R_w} \\ \omega_{M/GA} \end{bmatrix} \end{cases} \tag{2.15}$$

In a standard series architecture, $N_2 = 1$, which cancels the term that links the traction EM speed with the generator speed. This is also coherent with the third line from matrix A_ω defined in (2.5), because C_2 is set to zero. However, in multi-mode configurations, it is not always possible to have the two speeds decoupled, as it can be seen in Table 2.4, which defines the functional modes of GM Range Extender powertrain, depicted in Fig. 2.12. The above formulation models this architecture for $R_2 = 1 + \frac{1}{z}$, $rat^{prim}_{EM} = 1$ and N_2 is dependent on the selected mode, $N_2 \in \{1, R_2\}$.

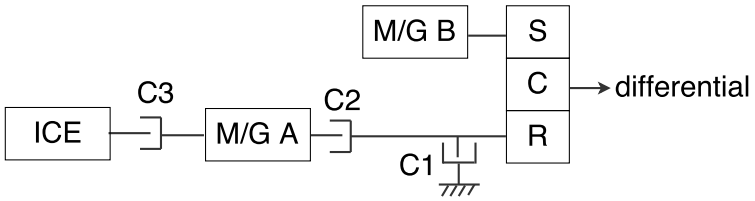

Fig. 2.12 – General Motors Range Extender (GM RE) hybrid powertrain with the 2ET50 transaxle [5]

Table 2.4 – Series architecture, GM RE case study; terms from (2.16)

Parameters / Mode	M_{11}	M_{12}	M_{21}	M_{22}
One-Motor EV $C_1 = 1, C_2 = C_3 = 0$	0	0	$1 + \frac{1}{z}$	0
Two-Motor EV $C_1 = 0, C_2 = 1, C_3 = 0$	0	0	$1 + \frac{1}{z}$	$-\frac{1}{z}$
Series One-Motor RE $C_1 = 1, C_2 = 0, C_3 = 1$	0	$const$	$1 + \frac{1}{z}$	0
Combined Two-Motor RE $C_1 = 0, C_2 = 1, C_3 = 1$	0	$const$	$1 + \frac{1}{z}$	$-\frac{1}{z}$

2.3.4 Series-parallel architecture

For series-parallel architectures only a generic description was provided in Table 2.3. It should be noted that such architectures exhibit an increased complexity for their transmissions, i.e. number of planetary gear sets (PGS) and their interconnection, as well as the potential presence of different clutches that allow a multi-mode functioning. A comprehensive description of these architectures can be found in [109], where it was shown, for instance, that a configuration with two planetary gear sets may contain up to 16 clutches. For a better understanding, in Fig. 2.13 three representative hybrid architectures based on PGS are provided:

(a) General Motors 2-mode hybrid powertrain with the 2MT70 transaxle (Saturn VUE)

(b) Toyota Hybrid System, first and second generation

(c) Lexus RX450h

Let M from (2.1) be defined as $M = \begin{bmatrix} M_{11} & M_{12} \\ M_{21} & M_{22} \end{bmatrix}$, $\omega_f = R_f \frac{v}{R_w}$ and $z = \frac{\omega_R - \omega_C}{\omega_C - \omega_S} = \frac{N_S}{N_R}$, where indexes R, S, C stand for *ring, carrier* and *sun*, respectively (see Fig. 1.4) and N_S, N_R - number of teeth. On each configuration, the B motor is the traction electric machine (connected to the driveshaft), whereas the A motor acts mainly as a generator and introduces an additional degree of freedom in the speed expressions. Relation (2.13) can then be written as:

$$\begin{bmatrix} \omega_{ICE} \\ \omega_{M/GB} \end{bmatrix} = \begin{bmatrix} M_{11} & M_{12} \\ M_{21} & M_{22} \end{bmatrix} \begin{bmatrix} R_f \frac{v}{R_w} \\ \omega_{M/GA} \end{bmatrix} \tag{2.16}$$

where the terms M_{ij} are defined in Table 2.5 for power-split architectures (a), (b) and (c).

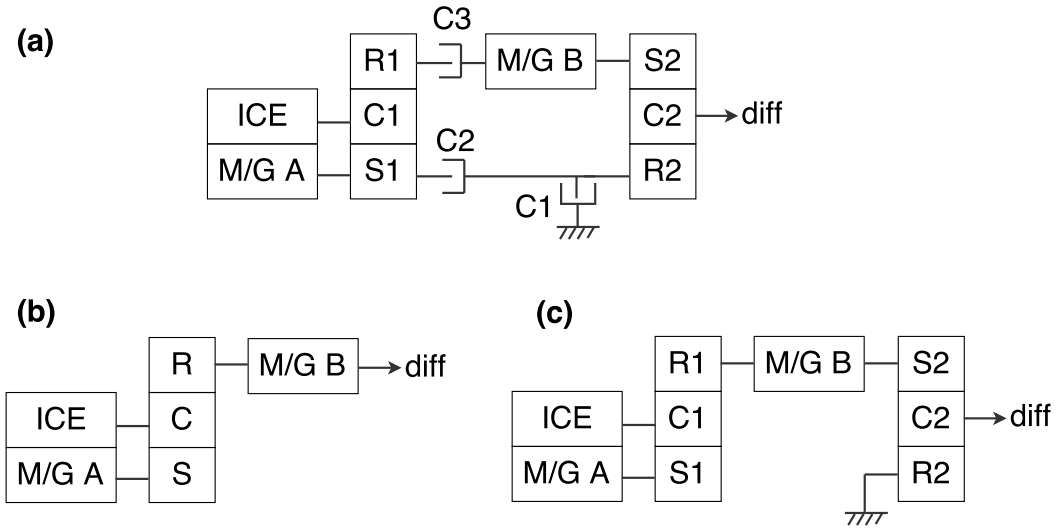

Fig. 2.13 – Three representative PGS-based hybrid architectures [5]; *diff* - differential

Table 2.5 – PGS-based hybrid architectures; terms from (2.16) for architectures in Fig. 2.13; z_1, z_2 are PGS ratios

Architecture \ Parameters		M_{11}	M_{12}	M_{21}	M_{22}
(a)	Mode 1 $C_1 = 1, C_2 = 0, C_3 = 1$	$\left(1 + \frac{1}{z_2}\right) \frac{1}{1+z_1}$	$\frac{z_1}{1+z_1}$	$1 + \frac{1}{z_2}$	0
	Mode 2 $C_1 = 0, C_2 = 1, C_3 = 0$	0	$\frac{z_1}{1+z_1}$	$1 + \frac{1}{z_2}$	$-\frac{1}{z_2}$
(b)		$\frac{1}{1+z}$	$\frac{z}{1+z}$	1	0
(c)		$\left(1 + \frac{1}{z_2}\right) \frac{1}{1+z_1}$	$\frac{z_1}{1+z_1}$	$1 + \frac{1}{z_2}$	0

Model (2.4)-(2.12) can also be used for these series-parallel architectures with a suitable parametrization. Relation (2.4) is detailed below, where only the EM connected to the secondary shaft was kept, which corresponds to M/G B, with the degree of freedom $\omega_{ice}^{ctrl} = \omega_{M/GA}$, as mentioned above.

$$\begin{bmatrix} \omega_{ICE} \\ \omega_{EM}^{sec} \end{bmatrix} = \begin{bmatrix} R_1 C_1 + R_2 C_2 & 1 - C_1 - N_2 C_2 \\ rat_{EM}^{sec} & 0 \end{bmatrix} \begin{bmatrix} R_f \frac{v}{R_w} \\ \omega_{M/GA} \end{bmatrix} \tag{2.17}$$

Configurations (b) and (c) correspond to the case with no clutch transmissions and they are well-defined for $C_1 = 0, C_2 = 1, N_2 = R_2$ and $rat_{EM}^{sec} = 1$. Here C_1 is not used and thus, set to zero, whereas C_2 is considered always closed and therefore, there is no need to check whether the shaft is decoupled from the wheel or not. Note that this decoupling feature imposes the use of an additional variable $N_2 = \min(R_2, 1)$, which was initially defined as a binary value. Here, a slight change is necessary in order to relax N_2 to take all the values of R_2, and thus provide a proper mathematical definition. From Table 2.5 and (2.17), for configuration (b) it can be extracted that

$$R_2 = \frac{1}{1+z}, \quad 1 - N_2 = 1 - \frac{1}{1+z}, \quad rat_{EM}^{sec} = 1 \tag{2.18}$$

Table 2.6 – PGS-based hybrid architectures; terms from (2.19)

Parameters / Architecture	R_2	final drive ratio	C_3
(a)	$\frac{1}{1+z_1}$	$R_f\left(1+\frac{1}{z_2}\right)$	{0,1}
(b)	$\frac{1}{1+z}$	R_f	1
(c)	$\frac{1}{1+z_1}$	$R_f\left(1+\frac{1}{z_2}\right)$	1

which validates the proposed parametrization. A similar relation can be written for configuration (c), but with one particularity: the presence of a second planetary gear set is included in the axle drive ratio, as detailed in Table 2.6.

Configuration (a) can be modeled in a similar way as (c) with an additional variable C_3 introduced in order to handle the two modes. Note also that for this case-study, C_1 and C_2 do no have the same significance as in Fig. 2.3, their use being related to multi-mode functioning.

A compacted expression, based on model (2.4)-(2.12), that describes the 3 series-parallel configurations, can therefore be written, with details provided by Table 2.6.

$$\begin{bmatrix} \omega_{ICE} \\ \omega_{M/GB} \end{bmatrix} = \begin{bmatrix} C_3 R_2 & 1-R_2 \\ 1 & -(1-C_3)\frac{1}{z_2} \end{bmatrix} \begin{bmatrix} R_f \frac{v}{R_w} \\ \omega_{M/GA} \end{bmatrix} \tag{2.19}$$

2.4 Fuel consumption approximation

As announced in the first chapter, the ultimate goal of the present thesis is to optimize the fuel gain for an HEV. Therefore, a consumption model is necessary and will be next introduced. Its development is based on the engine fuel consumption, which is provided as a nonlinear map in function of engine speed and torque, and allows its evaluation at each instant, for a measured speed and estimated torque. Depending on the type of application, several consumption models are conceivable, as summarized in [111]:

1. *white-box* models, based on engine physical processes (high fidelity, but very complex)
2. black-box models: engine-based (input data are engine torque and speed) and vehicle-based (different inputs are possible: vehicle speed, acceleration, road grade)
3. *gray-box* models, a synergy between *white-box* and *black-box*, which include some transient aspects, related to emissions or fuel consumption

For eco-driving or cruise control applications, a vehicle-based consumption model is generally used, whereas for supervisory powertrain control problems, such as energy management, an engine-based model is more suitable. Therefore, the scope of this section is to approximate the fuel map by an analytic expression in engine torque and speed.

The most common consumption model is Willans line [3], [112], [113] where a linear dependence with respect to power (P_{ice}) is introduced:

$$\dot{m}_f = \gamma_0\left(\omega_{ice}\right) + \gamma_1 P_{ice} \tag{2.20}$$

In the second chapter of [112] it is mentioned that this model is more suitable for a CI engine, because a SI shows a "fuel rate increase near maximum torque, which is typically related to an enriched fuel mixture commanded by the engine controller and meant to cool the valves". In [114] it is equally observed that an affine approximation in P_{ice} tends to underestimate the fuel rate at high loads for SI engines, due to enrichment. Therefore, for a SI engine, a quadratic expression in power would be more appropriate:

$$\dot{m}_f = \gamma_0\left(\omega_{ice}\right) + \gamma_1 P_{ice} + \gamma_2 P_{ice}^2 \tag{2.21}$$

as proposed in [22], too, but where a proportional term in vehicle speed was added. In [85] it is also stated that Willans line approximation is not appropriate for high speed, and therefore, a second-order term in speed is added.

In the literature, extensions of (2.20) are equally used: in [115] the slope γ_1 is piecewise constant; in [116] both coefficients γ_0 and γ_1 are expressed as 2^{nd} order polynomials in ω_{ice}. This is also the case for its quadratic counterpart: in [54], [117] a 2^{nd} order polynomial in torque was defined, with coefficients dependent on speed, but without an explicit definition, whereas in [118] the coefficients were detailed as:

$$\dot{m}_f = k_5 T_{ice}^2 + (k_4\omega_{ice} + k_3)T_{ice} + k_2\omega_{ice}^2 + k_1\omega_{ice} + k_0 \tag{2.22}$$

In addition to these attempts, more complicated consumption models can also be encountered: in [119], a ratio of polynomial expressions in torque and speed is used $\left(\frac{aT_{ice}\omega_{ice}+b\omega_{ice}c\omega_{ice}^3}{h+k\omega_{ice}+l\omega_{ice}^2}\right)$, which is deduced from a complex, vehicle speed-based model that represents an unified expression for the fuel rate of cruising and accelerating vehicle, introduced in [120]:

$$\dot{m}_f = \frac{F_d}{1+e^{\beta(\dot{v}+C)}} + e^{-\left(\frac{\dot{v}}{\sigma}\right)^2}(k_1 + k_2 v + k_3 v^3) + \frac{c_1 + c_2\dot{v}v}{1+e^{-\beta(\dot{v}-C)}}$$

where F_d is the consumption rate of decelerating vehicle (considered constant), c_1, c_2, k_1, k_2, k_3 are constants that appear in the approximation of the fuel rate for acceleration phases and cruising, respectively, whereas β and C define the suitable sigmoid functions and σ is the standard deviation of normal distribution. In [121] a 3^{rd} order polynomial in speed and torque $\left(\sum_{i=0}^{i=3}\sum_{j=0}^{j=3}\omega_{ice}^i T_{ice}^j\right)$ is used, whereas in [122] a 4^{th} order is proposed; in [123] a dynamical correction term is introduced, represented by engine torque variation, in order to correctly handle the transient fuel consumption.

Piecewise approximations are also used:

- in [124], a first order polynomial in ω_{ice}, divided in 10 partitions with respect to torque
- in [125] the engine map was divided into 18 subareas, for which a 2^{nd} order polynomial in speed and torque was defined

In [126], several low-degree polynomials in power and torque have been validated on engine dynamometer, chassis dynamometer and road tests measurements, respectively, with data coming from 15 different SI engines. None of the models has a cubic torque term, the stated argument being that they hardly bring an improvement in the approximation and they also "cause unnatural shape" in the brake specific fuel consumption. The 2 polynomials that yielded good results for all validation scenarios, with close performance one from another, are defined as:

$$\dot{m}_f = (k_8\omega_{ice}^2 + k_7\omega_{ice} + k_6)T_{ice}^2 + (k_5\omega_{ice}^2 + k_4\omega_{ice})T_{ice} + k_3\omega_{ice}^3 + k_2\omega_{ice}^2 + k_1\omega_{ice} \tag{2.23a}$$

$$\dot{m}_f = k_5 T_{ice}^2 + (k_4\omega_{ice} + k_3)T_{ice} + k_2\omega_{ice}^2 + k_1\omega_{ice} + k_0 \tag{2.23b}$$

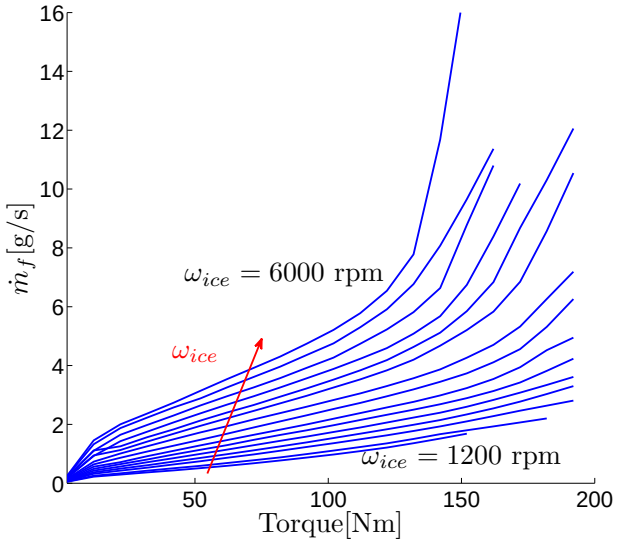

Fig. 2.14 – Fuel rate evolution with respect to engine torque, for different values of speed; turbocharged, 1.2 SI engine

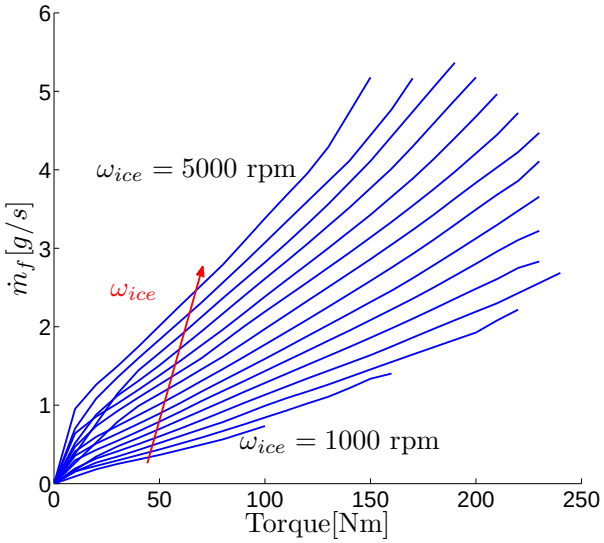

Fig. 2.15 – Fuel rate evolution with respect to engine torque, for different values of speed; turbocharged CI engine

In this work, the fuel maps for 2 engines are available: a turbocharged SI and CI engines, depicted in Fig. 2.14 and 2.15, as functions of engine torque, for different speed values.

It can be noticed that the CI engine shows a quasi-linear behavior in torque for all speed levels, whereas the SI exhibits a nonlinear tendency for high loads, starting with average speeds. In what follows, 3 polynomials are tested for curve fitting: first and second degree in torque, as well as second order in speed. Each of them represents a family of polynomials, with coefficients defined for a given engine speed (2.24a, 2.24b) or torque (2.24c).

$$\dot{m}_f = p_1(\omega_{ice})\, T_{ice} + p_0(\omega_{ice}) \tag{2.24a}$$

$$\dot{m}_f = p_2(\omega_{ice})\, T_{ice}^2 + p_1(\omega_{ice})\, T_{ice} + p_0(\omega_{ice}) \tag{2.24b}$$

$$\dot{m}_f = p_2(T_{ice})\, \omega_{ice}^2 + p_1(T_{ice})\, \omega_{ice} + p_0(T_{ice}) \tag{2.24c}$$

The accuracy of these approximations on the identification data is quantified in Table 2.7, where the root mean square error is presented.

Table 2.7 – RMSE (Root Mean Square Error) for different consumption approximations [g/s] and average $\overline{\dot{m}_f}$. Validation on identification data

Engine	$\overline{\dot{m}_f}$	(2.24a)	(2.24b)	**(2.24c)**
SI	2.67	0.75	0.5	**0.37**
CI	1.16	0.08	0.07	**0.06**

Note that for the CI engine, the difference between polynomials is insignificant and this can also be concluded from Fig. 2.15. A first order polynomial in torque can therefore be retained, which validates the aforementioned remarks about Willans line. For a SI engine, it can be seen from the results, as well as from Fig. 2.14, that a linear expression in torque is not suitable. The second order polynomial in speed (2.24c) is the most accurate, as shown in Table 2.8, too, where the validation was performed on different drive cycles. The torque dependence of polynomial parameters is depicted in Fig. 2.16 and it can be seen that it is highly nonlinear, but a piecewise linear approximation is feasible (see curves in red):

$$p_j^{(i)}(T_{ice}) = a_j^{(i)} T_{ice} + b_j^{(i)}, \quad j = 0 \dots 2 \tag{2.25}$$

with $i = 1 \dots N_{part}$ the index of the piecewise linear partition and N_{part} the number of partitions (for the specific case considered here: $N_{part} = 5$).

This approximation leads to a simplified version of (2.24c):

$$\dot{m}_f = \left(a_2^{(i)} \omega_{ice}^2 + a_1^{(i)} \omega_{ice} + a_0^{(i)}\right) T_{ice} + b_2^{(i)} \omega_{ice}^2 + b_1^{(i)} \omega_{ice} + b_0^{(i)} \tag{2.26}$$

Its accuracy was also evaluated on different drive cycles and quantified in Table 2.8. An improvement can be obtained either by increasing the number of partitions, or by performing the division directly on the fuel map (Fig. 2.14), that captures the changes in fuel rate slope with respect to torque. For instance, it can be noticed that the low torque region ($T_{ice} < 12$Nm) should be handled separately for both SI and CI engine and that a more frequent division is necessary for SI, for $T_{ice} > 120Nm$. Therefore, a family of PWL polynomials in torque can be obtained, similar to 2.24a, but calculated for a specific torque region i:

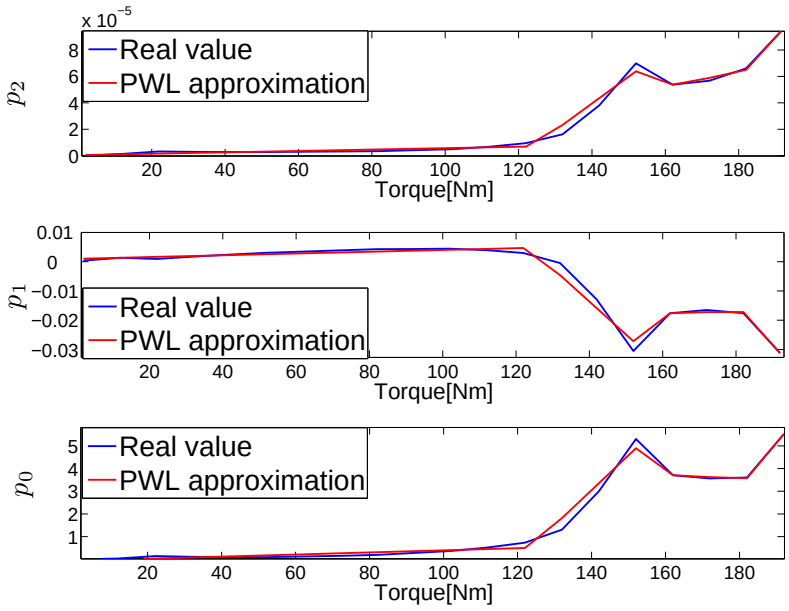

Fig. 2.16 – Torque dependence of polynomial parameters for (2.24c), SI engine case-study; real values and PWL approximation

$$\dot{m}_f = \alpha_i(\omega_{ice})T_{ice} + \beta_i(\omega_{ice}), \quad i = 1 \dots N_{part} \tag{2.27}$$

The granularity of the partition can be adapted in function of the engine type, with an increase from a CI (for which no more than 2 partitions are needed) to a turbocharged SI engine, which exhibits a more nonlinear behavior with respect to its normally aspired version, the proposed model being therefore generic. The approximation is depicted in Fig. 2.17 and its accuracy quantified in the last column of Table 2.8, where a significant improvement with respect to (2.26) can be observed.

Table 2.8 – RMSE for different consumption approximations [g/s] and average $\overline{\dot{m}_f}$. Validation on drive cycles

Drive cycle	$\overline{\dot{m}_f}$	(2.24a)	(2.24b)	(2.24c)	(2.26)	(2.27)
NEDC	0.816	0.0734	0.062	0.01	0.03	0.01
Artemis urban	0.97	0.062	0.053	0.027	0.042	0.012
FTP-75	0.9	0.071	0.058	0.017	0.04	0.01
Traffic Jam	0.6	0.061	0.038	0.007	0.03	0.015
Artemis road	1.1	0.077	0.062	0.06	0.072	0.008

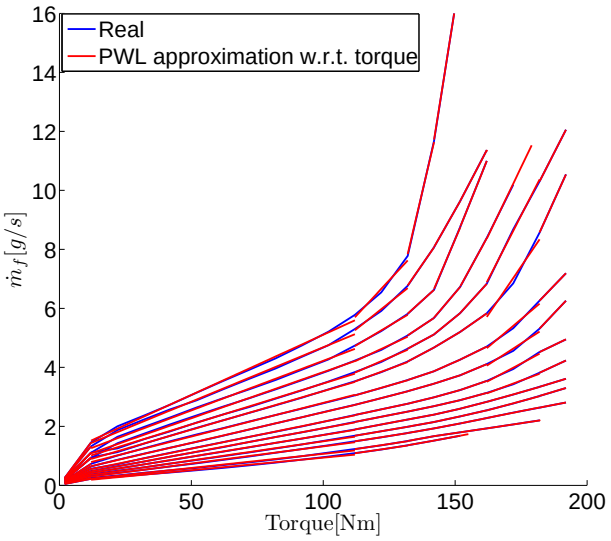

Fig. 2.17 – PWL approximation with respect to torque for the fuel rate of the SI engine

3 Conclusions

In this chapter, a control-oriented model for a variety of hybrid powertrains was proposed. The main contribution is the inclusion of dual-clutch transmission-based architectures, which are often neglected in the specialized literature. The static expressions of torque and speed were detailed for parallel HEV and extensions were provided for the remaining cases, with the exception of planetary gear set-based architectures, with multiple clutches, for which only some specific case-studies were handled. A generic fuel consumption approximation was also introduced, which will facilitate the formulation of the optimization problem that represents the next topic of this work.

Dans ce chapitre, un modèle orienté-contrôle pour une variété de GMP hybrides a été proposé. La contribution principale est la prise en compte des architectures basées sur des transmissions double-embrayage, qui sont souvent négligées dans la littérature spécialisée. Les expressions statiques du couple et de vitesse ont été détaillées pour un hybride parallèle et des extensions ont été fournies pour les cas restants, à l'exception des architectures basées sur des trains épicycloidaux, avec des contacts multiples, pour lesquelles seulement quelques études de cas spécifiques ont été adressées. Une approximation générique de la consommation de carburant a également été introduite, qui facilitera la formulation du problème d'optimisation qui représente le sujet suivant de cette thèse.

Chapter 3

Predictive energy management

In this chapter, an energy management strategy based on model predictive control is introduced. At a first stage, only the torque split between the combustion engine and the electric machine is addressed. The model introduced in the previous chapter will be used for prediction with the appropriate parametrizations. Besides the prediction model, one of the most challenging tasks in the MPC approach is the definition of the cost function (the control objective) to be minimized. Usually, it is expressed as a trade-off between the reduction of the setpoint tracking error and the command effort. Here, an energetic criterion needs to be conceived, that responds to the problem objectives i.e. the consumption minimization for a system with two energy sources.

The problem will be formulated in a standard quadratic programming form, for which dedicated solvers exist. Engine stop can provide a significant fuel gain, especially in urban driving, and therefore its inclusion is also considered. Hence, the MPC problem is extended with this functionality, but without introducing a binary decision variable (engine ON/OFF). This feature is remarkable as it avoids introducing a mixed-integer quadratic programming that demands adapting the solver and hence, introduces an additional degree of complexity. The engine stop-start strategy relies on a rule-based mechanism, which uses the command provided by the MPC.

Tuning is another major problem of model predictive control and it is often cumbersome. Moreover, for this specific problem, it is strongly dependent on drive cycle characteristics, which can be accurately foreseen for a limited time window. Here, the tuning is handled upstream of the MPC problem, by exploiting preview traffic data over a longer horizon than the one used by the MPC controller. The energy management problem is therefore structured as a two-layer predictive strategy.

In addition, the potential of free wheeling is analyzed and unlike previous work, it is addressed in an analytical manner. This functionality involves no pedal pressing and it usually concerns constant speed phases on highway. Here, the problem is extended to time-varying speed phases. The strategy evaluates the time-wise speed deviation between the reference and the free wheeling and it decides whether the solution is acceptable or not for a given coasting initiation and deactivation time.

Dans ce chapitre, une stratégie de gestion d'énergie basée sur le model predictive control *est introduite. Dans une première étape, seulement la distribution de couple entre le moteur et la machine électrique est adressé. Le modèle introduit dans le chapitre précédent sera employé pour la prédiction avec les paramétrisations appropriées. En dehors du modèle de prédiction, un des éléments les plus problématiques est la définition de la fonction coût (l'objectif) à minimiser. Traditionnellement, elle est exprimée comme un compromis entre la réduction de l'erreur de suivie de consigne et l'effort de commande. Dans ce travail, un critère énergétique doit être introduit, qui répond aux objectifs du problème i.e. la minimisation de la consommation pour un système avec deux sources d'énergie.*

Le problème sera formulé sous une forme quadratique standard, pour laquelle des solveurs dédiés existent. L'arrêt moteur peut apporter un gain signifiant, surtout en conduite urbaine, et par conséquent son inclusion est également considérée. Le problème MPC est donc étendu avec cette fonctionnalité, mais sans l'introduction d'une variable de décision binaire (moteur ON/OFF). Cette approche est remarquable car elle évite l'emploi d'une programmation quadratique mixed-integer *qui demande l'adaptation du solveur et qui, par conséquent, rajoute un dégrée de complexité. La stratégie d'arrêt moteur s'appuie sur un mécanisme* rule-based*, qui utilise la commande fournie par le MPC.*

La calibration est un autre problème majeur du MPC, souvent lourd. En outre, pour le problème considéré, elle est fortement dépendante des caractéristiques du cycle de conduite, qui peut être prédit pour un horizon limité. La calibration est traitée ici au niveau au dessus du MPC, en exploitant les informations du trafic sur un plus long horizon que celui utilisé par le contrôleur MPC. Le problème de la gestion d'énergie est donc structurée en deux couches.

En outre, le potentiel du free wheeling *est analysé et à la différence des travaux précédents, il est adressé sous une forme analytique. Cette fonctionnalité implique l'absence d'appui pédale et elle concerne notamment les phases de vitesses constante sur l'autoroute. Dans cette thèse, le problème est étendu pour les phases de vitesse variantes dans le temps. La stratégie évalue la déviation entre la vitesse de consigne et celle en roulage libre et décide si la solution est acceptable pour une initiation et désactivation du* coasting *données.*

1 State-of-the-art

In the first chapter an overview presentation of the energy management system for hybrid vehicles was introduced, aiming to present all the possible objectives and degrees of freedom, as well as the potential available inputs and the targeted case studies (vehicle and configuration type). Here, a more detailed characterization will be provided, focused on dynamical aspects with the ultimate goal of developing model-based control strategies.

Energy management strategies are expected to attain the objectives in real-driving conditions and thus, to integrate feedback from the system and to be real-time implementable. From a control perspective, this problem arises many challenges, due to a number of uncertainties such as trip characteristics (speed, slope), driver behavior (especially in change-of-mind situations), traffic status (jams, detours). Some of the elements are potentially predictable over a certain horizon, whereas others (driver's change-of-mind) cannot be anticipated. Usually, the first stage in the performance evaluation is to determine the maximum potential of the system to reduce the fuel consumption for regulated drive cycles. This implies finding offline the global optimum under the assumption that the drive cycle is entirely known and keep this result as the reference value.

The best candidate for this problem is the Dynamic programming (DP) [15], a method based on Bellman's optimality principle, which can be stated as follows [127]: "An optimal control policy has the property that whatever the initial state and initial decisions are, the remaining decisions must constitute an optimal policy with regard to the state resulting from the first decisions". The input and state variables are discretized at a representative step for the desired precision and at each instant a cost-to-go function is computed. The computational burden and the memory increase linearly with respect to grid size, but exponentially with respect to number of states, which considerably limits the potential for its use in real-time applications, its results remaining generally at the level of a benchmark solution [128], [91], [103]. There is however a possibility to integrate this solution in real-time, but only for one state variable and a short-term horizon, to numerically solve optimization problems under constraints as in [73], [32] or [102]. A description of this method can be found in [129] and details about its implementation in Matlab, on a HEV case study, is presented in [130].

Pontryagin's Minimum Principle (PMP) is another candidate for solving optimal control problems, which gives necessary conditions of optimality. If the control problem admits one solution, then these conditions are satisfied [131].

Given a system

$$\dot{x} = f(x, u), \quad x(0) = x_0 \tag{3.1}$$

a performance index over a time slot can be written as:

$$J(x_0, u) = \int_{t_0}^{t_f} L(x(t), u(t))\, dt \tag{3.2}$$

where $L(\cdot)$ denotes the quantity to be minimized. The Hamiltonian can be therefore constructed as:

$$H(x, u, \lambda) = L(x, u) + \lambda f(x, u) \tag{3.3}$$

where λ represents the co-state or the adjoint state (the variable t has been omitted for an easier reading). Then PMP states that the following necessary optimality conditions [1] are verified by the optimal control

[1] If state constraints are active, the co-state will exhibit discontinuities

$u^* \in \mathcal{U}$ [132]:

$$\dot{x} = \frac{\partial H}{\partial \lambda}(x, u, \lambda) \tag{3.4a}$$

$$\dot{\lambda} = -\frac{\partial H}{\partial x}(x, u, \lambda) \tag{3.4b}$$

$$u^* = \arg\min_{u \in \mathcal{U}} H(x, u, \lambda) \tag{3.4c}$$

For the energy management problem, the quantity to be minimized is the fuel consumption, whereas the state variable is the battery SOC. Therefore $L(x(t), u(t))$ is defined as:

$$L\left(u(t)\right) = \dot{m}_f\left(\omega_{ice}(t), T_{ice}(t)\right) \tag{3.5}$$

The cost function not being dependent on the state x, a simplified expression can be written for the adjoint state dynamics (3.4b):

$$\dot{\lambda} = \frac{\partial f(x, u)}{\partial x} \tag{3.6}$$

where $f(x, u)$ can be derived from the dynamics of the state of charge (1.11):

$$\dot{SOC} = -\frac{OCV((SOC)) - \sqrt{OCV((SOC))^2 - 4R((SOC))P_{bat}}}{2R((SOC))Q_{max}}$$

For a charge sustaining operation it can be assumed that the battery parameters OCV and R do not vary significantly w.r.t. SOC. Therefore, the function f does not depend on the state x and as a result, for a given drive cycle the assumption $\dot{\lambda} = 0$ i.e. $\lambda = constant$ is not restrictive [3], [26].

For each drive cycle there is a constant co-state, which can be determined offline, that ensures the optimality of the solution, as detailed in [131] and explained in Fig. 3.1. Therefore PMP is sometimes preferred to DP, due to its considerably faster implementation. The similarity in terms of performance between DP and PMP is also stated in [133].

The online version of PMP solution and the most popular energy management method is the ECMS (*Equivalent Consumption Minimization Strategy*) [25], [134], [26]. Among the first papers that introduced this strategy is [24], where the battery is seen as an energy buffer, that can be temporarily used. Each electrochemical consumption corresponds to an equivalent fuel consumption, hence the name of the method. The cost function to be minimized is formulated based on PMP, but with a physical interpretation for the terms appearing in the Hamiltonian (3.3):

$$\begin{aligned} H(t, u(t), \lambda(t)) &= P_f(t, u(t)) + \lambda(t) P_e(t, u(t)) \\ P_f(t, u(t) &= H_{LV} \dot{m}_f(t, u(t)) \\ P_e(t, u(t)) &= -\dot{SOC}(t, u(t)) OCV(t) \end{aligned} \tag{3.7}$$

where P_f is the fuel power, H_{LV} is the lower heating value of the fuel, P_e is the electrochemical power and the control variable is usually the engine torque $u = T_{ice}$. Therefore, the cost function is expressed as a weighted sum of two physical powers, the co-state $\lambda(t)$ being often referred to as the equivalence factor. The ECMS being exclusively oriented toward online implementation, the value of the tuning factor λ can no longer be constant, as is the case for its offline counterpart, PMP-based. The essence of the ECMS relies on the tuning procedure, for which several solutions have been proposed over the years:

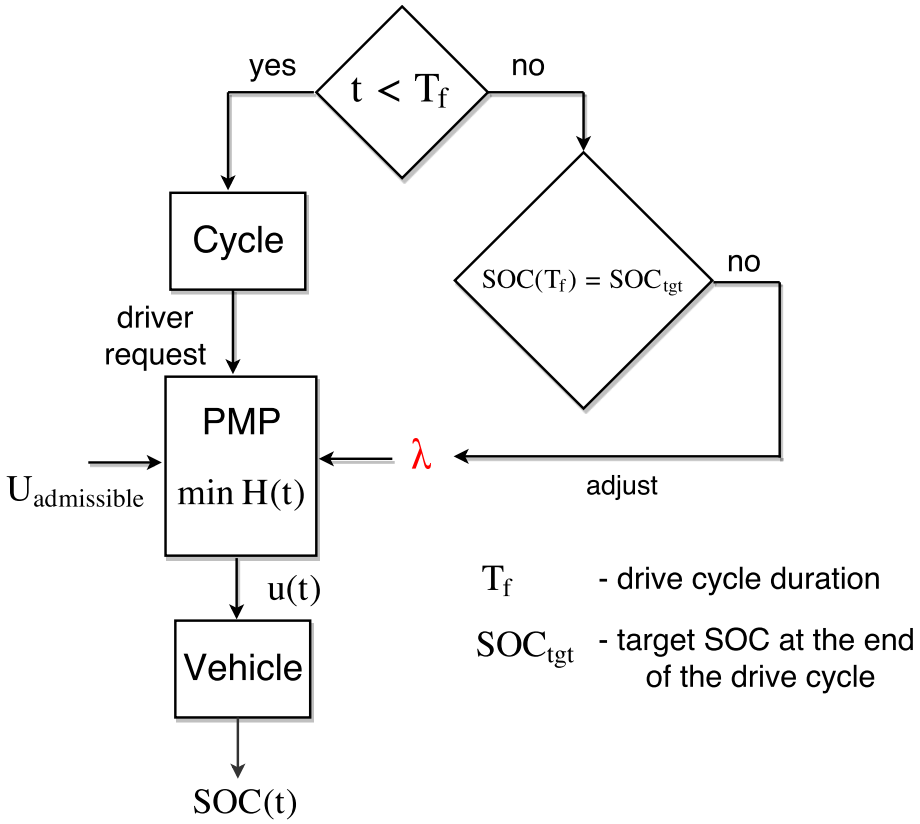

Fig. 3.1 – Schematic representation of PMP implementation, with the equivalence factor λ kept constant *a priori* during the entire drive cycle; if at the end of the drive cycle the SOC is different from the target, then an adjustment of the λ value is necessary; $U_{admissible}$ is a vector with admissible inputs for which the Hamiltonian H is evaluated

- an average efficiency-based method [24], which has the advantage of simplicity, but the disadvantage of lacking a SOC feedback from real-time evolution
- a constant term plus a PI-like controller with respect to the target SOC, which is constant and equal to the initial value [128], [135]:

$$\lambda(t) = \lambda_0 + k_p \left(SOC_0 - SOC(t)\right) + k_i \int_0^t \left(SOC_0 - SOC(\tau)\right) d\tau \tag{3.8}$$

  or just a proportional controller [136], with a variable SOC setpoint, which includes the energy potentially recovered during regenerative braking. A nonlinear adaptation of tuning factors is also possible: in [137] a tangent-like adaptation w.r.t. SOC is proposed, the goal being to slightly adjust the equivalence factor for small variations of SOC around the reference value, but to strongly penalize large variations
- adaptation based on driving conditions identification (based on past and predicted data) method referred to as Adaptive-ECMS [138]
- binary search such that SOC has a certain evolution at the end of a prediction horizon [139]

More details about these tuning strategies can be found in [140], [141] and Chapter 7 from [3].

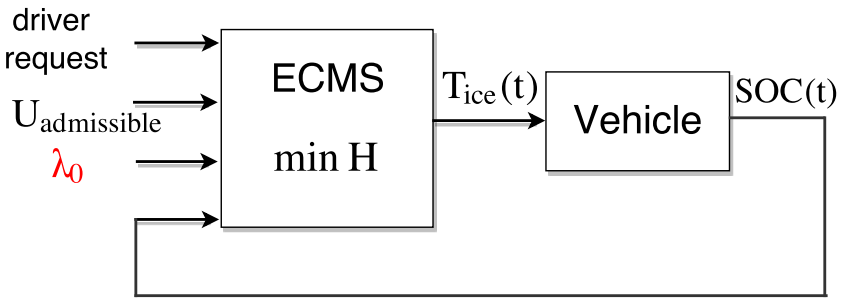

Fig. 3.2 – Schematic representation of ECMS implementation, with the equivalence factor λ adapted with respect to SOC; $U_{admissible}$ is a vector with admissible inputs for which the Hamiltonian (3.7) is evaluated. The output of the ECMS is the torque of the ICE.

Moreover, ECMS can be extended to handle emissions reduction, as in [59], [12], [142], [88] or battery thermal management [14], by introducing additional corresponding co-states. ECMS can be implemented either by evaluating the Hamiltonian for a set of admissible inputs and selecting the value that corresponds to the minimum, as in Fig. 3.2, or through lookup tables, constructed from offline calculations. They usually receive as inputs the driver demand, vehicle speed, SOC and the equivalence factor [37].

As summarized in the first chapter, current technologies allow to foresee different road elements over a certain distance, which can be exploited to reconstruct the future reference speed, sometimes in conjunction with a driver behavior model [64], [18]. This availability of upcoming trip information encourages the orientation toward finite-time moving horizon control structures. One of the most encountered predictive control method is Model Predictive Control (MPC), which will be introduced in the next subsection. It is an optimization-based control strategy under constraints, which calculates a sequence of commands that minimizes a cost function over a prediction horizon. Only the first command is applied to the system, combining therefore the open-loop optimal solution with feedback.

Among the first papers that exploited telemetry data for the torque split problem is [16], where the vehicle speed and wheel torque demand are estimated for a preview horizon between 250m and 3000m. This data is next introduced in a nonlinear MPC formulation that minimizes the fuel consumption over a future feasible horizon. The problem is solved using DP, for which some simplifications were made in order to make a real-time implementation possible: for instance, the grid was more finely discretized in the neighboring area of the current time and more roughly in the far regions, as a result of the receding horizon concept. In [17] information about the front vehicle is exploited, with a maximum headway of 400m, in order to correctly induce a deceleration that allows a maximum energy recovery. The speed profile is calculated at a supervisory level with DP and the torque split problem is handled with ECMS. In [32] the problem is formulated as a co-optimization of the speed profile and the torque split, into an MPC framework. The cost function is similar to (3.7), where a proportional SOC corrector was used for λ adaptation. A very simplified linear SOC model was used, but valid under the assumption that SOC variations are of only $\pm 10\%$. Constraints are imposed on vehicle speed and acceleration, and the problem was solved with a Sequential Quadratic Programming (SQP).

Due to its ability to cope with constraints, MPC gradually became in the last years an attractive solution for the energy management problem, in its stochastic or deterministic form. The former uses a stochastic model for the uncertainties of the predicted data: [101], [64], [121] and [143] use a Markov

chain to model the driver behavior and calculating therefore the wheel power demand, whereas in [103], Markov chains are used for the prediction of the road grade.

In the present work, it is assumed that the vehicle speed can be accurately predicted over a horizon up to 2 minutes, which will allow to estimate the wheel torque demand. Traffic forecast techniques are out of the scope of this work and therefore, no further information is provided regarding data acquisition.

The PHEV case is usually handled separately from the others HEV. In a tank-to-wheel analysis, the goal is to deplete the battery by the end of the trip, if this coincides with a charging point. If the trip distance is longer than the all-electric range, than a close-to-optimal solution is a linear SOC reference trajectory w.r.t distance, as in [144]. However, adjustments must be performed in order to appropriately accommodate different road characteristics. In [81] the considered road presents important elevation changes and the available potential energy is interpreted as an extension of the all-electric range. In [11], it is mentioned that for speed profiles with inconsistent driving pattern, i.e. that contain segments of very high and low power, the depletion rate is no longer constant, but rather piecewise constant as detailed in [82], where the trip is divided into several domains that verify a certain pattern. The same idea can be found in [83], with an improvement related to hilly subsections, for which a linear discharge with respect to energy, rather than distance, is introduced. One challenging problem is therefore long-term traffic prediction that allows a pattern-based division of the trip [145], [146]. It should be noticed that from a client-cost perspective, it can be more appropriate to explicitly consider the price of grid electricity and of fuel in the optimization problem. In [147] a range-extender with plug-in is tackled and it is considered that the engine is not owned by the user, but only rented when needed.

In the absence of an external charging, the battery should not be depleted by the end of the drive cycle, because it would have to be recharged later, via the engine, which involves an additional fuel consumption. For this type of hybrid, it is therefore important to maintain the final state-of-charge between certain limits and this framework will be adopted in the present thesis. In order to correctly evaluate the performance, it is required in simulation that final state-of-charge value must equal the initial one. The goal is twofold: a fair comparison with the consumption of a conventional vehicle and between different control strategies for a given hybrid vehicle.

As already announced, the torque split problem will be addressed in an MPC framework and before the problem formulation, a brief presentation of the MPC method will be next introduced.

2 Model predictive control-based torque split

2.1 MPC: an overview

Model Predictive Control is a relatively recent control technique that emerged in the late 70s, with a first application in the chemical industry. It is especially oriented toward problems of setpoint tracking where the anticipation of the system evolution subject to future commands improves the control performance. The setpoint can be constant or generated by a model. Traditionally, the goal is to minimize the tracking error and the command effort, under state and command constraints. However, in the absence of a setpoint tracking, MPC optimizes an energetic criterion under constraints, in which case it is referred to as Economic MPC [148]. MPC relies mostly on the following elements [149]:

- prediction of the system output over an horizon N_p, based on a mathematical model of the dynamical process
- calculation of a sequence of future commands of length N_c that minimize a cost function under constraints over a finite horizon

- application of only the first value of this optimal sequence to the system. At the next time step, new measurements are available and the procedure is repeated, in a receding horizon manner.

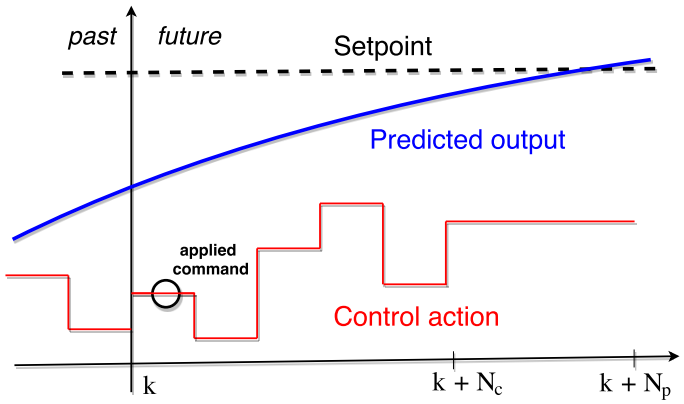

Fig. 3.3 – MPC principle; k is the current time index, N_c the control horizon and N_p the prediction horizon

Calculating a sequence of commands and using only the first value may seem computationally expensive, without an explicit performance improvement. The purpose is to combine open-loop optimal control with feedback from the system; simultaneous calculation of a block of optimization variables, instead of just one element, implies that in the calculation of the each element there is an anticipation of its effect over the considered horizon. If the entire block of commands is applied to the system, no feedback is incorporated and thus, model inaccuracies or unpredicted phenomena are not appropriately handled.

MPC was mostly used during the '80s and '90s for systems with rather slow dynamics, that can be approximated by linear models, but in the last 20 years it showed an expansion toward plants with fast dynamics, with nonlinear prediction models [150] or even hybrid systems [151]. In this case, MPC is referred to as *Nonlinear* and *Hybrid* MPC, respectively, due to the nature of the prediction model. Linear models can provide good results for an evolution of the system around the operating point, where the model is valid. Moreover, they are generally used in conjunction with a quadratic cost function, under linear constraints, leading to a convex optimization problem, for which efficient solvers exist. In what follows, MPC formulation will be presented under its standard, linear form. For its nonlinear counterpart, details can be found in [152].

In practice, there are several ways to enforce asymptotic stability, with a detailed review in [153]. The most common is the introduction of a terminal cost function; the approach is inspired from the infinite-time optimal control of unconstrained linear systems and it yields to adding in the cost function J from (3.26) a term usually expressed as $\frac{1}{2}y^T P_N y$, with $P_N > 0$ obtained from the Riccatti equation in reverse time and accounts for a control Lyapunov function in a neighborhood of the equilibrium point. For constrained and nonlinear systems, the stability can be achieved in conjunction with a final state confinement in a given compact set, which enjoys controlled positive invariance properties. The convergence and stability are implicitly handled by the final cost or a large enough prediction horizon. Both approaches intend to transform the optimal cost function in a control Lyapunov function.

Constraints handling represents a major advantage of MPC, but if not satisfied, they can lead to infeasibility. A solution to avoid this problem is to soften the constraints, i.e. to allow small violations,

but with a penalty in the cost function. For a given cost function $J(x,u)$, with a relaxed constraint on the control variable, this can be written as:

$$\min_{u,\epsilon} \quad J(x,u) + \rho\epsilon^2 \tag{3.9}$$

$$\text{s.t. } u_{min} - \epsilon \leq u \leq u_{max} + \epsilon \tag{3.10}$$

where ϵ is referred to as *slack variable*, whose value in case of constraints violation is highly penalized by $\rho > 0$.

To sum up, MPC relies on the following elements:

- a prediction model (linear, linear time-varying or nonlinear)
- a cost function with associated constraints, that incorporates the control objectives and considers the measurements and actuators availability
- a solver that allows a real-time implementation

In what follows, before proceeding with the presentation of the standard MPC form for energy management, the prediction model will be first introduced, followed by the cost function definition.

2.2 Prediction model

As mentioned in the first chapter, the energy management is a complex problem that can handle multiple objectives, through different degrees of freedom. Here, the torque split problem is mainly addressed and the only dynamics considered are related to the evolution of the battery state-of-charge, given by the nonlinear model from (1.11). These choices were dictated by the following assumptions:

1. the driver behavior is considered into a backward framework (see Section 3), i.e. a speed profile is pre-imposed, which generates a power reference for the driveline. Here, the speed tracking is handled at an upper level and assuming the speed known in advance for a certain horizon, the wheel torque can be calculated as in (1.2), given the vehicle parameters.

2. from the previous assumption and relation (2.2) it can be concluded that the real time decision on the engine torque T_{ice} can be considered as the unique control variable. The contribution of the electrical path is straightforwardly deduced from (2.2) i.e. $\sum_{pos} r_{em}^{w/pos} T_{em}^{pos} = T_w - r_{ice}^{w} T_{ice}$. In the case with several electric machines, the torque distribution between them relies exclusively on the static efficiency.

3. the gearshift is handled separately from the torque split and therefore, the gear numbers are set as inputs for the energy management problem, even for an automatic transmission. The optimization of the engine operating point can significantly reduce the consumption, but it is subject to NVH (Noise, Vibration and Harmonics) requirements, drivability constraints such as avoidance of frequent gearshifts or of rapid shifting back and forth, phenomenon called *hunting* [10], but also safety: a fuel-optimal solution is to upshift as much as possible, but this reduces the torque margin, hindering the reactivity possibilities in case of change-of-mind situations. The drawback is that the simultaneous optimization of the torque split and gearshift will significantly increase the computational burden due to the addition of a control variable (usually discrete) and to the formulation of constraints. The latter depend on the operating point that would need in this case to be

also optimized, making therefore their formulation over-complicated for the established objective. To summarize, physical and computational constraints outsource the gearshift strategy without a significant sacrifice of the fuel gain.

The state dynamics $x = SOC$ (1.11) can be detailed as below, where $u = T_{ice}$ and the electric torque T_{em} was expressed based on the static relation (2.2):

$$\dot{x} = -\frac{OCV(x) - \sqrt{OCV(x)^2 - 4R(x)\left(\frac{\pi}{30}\omega_{em}\frac{T_w - r^w_{ice}u}{r^w_{em}} + loss\left(\omega_{em}, \frac{T_w - r^w_{ice}u}{r^w_{em}}\right)\right)}}{2R(x)Q_{max}} \tag{3.11}$$

A nonlinear prediction model raises further difficulties in formulating the control problem and here, a linearization at the operating point (x_0, u_0) is introduced for $\dot{x} = f(x, u)$:

$$\dot{x} \approx f(x_0, u_0) + \left.\frac{\partial f}{\partial x}\right|_{x=x_0}(x - x_0) + \left.\frac{\partial f}{\partial u}\right|_{u=u_0}(u - u_0) \tag{3.12}$$

It is assumed, based on the high sampling rated and the battery time constants, that the battery parameters OCV and R do not vary significantly during the prediction and therefore $\frac{\partial f}{\partial x} = 0$. With this simplification and after discretization with sampling T_s at current engine torque u_{k0}, the linearized model becomes:

$$\frac{x_{k+1} - x_k}{T_s} = f(x_0, u_0) + \left.\frac{\partial f}{\partial u}\right|_{u=u_{k0}}(u_k - u_{k0}) \tag{3.13}$$

which can be written in a compact form as:

$$x_{k+1} = x_k + B_k u_k + D_k \tag{3.14}$$

where B_k and D_k are expressed as below:

$$B_k = \frac{\pi}{30}\frac{1}{Q_{max}}\frac{\omega_{em_k}}{f_k}\frac{r^w_{ice_k}}{r^w_{em_k}}T_s \tag{3.15a}$$

$$D_k = \frac{-OCV + f_k}{2RQ_{max}}T_s - B_k u_{k0} \tag{3.15b}$$

Let $T_{em}(k|k-1) = \frac{1}{r^w_{em_k}}\left(T_{w_k} - r^w_{ice_k}u_{k0}\right)$. Then:

$$f_k = \sqrt{OCV^2 - 4R\left(\frac{\pi}{30}\omega_{em_k}T_{em}(k|k-1) + loss(w_{em_k}, T_{em}(k|k-1))\right)}$$

The model complexity is given by the time-varying characteristic of B_k and D_k, which depend on EM rotational speed ω_{em_k} and torque demand T_{w_k}.

Table 3.1 – RMSE for SOC LTV model validation

Drive cycle	NEDC	Artemis urban	FTP-75	Traffic jam
RMSE[%]	0.0812	0.29	0.25	0.09

Model validity was tested for a prediction horizon of 5s and its accuracy is analyzed in Fig. 3.5 for different scenarios and quantified in Table 3.1. The validation consisted in applying a sequence of

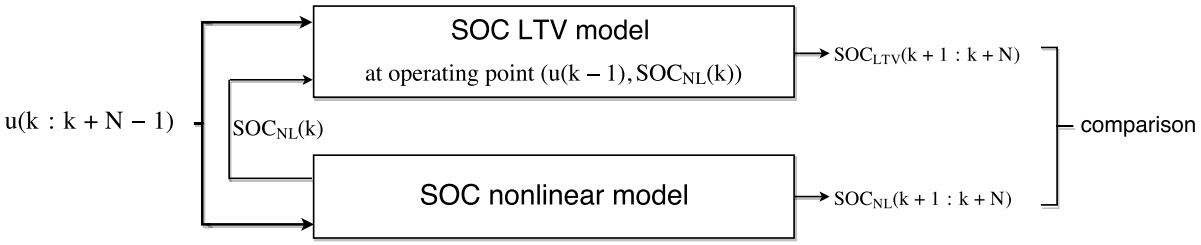

Fig. 3.4 – Principle of SOC LTV model validation

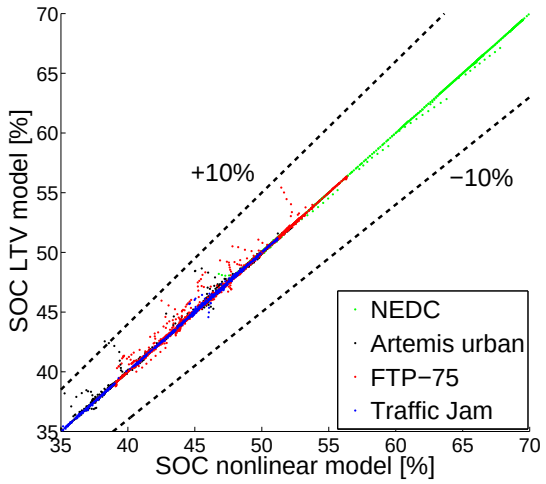

Fig. 3.5 – SOC LTV model vs SOC nonlinear model, for a prediction of 5s

a-priori calculated commands to both nonlinear and linearized model; every 5s the LTV model was updated with the SOC value given by the nonlinear model, as in Fig. 3.4 (for the considered case, the sampling time was of 0.5s and hence, $N = 10$). The purpose is to evaluate how distant the evolution of the approximated SOC trajectory is from the one provided by the nonlinear model.

The MPC problem is therefore formulated in a LTV framework, with a single control variable (engine torque T_{ice}), by assuming the vehicle profile and the driveline states foreseen over a given horizon, typically of 30s. In the next subsections, it will be shown that the engine state can be handled without introducing a dedicated ON/OFF control variable, but first the cost function needs to be defined.

2.3 Optimization criterion

The considered control problem focuses on the reduction of the fuel consumption, in the context of availability of an energy buffer, that can be replenished during driving, either by recovering the vehicle energy, or by shifting the engine operating point toward higher torques than necessary. A local fuel-friendly strategy would be to use the battery as much as possible, but the absence of external charging would imply to charge the battery later, via the engine, if the regenerative braking phases are not important enough and therefore, it is far from the global optimum.

Regarding the choice of the optimization criterion, there are two main approaches that can be distinguished in the literature:

1. construction of a cost function based exclusively on the fuel consumption, with an enforced constraint on final SOC
2. inclusion of the SOC variation in the cost function

The first approach can take different mathematical forms. In [102] the following cost function was defined as:

$$J_k = \int_{k\Delta t}^{(k+N_p)\Delta t} \left(\dot{m}_f(u(t))^2 + \lambda O(t)\right) dt \tag{3.16}$$

where $O(t)$ is the engine ON/OFF switching time and λ a penalty factor. With respect to the battery use, a very conservative approach is adopted, enforcing $SOC(k+N_p|k) = SOC_0$ where $SOC(k+N_p|k)$ denotes the predicted SOC trajectory. The problem is formulated into a nonlinear MPC framework and it is solved using DP.

In [117], the MPC problem is formulated as a Second Order Cone Problem (SOCP), which is a nonlinear convex problem and it minimizes "a linear function over intersection of affine set and product of second-order cones". Linear and quadratic programming are particular cases of SOCP. In addition to torque split, the quoted reference addresses also the engine stop. The cost function is the fuel consumption over an horizon and for the SOC trajectory, the following inequality constraint is imposed:

$$SOC(k) + \Delta t \sum_{i=0}^{N_p} \dot{SOC}(k+i|k) \geq SOC_{ref} \tag{3.17}$$

A similar approach is encountered in [31], with the difference that the fuel consumption is approximated by a linear model in engine torque, whereas [117] uses a second-order polynomial; in [154] the method follows the same logic, but using a nonlinear prediction model.

For real-time computation perspective, the MPC would rather use short-range prediction especially when constrained optimization is considered. Moreover, it relies on traffic preview data, which cannot always present an elevated precision or reliability, mainly in case of aggressive or unpredictable drivers. If the prediction model is resulted from a linearization at the operating point, its validity is restricted to a small neighborhood around this point. Hence, in the context of small prediction horizons, the approach (1) may lead to conservative results.

For the second approach, i.e. the inclusion of the SOC variation, there are 2 main methodologies. The first is to consider the electrochemical consumption similar to the ECMS design (3.7), but where the weighted sum of the two powers is evaluated over a prediction horizon.

$$J_k = \sum_{i=1}^{N_p} \left(P_f(i) + \lambda_k P_e(i)\right) \tag{3.18}$$

In [32] a linear SOC model is used and the problem (3.18) is solved using a Sequential Quadratic Programming (SQP) based optimization algorithm (the result being presented in Matlab simulation environment), for short-range prediction horizons (5-15s). The tuning factor λ_k is adapted with a proportional SOC corrector, similar to (3.8). In [155] the cost function includes also a penalty term for the engine ON/OFF. The prediction is of the order of 10s and the problem resolution relies on Matlab's *fmincon*.

The second method considers the tracking error between the SOC predicted trajectory and a setpoint SOC_{sp}, for each predicted step [73], [124] or exclusively for the final SOC [156]. Therefore, the cost function becomes:

$$J = \int_{t_0}^{t_f} \left(\dot{m}_f^2(\tau) + \lambda(SOC(\tau) - SOC_{sp}(\tau))^2\right) d\tau \tag{3.19}$$

This leads to a standard setpoint tracking formulation: trade-off between the tracking error and the energetic consumption $\dot{m}_f$. It should be noted that the SOC reference is set constant, the reason being that in a charge sustaining operation, the SOC evolution is maintained in a mid-range value. The cost function (3.19) may therefore not respond to the energetic objective that is to allow the free use of the battery, instead of following a fixed target. An alternative is to define a time-varying SOC reference, by exploiting traffic preview data. In [114] the SOC target is calculated such that energy recovery during braking is possible and by reducing the rate of change between the fixed segments of braking, which is performed in order to extend the NiMH battery lifetime. In [157], the trip is divided under several segments, defined by similar characteristics and for each segment a constant SOC setpoint is calculated with DP, which uses the fuel consumption as the performance index.

In view of all these previous attempts, the present work will adopt an energy-oriented optimization, placing the problem into an Economic MPC framework, already mentioned in [117]. As a difference with [117], here the cost function will also consider the electrochemical consumption and thus, anticipating a premature depletion through a trade-off at the consumption level, rather than by means of constraints. Therefore, the proposed optimization criterion meets the approach from (3.18), but in a quadratic form. With the linearized models introduced before, this choice allows the problem to be formulated in a standard convex form, which favors an efficient implementation. In its generic form this optimization problem will be written:

$$\min_{U_k} \sum_{i=1}^{N_{mpc}} P_{f_k}^2\left(U_k(i)\right) + \lambda_k^2 \left(P_{e_k}(U_k(i)) - P_{emin_k}(U_k(i))\right)^2 \tag{3.20}$$

where $U_k = \begin{bmatrix} u_k & u_{k+1} & \cdots & u_{k+N_{mpc}-1} \end{bmatrix}$, N_{mpc} is the prediction horizon and P_{emin_k} is the electrochemical power minimal value. This latter element is used as an offset term, in order to properly include the sign information of the electrochemical power, that would otherwise be lost if only the squared value were used. This choice and the argument behind its construction can be analyzed in Fig. 3.6, where for the linear approximations of the two powers, their dependence of the control variable u is depicted. If the engine provides a greater torque than the demand, the torque in excess is used to charge the battery, making P_{emin} negative.

2.4 Linear Time-Varying MPC framework

Once the prediction model and the cost function are introduced, the next step is to present the MPC framework that solves the optimization problem. The SOC model is linear time-varying, due to variations of B_k and D_k, resulting into a LTV-MPC problem, whose standard formulation is introduced below, followed by its application to the torque split problem.

2.4.1 Standard formulation

Let:

$$\begin{cases} x_{k+1} = A_k x_k + B_k u_k + D_k \\ y_k = C x_k \end{cases} \tag{3.21}$$

be the state-space evolution of a linear time-varying dynamical system, with $x \in \mathbb{R}^n, u \in \mathbb{R}^m, y \in \mathbb{R}^{n_y}$, $A_k \in \mathbb{R}^{n \times n}$, $B_k \in \mathbb{R}^{n \times m}$, affine term $D_k \in \mathbb{R}^n$ and the sensors constant matrix $C \in \mathbb{R}^{n_y \times n}$.

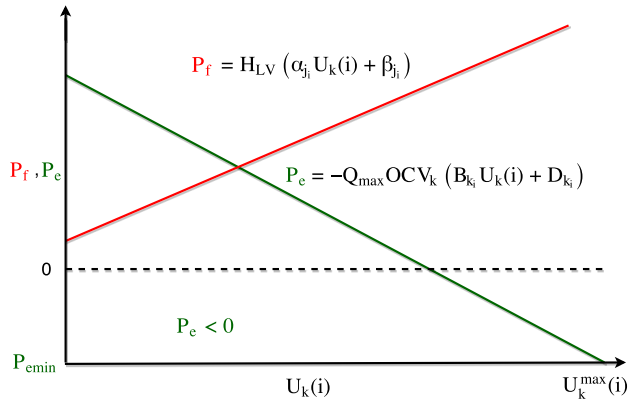

Fig. 3.6 – Graphic representation of fuel and electrochemical power evolution w.r.t. the control variable; α and β are the coefficients that define the fuel consumption approximation; B_k and D_k define the SOC linearized model

Let $\hat{y}(k+i)$ denote the i^{th} step prediction of the output from the current state. Then:

$$Y_k = \begin{bmatrix} \hat{y}(k+1) & \hat{y}(k+2) & \cdots & \hat{y}(k+N_p) \end{bmatrix}^T \tag{3.22}$$

$$U_k = \begin{bmatrix} u(k) & u(k+1) & \cdots & u(k+N_c-1) \end{bmatrix}^T \tag{3.23}$$

where N_p is the prediction horizon and $N_c \leq N_p$ is the control horizon and it represents the dimension of the optimization problem. In some cases, it is preferred to enforce the constraints only at the beginning of the prediction, the purpose of the rest of the prediction being only to maintain a proper direction for the future trajectory. The output evolution from the current state x_k, under the influence of the future commands can be expressed into a compacted form:

$$Y_k = \Phi_k x_k + \Psi_k U_k + W_k \tag{3.24}$$

with

$$\Phi_k = \begin{bmatrix} CA_k \\ CA_{k+1}A_k \\ \vdots \\ C\prod_{i=0}^{N_p-1} A_{k+i} \end{bmatrix} \tag{3.25a}$$

$$\Psi_k = \begin{bmatrix} CB_k & 0 & \cdots & 0 \\ CA_{k+1}B_k & CB_{k+1} & \cdots & 0 \\ \vdots & & & \\ C\prod_{i=1}^{N_p-1} A_{k+i}B_k & C\prod_{i=2}^{N_p-1} A_{k+i}B_{k+1} & \cdots & C\prod_{i=N_c}^{N_p-1} A_{k+i}B_{k+N_c-1} \end{bmatrix} \tag{3.25b}$$

$$W_k = \begin{bmatrix} C & 0 & \cdots & 0 \\ CA_{k+1} & C & \cdots & 0 \\ \vdots & & & \\ C\prod_{i=1}^{N_p-1} A_{k+i} & C\prod_{i=2}^{N_p-1} A_{k+i} & \cdots & C \end{bmatrix} \begin{bmatrix} D_k \\ D_{k+1} \\ \vdots \\ D_{k+N_p-1} \end{bmatrix} \tag{3.25c}$$

where $\Phi_k \in \mathbb{R}^{n_y N_p \times n}, \Psi_k \in \mathbb{R}^{nN_p \times mN_c}, W_k \in \mathbb{R}^{n_y N_p \times 1}$.

The predictor has therefore a linear affine structure and under controllability assumptions, the rank of these matrices is full. With these notations, a quadratic cost function is introduced, which minimizes over a finite horizon the tracking error between the output Y_k and the setpoint Y_{ref_k} (that can be time-varying, based on the anticipatory data), as well also the command effort U_k. Moreover, constraints on output and command are imposed:

$$\min_{U_k} \quad J_k = (Y_k - Y_{ref_k})^T Q_k (Y_k - Y_{ref_k}) + U_k^T R_k U_k \tag{3.26}$$

$$\text{s.t.} \begin{cases} Y_{min_k} \leq Y_k \leq Y_{max_k} \\ U_{min_k} \leq U_k \leq U_{max_k} \end{cases} \tag{3.27}$$

where $Q_k \geq 0, R_k \geq 0$ are matrix of penalties for the tracking error and the command, respectively, usually diagonal.

Then the problem (3.26) can be formulated into a quadratic programming (QP) framework:

$$\min_{U_k} \quad \frac{1}{2} U_k^T H_k U_k + F_k^T U_k \tag{3.28a}$$

$$\text{s.t.} \begin{cases} A_{ineq} U_k \leq b_{ineq} \\ A_{eq} U_k = b_{eq} \end{cases} \tag{3.28b}$$

where $H_k = \Psi_k^T Q_k \Psi_k + R_k > 0$ and $F_k^T = \left(\Phi_k x_k + W_k - Y_{ref_k}\right)^T Q_k \Psi_k$.

Note that the cost function can also be expressed as an ℓ_1 norm, transforming the optimization into a Linear Programming (LP) problem.

$$\min_{U_k} \quad F_k^T U_k \tag{3.29}$$

$$\text{s.t.} \begin{cases} A_{ineq} U_k \leq b_{ineq} \\ A_{eq} U_k = b_{eq} \end{cases} \tag{3.30}$$

Traditionally, the standard choice is the QP formulation, due to its smoother command in comparison to the *bang-bang* control usually provided by LP [158]. Moreover, even in the unconstrained case, the LP formulation makes the structural analysis more involved as long as it is not reducible to the linear feedback closed-form [159].

The most common tool for stability analysis remains the Lyapunov theory, which proved its effectiveness for LQR (Linear Quadratic Regulator) control and its closely related MPC formulation [129]. In [160] the stability for a receding horizon controller is proven for an infinite horizon, under the assumption of controllability. The analysis is extended and it is shown that global asymptotic stability can be assured for a finite prediction horizon N_p, if this is large enough, under assumptions on stabilizability

and feasibility. With respect to the present formulation we note two features: on one side the fact that the model being time-varying, the MPC solution (3.28) will be linear time-variant itself and the rate of variation needs to be accounted for in the closed-loop analysis. Secondly, the control formulation is that of a tracking problem, with the reference trajectory known on a relatively short horizon, thus placing the closed-loop analysis on the ground of economic performance and less on the stability guarantees.

2.4.2 Application to the torque split problem

With the prediction model and the cost function defined in the previous sections, it will be shown how the energy management problem can be formulated into a standard LTV MPC form, introduced above. For a better understanding, the definitions from (3.7) are recalled here:

$$P_f(k) = H_{LV}\dot{m}_f(\omega_{ice}(k), T_{ice}(k)), \quad P_e(k) = -Q_{max}\Delta SOC(k)OCV(k)$$

and with the SOC LTV model (3.14), the dependence between P_e and the control variable u can be expressed as:

$$P_e(k) = -Q_{max}OCV(k)(B_k u_k + D_k) \tag{3.31}$$

The minimum value of the electrochemical power P_{emin_k} corresponds to the maximum value of the control variable U_k^{max} as depicted in Fig. 3.6 and hence $P_{emin_k} = Q_{max}OCV(k)(B_k U_k^{max} + D_k)$. Therefore, with the PWL consumption model (2.27):

$$\dot{m}_f = \alpha_j(\omega_{ice})T_{ice} + \beta_j(\omega_{ice}), \quad j = 1 \dots N_{part}$$

as well as the above definitions, the cost function (3.20) can be written as:

$$\min_{U_k} \sum_{i=1}^{N_{mpc}} H_{LV}^2 \left(\alpha_{j_i}(\omega_{ice})U_k(i) + \beta_{j_i}(\omega_{ice})\right)^2 + \lambda_k^2 Q_{max}^2 OCV_k^2 \left(B_{k_i}U_k(i) - B_{k_i}U_k^{max}(i)\right)^2 \tag{3.32}$$

where the index j_i denotes the fuel consumption region j (2.27) for the i^{th} element in the array U_k and U_k^{max} is an array with the control upper bounds. This can be formulated as a QP problem (3.28), with:

$$H_k = \bar{\alpha}_k^2 + q_k^2 \bar{B}_k^2 \tag{3.33a}$$

$$F_k = \bar{\alpha}_k \bar{\beta}_k - q_k^2 \bar{B}_k U_k^{max} \tag{3.33b}$$

where $q_k = \lambda_k \frac{1}{H_{LV}} Q_{max} OCV_k$, $\quad \bar{B}_k = diag\left(B_{k_i}\right)$,

$$\bar{\alpha}_k = \begin{bmatrix} \alpha_{j_1}\left(\omega_{ice_k}\right) & \cdots & 0 \\ \vdots & \ddots & \vdots \\ 0 & \cdots & \alpha_{j_{N_{mpc}-1}}\left(\omega_{ice_{k+N_{mpc}-1}}\right) \end{bmatrix} \tag{3.34a}$$

$$\bar{\beta}_k = \begin{bmatrix} \beta_{j_1}\left(\omega_{ice_k}\right) & \cdots & \beta_{j_{N_{mpc}-1}}\left(\omega_{ice_{k+N_{mpc}-1}}\right) \end{bmatrix} \tag{3.34b}$$

If penalties on torque variations are also considered (for drivability improvement, for instance), the relations (3.33) are updated as below, with $R_{\Delta_k} \geq 0$ the matrix of penalties:

$$H_k = \bar{\alpha}_k^2 + q_k^2 \bar{B}_k^2 + D_\Delta^T R_{\Delta_k} D_\Delta \tag{3.35a}$$

$$F_k = \bar{\alpha}_k \bar{\beta}_k - q_k^2 \bar{B}_k U_k^{max} + D_\Delta^T R_{\Delta_k} U_{k0} \tag{3.35b}$$

where:

$$\Delta U_k = D_\Delta U_k + U_{k0} \tag{3.36a}$$

$$U_{k0}^T = \begin{bmatrix} -u_{k0} & 0 & \dots & 0 \end{bmatrix} \tag{3.36b}$$

$$D_\Delta = \begin{bmatrix} 1 & 0 & 0 & \cdots & 0 & 0 \\ -1 & 1 & 0 & \cdots & 0 & 0 \\ 0 & -1 & 1 & \cdots & 0 & 0 \\ & & & \ddots & & \\ 0 & 0 & 0 & \cdots & -1 & 1 \end{bmatrix} \tag{3.36c}$$

2.4.3 Constraints formulation and SOC balance problem

For a charge-sustaining operation mode, a particular attention must be paid to SOC balance, i.e. final SOC value should coincide with the value at the start of the trip. The integration of this objective remains largely an open problem, due to the differences between simulation and real-driving operation. For example, in [142] is stated to be "justified mainly as a way to compare the results of different solutions by guaranteeing that they reach the same level of battery energy. In real vehicles, there is no need to have a fixed battery SOC at the end of each cycle but only to keep it always between two boundary values". In [37] it is also mentioned that final SOC value does not necessarily need to be defined w.r.t. to the starting value, but chosen such that it verifies conditions related to the battery health. Therefore, the SOC balance is especially useful in simulation, but in practice this constraint can be relaxed, as the interest is on maintaining SOC within a certain range (in average).

The proposed strategy allows to handle both situations: simulation and real-driving. Instead of adapting the tuning in order to avoid important deviations from the starting value SOC_0, distance-varying limits for SOC are introduced, as expressed below:

$$\begin{aligned} SOC^{min}(k) &= SOC_0 - (SOC_0 - SOC_{min})\, e^{1-\frac{1}{1-\frac{dist(k)}{distTot}}} \\ SOC^{max}(k) &= SOC_0 + (SOC_{max} - SOC_0)\, e^{1-\frac{1}{1-\frac{dist(k)}{distTot}}} \end{aligned} \tag{3.37}$$

The idea is to constrain SOC to gradually approach its initial value as the ratio between the actual distance and the total distance increases and, at the same time, allowing it a wide range of variation in the first part of the trajectory (SOC_{min}, SOC_{max} represent the physical limitations of the battery which were set at 20% and 90%, respectively). Moreover, the trajectory can be adjusted for a given final SOC value. However, this implies the knowledge of the trip distance, which cannot always be available. In this case, a pre-defined reset distance can be introduced, as for the red curve in Fig. 3.7. In simulation, it can be set to 5 or 10 km, but in real-driving situations this value could be chosen with respect to driver's history data.

These constraints do not influence the algorithm design, they only provide a mechanism to address the SOC balance problem. Moreover, relaxations can be included in the formulation of boundaries (3.7). For $\alpha \in (0,1)$, the exponential $e^{1-\frac{1}{1-\alpha\frac{dist(k)}{distTot}}}$ will determine a slower convergence (red curve in Fig. 3.8) whereas $e^{1-\frac{1}{\frac{1}{\alpha}-\frac{dist(k)}{distTot}}}$ will enlarge the domain between the boundaries (black curve in Fig. 3.8).

In addition to SOC limitations (3.37), the powertrain is subject to several physical constraints: engine torque upper bound, as depicted in Fig. 1.11, electric machine torque and power limits as in Fig. 1.12,

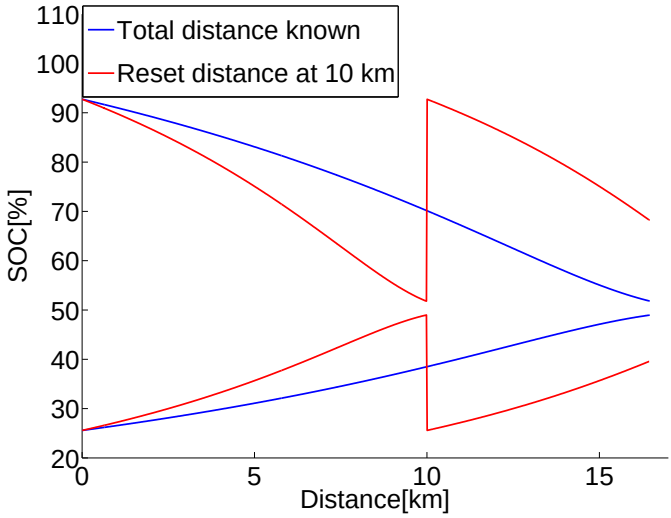

Fig. 3.7 – SOC limits for 2 cases: total distance known and reset distance fixed at 10 km, respectively

which depend on the operating points ω_{ice} and ω_{em}, respectively. In same cases, new constraints may need to be enforced by external systems, such as the aftertreatment: for the catalyst warm-up the engine speed is adapted, changing therefore the upper and lower torque limits.

The constraints can be classified into 3 main categories:

- reliability: physical constraints of the components

- emissions and OBD (On-Board Diagnosis) [161]

- driveability: engine overboost, which allows dynamic torque limitations that exceed the static ones

Here, only the reliability constraints are considered and for a time step k these time-varying limitations can be expressed as:

$$T_{ice}^{min}(\omega_{ice}(k)) \leq T_{ice}(k) \leq T_{ice}^{max}(\omega_{ice}(k)) \tag{3.38a}$$
$$T_{em}^{min}(\omega_{em}(k)) \leq T_{em}(k) \leq T_{em}^{max}(\omega_{em}(k)) \tag{3.38b}$$
$$P_{em}^{min}(\omega_{em}(k)) \leq \frac{\pi}{30}\omega_{em}(k)T_{em}(k) \leq P_{em}^{max}(\omega_{em}(k)) \tag{3.38c}$$
$$SOC^{min}(k) - \epsilon_k \leq SOC(k) \leq SOC^{max}(k) + \epsilon_k \tag{3.38d}$$

where ϵ_k is a slack variable and it is introduced to relax the constraints, in order to avoid infeasibility of the optimization problem. This can especially occur toward the end of the trip, where the range of SOC variation is considerably narrow. Moreover, the system is inherently bounded and it is not needed to enforce hard stability constraints.

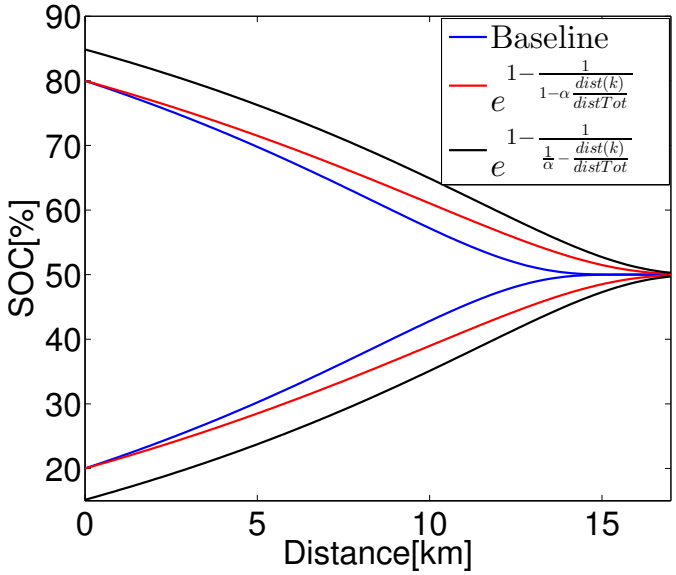

Fig. 3.8 – SOC limits relaxation for $\alpha = 0.85$

3 Analysis of the control law

3.1 Tuning

The penalty factor λ has a tremendous impact on the performance and its tuning encounters the same challenges as for the ECMS, i.e. dependence on the drive cycle characteristics. At the beginning of the chapter a summary of tuning methods for the equivalence factor was introduced. Here, an approach similar to (3.8) is chosen, but with an adaptation of the feedforward term λ_0. If this term is set constant, the tuning depends strongly on the initial guess, which cannot be suitable for all drive cycles. In [162] an adaptation based on an auto-regressive moving average (ARMA) model was proposed

$$\lambda(k) = \frac{\lambda(k-1) + \lambda(k-2)}{2} \tag{3.39}$$

However, this does not take into account the future characteristics of the drive cycle. Here, an adaptation that exploits the availability of predicted data is introduced, as detailed below.

Given the lower and upper bound of the command at each predicted step i, the solution explored in the present study is to express λ as a ratio of the 2 powers variations between these bounds, as defined below, where k is the optimization step:

$$\lambda_{k,i} = -\frac{P_f(\overline{u}_{k,i}) - P_f(\underline{u}_{k,i})}{P_e(\overline{u}_{k,i}) - P_e(\underline{u}_{k,i})}, \quad \text{for } T_w(k+i) \geq 0 \tag{3.40}$$

which guarantees $\lambda_{k,i} > 0$, due to the characteristics in Fig. 3.6.

However, instead of using a pointwise penalty, an average-based expression can be introduced over an horizon N_λ, which can be greater or equal to the horizon used for the MPC problem:

$$\lambda_{k0} = \frac{1}{N_\lambda - N_\lambda^{stop}} \sum_{i=1}^{N_\lambda} \lambda_{k,i} \tag{3.41}$$

where $\lambda_{k,i}$ is given by (3.40) and N_λ^{stop} is the number of predicted steps of vehicle standstill.

$$\lambda_k = \lambda_{k0} + k_p \left(SOC_{sp} - SOC_k\right) \tag{3.42}$$

where SOC_{sp} is the SOC setpoint, which can be set constant or generated by exploiting data from the navigation system, as shown in Fig. 3.9. It can be observed that the control problem is structured as a two-layer optimization: the upper layer handles the tuning and it exploits the navigation data over an horizon N_λ to calculate the feedforward component of λ, which will be next used by the MPC controller in the cost function. This layer handles the torque split and the stop & start (S&S), as will be detailed in the next section; the engine torque reference and S&S command are sent to a powertrain supervisor, that will process the commands (engine idle speed control, for instance) and calculate the torque and gearbox setpoints for the vehicle. In addition to the driver request and preview data over an horizon N_{mpc}, the MPC controller receives as well the on-board estimated SOC and engine torque.

The expression contains therefore 2 terms: a feed-forward component (λ_{k0}) and a feedback part (the proportional SOC control). The purpose of the latter is to adjust the penalty factor with respect to an SOC setpoint:

- if the trajectory is below the setpoint, λ increases, thus penalizing more the use of the battery
- if the trajectory is greater than the reference, λ will diminish and this will correspond to a greater use of the battery.

In this study, the setpoint was chosen constant and equal to the initial value. Again, the goal is not to track a certain SOC reference, but to allow the trajectory to freely vary and to avoid overcharge or discharge.

The braking phases need to be included in the average calculation, but in this case $\lambda_{k,i}$ can no longer be expressed as a ratio of differences, because these modes are pre-imposed: the maximum possible energy is recovered and the rest is dissipated in the friction brakes. Therefore, a particular expression is adopted in the present study:

$$\lambda_{k,i} = \frac{P_f^{idle}}{P_e^{regen}(k+i|k)}, \quad \text{for } T_w(k+i) < 0 \tag{3.43}$$

where $P_f^{idle} = H_{LV}\dot{m}_f^{idle}$ and $P_e^{regen}(k+i|k)$ is the predicted electrochemical power obtained by regenerative braking.

With this formulation λ will decrease if braking phases are anticipated. Thus, the use of the electric motor is encouraged if it is possible to compensate the electric consumption by regenerative braking.

A choice for the proportional factor k_p can be made such that λ_k remains positive:

$$\lambda_{k0} + k_p \left(SOC_{sp} - SOC_k\right) \geq 0 \tag{3.44}$$

For worst-case scenario i.e. $SOC = SOC_{max}$, this leads to:

$$k_p \leq \frac{\lambda_{k0}}{|SOC_{sp} - SOC_{max}|} \tag{3.45}$$

Usually, $SOC_{sp} \in [40\%; 60\%]$ and $\lambda_{k0} \in [2; 4]\frac{Q_{max}OCV}{H_{LV}}$, which gives:

$$k_p \leq 2 \tag{3.46}$$

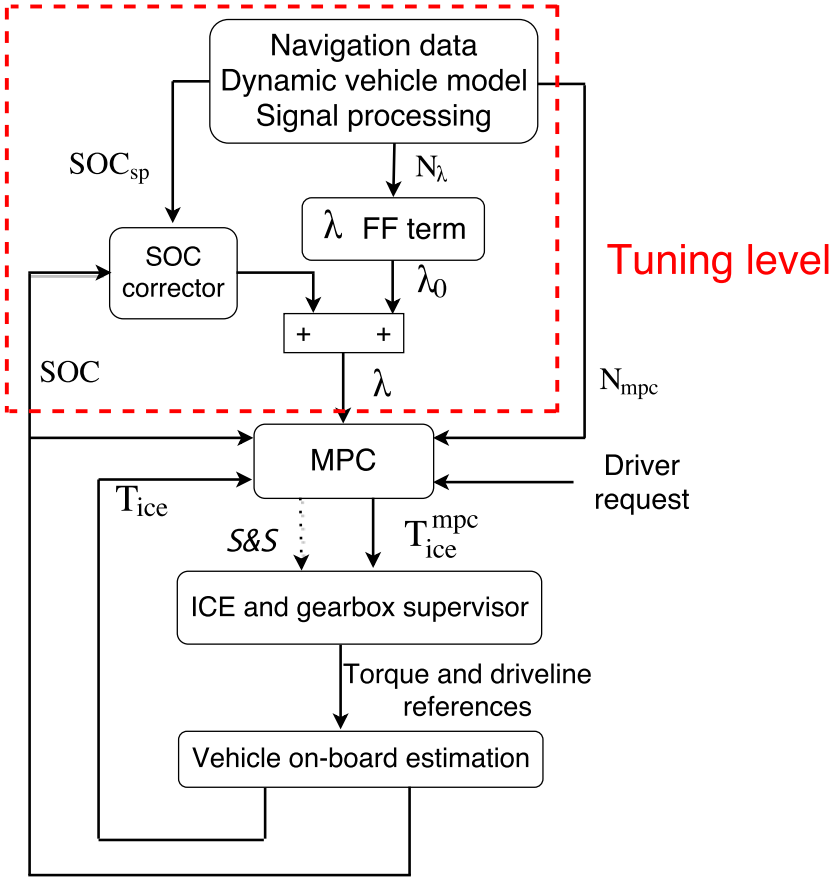

Fig. 3.9 – Control structure with a high-level tuning block

Choice of the horizon in the tuning procedure

The feed-forward component should encapsulate the trade-off between general tendency and aggressiveness of the drive cycle along a receding window. The longer the horizon N_λ, the smoother the feed-forward component becomes. MPC performs a local optimization and therefore, λ should be able to adapt fast enough with respect to drive cycle aggressiveness. In [6], a measurement of traffic and driver aggressiveness based on jerk periodograms has been introduced, see Fig. 3.10. The periodogram for a signal y is an estimate of the spectral density and it is given by the squared modulus of the Discrete Fourrier Transform [163]:

$$p(f) = \frac{1}{N}\left|\sum_{t=1}^{N} y(t)e^{-i2\pi ft}\right|^2 \tag{3.47}$$

Here, the periodogram of the wheel power will be used to analyze the aggressiveness information incorporated into λ, by using the frequency cumulative content for different prediction horizon values as in the expression below, where p stands for periodogram.

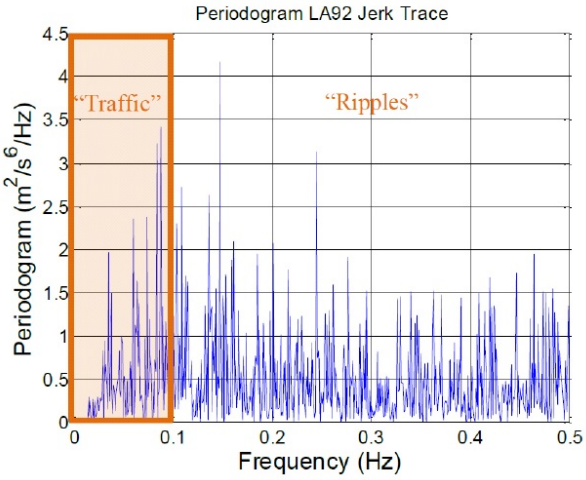

Fig. 3.10 – Jerk periodogram for LA92 cycle; low frequencies correspond to traffic-related aggressiveness (unavoidable situations) and high frequencies indicate the driver characteristics [6]

$$r(N_\lambda) = \frac{\int_{f=0}^{\frac{1}{2}f_{N_\lambda}} p(f)df}{\int_{f=0}^{\frac{f_s}{2}} p(f)df} \tag{3.48}$$

where f_s is the sampling frequency (here: $f_s = 1$Hz), $f_{N_\lambda} = \frac{1}{N_\lambda}$. This definition implies that for $N_\lambda = 1$s, the ratio is 1, that is, all drive cycle variations are included because no averaging is performed. If N_λ increases, the ratio diminishes due to smoothing. This can be observed in Fig. 3.11, where the evolution of the aggressiveness indicator with respect to the prediction horizon is depicted for several drive cycles. For values greater than 60s, the smoothing is sufficiently significant for all the scenarios considered. In certain cases, such as Artemis urban and traffic jam, the loss of aggressiveness information occurs at even lower horizons and therefore, the prediction horizon choice is drive cycle dependent.

The presence of a road grade may lead to the need of adapting the parameters that appear in the formulation of the tuning factor λ: N_λ (changing therefore the feedforward component) or SOC_{sp}, which defines the feedback part, as shown in Fig. 3.12. A simple example is analyzed in Fig. 3.13, described by a constant speed phase with variable slope: for the first half the road grade is set to 5% and for the other half: -5%. The frequency content of the wheel power periodogram is depicted in the third plot for the case with a flat road (blue line) and with slope (red line), respectively. This simple benchmark points to the need of adaptation for N_λ. An alternative would be to reduce the value of SOC_{sp} before the phase with negative slope, anticipating therefore the energy recovery. A comparison between these 2 strategies will be made in Chapter 4, dedicated to simulation results.

3.2 Influence of PWL approximation for fuel consumption

As mentioned in Chapter 2, the fuel consumption map is partitioned in several torque-dependent regions to which a first order polynomial approximation is associated. As introduced earlier, the cost function includes the fuel consumption and therefore parameters α_j and β_j from (3.34) need to be de-

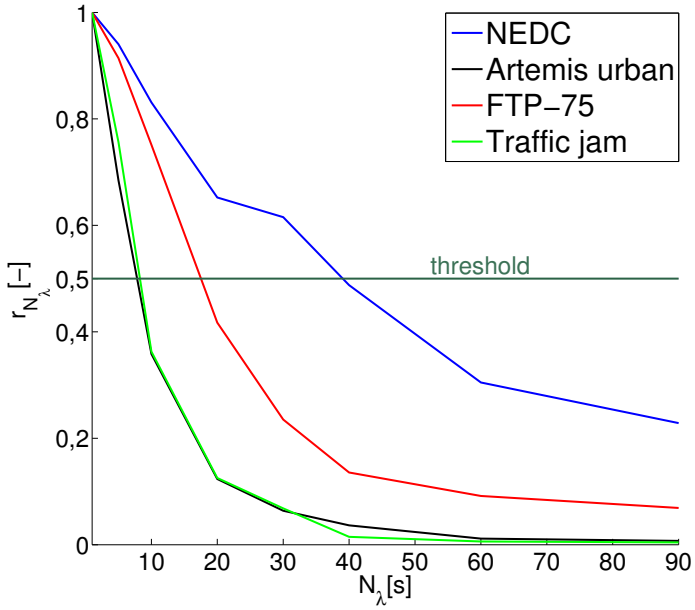

Fig. 3.11 – Ratio (3.48) of the frequency content for different prediction horizon values and drive cycles

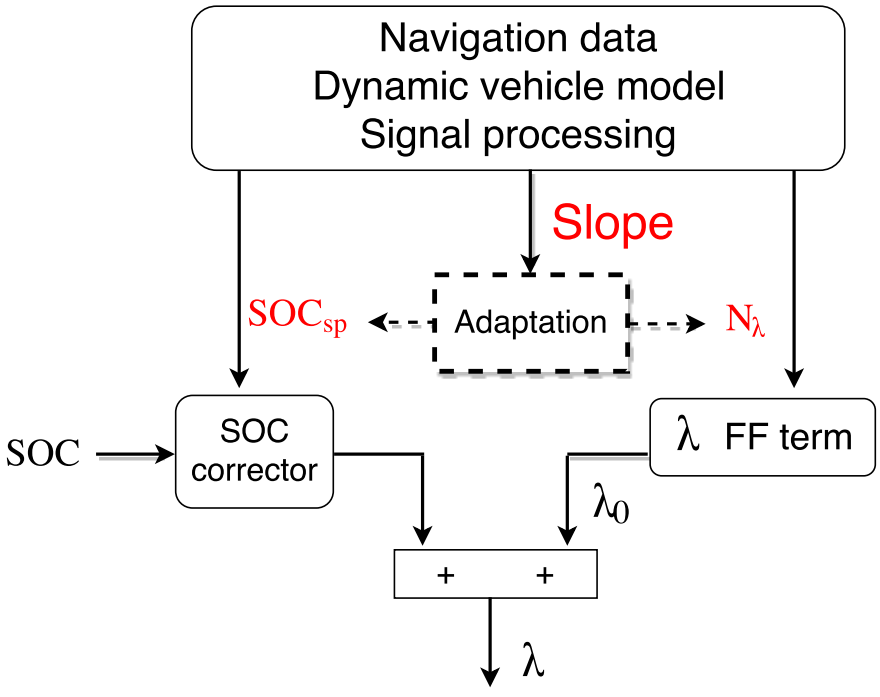

Fig. 3.12 – Tuning parameters (SOC_{sp} and N_λ) adaptation w.r.t. slope

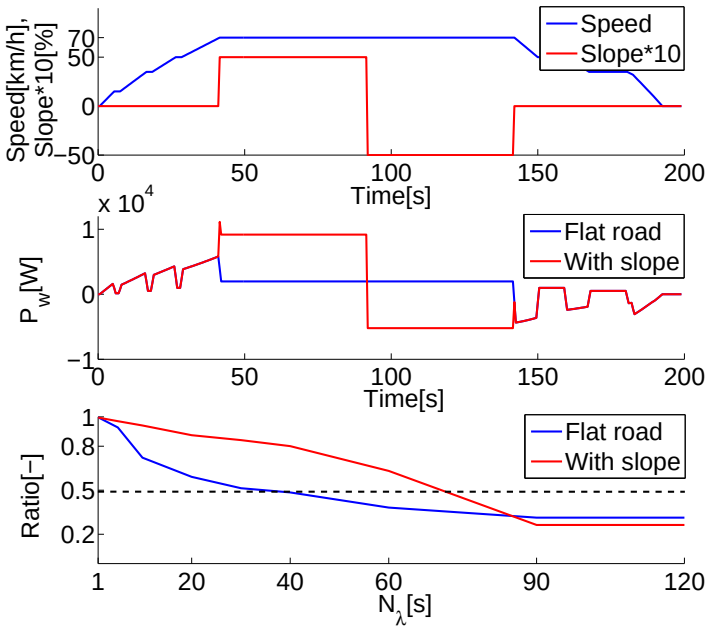

Fig. 3.13 – A case study with variable slope profile. Top figure: the speed profile and the slope; middle: the wheel power; bottom: ratio (3.48) of the frequency content

fined, i.e. a consumption region j needs to be selected. A drawback of such piecewise approximation approach is that the physical constraints of commands usually span several regions.

Let k be the current optimization step, i the index of a command from the vector U_k (the output of the MPC controller), n_{pwl} a vector with the consumption regions associated to each command from U_k, T_{ice}^{part} a vector with the torque values that demarcate the consumption approximation regions and U_k^{min}, U_k^{max} vectors that contain the lower and upper limits, respectively, of the commands.

The first step is to verify if for each command $U_k(i)$ a unique consumption partition j can be identified. The uniqueness can only be seldom encountered, the admissible torque interval for a command usually spans several partitions, but it is a possible case for approximations with a sparse division. The principle of selection can be expressed readily as:

$$\begin{aligned} &\text{if } \exists j \text{ s.t . } \left[U_k^{min}(i); U_k^{max}(i)\right] \subseteq \left[T_{ice}^{part}(j); T_{ice}^{part}(j+1)\right] \\ &\qquad \text{then } n_{pwl}(i) = j, \quad j = 1 \dots N_{part} \end{aligned} \tag{3.49}$$

where $T_{ice}^{part}(j), T_{ice}^{part}(j+1)$ represent the torque limits for the jth region, as in (2.27).

If this condition is not satisfied, the choice of the consumption region relies mostly on the current engine torque value. Let n_0 denote the region that corresponds to this torque value. Then:

$$\begin{aligned} &\text{if } \left[T_{ice}^{part}(n_0); T_{ice}^{part}(n_0+1)\right] \cap \left[U_k^{min}(i); U_k^{max}(i)\right] \neq \emptyset \\ &\qquad \text{then } n_{pwl}(i) = n_0 \end{aligned} \tag{3.50}$$

Finally, if no intersection is found between the torque limits and the current region, a neighbor

interval is selected. This situation can occur for instance when the current engine torque is very high and the operating point at step i has an average upper torque limit i.e. $T_{ice}^{part}(n_0) > U_k^{max}(i)$.

$$\begin{aligned} & n_{pwl}(i) = j, \quad j = 1 \dots N_{part} \\ & \min_j |n_0 - j| \\ & \quad \text{s.t.} \left[T_{ice}^{part}(j); T_{ice}^{part}(j+1) \right] \cap \left[U_k^{min}(i); U_k^{max}(i) \right] \neq \emptyset \end{aligned} \tag{3.51}$$

New limits are thus imposed:

$$\begin{aligned} U_k^{min}(i) &= \max \left(U_k^{min}(i), T_{ice}^{part}\left(n_{pwl}(i)\right) \right) \\ U_k^{max}(i) &= \min \left(U_k^{max}(i), T_{ice}^{part}\left(n_{pwl}(i+1)\right) \right) \end{aligned} \tag{3.52}$$

After each optimization step, a verification is performed for the commands whose physical limitations span several consumption regions. If the command i lies within its defined limits (3.52), no action is taken. If saturation occurs, $n_{pwl}(i)$ is shifted toward left or right, depending on whether the lower or the upper bound was activated, and a new optimization is launched with this update. The procedure is repeated until a chattering effect is encountered, as in (3.53), or a maximal number of iterations is reached.

$$U_k^{(iter)}(i) = \begin{cases} U_k^{min,(iter)}(i), & n_{pwl}^{(iter)}(i) = n_{pwl}^{(iter-1)}(i) + 1 \\ U_k^{max,(iter)}(i), & n_{pwl}^{(iter)}(i) = n_{pwl}^{(iter-1)}(i) - 1 \end{cases} \tag{3.53}$$

where the superscript $iter$ denotes the iteration number.

4 Stop-start inclusion: a model-based activation

Engine Stop&Start (S&S) is a functionality that automatically shuts and restarts the engine, avoiding thus unnecessary idling. If handled properly, it can bring an additional fuel gain up to 5% [164] and it is especially useful in urban traffic, as a result of frequent stops due to red lights or traffic jams. It is applied to a stationary vehicle, but enhanced stop-start systems allow extensions for speeds > 0 km/h too, but for safety reasons, they need to be equipped with an additional energy storage (in case of failure of the primary battery) [165].

The most encountered stop-start strategy is a rule-based method, largely adopted by car manufacturers [166]: for a manual transmission, the engine is stopped when the transmission is disengaged and the clutch pedal released, the restart being performed at clutch pedal activation; for an automatic transmission, the only control is the brake pedal, technique referred to as *stop-in-drive*, because the driveline is still engaged; the restart occurs at brake pedal release [167].

The simplicity of this rule-based strategy comes with the cost of fuel-inefficient or unwanted stops from a drivability perspective. An engine start implies an electric consumption (torque transfered to the engine in order to accelerate it) and an additional injected fuel to build the wall film in the intake manifold [114], in the case of a port injection. Therefore, an equivalent fuel cost associated to an engine restart must be introduced. It is usually defined in seconds of idling t_{idle} i.e. instead of keeping the engine idling for t_{idle}s, it is preferable to switch it off. This value depends mostly on the engine type (SI or CI) and displacement, as well as the transmission type (for instance, automatic transmissions have lower t_{idle} values than manual transmissions).

Improvements can be made by considering the cost of the engine restart and data about the driver's behavior, as in [168] where a machine learning-based strategy is proposed: the reinforcement learning. This method is based on the interaction of agents with their environment, in order to minimize a cost or to maximize a reward, the goal being therefore to optimize their performance. For the stop-start problem, 3 inputs are considered: vehicle speed, accelerator pedal position and brake pressure. A comparison is made with Ford rule-based strategy, which is similar to the one briefly introduced earlier and an improvement up to 12% is observed.

For an HEV, S&S presents an even greater interest, the engine can also be stopped during electric traction phases and hence, at higher speeds. Similar to the torque split problem, the strategies can be classified into heuristic and model-based. In [169] a fuzzy logic controller is proposed, which receives as inputs the required torque, the electric machine speed, the SOC value, the time after an engine start or stop and the temperature of the catalytic converter. Therefore, emissions are considered in addition to the fuel consumption reduction. In [74] a rule-based strategy, modeled with a finite state machine, is proposed for a power-split HEV. The focus is to improve the engine efficiency, by exploiting the multi-mode functioning of the power-split configuration.

Regarding the model-based strategies, there are two main approaches: introduction of a binary decision variable in the optimization procedure or separation into a two-layer optimization. The former can be encountered in [31], where the problem is formulated as a Mixed-Integer Quadratically Constraint Linear Program (MI-QCLP) and implemented with the help of a dedicated solver; [155] uses a nonlinear model, with an accurate description of the engine start-up and crank-to-idle phenomena and a cost function that minimizes the consumption over an horizon, with a SOC correction term and ICE restart cost penalty; the problem is solved with Matlab *fmincon* function, which is also the choice for [156], where the problem is formulated into a nonlinear programming (NP) framework. The advantage of this approach is the simultaneous handling of the two problems (torque split and engine ON/OFF), but in the same time the solver may be too computationally demanding for real-time applications.

The two-layer optimization is encountered on different forms: in [170] a constrained LP is used to compute the power distribution at the top level, whereas the engine operating point optimization is performed at a lower level, which includes S&S. Time constraints related to the duration to start the engine and to bring it to a specific operating point, as well as the time to declutch and to shut off the engine, are also considered; the problem is solved with a MILP (Mixed-Integer Linear Programming) solver. In [30] the upper level uses dynamic programming for engine ON/OFF decision and gear choice, whereas the lower level uses convex optimization to provide the torque split. The MPC benefit for stop-start strategy has been analyzed in [68] for a city bus, where the torque-split is also handled as a separated, low-level problem. In [73] a LTV-MPC framework is introduced for the energy management of a power-split architecture, where the engine speed is an additional optimization variable and therefore, it includes by default the S&S strategy. The drawback of this approach is that the cost of an engine restart is not considered and the variation of torque limitations w.r.t. speed is not explicitly addressed.

In our work, the interest is to introduce new functionalities without essentially changing the control structure, such as the number of control variables or the type of solver, the request being allowed by MPC, due to its design principle. The MPC advantage of calculating a sequence of commands can provide, via the complete finite-time optimal-control solution, short-term information about the duration of the phases where the engine can potentially be stopped. The proposed approach is to generate a stop-start command based on the analysis of the MPC control sequence, without introducing a binary optimization variable in the problem, as will be detailed below.

Let t_{idle} be the number of seconds of idling which reflects the cost of an ICE restart, ct_{on} the number

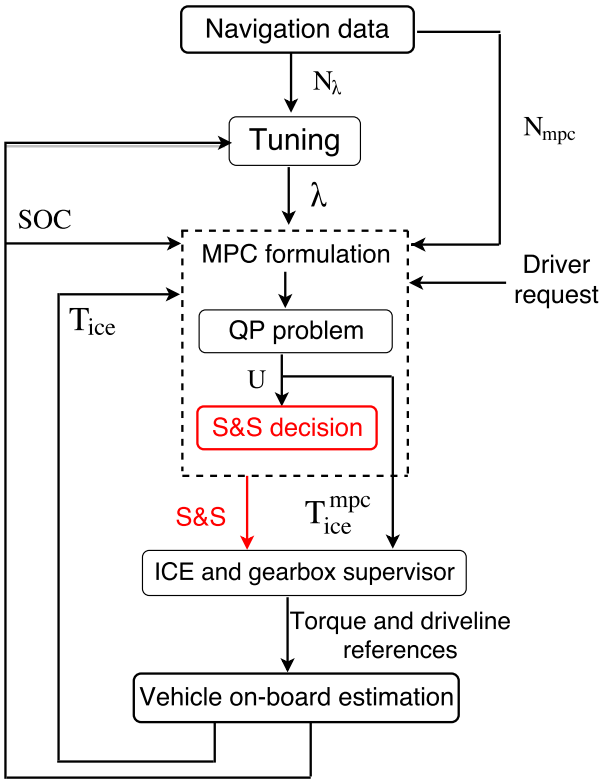

Fig. 3.14 – Control structure with S & S included

of steps since an ICE restart and ct_{off} the number of steps since an ICE stop. Then at step k the engine is shut off for:

$$U_k\left(1:N_{stop}\right) \leq T_{ice}^{thr} \tag{3.54a}$$

$$ct_{on} > N_{start} \tag{3.54b}$$

where

$$N_{stop} = \frac{t_{idle}}{\Delta t_{opt}} \tag{3.55}$$

and T_{ice}^{thr} is a threshold value for ICE torque below which the stop of the engine is preferable over the considered length of the prediction horizon. The condition (3.54b) assures that the engine is not stopped shortly after a restart decision. If the engine is already stopped, a restart is demanded if the first calculated command is greater than T_{ice}^{thr}.

Engine restart is not an instantaneous event and for speed tracking improvement, an anticipation is suitable. Here, as a contribution, a N_{on}- step anticipation for ICE restart is introduced: if a sequence of commands with length N_{stop} from position $1 + N_{on}$ exceeds the threshold torque value and the engine has already been stopped for at least N_{stop} steps, a restart command is activated. For the case considered, with an MPC sampling time of 0.5s, N_{on} was set to 1.

$$U_k(1 + N_{on} : 1 + N_{stop}) > T_{ice}^{thr} \tag{3.56}$$

In addition, all stop conditions are subject to powertrain inhibition functions, where safety requirements are formulated (SOC level, fuel temperature, altitude value, aftertreatement etc). This stop-start strategy is described by the diagram in Fig. 3.15.

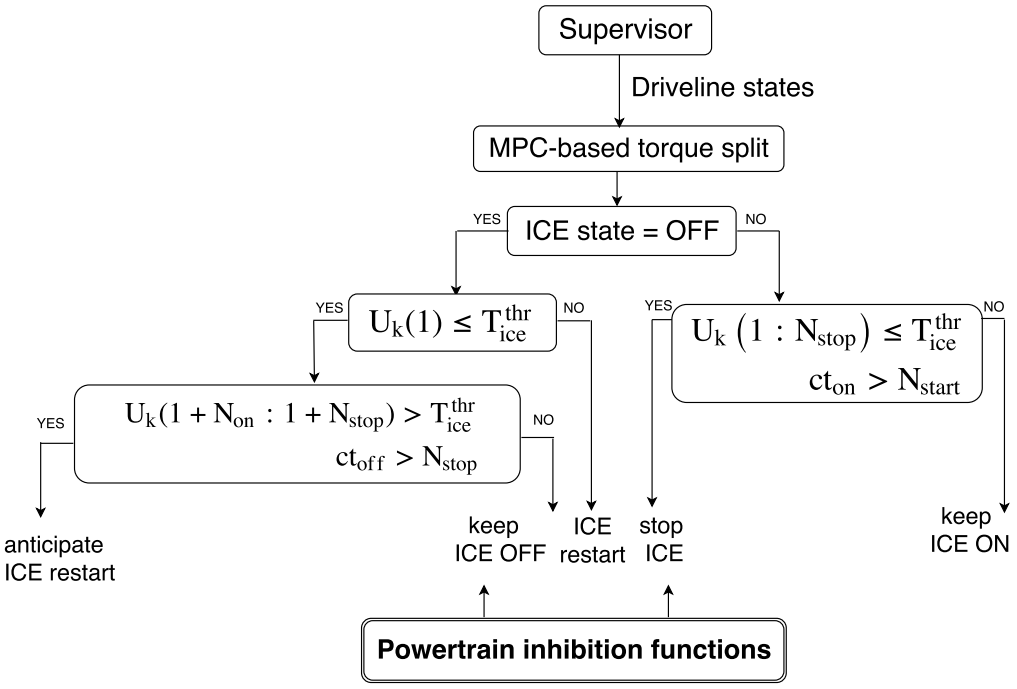

Fig. 3.15 – Schematic representation of the S & S strategy

The PWL approximation introduced in the previous section is suitable for this problem because it allows the demarcation of the low torque region, where T_{ice}^{thr} is included: $T_{ice}^{part}(1) \leq T_{ice}^{thr} \leq T_{ice}^{part}(2)$. The first step is to identify the sequences of commands with a length of at least N_{stop} for which the first region was selected for the fuel consumption approximation. Then, for these sequences, penalties on torque variations are introduced through the matrix R_{Δ_k}, as it appears in formulation (3.35) of the optimization criterion.

$$U_k^T = \begin{bmatrix} U_k(1) & U_k(2) & \dots & \underbrace{U_k(i) \dots U_k(j)}_{\substack{\geq N_{stop} \\ 0 \leq U_k(i:j) \leq T_{ice}^{part}(2) \\ \downarrow \\ R_{\Delta_k}(i+1:j, i+1:j) \neq 0}} & \dots & U_k(N) \end{bmatrix}$$

$R_{\Delta_k} \geq 0$ matrix of penalties

$T_{ice}^{part}(2)$ upper limit of the first torque region

$$R_{\Delta_k}(i+1:j, i+1:j) \neq 0, \text{ for } \begin{cases} j - i \geq N_{stop} \\ n_{pwl}(i:j) = 1 \end{cases} \tag{3.57}$$

The purpose of this strategy is to force the entire sequence to either go toward zero (and the engine to be stopped) or to reach the upper limit of the interval and then to commute toward higher values. The

cost of an ICE restart is implicitly handled by the length of the sequence, N_{stop}. If the engine has been stopped for $ct_{off} < N_{stop}$, then penalties are introduced for the first $N_{stop} - ct_{off}$ commands, in order to maintain the calculated torque close to zero and hence, the ICE stopped:

$$\begin{aligned} &R_{\Delta_k}\left(1 : N_{stop} - ct_{off}, 1 : N_{stop} - ct_{off}\right) \neq 0 \\ &ct_{off} < N_{stop} \end{aligned} \tag{3.58}$$

5 Coasting functionality

Coasting, sometimes also referred to as *free-wheeling*, is a special functional mode in which the vehicle motion is described only by resistive forces, no pedal being pressed. During coasting, the engine is usually disengaged, in order to avoid the friction torque. In some cases however, an additional negative torque from the engine can be useful, when a fast decrease of vehicle speed is demanded. If the engine is disconnected from the wheels, it can either be on idle or stopped.

One of the first papers which addressed the benefit of coasting (with engine stop) in terms of fuel consumption for conventional vehicles is [164]. Two types of drive cycle were considered: NEDC (hard deceleration) and FTP-75 (small deceleration). Although the NEDC in its initial form is not representative for coasting, a tolerated speed deviation allows early coasting initiation during phases of constant reference speed. It was shown that a gain up to 6% can be obtained, whereas for FTP-75, the best-case scenario provides a gain of 10%.

In [171] the performance of coasting was analyzed for constant speed phases on highway, with slope information included. The focus is on conventional vehicles and two main topics are addressed: coasting initiation and influence of boost acceleration before coasting. The performance of HEV is also tackled for a downhill road profile and results showed that coasting is more fuel-efficient than energy recovery.

Pulse and glide (PnG) [172], [122] is a method that uses the vehicle inertia as an energy buffer: the vehicle accelerates more than necessary instead of cruising, and thus, the engine operating point is shifted toward a more efficient zone. The consequent additional fuel consumption is made profitable due to the vehicle extra kinetic energy that allows a longer free-wheeling time, with the engine stopped. This strategy implies an interference in the accelerator pedal displacement, which is out of the scope of the present study, where only pedal release is concerned. It is assumed that once the driver is pressing the pedal, he/she is following the reference speed (in simulation, there will be a driver model implemented). A supervisory controller can display a message to suggest coasting initiation and under the assumption that the driver follows the indication, the functionality is activated.

In this section, we aim to show that model-based control design can integrate readily this supplementary feature with respect to the predictive energy management and therefore, an analysis of the coasting functionality and its performance for an HEV is introduced. First, a framework for the scenarios where coasting is potentially preferable over regeneration needs to be defined. Second, a strategy that determines coasting acceptance in terms of speed deviation and position, as well as the satisfaction of time-dependent constraints will be designed. A method to determine coasting initiation and duration is also detailed. The analysis considers exclusively coasting with engine stop.

5.1 Motivation: basic case study

In order to motivate the coasting, a basic case study is considered, described by a constant speed, followed by a decrease and shortly afterwards, a new increase phase, as the one depicted in Fig. 3.16

(black, dashed curve). Two scenarios are handled: basic coasting (red) and *e-coasting* (blue), conceptually illustrated in the same figure. The latter is defined by free-wheeling with energy recovery and it can be preferred if the vehicle cannot be slowed down fast enough by basic coasting, as it will be presented in the next example. If coasting is initiated around $t = 82$s , after 21s the vehicle will reach the new reference speed from the acceleration section, without showing an important deviation from the setpoint. The e-coasting can be started later and as a result of the energy recovery, the speed decreases faster and thus, remains closer to the setpoint.

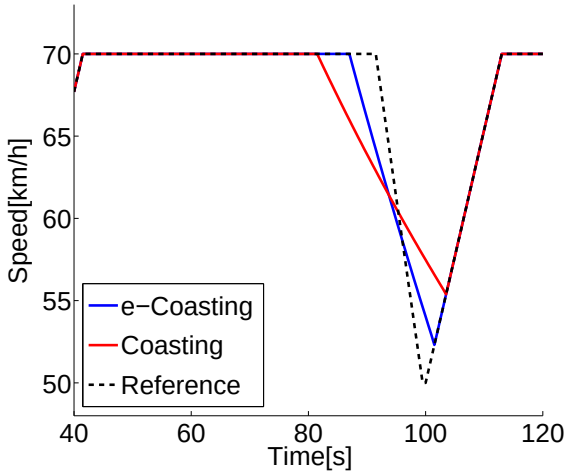

Fig. 3.16 – Speed profile of a basic case study with flat road (zoom). Comparison between coasting with recovery (blue) and baseline coasting (red)

Table 3.2 – Performance of the considered scenarios, speed from Fig. 3.16

Performance \ Scenario	e-Coasting	Coasting	Baseline
Consumption [L/100km] (final SOC)	5.07 (52%)	4.98 (52.05%)	5.15 (51.9%)
Distance[km]	2.51	2.505	2.517
RMS error speed [km/h]	0.72	1.66	0

The coasting decision is taken at the supervisory level, as depicted in Fig. 3.17, from the exploitation of the navigation data. This will influence the current driver request (coasting activation implies no pedal pressed), as well as the wheel torque prediction, that will affect the value of the feedforward component of the MPC tuning factor (λ_{k0}), as shown in Fig. 3.18. The aim of our work in this context is the evaluation of the benefit of coasting from a fuel consumption perspective, within a MPC-based energy management. For the subsequent analysis, the coasting decision was taken offline.

The analysis of coasting will be built on three main simulations, carried out for the three scenarios: baseline, coasting and e-coasting for $N_{MPC} = 5$s, $N_\lambda = 10$s and an initial SOC value of 50%, which is a representative framework with respect to the prior MPC synthesis. Consumption results show that coasting brings an improvement of almost 3%: 4.98 L/100 km vs 5.15 L/100 km, as it is obtained with

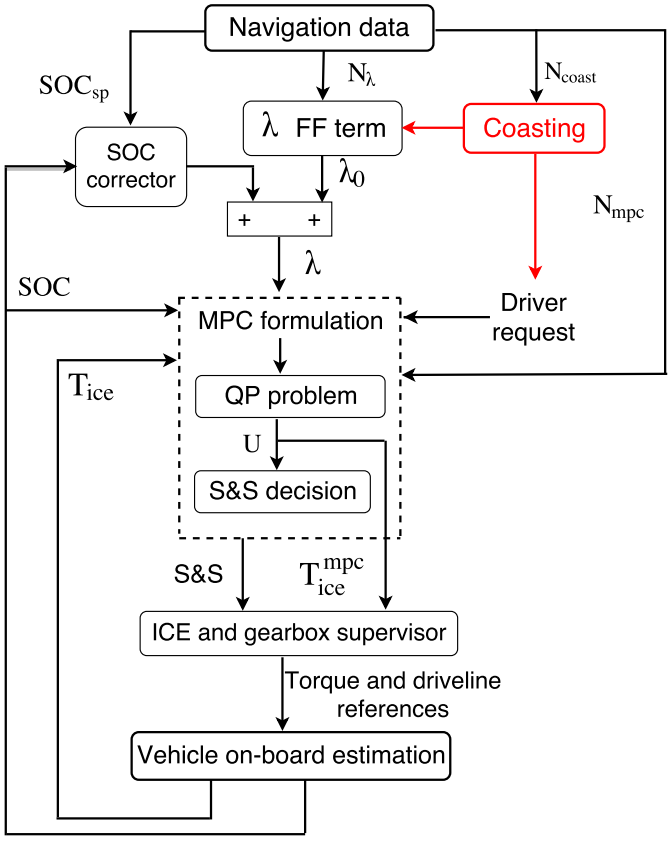

Fig. 3.17 – Extension of the control structure from Fig. 3.14 with coasting functionality

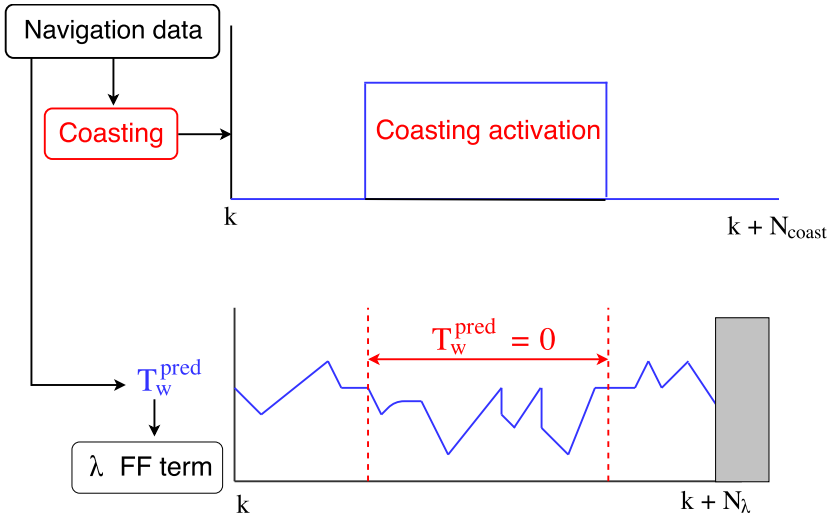

Fig. 3.18 – Coasting initiation: details about influence on the wheel torque prediction and impact on the λ feed-forward component

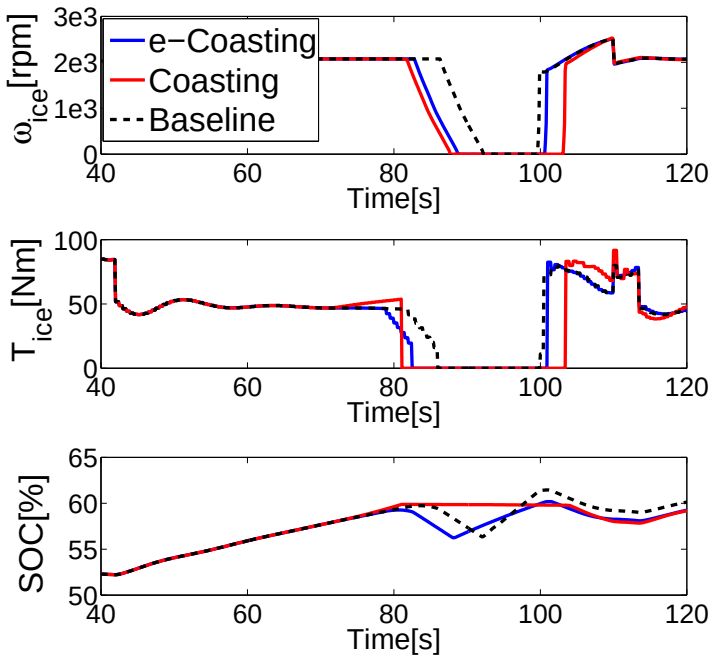

Fig. 3.19 – Simulation results for a basic case study with flat road: coasting with recovery (e-Coasting), coasting and baseline

the baseline strategy, for almost the same distance, whereas the e-coasting shows a less important improvement, as in Table 3.2. It is worth mentioning that our analysis is coherent with respect to similar coasting analyses performed with different control strategies [171]. The evolution of engine speed, engine torque and battery SOC is depicted in Fig. 3.19. We stress the fact that the red trajectory of SOC remains constant in the interval $[82; 103]$s i.e. during coasting, whereas the curve in black shows a slight decrease before increasing due to regenerative braking, followed by a new decrease in the acceleration part. The early initiation of coasting (during the constant speed phase) allows the engine to be stopped earlier. Moreover, due to coasting, the engine is kept shut off longer, even during the beginning of the acceleration, thus improving the fuel gain. It can be noticed that the engine torque before coasting initiation is different in the three cases. This is due to variations in the calculation of the feed-forward component λ_{k0}: the predicted wheel torque is different, zero during coasting and constant negative during e-coasting. The engine torque continues to have a different evolution, even after coasting deactivation (when λ_{k0} is practically the same). This behavior can be readily explained by following the MPC functioning: SOC trajectory changes after coasting deactivation and therefore the feedback component is different, a straightforward implication being the fact that the prediction model is linearized at a distinct operating point (current engine torque and SOC). The e-coasting speed trajectory is very close to the reference speed and hence, the performance is similar too, with the major difference that the engine can be stopped earlier.

This elementary case study demonstrated within a formal model-based strategy that a sequence of deceleration-acceleration is disadvantageous from energy management point of view and leaving the vehicle in free-wheeling is a fuel-friendly alternative. Coasting avoids the efficiency degradation of the

battery use, as a result of bidirectional power exchanges (charge, followed by a discharge) and allows the engine to be stopped for a longer time, not only during deceleration, but also at the beginning of the acceleration phase. Coasting feasibility depends on the vehicle self-deceleration possibility: if the resistive forces are not important enough, the free-wheeling may be too slow with respect to the real speed. The acceptance of the solution may be defined by limits on speed deviation, constraints on position (obstacles, stop points) and preservation of the total distance.

In Fig. 3.20 a different case study with a lower speed is introduced. This scenario details the configuration for which coasting may be unacceptable, in the presence of a deviation from 35 km/h to 45 km/h. In Fig. 3.21 simulations results are depicted and Table 3.3 summarizes the performances.

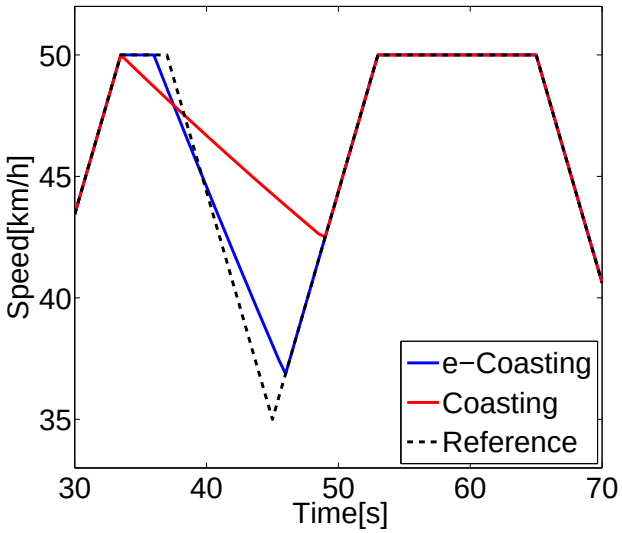

Fig. 3.20 – Speed profile of a basic low-speed case study with flat road. Comparison between coasting with recovery (blue) and baseline coasting (red)

Table 3.3 – Performance of the considered scenarios, speed from Fig. 3.20

Performance \ Scenario	e-Coasting	Coasting	Baseline
Consumption [L/100km] (final SOC)	5.46 (51.3%)	5.52 (54.52%)	5.76 (52.87%)
Distance[km]	0.69	0.7	0.695
RMS error speed [km/h]	0.55	2.05	0

In comparison to the previous case studies, similar observations can be made about the torque and the SOC evolution, but there is no longer an engine stop anticipation for the coasting, the electrical traction being initiated during the constant speed phase for the baseline strategy, too. The final SOC is not the same for the three strategies and hence, a fair comparison between them is not possible, but it can be noticed that e-coasting, with a slightly different speed trajectory, has the potential of improving fuel gain.

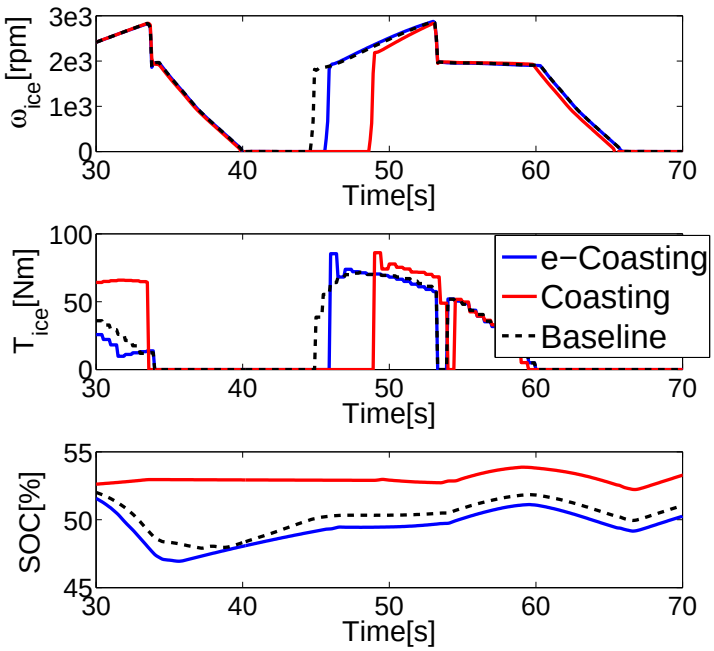

Fig. 3.21 – Simulation results for a basic low-speed case study with flat road: coasting with recovery (e-Coasting), coasting and baseline

In all the case studies, coasting is deactivated later than the e-coasting and therefore, it benefits from a fuel gain given by a reduced time of acceleration. It would be useful to compare the two approaches for a case when they are deactivated at the same instant and the engine is stopped during the same amount of time, as shown in Fig. 3.22 and 3.23.

The performance of each scenario is summarized in Table 3.4; the total distance is comparable, but the final SOC is slightly different, which makes the comparison between the consumption values a difficult task. It can be noticed that coasting and e-coasting have similar performances, with a small advantage for the latter. The difference not being significant, it is preferable to use recovery during coasting for the case when a fast deceleration is needed and basic coasting is too slow.

Coasting initiation influences therefore the driver demand and the speed profile, but also the MPC tuning factor. As shown in the previous section, the feedforward tuning term λ_{k0} is calculated as an average over a prediction horizon N_λ, by using the predicted wheel torque, which is zero during coasting. Engine torque and consequently, SOC trajectory, are different from the baseline case even before coasting activation, as observed for the representative case studies presented.

Next, an analysis is made for a similar speed profile depicted in Fig. 3.22 with the same coasting strategy, but with a constant feedforward term λ_{k0} within the MPC design. Consumption results with final SOC are summarized in Table 3.5 and engine speed, torque, as well as SOC trajectories are depicted in Fig. 3.24, 3.25 and 3.26. While for the first two case studies the final SOC is almost identical in the considered scenarios, the comparison between them becomes possible. Coasting shows an improvement of around 4% for the first case study and it outperforms e-coasting. A similar remark can be made about the second case study, with the difference that coasting will be conditioned in this case by the feasibility

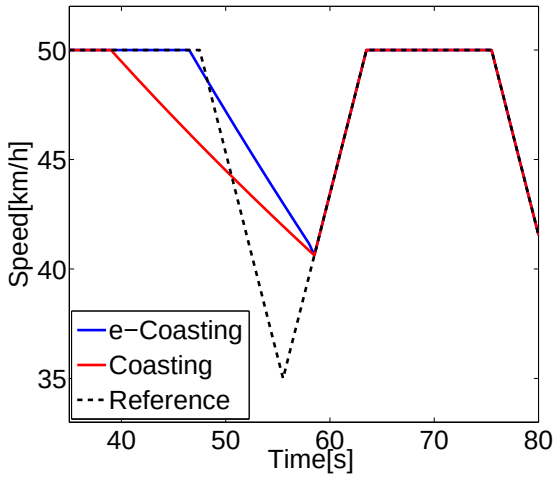

Fig. 3.22 – Basic case study, with coasting and e-coasting deactivated at the same time; speed profile

Table 3.4 – Performance for the considered scenarios, speed from Fig. 3.22

Performance \ Scenario	e-Coasting	Coasting	Baseline
Consumption [L/100km] (final SOC)	5.23 (55%)	5.28 (55.71%)	5.78 (56.7%)
Distance[km]	0.85	0.843	0.846
RMS error speed [km/h]	1.5	1.54	0

Table 3.5 – Normalized consumption [L/100km] and final SOC [%] for scenarios Fig. 3.16 and Fig. 3.20; constant feedforward tuning factor λ_{k0}

Case study \ Scenario	e-Coasting	Coasting	Baseline
Speed from Fig. 3.16	4.93 (48.57%)	4.8 (48.54%)	5.02 (48.63%)
Speed from Fig. 3.20	5.28 (48.47%)	5.12 (48.77%)	5.44 (48.4%)
Speed from Fig. 3.22	5.14 (50.57%)	4.71 (49.13%)	5.64 (51.94%)

from speed deviation perspective. The third case, whose purpose was to evaluate the performance when coasting and e-coasting are deactivated at the same instant, leads to a slightly different final SOC for the three scenarios, a comparison between them being less accurate. However, it can be observed that coasting exhibits a greater consumption gain due to a longer engine stop phase, as in Fig. 3.26. The e-coasting in this case does not shut-down the engine earlier, as in Fig. 3.23, because the tuning factor no longer decreases as a result of the energy recovery anticipation, but remains constant.

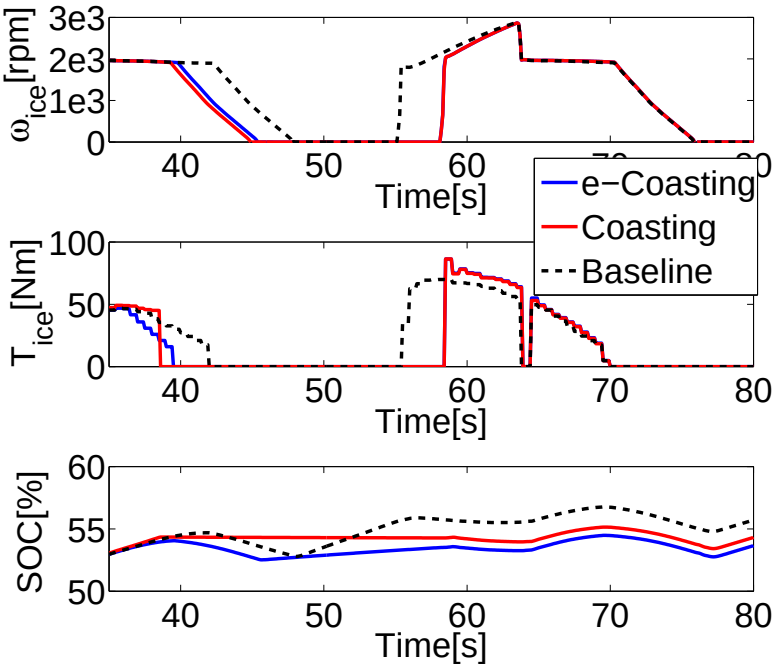

Fig. 3.23 – Basic case study, with coasting and e-coasting deactivated at the same time; simulation results

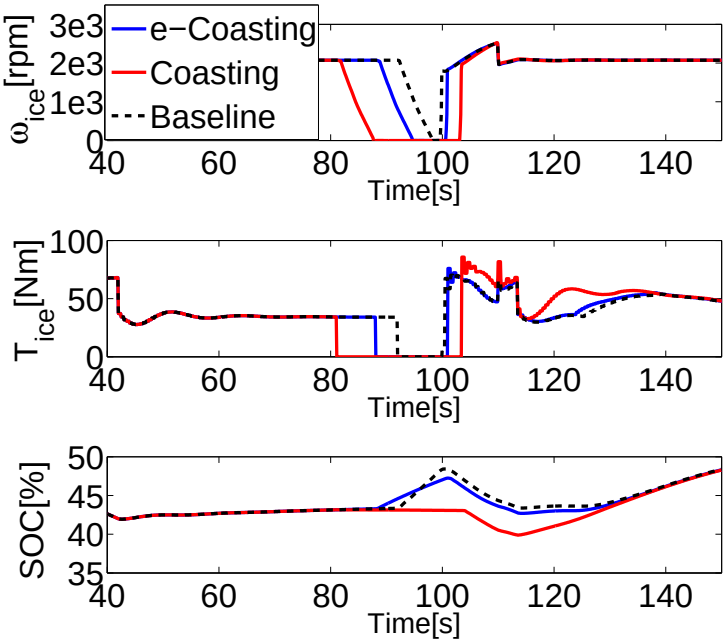

Fig. 3.24 – Simulation results for case study Fig. 3.16 with constant feedforward tuning factor λ_{k0}

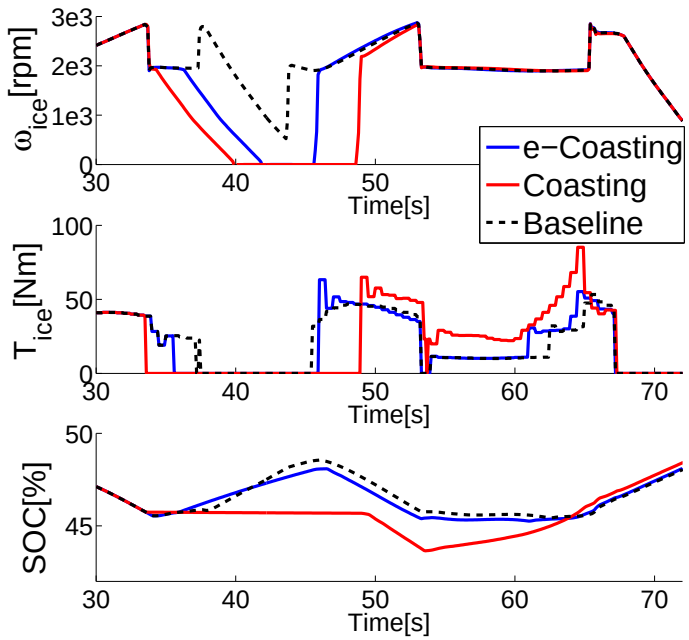

Fig. 3.25 – Simulation results for case study Fig. 3.20 with constant feedforward tuning factor λ_{k0}

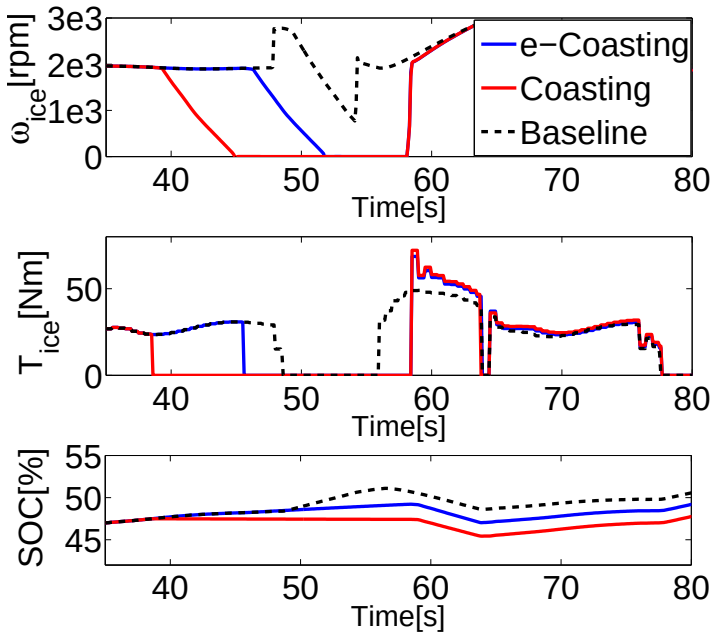

Fig. 3.26 – Simulation results for case study Fig. 3.22 with constant feedforward tuning factor λ_{k0}

5.2 Problem formulation and proposed solution

In [171] an analytical approach was introduced for coasting initiation, by writing the energy balance: work and kinetic and potential energy variation. The resistive forces expression however does not contain the viscous loss, only the dry friction and aerodynamic drag. Moreover, only the constant speed scenario is considered and therefore it is enough to evaluate speed deviation at the end of the coasting in order to decide the acceptance of the operation. In a general framework, with a variable reference speed as presented in the previous section, the speed evolution during coasting needs to be explicitly considered at each time step or position. In [173], analytical expressions for speed and distance as functions of time were provided and remain valid in the case of the present MPC design framework. Following the notations from the aforementioned paper, free-wheeling equation can be expressed as:

$$-\frac{\delta}{g}\frac{dv}{dt} = a + bv + cv^2 \tag{3.59}$$

$$\delta = 1 + \frac{nI_w + I_d}{m_v R_w^2} \tag{3.60}$$

where n - number of wheels, I_w - inertia of one isolated wheel, I_d - driveline inertia and a, b, c represent the coefficients of the resistive forces from (1.1), divided by the vehicle weight $m_v g$. The following calculations are valid under the assumption that these coefficients are constant, which implies a road with piecewise-constant slope.

If expression (3.59) is inverted, then: $-\frac{g}{\delta}dt = \frac{1}{a+bv+cv^2}dv$. The coasting time can therefore be directly extracted:

$$-\frac{gc}{\delta}T = \int \frac{1}{\frac{a}{c} + \frac{b}{c}v + v^2}dv \tag{3.61}$$

Let:

$$\begin{aligned} B &= \frac{g}{2\delta}\sqrt{4ac - b^2}, \quad h = \frac{gb}{2\delta} \\ \beta &= \arctan\left(\frac{1}{B}\left(\frac{g}{\delta}cv + h\right)\right) \end{aligned} \tag{3.62}$$

The nominator can be expressed as:

$$\frac{a}{c} + \frac{b}{c}v + v^2 = \left(v + \frac{b}{2c}\right)^2 + \left(\frac{\sqrt{4ac - b^2}}{2c}\right)^2$$

By using:

$$\int \frac{1}{(x+a)^2 + b^2}dx = \frac{1}{b}\arctan\frac{x+a}{b}$$

relation (3.61) becomes:

$$-\frac{gc}{\delta}T = \frac{2c}{\sqrt{4ac - b^2}}\arctan\frac{v + \frac{b}{2c}}{\frac{\sqrt{4ac-b^2}}{2c}}$$

With the notations introduced earlier, the coasting time T_{coast} between speed v_1 and v_2 is given by $T_{coast} = \frac{\beta_1 - \beta_2}{B}$.

By noting $T = T_{coast} - t$, the speed evolution in time in the new coordinates is:

$$v(T) = \frac{\delta}{gc}\left[B\tan\left(BT + \beta_2\right) - h\right] \tag{3.63}$$

which gives for $t = 0$, $v = v_1$ (speed at the start of coasting) and for $t = T_{coast}$, $v = v_2$ (speed at the end of coasting).

The evolution in time of the position can be determined by integrating the speed expression. By using $\int \tan x dx = -\ln(\cos x)$, we have:

$$d(T) = \frac{\delta}{gc}\left(ln\frac{\cos\beta_2}{\cos\left(BT + \beta_2\right)} - hT\right) \tag{3.64}$$

In the current MPC framework, the decision of coasting is taken after the evaluation of a cost function that includes the speed deviations in time. This maximizes the coasting time T_{coast} and ensures that at the end of the coasting, the vehicle speed is close to reference speed (and thus, avoiding a strong compensation from the driver model, that will result in an additional fuel consumption). Two approaches are proposed. Let t_{k_1}, t_{k_2} denote the moment of coasting start and stop, respectively and therefore, $t_{k_2} = t_{k_1} + \frac{T_{coast}}{\Delta t_{opt}}$; v_{ref} the reference speed and $\Delta v\left(t_k\right) = v\left(t_k\right) - v_{ref}\left(t_k\right)$.

The first cost function has the following expression:

$$J_1\left(t_{k_1}, t_{k_2}\right) = \alpha\Delta v(t_{k_2})^2 + \beta\frac{1}{T_{coast}^2} + \frac{1}{N_t}\sum_{t_k=t_{k_1}}^{t_k=t_{k_2}-1}\Delta v(t_k)^2 \tag{3.65}$$

where $N_t = t_{k_2} - t_{k_1} - 1$.

The second cost function considers the cumulative speed error during coasting, relative to the reference speed, but not for the final speed deviation, too. The purpose is to assign important penalties to variations at lower speeds (a deviation from 90 km/h to 80 km/h is acceptable, whereas from 50 km/h to 40 km/h may not be possible), but at the end of the coasting, it is necessary to have a speed as close as possible to the reference, regardless of its order of magnitude.

$$J_2\left(t_{k_1}, t_{k_2}\right) = \alpha|\Delta v(t_{k_2})| + \beta\frac{1}{T_{coast}} + \frac{1}{N_t}\sum_{t_k=t_{k_1}}^{t_k=t_{k_2}-1}\Delta v(t_k)\frac{\Delta v(t_k)}{v_{ref}(t_k)} \tag{3.66}$$

Differences between the results given by the two cost functions are depicted in Fig.3.27 and 3.28. It can be noticed that the second cost function avoids coasting initiations at low speeds (Fig. 3.27, upper left corner) as a result of using the relative error.

Cost function evaluation

Coasting initiation relies on three aspects:

- start of coasting (t_{k_1})
- end of coasting (t_{k_2})
- validation of the solution acceptance (value of $J_i, i \in \{1, 2\}$)

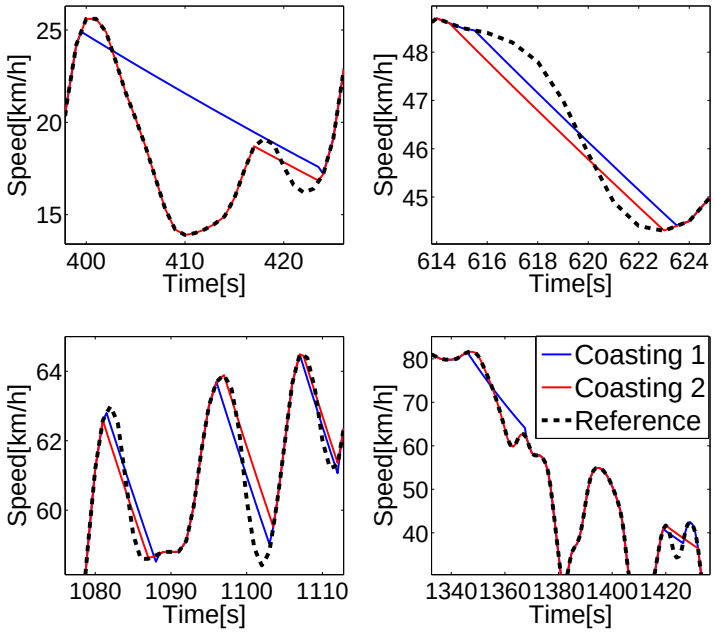

Fig. 3.27 – Comparison between the speed profiles given by J_1 and J_2; speed profile - WLTC

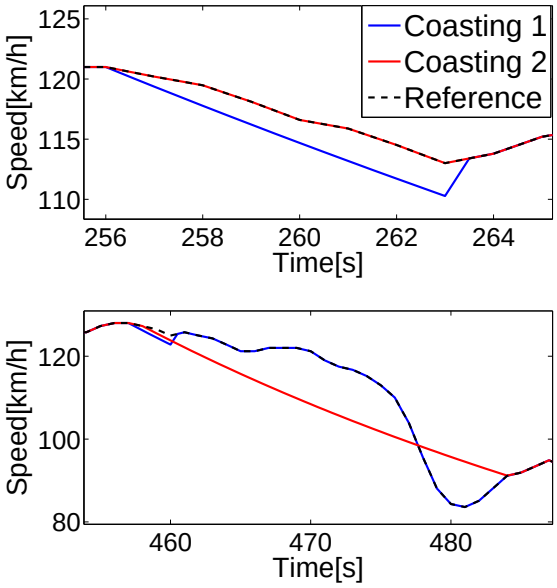

Fig. 3.28 – Comparison between the speed profiles given by the 2 cost functions; speed profile - Artemis highway

Given a road preview of length N_{coast}, the first step is the detection of potential coasting initiation. As shown in the previous subsection, the target scenarios are described by a deceleration, followed immediately by an acceleration. Hence, a check is performed on the acceleration sign change in 2 consecutive steps, from negative to strictly positive. The coasting should therefore be initiated the latest at the start of deceleration ($t_{k_1}^{max}$). An early start is also possible, for constant speed phases or with only minor variations. Therefore, $t_{k_1} \in \left[t_{k_1}^{min}, t_{k_1}^{max}\right]$, where the lower bound is several steps ahead the upper limit. The next aspect is the end of coasting, which has a lower bound given by the duration of deceleration. Strong accelerations and decelerations are *a-priori* penalized.

The cost function J_1 or J_2 is evaluated by varying t_{k_1} and t_{k_2} between their lower and upper bounds. The values of t_{k_1} and t_{k_2} that correspond to the minimum are retained, provided the solution is acceptable, by comparing the minimal value with a pre-defined threshold (in order to avoid large speed deviations). The following thresholds for the cost functions have been empirically chosen:

$$J_1^{thr} = \left(\frac{5}{3.6}\right)^2 + \alpha\left(\frac{1}{3.6}\right)^2 + \beta\left(\frac{1}{T_{coast}^{min}}\right)^2 \tag{3.67a}$$

$$J_2^{thr} = 0.1 + \alpha\frac{1}{3.6} + \beta\frac{1}{T_{coast}^{min}} \tag{3.67b}$$

For J_1, this threshold value indicates that an average speed deviation of 5 km/h is preferable (expressed in m/s), whereas for J_2 the term 0.1 is related to an average relative deviation. In both cases, a final speed error of 1 km/h is desired.

A synthesis of this method is given by algorithm 1, whose notations refer to Fig. 3.29. The cost functions J_1 and J_2 dependence on different starting points and coasting durations is depicted in Fig. 3.30 and 3.31, respectively. The tuning terms were chosen $\alpha = 2, \beta = 1$ for J_1 and $\alpha = 0.7, \beta = 0.2$ for J_2. Both give similar results, the best performances being obtained for an initiation at $t_{k1} = 120$s and a coasting duration of 13s i.e. a stop point at $t_{k2} = 133s$, as trajectory (3). Close results can be obtained for an earlier initiation at $t_{k1} = 118.5$s, but with a reduced coasting duration of only 8s (trajectory (1)) or for $t_{k1} = 119.5$ and $t_{k2} = 127$s (trajectory (2)). A longer duration for these starting points would give a speed trajectory with a more important deviation from the reference, due to the acceleration around 128s, which explains the increase in the cost functions for coasting times superior to 9s for early starts. Moreover, it was noticed that for $\beta = 0$ i.e. no maximization of the coasting time, the best value given by J_1 is trajectory (2).

If the cost function evaluation at each point is to be avoided, an approximation based on Gauss quadrature can be an alternative solution. This method is used to approximate the integral of a function, by using a decomposition in basic functions and evaluate them at some specific points between the domain of integration. It can provide reliable results if the initial function can be accurately approximated by a polynomial. Therefore, if a piecewise polynomial approximation for the reference speed can be found, then the aforementioned exhaustive research can be replaced with a faster evaluation in a reduced number of points.

By summing up all the analysis conducted in the present section, coasting should be excluded from the basic MPC-based energy management and its management should be handled at the supervisory level, as in Fig. 3.17. This choice is dictated by several reasons:

- the two problems do not operate with the same prediction horizons ($N_{coast} > N_{mpc}$) and therefore, a time-scale separation needs to be performed
- coasting activation implies a modified driver behavior, which is situated by design at a supervisory level, the MPC structure receiving as input the actual wheel torque demand and the foreseen values

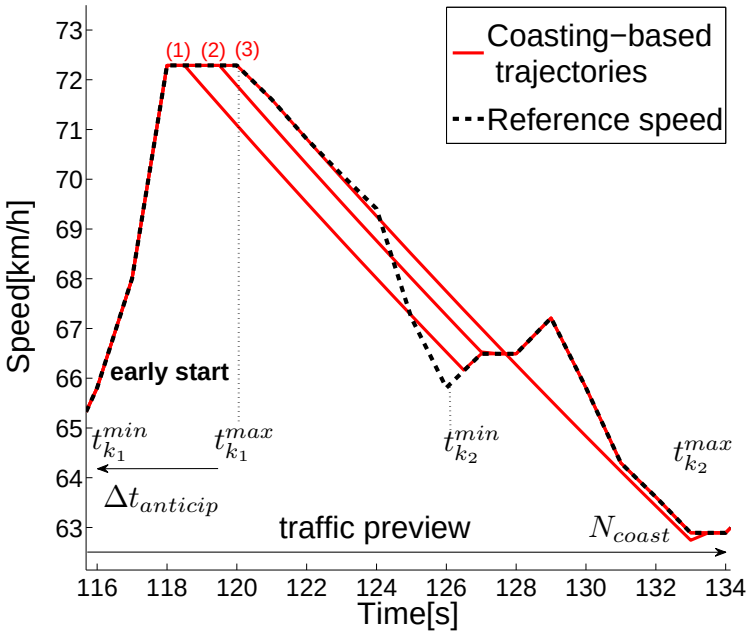

Fig. 3.29 – Example of coasting trajectories for different starting points

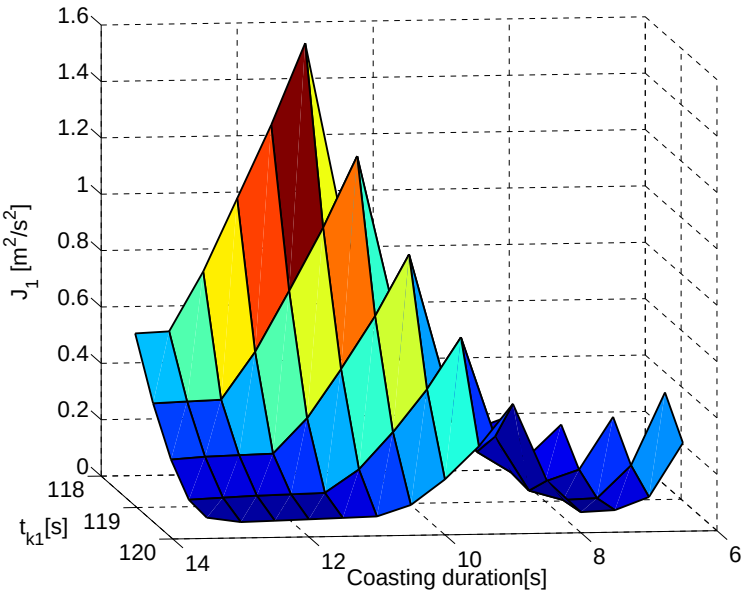

Fig. 3.30 – Cost function J_1 for case study from Fig. 3.29

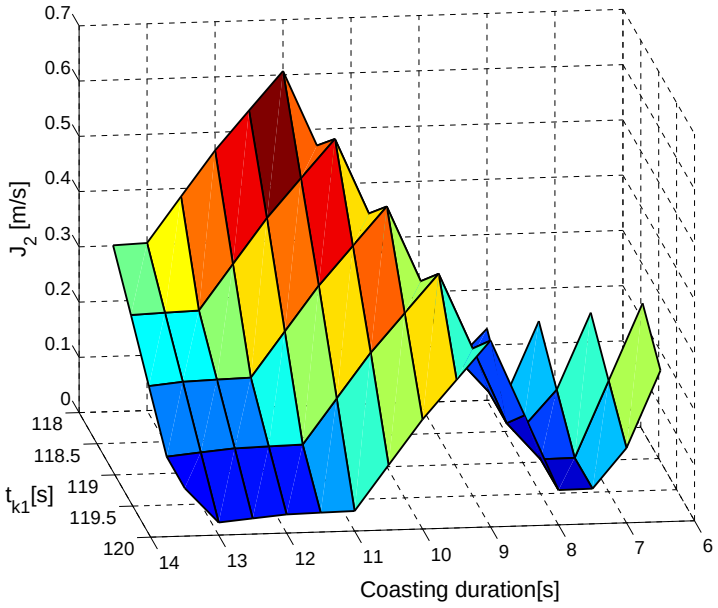

Fig. 3.31 – Cost function J_2 for case study from Fig. 3.29

Algorithm 1 Coasting activation

Require: Predicted vehicle speed $v(k : k + N_{coast})$

Find t_k s.t. $a(t_k) < 0 \quad \& \quad a(t_k + 1) > 0$
$t_{k_2}^{min} \leftarrow t_k$
$t_{k_2}^{max} \leftarrow k + N_{coast}$
Find $\min t_k$ s.t. $a\left(t_k : t_{k_2}^{min}\right) < 0$
$t_{k_1}^{max} \leftarrow t_k$ *% beginning of deceleration*
$t_{k_1}^{min} \leftarrow t_{k_1}^{max} - \Delta t_{anticip}$ *% early start of coasting*
for $t_{k_1} = t_{k_1}^{min}$ to $t_{k_1}^{max}$ **do**
  for $t_{k_2} = t_{k_2}^{min}$ to $t_{k_2}^{max}$ **do**
    calculate $J(t_{k_1}, t_{k_2})$
  end for
end for
Find t_{k_1}, t_{k_2} s.t. $J(t_{k_1}, t_{k_2}) = \min J$
if $\min J \leq J^{thr}$ **then**
  $T_w^{pred}(t_{k_1} : t_{k_2}) = 0$ *% update of torque prediction*
  if $t_{k_1} = k$ **then**
    pedal release *% change in driver request*
  end if
else
  no coasting initiation
end if

- under the assumption that the predictive control problem had not the aforementioned hierarchical structure (i.e. simultaneous optimization of the torque split and of the vehicle speed), the problem would be formulated in a *hands-off control* framework [174]. This implies however the use of a non differentiable cost and hence, a bi-level optimization is necessary.

6 Conclusions

In this chapter, a comprehensive model predictive control-based energy management strategy was proposed, which handles the torque distribution and the engine stop-start feature. The problem was constructed as a standard QP form, which allows an efficient implementation. The main contribution from a problem formulation perspective is the introduction of the stop-start functionality without the use of a binary decision variable, but rather as a model-based *a-posteriori* rule. Moreover, the calculation of a sequence of commands allows an anticipation of engine start, for speed tracking improvement.

Another contribution is related to the tuning mechanism, which is a crucial aspect in the MPC. A predictive adaptation of the équivalence factor was proposed, leading to a two-layer predictive control strategy: an upper layer that handled the tuning and exploited preview information over a certain horizon, and a low layer for the MPC controller that used a shorter horizon, which is suitable for real-time implementation, as well as for reducing the impact of inaccuracies of the linearized prediction model. A frequency analysis was employed to define an indicator of the aggressiveness content of the drive cycle over the tuning horizon and providing therefore a tool to determine the horizon value that ensures a trade-off between transient and average behavior.

Finally, an analytical method for coasting was proposed, with an evaluation for specific case studies. The algorithm provides the time of coasting initiation and its duration, as well as an indicator of the acceptance of the solution. This was made possible by the definition of a cost function which included the speed deviation from the reference during coasting, with a special penalty for the deviation at the end of coasting, in order to avoid high compensations from the speed regulator, as well as a term that maximizes the duration of coasting.

Dans ce chapitre, une stratégie de gestion d'énergie basée sur *model predictive control*, qui gère la distribution de couple et stop-start moteur a été proposée. Le problème a été construit sous une forme QP, qui permet une implémentation efficace. La contribution principale d'une perspective formulation du problème est l'introduction de la fonctionnalité stop-start sans l'utilisation d'une variable de décision binaire, mais comme une règle *a-posteriori* à la base de modèle. De plus, la calcul d'une séquence des commandes permet l'anticipation du démarrage moteur, pour une amélioration du suivi de vitesse.

Une autre contribution est liée au mécanisme de calibration, qui est un aspect crucial dans le MPC. Une adaptation prédictive du facteur d'équivalence a été proposée, conduisant à une structure de contrôle double-niveau : un niveau supérieur qui gérait la calibration, en exploitant les données prédictives sur un certain horizon, et un niveau inférieur, avec un horizon plus court, souhaitable pour l'implémentation en-ligne, ainsi que pour réduire l'impact des imprécisions du modèle linéarisé. Une analyse fréquentielle a été employée pour définir un indicateur du contenu d'agressivité du cycle de conduite sur l'horizon de calibration, fournissant donc un outil pour déterminer la valeur de l'horizon qui assure un compromis entre le comportement transitoire et celui moyen.

Dernièrement, une méthode analytique pour le coasting a été proposée, avec une évaluation pour des études de cas spécifiques. L'algorithme fournit l'instant pour l'initiation du coasting, sa durée et un indicateur pour l'acceptabilité de la solution. Ceci a été rendu possible par la définition d'une fonction

coût qui inclut l'écart entre la vitesse cible et celle pendant le coasting, avec une pénalité particulière pour la déviation à la fin, afin d'éviter les compensations élevées du régulateur de vitesse, ainsi qu'un terme qui maximise la durée du coasting.

Chapter 4

Model-in-the-Loop validation

The static model and the control strategy presented in the previous chapters are validated on a parallel mild hybrid, with a dual-clutch transmission and one electric machine connected to the even primary shaft. Simulations are carried out for different scenarios in a Model-in-the-Loop framework, in Matlab/Simulink environment. The vehicle behavior is simulated by a high-fidelity model, designed in AMEsim, where slow and fast dynamics are handled.

The simulations are performed on 4 drive cycles, where urban driving phases predominate: NEDC, FTP-75, Artemis urban and Traffic jam. The proposed energy management algorithm is organized as a two-layer predictive strategy and therefore the validation procedure will consider this separation. First, the influence of the tuning horizon is addressed and explained through the frequency analysis introduced in the previous chapter. Next, for a fixed tuning, the influence of the MPC horizon is analyzed, showing that an increase leads to an improvement in the fuel gain is due to the engine stop-start. A comparison is also made with a PMP-based method, implemented offline and which often serves as a benchmark solution.

The control law needs real-time estimations of the battery SOC and engine torque, which cannot always be accurately determined. Therefore, a robustness analysis with respect to these estimations is performed. All the simulations are carried out for a fixed sizing, but it would be useful to validate the robustness of the tuning strategy with respect to battery size. The road grade is another important element, but standard drive cycles do not include information about it. Here, basic case-studies with constant speed and variable slope are considered and the main focus is on the influence of the tuning factor. A comparison between the adaptation of the feedforward component (via the tuning horizon) and the feedback (via the SOC setpoint) is performed.

Le modèle statique et la stratégie de contrôle présentés dans les chapitres précédents sont validés sur un mild *hybride parallèle, avec une transmission double embrayage et une machine électrique connectée sur l'arbre primaire paire. Des simulations ont été effectuées sur plusieurs scénarios, dans un cadre* Model-in-the-Loop*, dans l'environnement Matlab/Simulink. Le comportement véhicule est simulé par un modèle haute fidélité, conçu en AMEsim, qui gère les dynamiques rapides, ainsi que celles lentes.*

Les simulations ont été testées sur 4 cycles de conduites, où les phases urbaines sont prédominantes : NEDC, FTP-75, Artemis urbain et Traffic jam. L'algorithme de gestion d'énergie est organisé comme une stratégie prédictive double-niveau et par conséquent, la procédure de validation va prendre en compte cette séparation. Premièrement, l'influence de l'horizon de calibration est adressée et expliquée à travers l'analyse fréquentielle introduite dans le chapitre précédent. Ensuite, pour une calibration fixée, l'influence de l'horizon MPC est examinée, montrant qu'une augmentation de cette valeur conduit à une amélioration dans la consommation grâce à l'arrêt moteur. Une comparaison est également faite avec une méthode basée sur le PMP, implémentée offline et qui est souvent utilisée comme solution de référence.

La stratégie de contrôle a besoin des estimations en temps réel pour le SOC et le couple moteur, qui ne peuvent pas être toujours estimés avec précision. Par conséquent, une analyse de robustesse par rapport à ses estimations est effectuée. Toutes les simulations ont été faites pour un dimensionnement fixe, mais il serait utile de valider la robustesse de la stratégie de tuning par rapport à la capacité de la batterie. La pente est un autre élément important, mais les cycles standardisés n'incluent pas cette information. Cette thèse considère des études de cas élémentaires, avec une vitesse constante et pente variable et le but principal est l'influence du terme de calibration. Une comparaison entre l'adaptation de la composante feedforward (via l'horizon pour la calibration) et celle de feedback (via la consigne de SOC) est proposée.

1 Simulation framework

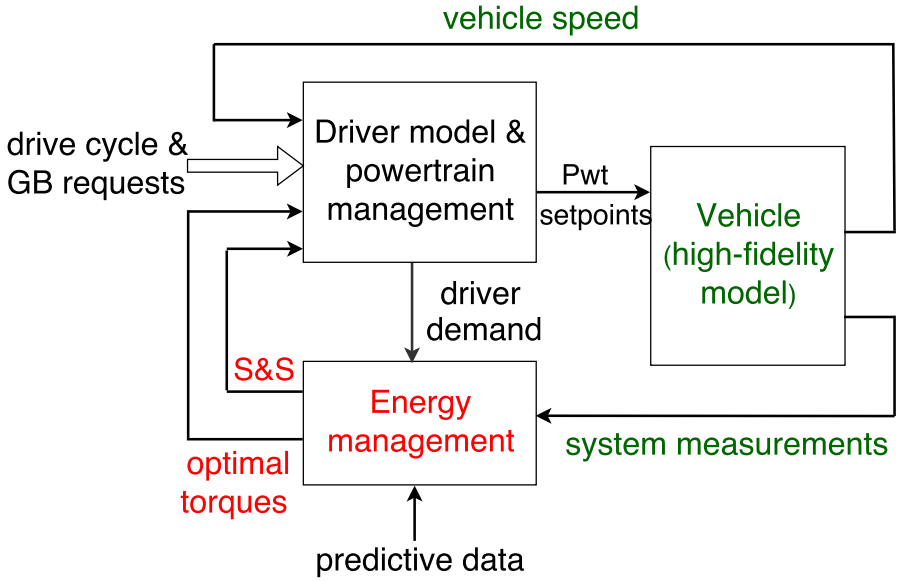

Fig. 4.1 – Simulation framework: basic representation with the 3 main components: the plant (vehicle), driver and powertrain management and the controller (energy management); *GB* - gearbox, *pwt* - powertrain

The proposed control strategy is validated in a Model-in-the-Loop environment, with a basic repre-

sentation depicted in Fig. 4.1, with the 3 main elements: driver and powertrain management, the plant (given by a high-fidelity model) and the energy management controller. A detailed description is given by Fig. 4.2, whose blocks are next introduced.

A *high-fidelity model* designed in AMEsim, validated independently of the control law, is used to simulate the vehicle behavior and it handles the slow and fast dynamics, as well. It provides the physical vehicle speed v_{veh}^{ame}, ICE and EM rotational speeds $\omega_{ice}^{ame}, \omega_{em}^{ame}$, the effective torques $T_{ice}^{ame}, T_{em}^{ame}$ and the battery state-of-charge SOC^{ame}.

A *driver model* ensures the speed tracking by providing the wheel torque demand T_w and the displacement of the accelerator and brake pedal. For the latter, it is assumed that the vehicle is equipped with a brake-by-wire technology which allows the distribution between the regenerative and mechanical braking. The rule of splitting is to use the electric machine as much as possible and dissipate the rest of energy. Therefore, in order to calculate the brake pedal displacement, the electric machine regenerative torque is needed. Moreover, the driver model can be disabled if coasting is active, see Fig. 3.17. As presented in Chapter 3, coasting implies no action from the driver, no pedal being pressed and hence, the speed tracking is deactivated.

The *ICE supervisor & coordinator* block handles the idle speed control and the transitions between the engine states, in order to appropriately address its transient behavior. It can be observed that it receives the start request, but also a manual start command (for safety reasons) that together form the starter signal. The block provides also the indicated torque T_{ice}^{ind}, calculated as the sum between the effective torque and the losses, which will be next used as an input in the high-fidelity vehicle model. The indicated torque contains also information about the engine stop decision; in this case, to reflect the fuel cut-off functioning, it takes a negative value equal to engine losses $T_{ice}^{ind} = -T_{ice}^{loss}$.

The driveline requests (gear numbers $R_{1,2}^{req}$ and clutches request $C_{1,2}^{req}$) are calculated outside the energy management controller, in the driveline supervision and management block, which receives the driver intention, the engine state, as well as the stop-start command. The driveline setpoints ($C_{1,2}^{sp}, R_{1,2}^{sp}$) are calculated from these requests after taking into account the stop-start command from the MPC controller and they are afterwards sent to the AMEsim model.

The energy management controller receives the current wheel torque demand and the driveline requests, the current SOC and ICE torque value (for the linearization at the operating point), as well as the number of steps after an ICE start ct_{ON} or an ICE stop ct_{OFF}. Moreover, predictive data from navigation system are exploited over a N_λ horizon. Coasting can also be implemented, by using traffic preview data and the anticipation of its activation influence the MPC tuning (the predicted wheel torque will be thus set to zero).

The high-fidelity vehicle model receives the powertrain setpoints i.e. the torque references for the components, the clutches and gear numbers references, as well as the brake pedal displacement, the starter command and the slope from the environment, when considered. Its outputs are the physical torque values (available at different levels; here, only the components torque are needed), the rotational speeds, the real-time vehicle speed, the battery SOC. This allows to validate if the proposed strategy, in spite of its simplifications, verifies the physical constraints and the speed tracking.

2 Case-study: hybrid dual-clutch transmission

One of the main contributions of the model defined in the second chapter was to cover hybrid configurations with a dual-clutch transmission (DCT). Here, a case-study of a hybrid passenger car with an EM placed at the primary shaft is considered, as in Fig. 4.3. The engine is a 1.2 L SI, whose fuel rate

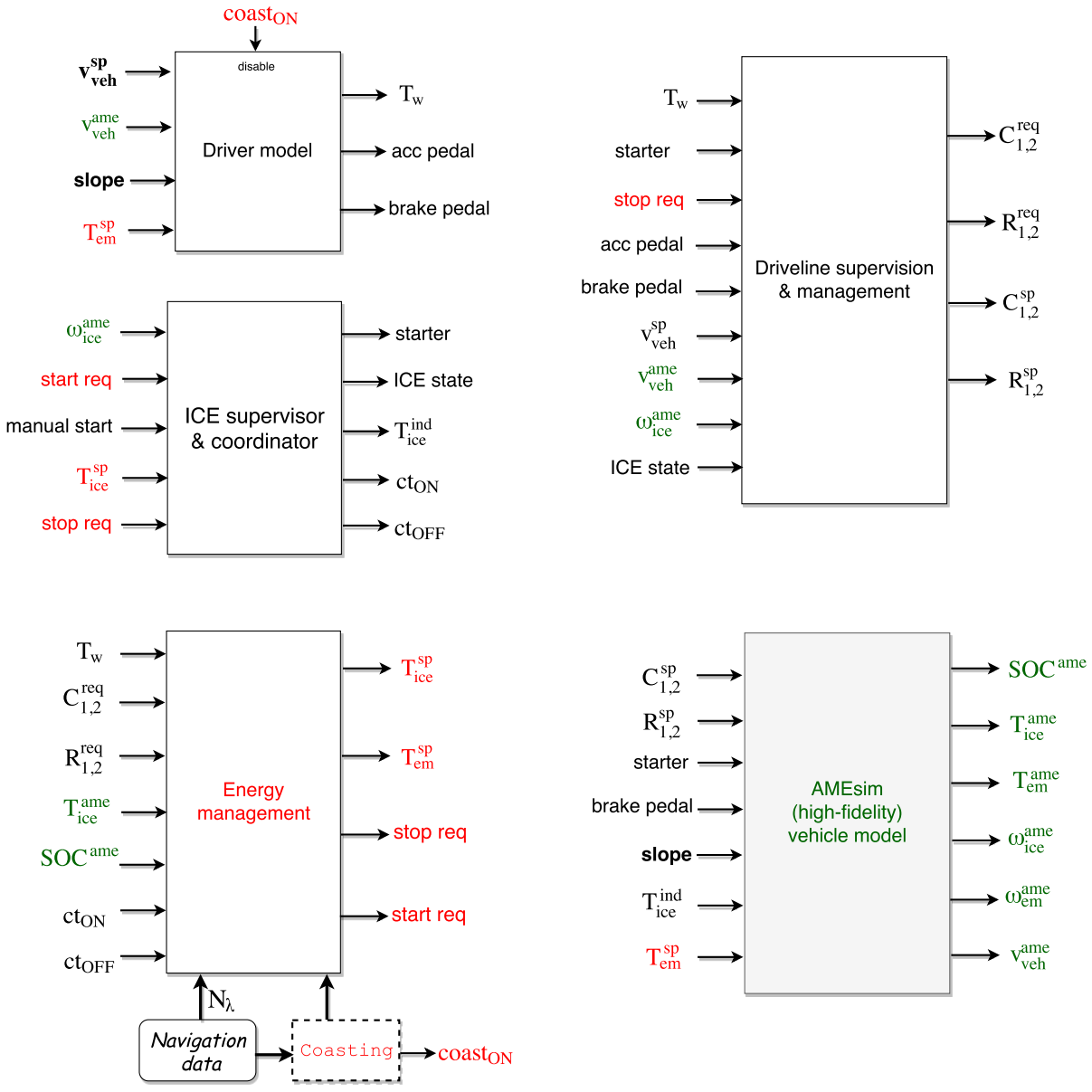

Fig. 4.2 – Validation framework - block representation; sp - setpoint, req - request, ind - indicated, acc - accelerator; green signals: output from the high-fidelity model; red: energy management controller, with a possible extension to coasting (dashed block); black: driver and powertrain management blocks (Driver model, Driveline supervision & management, ICE supervisor & coordinator); bold black signals: exogenous inputs (vehicle speed and slope)

and its corresponding PWL approximation are depicted in Fig. 2.17.

For a better understanding of the system and of the proposed model, Table 4.1 summarizes the clutches states with respect to potential functional modes.

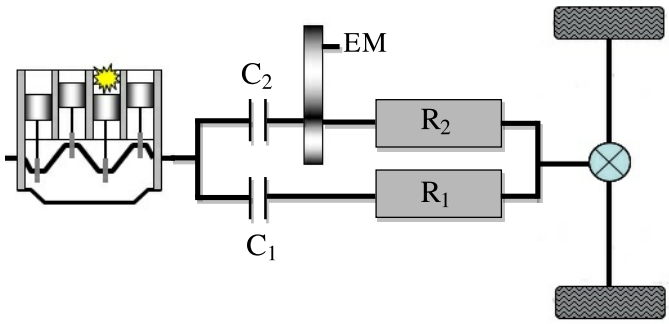

Fig. 4.3 – Case-study: hybrid DCT, with EM connected to the primary shaft

Table 4.1 – Hybrid DCT functional modes; $N_2 = \min(R_2, 1)$

C_1	C_2	N_2	*Case*
0	0	0	standstill, sailing
0	0	1	electric driving, regenerative braking
0	1	1	hybrid or conventional, even gear engaged
0	1	0	charge during standstill
1	0	0	conventional driving, odd gear engaged
1	0	1	hybrid driving
1	1	0	take-off, charge during driving (parallel mode)

Rotational speeds expression (2.4) are validated by comparing them with the values given by a high fidelity model (AMEsim), for several driving cycles: Artemis urban, road, highway NEDC and FTP-75. For the latter, the 10-minute standstill part was omitted, because the thermal analysis is beyond the scope of this work. The transient behavior of clutches having not been considered, inaccuracies appear especially in the case of components decoupling. Thus, the comparison is made with AMEsim corrected values ($\omega^{ame}_{ICE,EM}$), as in (4.1). In this way, the engine speed is instantaneously set to idle speed when decoupled ($C_1 + N_2 C_2 = 0$), because no engine stop was considered in this example, and EM speed is set to zero, when it is neither connected to the engine ($C_2 = 0$), nor to the wheel ($N_2 = 0$). If at least one of the terms C_2, N_2 is different from zero, ω^{ame}_{EM} value remains unchanged.

$$\omega^{ame}_{ICE} \leftarrow max\left(\omega^{ame}_{ICE}\left(C_1 + C_2 N_2\right), \omega_{idle}\right) \tag{4.1a}$$

$$\omega^{ame}_{EM} \leftarrow \omega^{ame}_{EM}\left(C_2 + N_2 - C_2 N_2\right) \tag{4.1b}$$

If the rotational speeds are directly calculated from the vehicle velocity, more than 98% of the values present a relative error inferior to 10%, for all the considered driving cycles. However, for a predictive control strategy, only the reference speed is available and in this case, the proposed model accuracy is affected by the driver model. The results are summarized in Table 4.3, where the RMSE for the speed tracking was also included. It can be seen that for all the cases the precision is superior to 85%, except for ω_{EM} from Artemis urban, but it corresponds to a high RMSE for vehicle speed.

3 Simulation results

All the simulations were carried out in the Matlab/Simulink environment introduced in the beginning of this chapter, on the DCT-based architecture from Fig. 2.5. The results are representative for a parallel hybrid architecture, without an external charging. As mentioned in state-of-the-art of Chapter 3, the case with a plug-in is usually handled separately and therefore, it will not be included in this simulation framework. The selected drive cycles are depicted in Fig. 4.4. It should be noted that the fuel consumption of a vehicle is usually expressed in L/100 km, commonly referred to as the normalized fuel consumption.

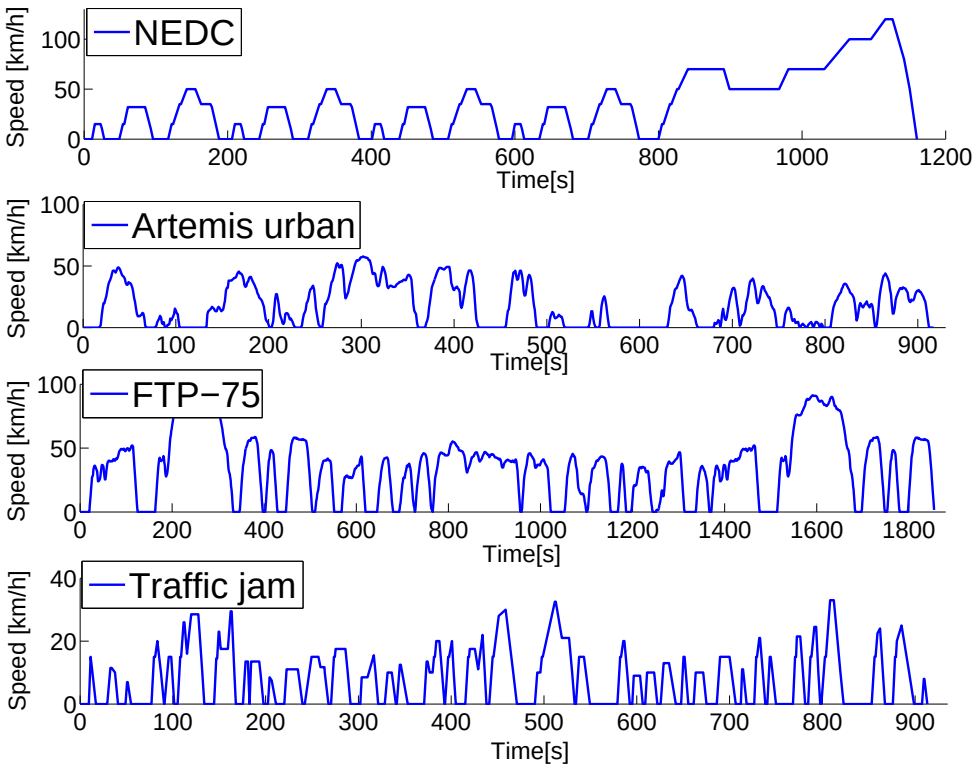

Fig. 4.4 – Speed profiles for the considered drive cycles

As introduced in Chapter 3, the energy management strategy relies on a double-layer predictive structure, with a long-term prediction horizon for tuning and a short-term for the MPC controller. In order

Table 4.2 – Percentage of points with relative error $\leq 10\%$, speeds calculated from v_{veh} AMEsim

Cycle	ω_{ICE}	ω_{EM}
Artemis road	98.1	91.8
Artemis urban	96.7	94.7
Artemis highway	98.8	99
FTP-75	96.7	96
NEDC	99.3	99

to evaluate the performance of the proposed MPC-based strategy, several aspects need to be analyzed:

- the influence of the upper layer prediction horizon, used for tuning
- the influence of the MPC control horizon
- the gain due to stop-start functionality
- robustness to torque and SOC estimation

3.1 Influence of the tuning horizon

First, the influence of the upper layer horizon N_λ is addressed, for an MPC control horizon of 5s which is long enough to include the stop-start decision. The longer the horizon, the smoother the tuning term λ_0 becomes, phenomenon depicted in Fig. 4.5, which presents the dependence of the standard deviation as a function of N_λ for different drive cycles. Fig. 4.6 depicts the ratio between the standard deviation and the average and it can be concluded that Artemis urban and Traffic jam are more aggressive than NEDC and FTP-75, which have a ratio inferior to 1. The evolution of λ_0 can be seen in Fig. 4.7, whereas the SOC trajectories for these values are depicted in Fig. 4.9, together with their SOC distance-varying limits.

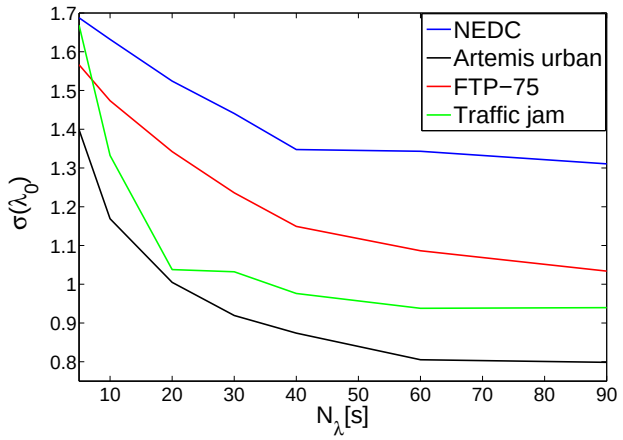

Fig. 4.5 – Standard deviation σ of the feedforward component λ_0 for different tuning horizons N_λ

Table 4.3 – RMSE for vehicle speed tracking and average speed

Cycle	RMSE v_{veh} [km/h]	$\overline{v}_{veh}$ [km/h]
Artemis road	1.96	60.2
Artemis urban	2.43	17.6
Artemis highway	1.53	97.7
FTP-75	1.73	34.1
NEDC	1.36	33.6

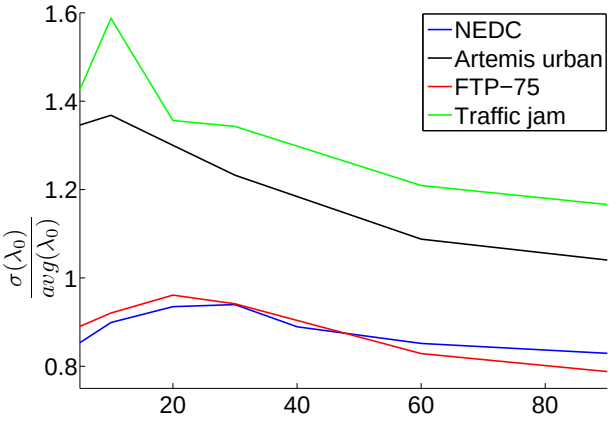

Fig. 4.6 – Ratio between standard deviation σ and average avg of the feedforward component λ_0 for different tuning horizons N_λ

The consumption sensitivity with respect to N_λ is illustrated in Fig. 4.8. NEDC shows a decrease in consumption until $N_\lambda = 40$s and then, an increase (final SOC is the same for all the cases). From Fig. 4.9 it can be observed that the SOC trajectories for $N_\lambda = 5$s and $N_\lambda = 10$s are characterized by large values of λ_0 which favor battery charging via the ICE, but without taking advantage of this energy buffer at a later stage. An appropriate balance is ensured by $N_\lambda = 40$s, which gives the best consumption results. For Artemis urban, $N_\lambda = 5$s gives the lowest normalized consumption, for a final SOC slightly greater than the one for the other horizons ($SOC_f = 52.58\%$ for $N_\lambda = 5$s vs $SOC_f = 51.15\%$ for the other values). FTP-75 shows an improvement up to 20s, and then a constant degradation, with a final SOC that slightly decreases starting with N_λ. For Traffic jam, an horizon of 10s provides the lowest consumption value, with a non-monotonic behavior for higher horizons.

These results can be interpreted through the aggressiveness analysis introduced in the previous chapter, based on the wheel power periodogram. From Fig. 3.11 it is possible to extract a limit for the upper layer horizon and its optimal value can be determined by empirically choosing the value of 0.5 for the ratio defined by (3.48), which would reflect the trade-off between average and transient behavior. This gives $N_\lambda = 40$s for NEDC, 5s for Artemis urban, 20s for FTP-75 and 10s for Traffic jam. The values are therefore around 30s, which is coherent with the current availability of accurate preview data.

3.2 Influence of the MPC horizon and of S&S

The tuning analysis in the previous section was carried out for a constant MPC horizon of 5s, with stop-start functionality included, which provided an optimal value of the upper horizon N_λ for each drive cycle. Here, for the corresponding optimal N_λ value, the control strategy performance is evaluated for two MPC horizons $N_{mpc} = 1$s and $N_{mpc} = 5s$, as well as two cases: with and without MPC-based S&S, respectively. A greater value for N_{mpc} would not be suitable due to the uncertainties resulting from model linearization, but also from wheel torque prediction: it is assumed that the vehicle speed, and therefore the wheel torque, are known for a given horizon, but the simulations being carried out with a driver in the loop, the future wheel torque cannot be perfectly predicted.

For this problem, the prediction and the control horizon are considered equal $N_p = N_c = N_{mpc}$. The cost of a restart was set to $t_{idle} = 2s$ and for all scenarios the engine is stopped for sequences

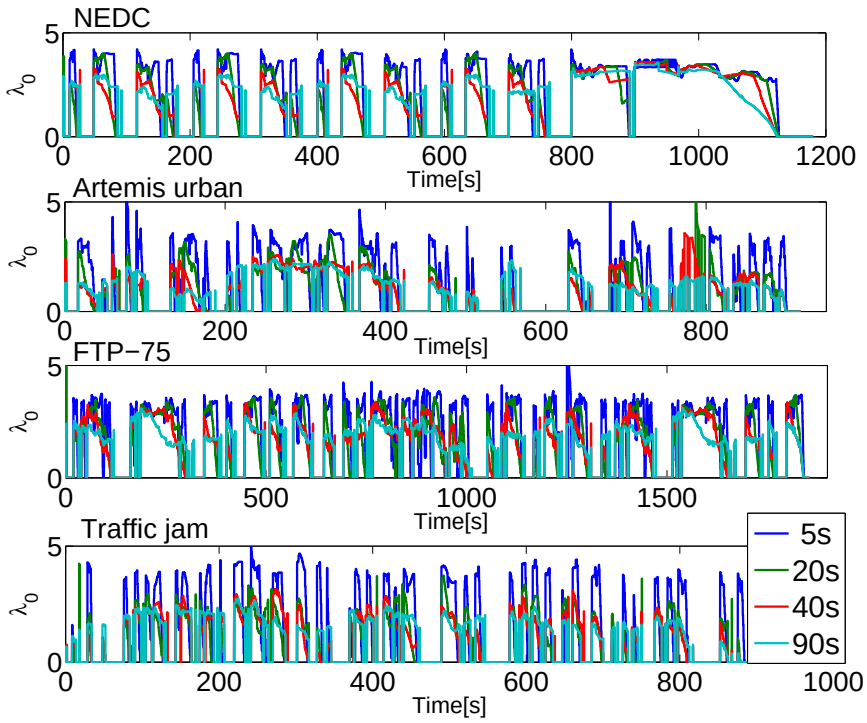

Fig. 4.7 – Evolution of the feedforward component λ_0 for different tuning horizons N_λ and drive cycles

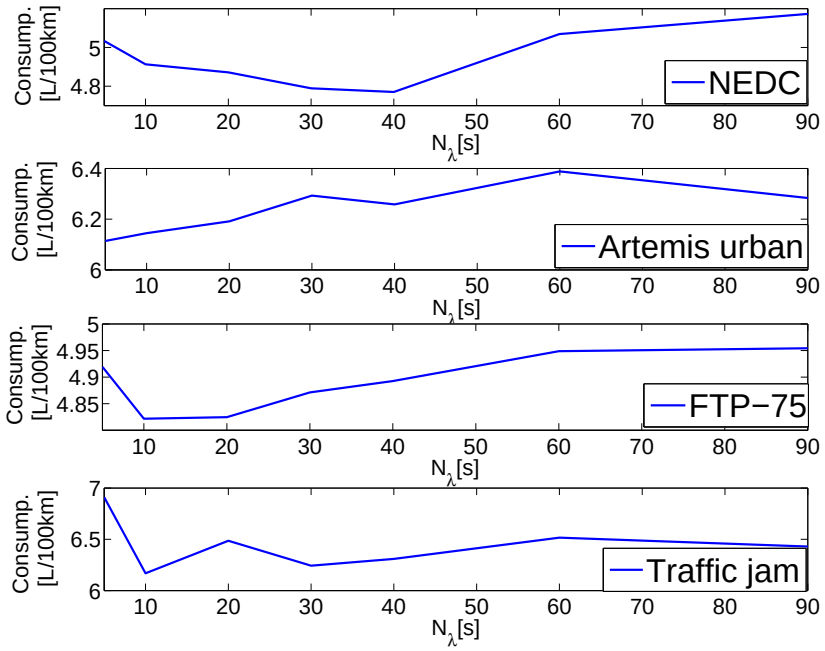

Fig. 4.8 – Evolution of the normalized consumption w.r.t. N_λ for different drive cycles

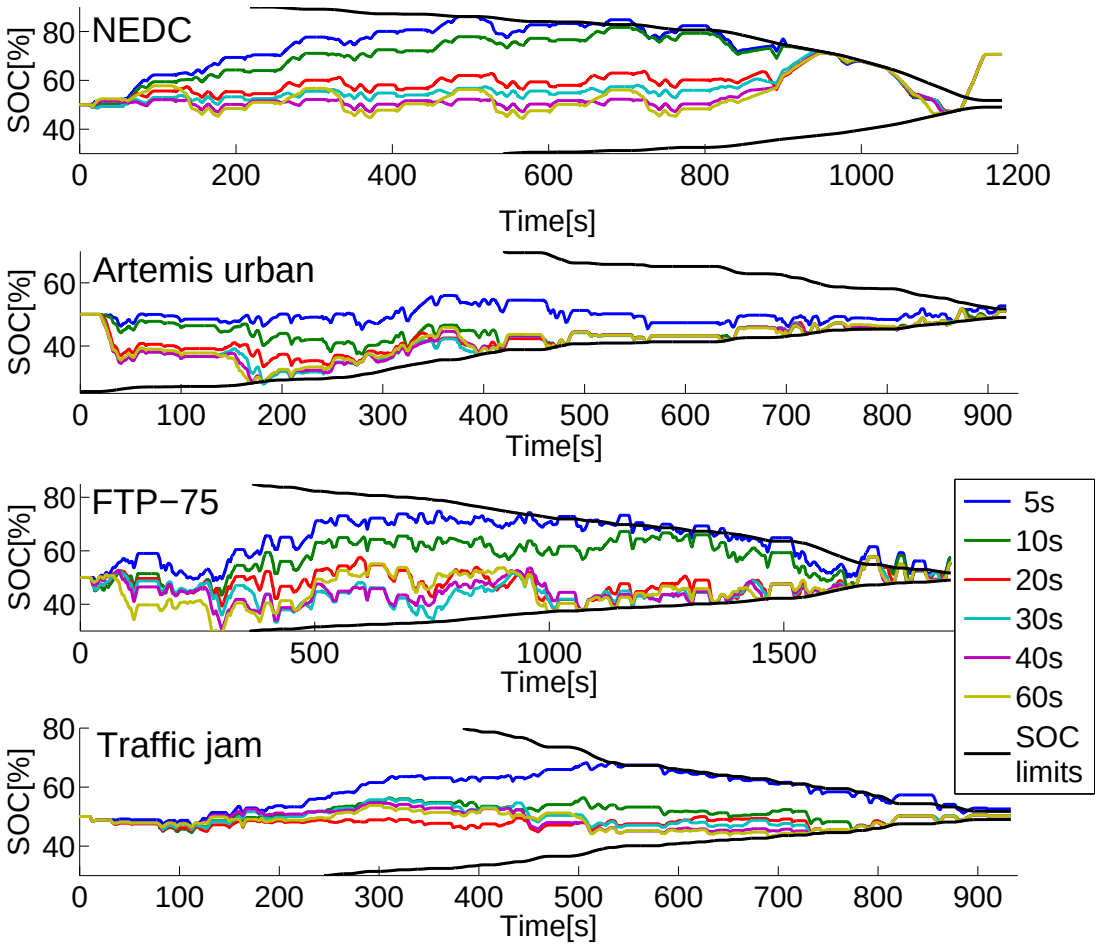

Fig. 4.9 – SOC trajectories for different tuning horizons N_λ; 4 drive cycles

of standstill or regenerative braking that last at least 2s. It is reminded that the preview information is considered available for an horizon of length N_λ (used for tuning), but the MPC controller uses only an horizon of $N_{mpc} \leq N_\lambda$.

From Table 4.4, where results are summarized, it can be concluded that a longer prediction horizon brings an improvement due to the engine stop decision. Indeed, the difference in consumption between the two values of N_{mpc} is virtually absent when the MPC-based engine stop is not considered. A longer N_{mpc} may improve the results if state constraints are active, but for the SOC this is the case only toward the end of the drive cycle, when the variation range becomes narrow.

Table 4.4 – Fuel consumption [L/100km] and final SOC[%] with MPC strategy

Strategy	MPC		MPC with S&S		
N_{mpc} / Cycle	1s	5s	1s	5s	Relative gain
NEDC	4.97 (70.03%)	4.96 (70.04%)	4.89 (70.03%)	4.76 (70.57%)	2.9%
Artemis urban	6.77 (52.88%)	6.76 (52.76%)	6.33 (53.33%)	6.11 (52.58%)	3.45%
FTP-75	5.06 (55.52%)	5.06 (55.4%)	4.93 (55.53%)	4.82 (55.16%)	2.23%
Traffic jam	7.65 (50.12%)	7.63 (50.32%)	7.03 (50.01%)	6.16 (50.32%)	12.37%

The parameters that interfere in the model-based stop decision (3.54) are $N_{stop} = 4$ (the optimization sampling time is $\Delta t_{opt} = 0.5$s), $T_{ice}^{thr} = 5$Nm and $N_{start} = 4$. An horizon of 5s is therefore long enough to include the engine stop. Intermediate values between 1s and 5s could have been tested as well, but the purpose of the study was to emphasize the benefit of engine stop, by using the longest possible accurate prediction.

The SOC trajectory, the engine speed and torque are compared for the two horizons in Fig. 4.10, 4.11, 4.12, 4.13 for NEDC, Artemis urban, FTP-75 and Traffic jam, respectively. It can be observed that the SOC trajectories are similar for the two N_{mpc} values, except for Traffic jam, where after almost 100s the SOC value drops for $N_{mpc} = 1$s and afterwards, the trajectories have a similar behavior. This is due to a problem of speed following for $N_{mpc} = 1$s that corresponds to a more important compensation demanded by the speed regulator and hence, a more important battery use.

Another observation that can be made about the influence of S&S is that a fuel gain already appears for $N_{mpc} = 1s$, even if it is less than the cost of a restart. This is due to the fact that once the engine is stopped (due to a regenerative braking or vehicle standstill) the strategy maintains the engine in the current state if the first command is inferior to the torque threshold value T_{ice}^{thr}, as depicted in Fig. 3.15. For a better understanding, Fig. 4.14 and 4.15 present the influence of MPC-based S&S for $N_{mpc} = 1s$, for sections of NEDC and Artemis urban. It can be noticed that for NEDC, around $t = 160$s the vehicle is braking (the engine is in fuel cut-off) and afterwards is stabilizing at constant low-speed.

The model-based S&S allows the engine to be stopped during this constant speed phase, improving thus the fuel gain. For Artemis urban (Fig. 4.15) the engine is kept shut off for low speed phases: around $t = 500$s, after a standstill phase and around $t = 800$s after braking, for instance.

In Chapter 3 it was mentioned that penalties on torque variations are introduced for those sequences

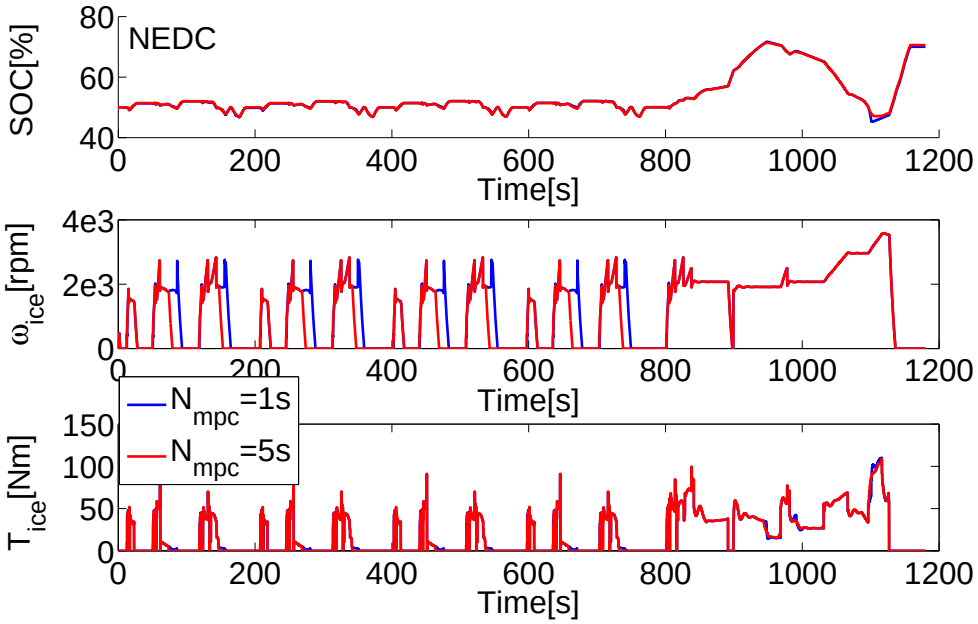

Fig. 4.10 – Comparison between $N_{mpc} = 1$s and $N_{mpc} = 5$s; NEDC

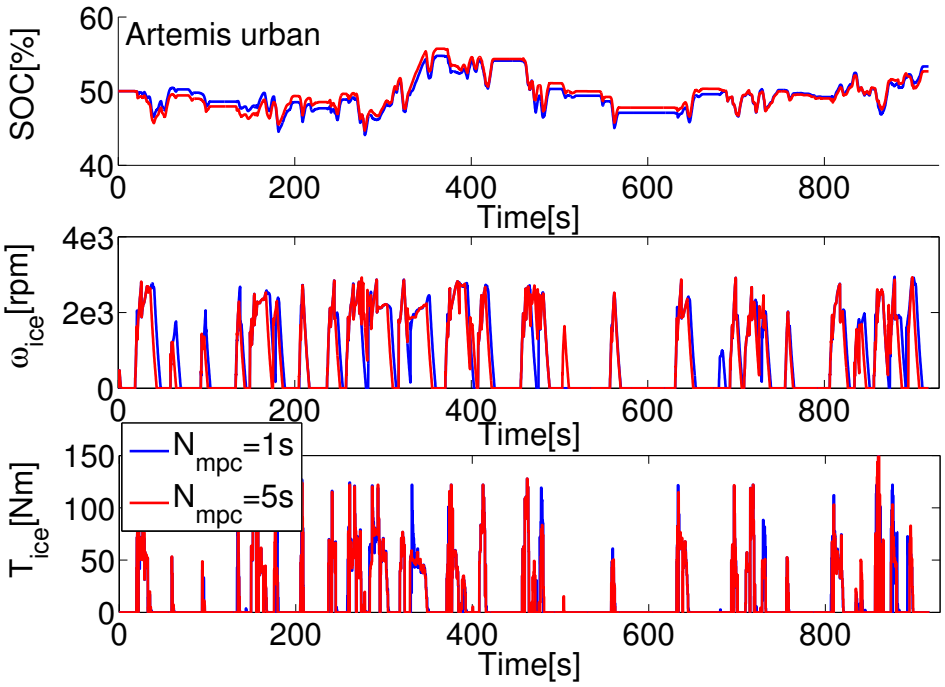

Fig. 4.11 – Comparison between $N_{mpc} = 1$s and $N_{mpc} = 5$s; Artemis urban

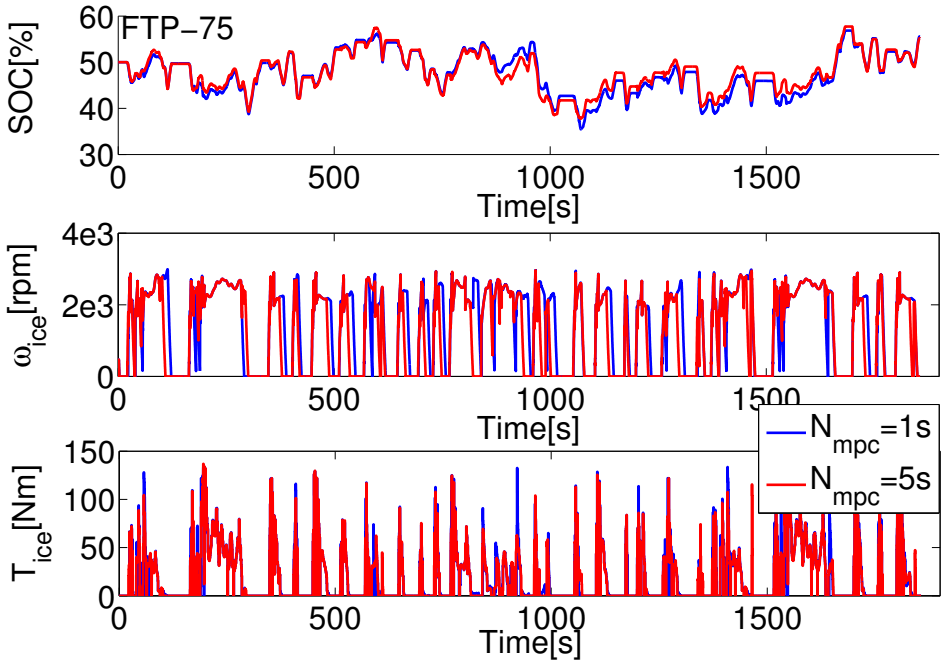

Fig. 4.12 – Comparison between $N_{mpc} = 1$s and $N_{mpc} = 5$s; FTP-75

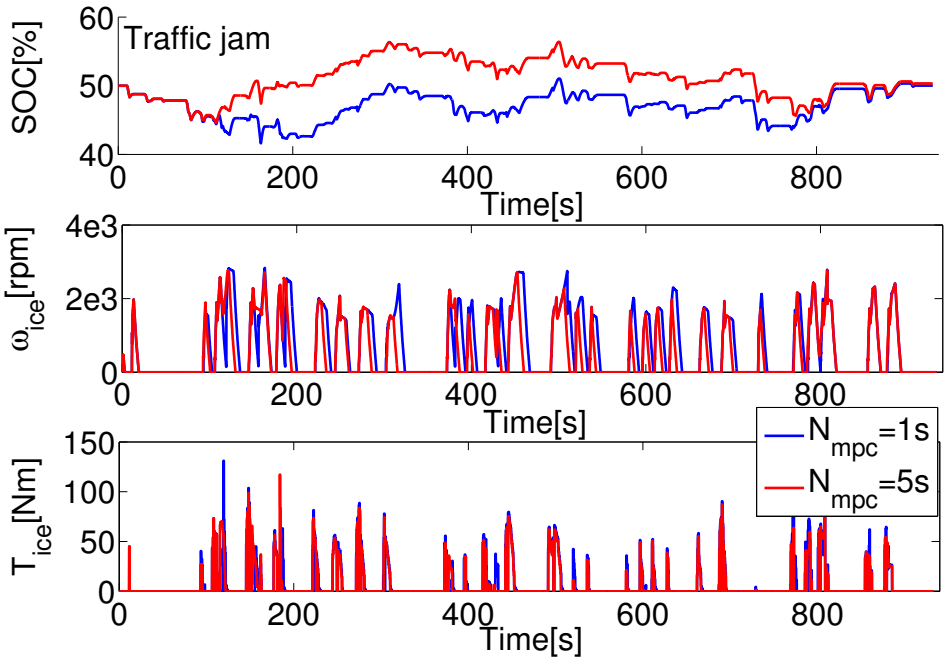

Fig. 4.13 – Comparison between $N_{mpc} = 1$s and $N_{mpc} = 5$s; Traffic jam

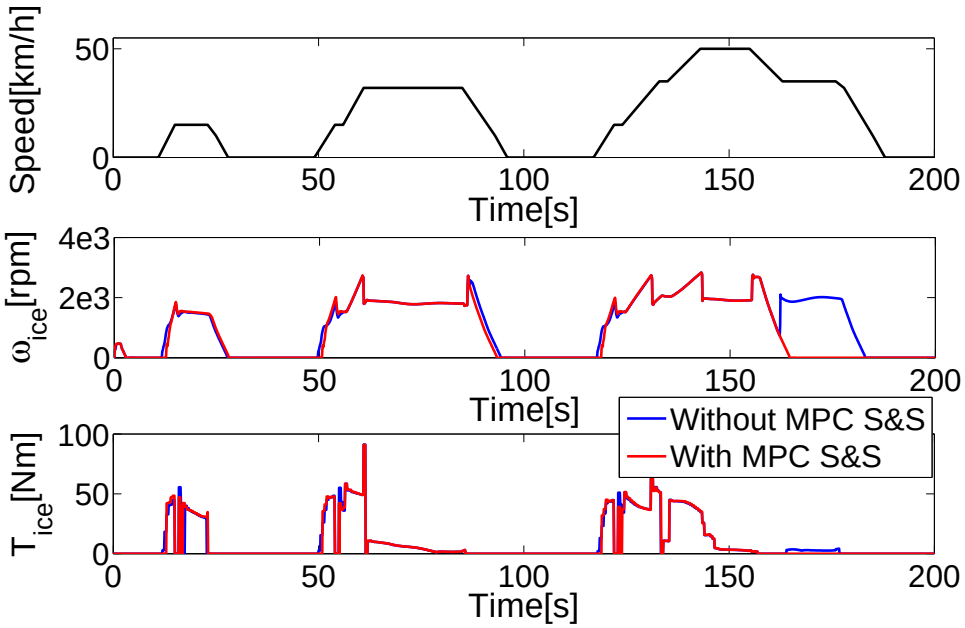

Fig. 4.14 – Comparison between MPC with and without S&S, $N_{mpc} = 1$s; NEDC, zoom

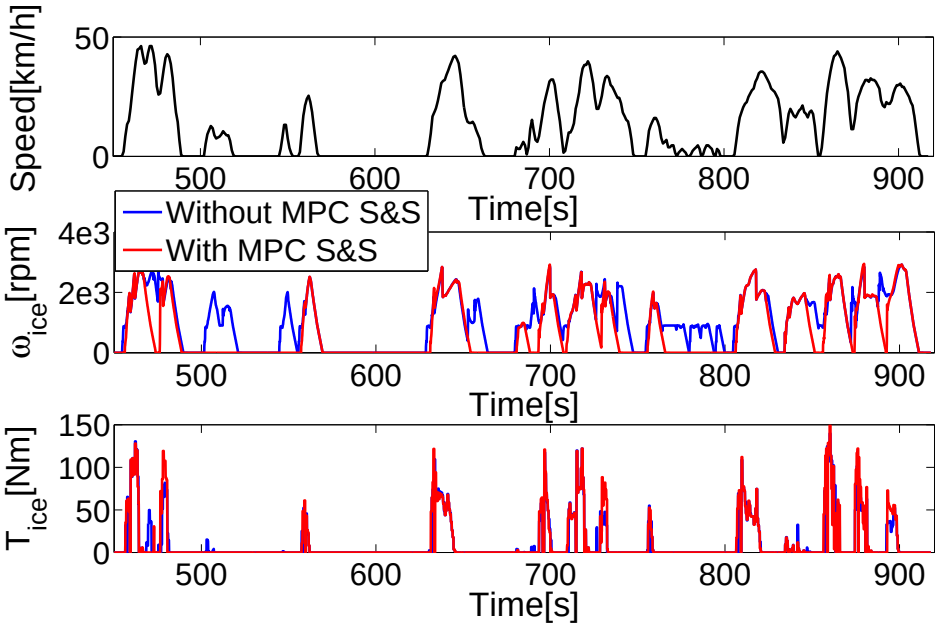

Fig. 4.15 – Comparison between MPC with and without S&S, $N_{mpc} = 1$s; Artemis urban, zoom

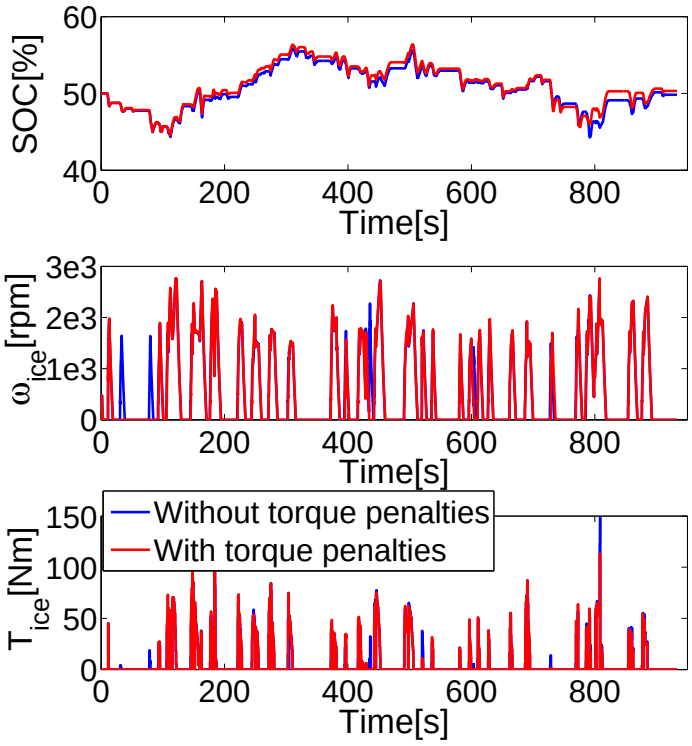

Fig. 4.16 – Traffic jam; influence of penalties on torque variations, as in (3.57)

for which the first consumption approximation region was assigned, as in (3.57). The purpose is to force all the sequence either toward zero, or toward higher torque values. Here, $R_{\Delta_k}(i,i) = 2$ was empirically chosen and found to provide good results, for each i that verifies the conditions from (3.57). In Fig. 4.16 the two cases (absence and presence of torque penalties) are confronted for Traffic jam, where an improvement in the engine stop decision can be observed especially at the beginning of the drive cycle. The fuel gain due to these penalties is of almost 1.5%: 6.25 L/100 km vs 6.16 L/100 km for an almost identical final SOC.

3.3 Comparison with offline method PMP

A comparison with a PMP - based method, as defined in (3.7), is summarized in Table 4.5, where for the MPC strategy the N_λ with the best consumption was retained. For the PMP -based method a constant equivalence factor was determined offline for each drive cycle such that the final SOC is identical to the one from the MPC trajectory, in order to make a fair comparison between the two strategies. At a first stage, PMP provides a torque distribution without considering the engine stop. From the ICE torque command, a stop signal is subsequently generated offline, for sequences of at least 2 seconds of zero torque. A new simulation is performed, with this ICE stop signal incorporated. The evolution of the SOC, engine speed and torque, as well as of the electric machine torque are compared in Fig. 4.17, 4.18, 4.19, 4.20 for the 4 considered drive cycles.

For NEDC, the main differences are observed for the extra-urban part, after $t = 800s$. The PMP -

Table 4.5 – Fuel consumption [L/100km] and final SOC[%], PMP and MPC with $N_{mpc} = 5$s

Strategy / Cycle	PMP	MPC	Relative difference
NEDC	4.5 (70.26%)	4.76 (70.57%)	5.77%
Artemis urban	5.61 (52.76%)	6.11 (52.58%)	8.9%
FTP-75	4.5 (55.74%)	4.82 (55.16%)	7.11%
Traffic jam	5.55 (50.12%)	6.16 (50.32%)	11%

based method provides a very aggressive torque around 850s and 1000s, time slots that correspond to constant speed of 70 km/h, where the optimal command is ON/OFF. Around 900s, PMP stops the engine, whereas MPC displaces the engine operating point and it provides a greater torque than necessary, the extra torque being used to charge the battery, which explains the difference in the SOC evolution for the 2 strategies. The MPC behavior is due to the choice of the cost function (3.20) that shifts the electrochemical power before using its square value. For cruising phases, this displacement term induces the tendency to charge the battery via the engine, rather than pure electric driving. This strategy is beneficial if torque assist is needed later, because it ensures an energy buffer. For NEDC, this advantage is less exploited, because toward the end of the drive cycle, there is an important phase of regenerative braking, the battery being therefore replenished. The relative difference between the 2 methods is however less than 6% for this drive cycle. More important deviations are noticed for urban profiles.

Table 4.6 contains the standard deviation for the engine torque $\sigma(T_{ice})$ and the ratio between the standard deviation and the average. MPC provides a smoother torque and this is mainly due to the quadratic formulation.

Table 4.6 – Standard deviation σ and ratio between standard deviation and the average of T_{ice}; comparison between PMP and MPC

Strategy / Cycle	$\sigma(T_{ice})$		$\sigma(T_{ice})/avg(T_{ice})$	
	PMP	MPC	PMP	MPC
NEDC	30.13	23.97	1.67	1.24
Artemis urban	31.66	28.27	2.4	2.01
FTP-75	35.06	28.02	1.8	1.44
Traffic jam	19.02	17.48	2.88	2.45

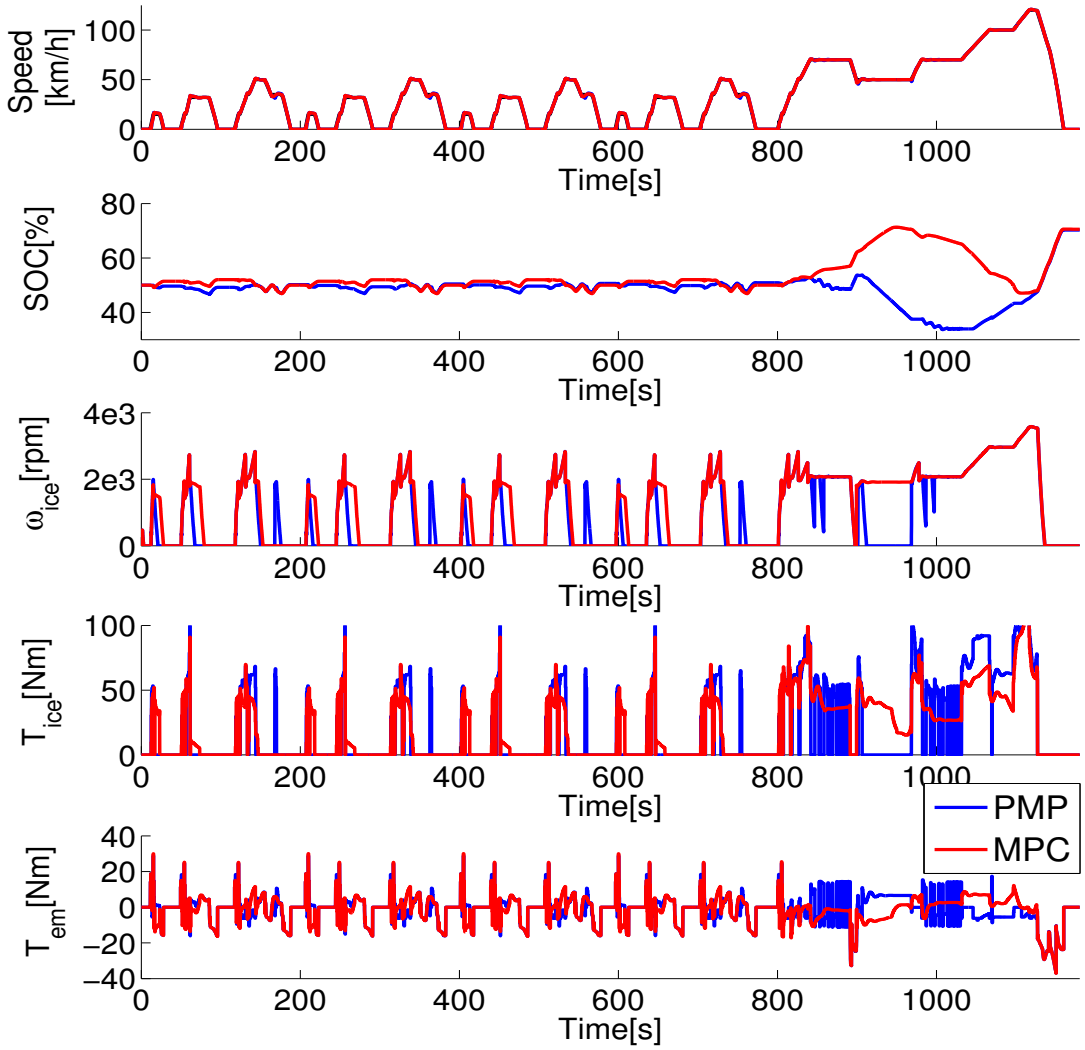

Fig. 4.17 – PMP vs MPC with $N_{mpc} = 5$s; NEDC

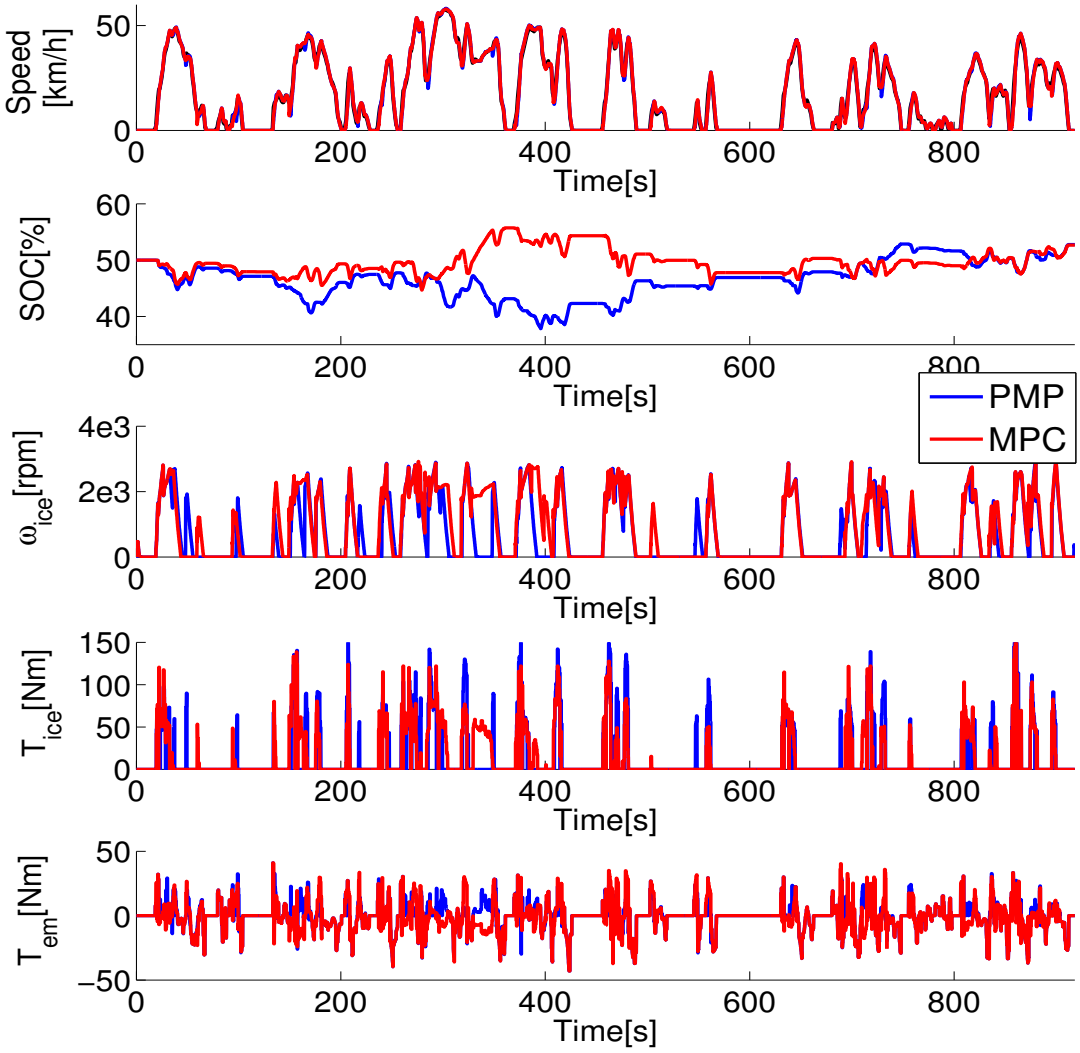

Fig. 4.18 – PMP vs MPC with $N_{mpc} = 5$s; Artemis urban

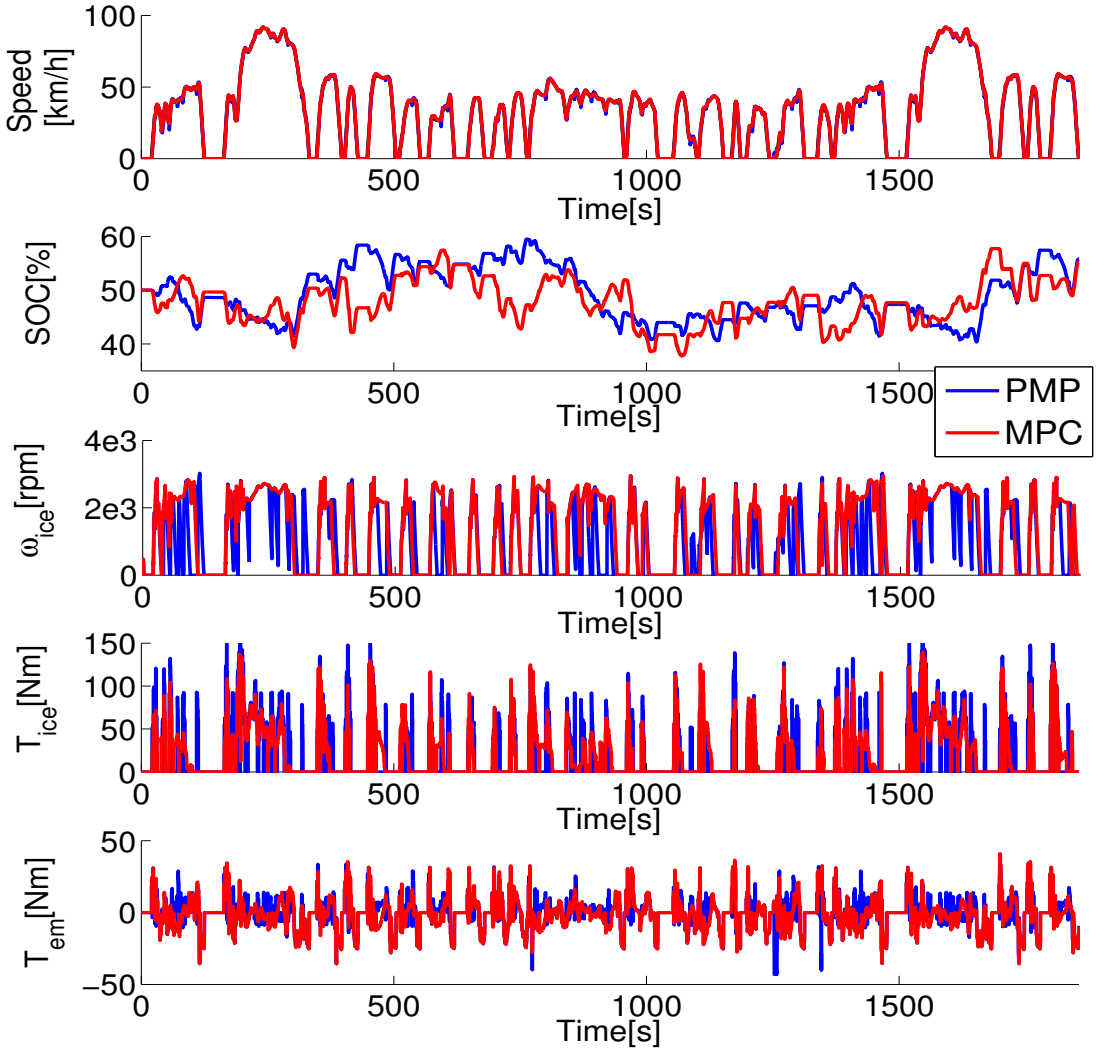

Fig. 4.19 – PMP vs MPC with $N_{mpc} = 5$s; FTP-75

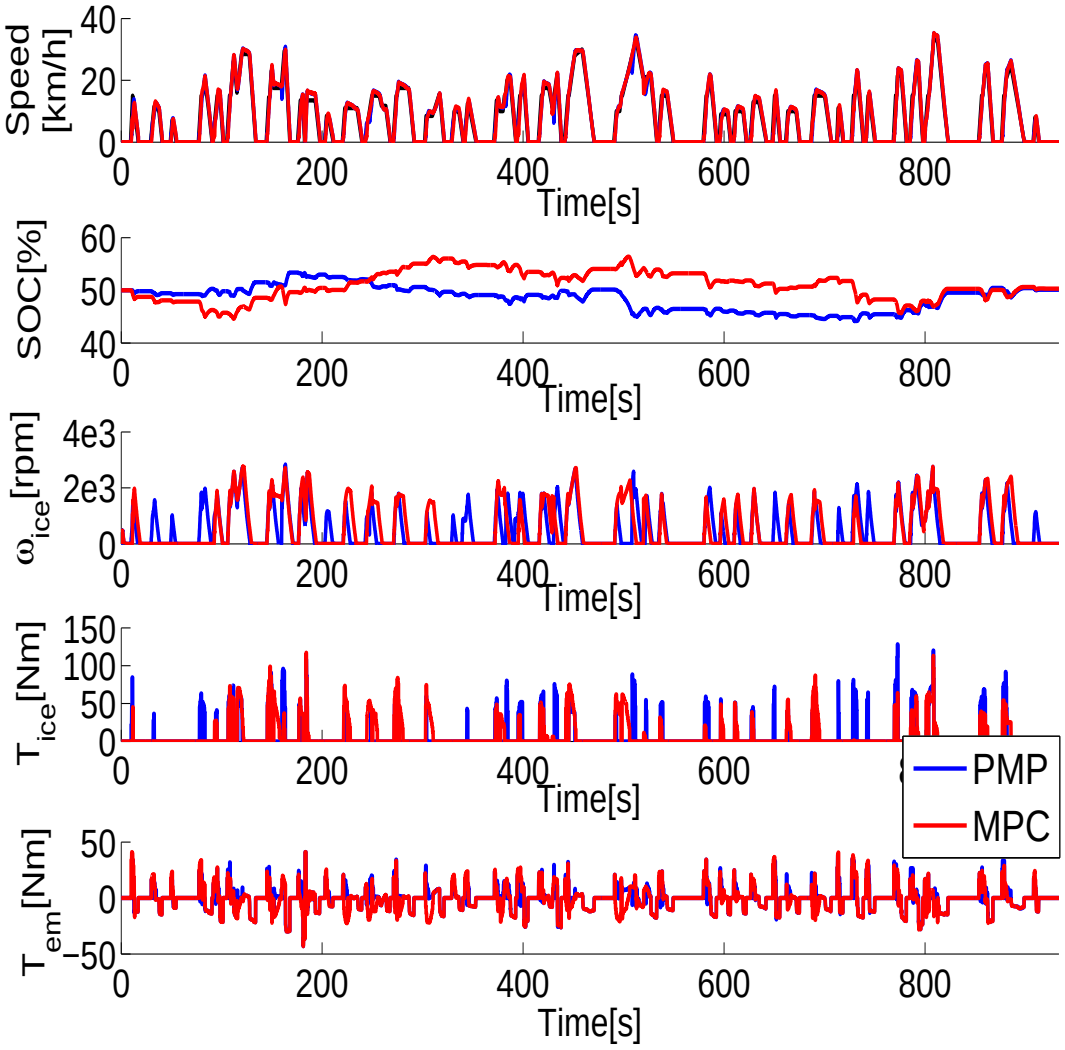

Fig. 4.20 – PMP vs MPC with $N_{mpc} = 5$s; Traffic jam

4 Robustness analysis

The MPC controller, as shown in Fig. 3.14, receives at each optimization step the estimated engine torque T_{ice} and the battery SOC from the vehicle high-fidelity model. The former is used in the model linearization at the operating point and the latter represent the current state which interferes in the calculation of the model parameters (OCV and R in (1.11)) and also in the feedback correction term of the penalty factor. The technical specifications state that the SOC can be estimated with a precision of $\pm 1\%$ of its value, whereas for the torque, the estimation accuracy is of $\pm 5\%$. Five scenarios that will be next introduced, are evaluated on each drive cycle. The results are summarized in Table 4.7 for two different N_λ values for each drive cycle and a comparison is made with the baseline strategy, where no disturbances are present on the measurements.

The robustness scenarios are:

1. positive offset for T_{ice}, accurate SOC
2. negative offset for T_{ice}, accurate SOC
3. signed offset for T_{ice}, but with a random distribution, accurate SOC
4. random offset of $\pm 1\%$ of its current value for SOC, accurate T_{ice}
5. random offsets on both inputs

Table 4.7 – Fuel consumption [L/100km] and final SOC[%], 5 scenarios for robustness for 2 values of the tuning horizon N_λ

Cycle \ Case		Baseline	1	2	3	4	5
NEDC	20s	4.87 (70.57%)	4.875 (70.57%)	4.81 (70.57%)	4.86 (70.57%)	4.85 (70.33%)	4.85 (70.32%)
	40s	4.76 (70.57%)	4.78 (70.57%)	4.75 (70.57%)	4.77 (70.57%)	4.76 (70.33%)	4.77 (70.32%)
Artemis urban	5s	6.11 (52.58%)	6.115 (52.58%)	6.113 (52.54%)	6.11 (52.68%)	6.11 (52.26%)	6.11 (52.28%)
	10s	6.14 (51.15%)	6.15 (51.15%)	6.07 (51.16%)	6.12 (51.16%)	6.25 (50.62%)	6.22 (51.04%)
FTP-75	10s	4.82 (57.07%)	4.82 (57.1%)	4.82 (57.1%)	4.82 (57.06%)	4.81 (56.88%)	4.82 (57%)
	20s	4.82 (55.16%)	4.83 (54.91%)	4.81 (55%)	4.83 (55.04%)	4.85 (55.9%)	4.83 (55.88%)
Traffic jam	10s	6.16 (50.32%)	6.2 (50.33%)	6.17 (50.32%)	6.16 (50.32%)	6.2 (50.52%)	6.21 (50.52%)
	20s	6.48 (50.28%)	6.58 (50.29%)	6.5 (50.28%)	6.51 (50.29%)	6.52 (50.53%)	6.54 (50.56%)

The fuel consumption degradation is less than 2% for the considered scenarios, which is a good performance. It can be noticed that the first scenario, with a positive offset for the engine torque, shows

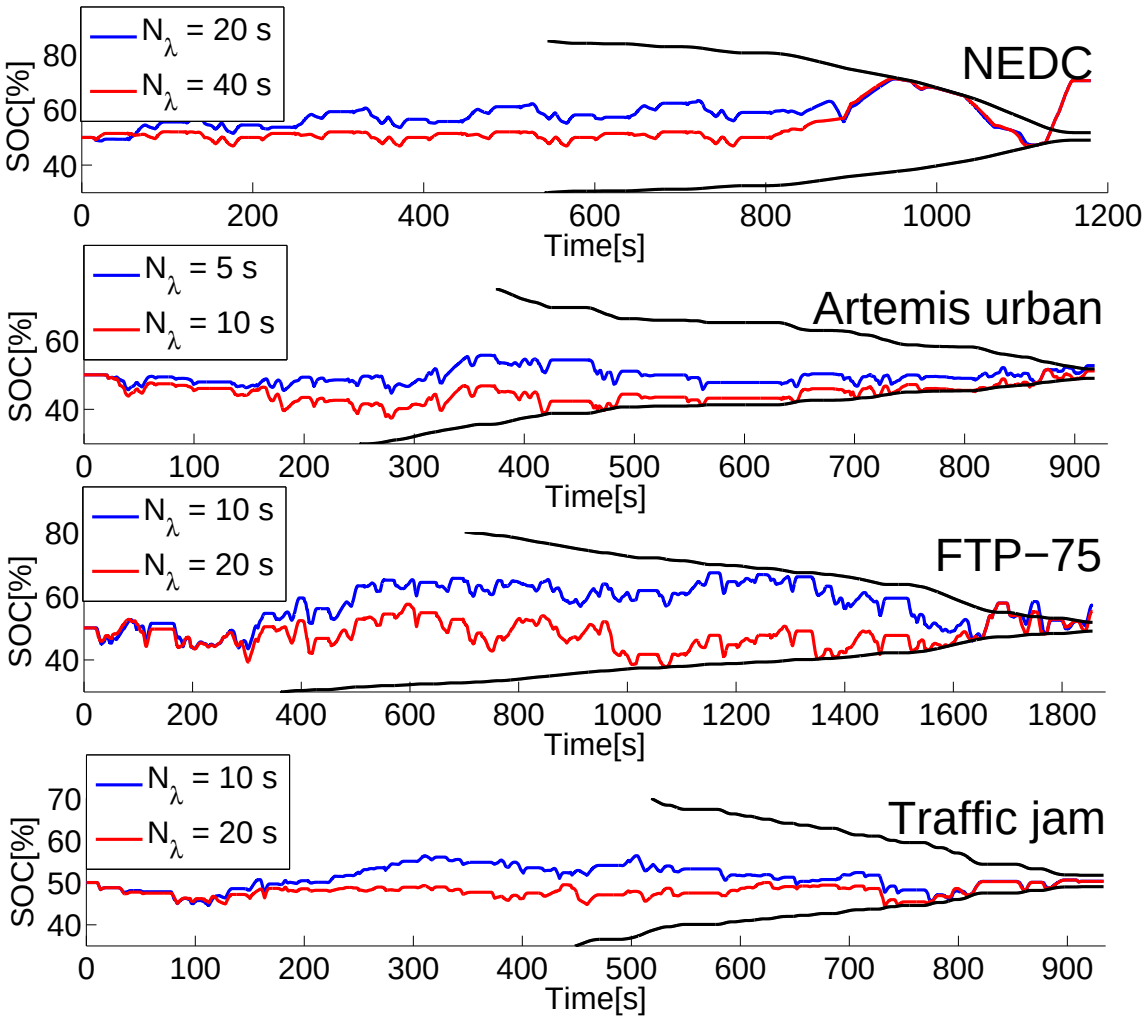

Fig. 4.21 – SOC trajectories for 2 different N_λ values, used in the robustness analysis scenarios; black curves represent SOC distance-varying limits

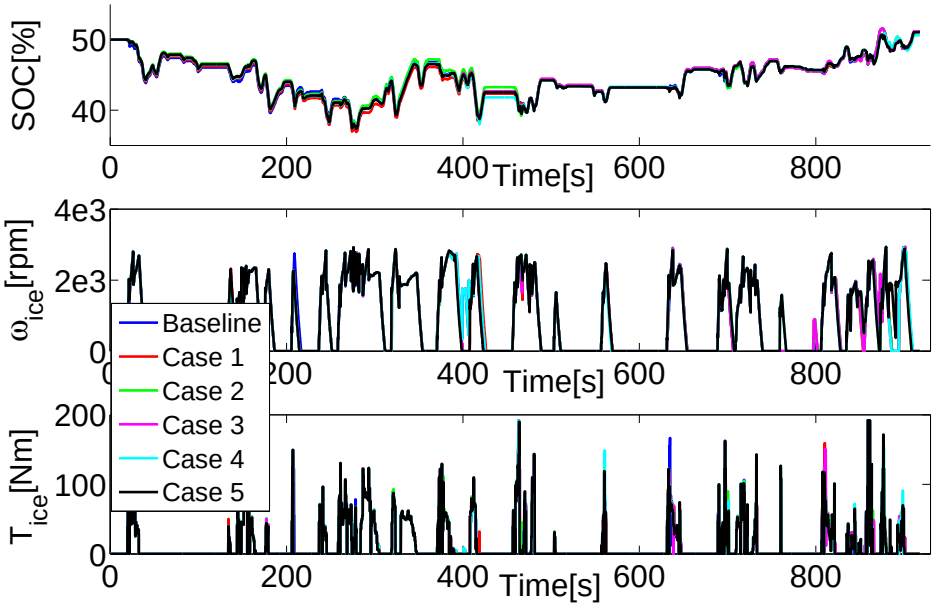

Fig. 4.22 – Trajectories for Artemis urban, $N_\lambda = 10$s, different robustness scenarios

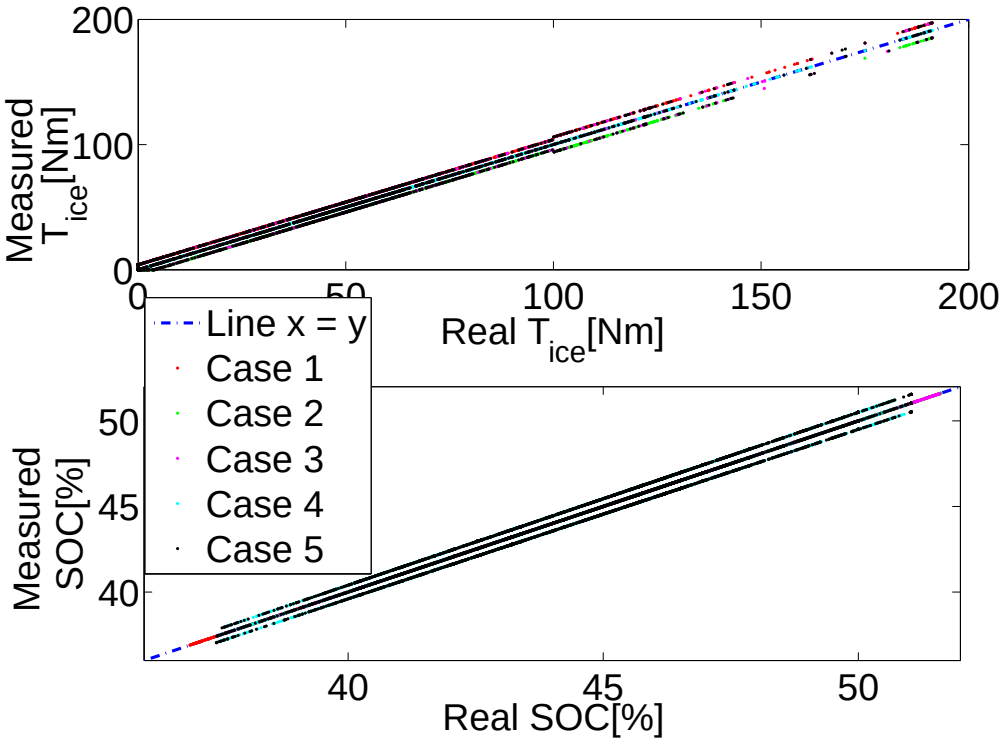

Fig. 4.23 – Comparison between real values and measurements (engine torque and SOC); Artemis urban, $N_\lambda = 10$s

a more important increase in consumption, whereas the second (negative offset) may lead to a decrease, as it is the case for Artemis urban. This is due to the impact on the stop decision, which may be favored by the latter. Disturbances on SOC have a stronger impact on trajectories where the constraints are active: Artemis urban, $N_\lambda = 10$s and FTP-75, N_λ = 20s, as it is depicted in Fig. 4.21. For Artemis urban, the lower constraints are activated during a proportionally longer amount of time than for FTP-75, which explains the difference in the consumption degradation. It can be noticed that SOC limitations are sometimes violated, but this is due to the use of slack variables, as in (3.38d).

For a better visualization, Fig. 4.22 depicts the trajectories for SOC, engine speed and torque for all the considered scenarios, for Artemis urban with $N_\lambda = 10s$. The differences between real values and disturbed measurements of torque and SOC are presented in Fig. 4.23.

In addition to the robustness analysis with respect to measurements, tuning sensitivity to the battery capacity is another robustness indicator of the proposed strategy. The tuning mechanism introduced in the previous chapter has a generalized expression and the choice of the tuning horizon N_λ depends exclusively on the drive cycle. For the present analysis, a battery with a capacity twice the size of the baseline case is considered and simulations were carried out for representative values of N_λ for each drive cycle. Consumption results and their sensitivity to tuning is depicted in Fig. 4.24, where it can be observed that the optimal N_λ is the same as for the baseline case (40s for NEDC, 5s for Artemis urban, 20s for FTP-75 and 10s for Traffic jam), which proves the robustness with respect to the battery size.

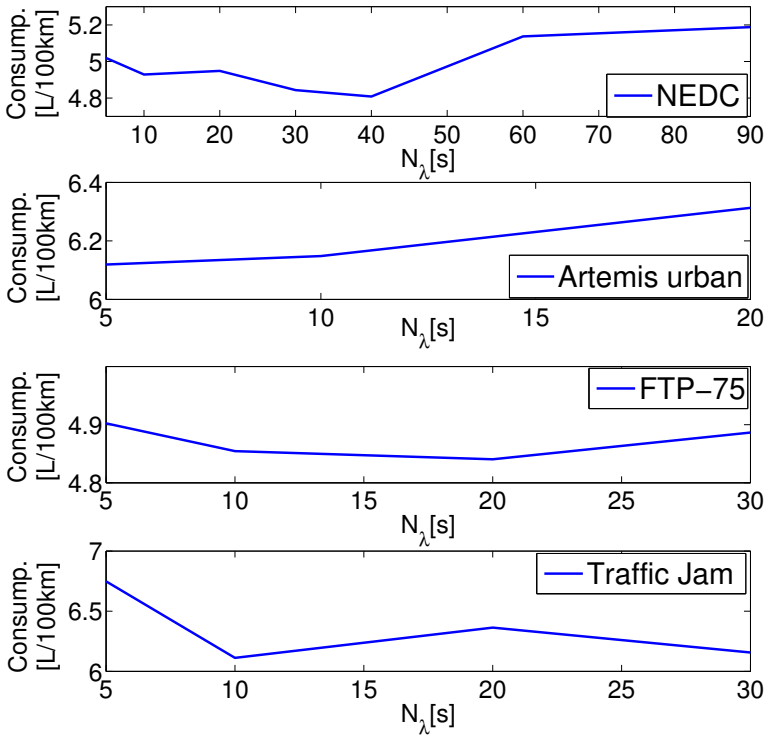

Fig. 4.24 – Evolution of the normalized consumption as a function of N_λ for a battery with a double capacity than the baseline case

5 Slope influence

Standard drive cycles do not provide any information about the slope, but its influence cannot be neglected. Here, two basic speed profiles with variable slope were selected, depicted in Fig. 4.25, for which two approaches are compared:

1. the use of a longer prediction horizon for tuning
2. the adaptation of the SOC_{sp}, as announced in the previous chapter and depicted in Fig. 3.12

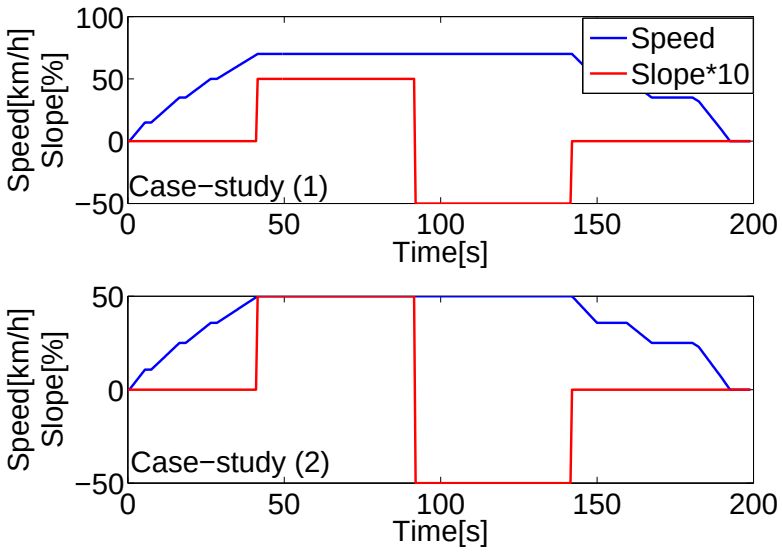

Fig. 4.25 – Speed profiles (blue) and slope (red) of basic case-studies

First, simulations are presented for case study (1), with a constant SOC setpoint $SOC_{sp} = 50\%$, which interferes in the feedback calculation (see (3.42)) and with distance-varying SOC limits (3.37), for different tuning horizons N_λ. The results are depicted in Fig. 4.26, where it can be seen that the SOC constraints activate early and therefore, it would be interesting to see the consumption evolution for a constant minimum value of SOC, $SOC_{min} = 20\%$, even though the final SOC will not be the same. The results with a constant SOC_{min} will be compared with the case where an adaptation of SOC_{sp} is introduced. For the considered case-study, with a positive slope of 5%, followed by a negative one, it may be more appropriate to diminish the SOC_{sp} before the start of the negative slope phase, in anticipation to the energy recovery. Therefore, the last tested scenario is defined by a constant SOC_{min} value and a variable SOC setpoint: $SOC_{sp} = 30\%$ during the first part and then, $SOC_{sp} = 50\%$.

The consumption results are summarized in table 4.8 for different N_λ. There is a saturation in consumption improvement toward $N_\lambda = 90s$ for all the scenarios, but present to a lesser extent for the second case, defined by constant SOC_{min} and SOC_{sp}. The absence of an identical final SOC makes a comparison between the performances associated to different N_λ relatively difficult, except when distance-varying limits are used: $N_\lambda = 60s$ and $N_\lambda = 90s$ outperform $N_\lambda = 30s$, which is coherent with the periodogram-based analysis from Fig. 3.13. It must be mentioned that for $N_\lambda = 10s$ the final SOC is not the same as for the other values because upper distance-varying SOC limits are not

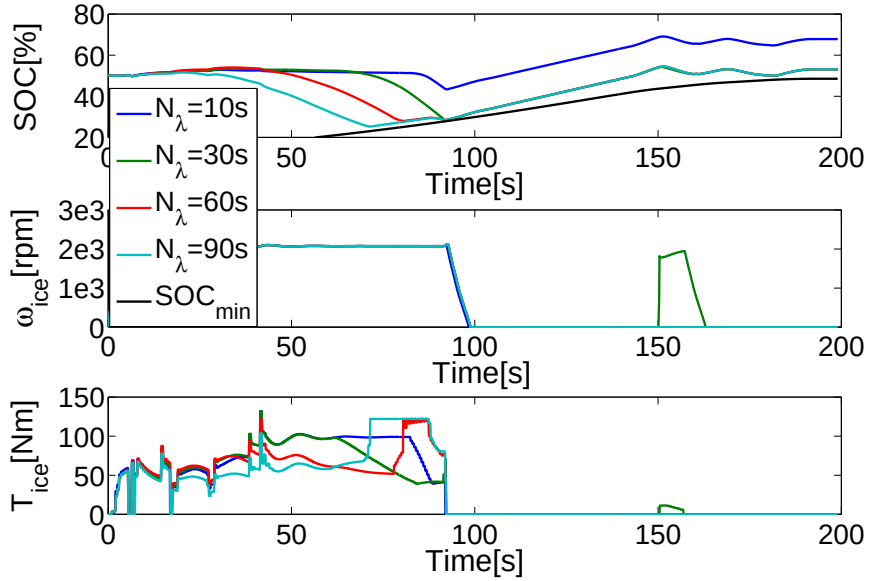

Fig. 4.26 – Case-study (1), SOC distance-varying limits, constant SOC_{sp}

activated during regenerative braking. At the beginning of the braking phase the SOC is greater than for the other N_λ values, which explains the difference in the final SOC.

Table 4.8 – Fuel consumption [L/100km] and final SOC[%], case study (1)

Scenario \ N_λ	10s	30s	60s	90s
Constant SOC_{sp}, Distance-varying SOC limits	4.49 (67.81%)	4.2 (53.05%)	4.07 (53.1%)	4.08 (53.1%)
Constant SOC_{sp} Constant SOC_{min}	4.49 (67.81%)	4.19 (52.73%)	3.86 (45.68%)	3.8 (45.62%)
Variable SOC_{sp} Constant SOC_{min}	4.09 (55.03%)	4.01 (48.37%)	3.82 (45.64%)	3.82 (45.64%)

Table 4.9 – Fuel consumption [L/100km] and final SOC[%], case study (2)

Scenario \ N_λ	10s	30s	60s	90s
Constant SOC_{sp} Constant SOC_{min}	4.58 (60.13%)	4.21 (46.04%)	3.75 (39.64%)	3.66 (39.64%)
Variable SOC_{sp} Constant SOC_{min}	4.55 (51.38%)	4.09 (41.52%)	3.89 (39.6%)	3.81 (39.61%)

An adaptation of the SOC_{sp} can lead to a consumption improvement for low values of N_λ: $N_\lambda = 10s$ for the third scenario outperforms the constant SOC_{sp} case with $N_\lambda = 30$s. The SOC trajectories for these two scenarios are depicted in Fig. 4.27, where it can be observed a faster battery depletion for the case with $SOC_{sp} = 30\%$. For higher N_λ values the two scenarios behave similarly i.e. it is enough to use a longer tuning horizon to improve the consumption, instead of introducing an additional tuning parameter (SOC_{sp}). This conclusion is also valid for the second case-study, with a lower speed, whose results are summarized in Table 4.9. Here, for $N_\lambda = 60s$ an adapted SOC_{sp} provides better results than a constant setpoint, but a greater N_λ ensures a better fuel gain improvement for the case with a constant setpoint. This result reinforces the choice of adapting the tuning horizon, rather than the SOC_{sp}.

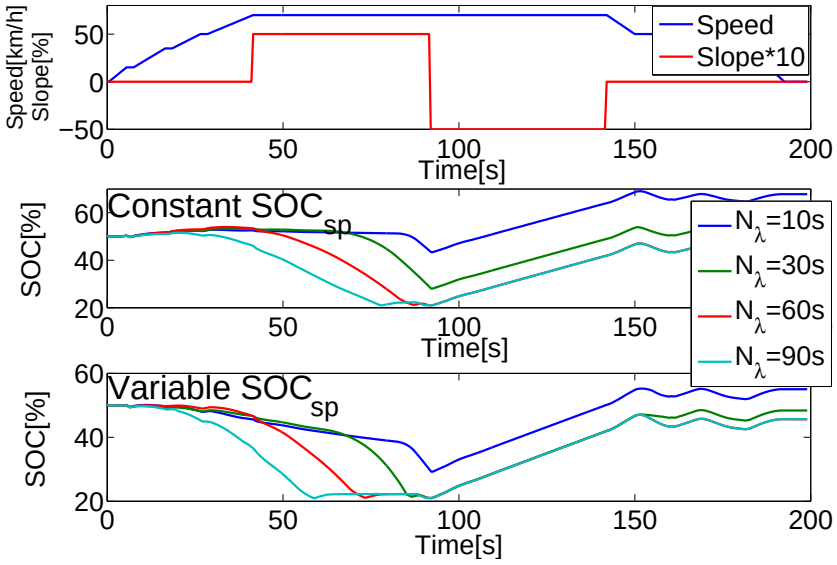

Fig. 4.27 – Case-study (1), SOC trajectories for different N_λ values; constant and variable SOC_{sp}, respectively; constant SOC_{min}

6 Conclusions

This chapter presented a series of case-studies considered to be representative for the overall test campaign. The results validated the proposed powertrain control-oriented model and evaluated the MPC performance for a parallel hybrid passenger car with fixed sizing, for different driving scenarios and tuning parameters. The influence of the tuning prediction horizon was explained through the mechanism proposed in chapter 3, based on the frequency analysis. One of the conclusion is that in the nominal case, the benefit in fuel gain of increasing the MPC horizon is due to S&S functionality. The robustness of the controller was proven with respect to disturbances on torque and SOC, but also with respect to the battery size, which was varied only in view of a sensitivity analysis, and not for sizing optimization. An analysis of the slope influence completes the evaluation and it is concluded that it is preferable to adapt the tuning horizon (and hence, the feedforward component of the tuning factor) rather than the SOC setpoint that interferes in the feedback term.

Ce chapitre a présenté une série d'études de cas, considérées comme représentatives. Les résultats ont validé le modèle de GMP orienté-contrôle et évalué la performance MPC pour un hybride parallèle, avec un dimensionnement fixe, pour des différents scénarios de conduite et des paramètres de calibration. L'influence de l'horizon de prédiction a été expliquée à travers le mécanisme proposé dans la chapitre 3, basé sur une analyse fréquentielle. Une des conclusions est que dans le cas nominal, le bénéfice en termes de gain en consommation d'augmenter l'horizon MPC est dû à la fonctionnalité stop-start. La robustesse du contrôleur a été prouvée par rapport aux perturbations sur le couple et le SOC, mais aussi à la capacité de la batterie, qui a été faite varier uniquement en vue d'une analyse de sensibilité et non pas pour une optimisation du dimensionnement. Une analyse de l'influence de la pente a complété l'évaluation et on a conclu que c'est préférable d'adapter l'horizon de calibration (et par conséquent, la partie feedforward du terme de calibration) plutôt que la référence de SOC qui intervient dans la partie feedback.

Conclusions and perspectives

The present research started from the acknowledgment that in the current context of restrictive environmental legislation, hybrid electric vehicles offer an alternative to conventional transportation systems. Although sometimes regarded as a transient solution toward all-electric vehicles, HEV gradually started to position themselves as a standalone actor on the automotive market. This justifies the abundance of research work that covers a wide range of topics, from design to control, but concomitantly nourish the academic investigations on switched systems, hybrid control or decision making in the activation of different strategies. The main advantage of hybridization being the reduction of CO_2 emissions, this thesis focused on the energy management in view of fuel consumption reduction. Traffic forecast is nowadays made possible by improved technologies, encouraging therefore the use of predictive control algorithms, with a model-based approach. Flexibility, robustness and reduced complexity of implementation are common requirements in automotive industry and for the considered problem, model-based strategies offer the best compromise, in comparison with heuristic or data-based approaches. Our work fits within this framework and its main goal was to exploit the potential of model predictive control for the torque distribution problem.

The first achievement was the establishment of a control-oriented powertrain model, regardless of the configuration. The wheel level, which is the uppermost powertrain position was chosen as the level for the problem formulation, because it includes complete information about the system i.e. transmission type and electric machine placement. For a complete description, intermediate levels were also defined (crankshaft, gearbox primary and secondary shaft). The model was parametrized with the help of two clutches and this allowed to include the case of dual-clutch transmissions, which are often neglected in the literature, as well as to define different architectures: in particular, it makes a distinction between series and parallel hybrid architectures, but it can also handle, to a certain extent, multi-mode power-split architectures. For the latter, due to their complexity, an additional degree of freedom is usually needed and the proposed model was extended for some specific case-studies, encountered on the market. To sum up, a compact static model was designed, that defined the torque at different levels and the speeds of traction elements (combustion engine and electric machines) and which covered a large class of hybrid architectures. The dynamical part of the model was linked to the battery SOC, for which a standard, internal resistance model was used. As an improvement of the static model, which can be considered for further studies, would be to introduce an additional clutch, in order to handle in a generalized form multi-mode configurations.

The reduction of fuel consumption being the main goal of this thesis, a tool for its evaluation was needed. In general, it is modeled as a lookup table in engine torque and speed, but in a model-based framework, an analytical formulation is preferred. The high level of complexity of physical models, characterized by fast dynamics, makes them unsuitable for a supervisory controller. In general, an ap-

proximation of the static model is instead used and the most encountered model in the literature is Willans line. However, a linear expression is not always accurate, especially for turbocharged SI engines. Therefore, a generalization of this model was proposed and the fuel consumption was expressed as piecewise linear in torque, with speed-dependent coefficients. This approximation can be applied to all types of engines, the distinguishing element being the number of torque partitions. The advantage of this model is therefore its general application and its improved accuracy.

The energy management formulation in the MPC framework was the central part of this thesis and represented the main contribution from the design point of view. For the cost function definition, an energetic criterion was proposed, expressed as a trade-off between the fuel and the electrochemical consumption, placing the problem into an economic MPC framework. The linearized SOC model at the operating point, along with the PWL consumption model define an LTV MPC problem, which was formulated in a standard quadratic form, allowing therefore an efficient implementation. Noteworthy, in addition to the torque split, the MPC formulation can also handle the engine stop-start, but without the use of a discrete optimization variable (engine ON/OFF), nor the introduction of a cost of a restart, which represents one of the main advantages as it emerges from the exhaustive studies conducted in the present. The engine stop was implemented as an *a-posteriori* decision from the sequence of optimal commands given by the MPC.

The model-in-the-loop validation showed on one side the versatility of the model-based design and the optimization-based implementation of the energy management, which often appeals to rule-based techniques. From a fuel consumption reduction point of view, it was shown that the benefit of prediction in the MPC framework is almost exclusively related to S&S functionality, as long as hard constraints activation is avoided. This phenomenon resides in the fact that the cost function was not expressed in a standard form i.e. a trade-off between tracking error and effort reduction, but as an energetic criterion, and that state constraints are only active a proportionally small amount of time, at the end of the drive cycle. If the main advantage of the MPC design is the versatility and relative robustness with respect to the changes in the scenarios, the disadvantage resides in the inaccuracies due to linearization and driver request prediction, both limiting the MPC prediction horizon to only several seconds. A nonlinear prediction model could be the object of a future work for accuracy enhancement, but in this case the MPC problem would need a more complicated solver. Concerning the driver request, there is a significant potential of improvement in the current context of connected cars.

The tuning of the MPC criterion represents a longstanding subject in the finite-time optimal control studies and it represented, also, an important part of the present thesis. Speed and wheel torque preview were exploited in the calculation of the feedforward component, over a longer horizon than the one used in the MPC algorithm. This was justified by its average-based definition, which can filter inaccuracies in the prediction. Simulations results showed that the optimal value of the prediction horizon used for tuning is drive cycle-dependent, which was explained on the basis of a frequency analysis that gives information about the trade-off between tendency and aggressiveness. In real driving situations it is not possible to have access to the entire speed profile and this constraint will limit the range of the analysis and consequently, the optimal adaptation of the prediction horizon. However from the present study, we concluded that for drive cycles with urban characteristics, an horizon of 10s is a suitable choice. The main advantage is therefore the inclusion of a self-tuning mechanism, by automatically exploiting drive cycle and powertrain-related data.

If hybridization can only ensure a limited fuel gain for road and highway speed profiles, coasting (otherwise known as *free-wheeling*) emerges as a potential solution for fuel reduction in extra-urban scenarios, in particular in view of the next generations of autonomous driving. Therefore, in addition to torque split and stop-start problem, coasting was another topic addressed in a predictive framework. Coasting was proven to be more fuel efficient that energy recovery, result that supports the state-of-the-art analysis for HEV. The novelty of the proposed solution was to address it in an optimization-based approach i.e. to evaluate a cost function and to subsequently decide the initiation and duration of coasting, as well as the acceptance of the result, in terms of speed deviation. This approach presents several advantages: adaptability with respect to vehicle parameters, it avoids high compensations from the speed regulator at pedal pressing and it can be applied to time-varying speed sections. The main drawback is the variable-structure form: the vehicle speed during free-wheeling can only be evaluated for a pair "coasting start-coasting stop" time, which are to be determined. Moreover, the reference speed does not have a parametrized expression, it is only provided as a time series, leading to a pointwise evaluation of the cost function, which can be computationally complex. As a perspective, a functionality that handles position-related obstacles may be introduced.

Vehicle speed tracking was supposed handled at a supervisory level, by a virtual driver. An extension of this work might be the co-optimization of the speed and torque split, in a predictive eco-driving framework. Moreover, information about the drive cycle was supposed known in advance for a certain time window, without the inclusion of a mechanism of speed prediction, such as reconstruction from the leading vehicle speed or from driver's past information. The MPC cost function could be modified in order to cope with different data reliability or with multiple scenarios, enhancing therefore the strategy robustness. Another direction of improvement could be the prediction model, which might include the battery aging. Concerning the validation, a MIL environment was used, but a hardware-in-the-loop validation would complete the evaluation of the proposed strategy.

Conclusions et perspectives

Le travail de recherche courant a démarré de l'acquiescement que dans le contexte actuel d'une législation environnementale restrictive, les véhicules hybrides offrent une alternative aux systèmes de transportation conventionnels. En dépit d'être perçus comme une solution transitoire vers les véhicules purement électriques, HEV ont graduellement commencé à se positionner sur le marché d'automobile comme un acteur indépendant. Ceci justifie le travail de recherche abondant qui couvre une large gamme de sujets, du design au contrôle, en nourrissant les investigations académiques sur les systèmes hybrides ou la prise de décision dans l'activation des différentes stratégies. L'avantage principal de l'hybridation étant la réduction des émissions CO_2, cette thèse s'est concentrée sur la gestion d'énergie en vue de réduire la consommation. La prédiction du trafic est maintenant rendue possible par l'avancement de la technologie, encourageant donc l'utilisation des algorithmes de contrôle prédictif, avec une approche basée modèle. Flexibilité, robustesse et complexité d'implémentation réduite sont les exigences courantes dans l'industrie de l'automobile et pour le problème considéré, les stratégies basées modèles offrent le meilleur compromis, comparé aux approches heuristiques ou *date-based*. Ce travail s'inscrit dans ce cadre et son but principal était d'exploiter le potentiel du MPC pour le problème de la distribution de couple.

Le premier résultat a été la définition d'un modèle GMP orienté-contrôle, indépendant de la configuration. Le problème a été formulé au niveau le plus haut, la roue, parce qu'il contient des informations complètes sur le type de transmission et la position de la machine électrique. Pour une description complète, des niveaux intermédiaires ont également été définis (vilebrequin, l'arbre primaire et secondaire de la boîte). Le modèle a été paramétrisé à l'aide de deux embrayages, ce qui a permis l'introduction des transmissions double-embrayage, qui sont souvent négligées dans la littérature, ainsi que la définition de différentes architectures: en particulier, il distingue l'architecture série de celle parallèle, mais il peut aussi gérer certains cas d'architectures multi-modes à puissance dérivée. Pour celles-ci, en raison de leur complexité, un dégrée de liberté supplémentaire est nécessaire en général et le modèle proposé a été étendu pour des études de cas spécifiques, présents sur le marché. Pour résumer, un modèle statique compact a été conçu, qui a défini le couple aux différents niveaux et les vitesses des éléments de traction (moteur et machines électriques) et qui a couvert une large classe des architectures hybrides. La partie dynamique du modèle était liée à l'état de charge de la batterie, pour laquelle un modèle standard, à résistance interne a été utilisé. Une amélioration du modèle statique, qui pourrait être considérée pour des études futures, serait l'introduction d'un nouvel embrayage, afin d'adresser sous une forme généralisée les configurations multi-modes.

La réduction de la consommation étant le but principal de cette thèse, un outil pour son évaluation était nécessaire. En général, elle est modélisée comme une cartographie en couple moteur et régime, mais dans le cadre d'une approche basée modèle, une formulation analytique est préférée. Le niveau

élevé de complexité des modèles physiques, caractérisés par des dynamiques rapides, les rend inutilisables pour un contrôleur au niveau superviseur. En général, une approximation du modèle statique est utilisée et le modèle le plus répandu dans la littérature est Willans line. Cependant, une expression linéaire n'est pas toujours précise, particulièrement pour des moteurs essence turbochargés. Par conséquent, une généralisation de ce modèle a été proposée, la consommation carburant étant exprimée comme linéaire par morceaux en couple, avec les coefficients dépendants du régime. Cette approximation peut être appliquée à tout type de moteur, l'élément discriminatoire étant le nombre de partitions de couple. En conclusion, l'avantage de ce modèle est son application générale et sa précision améliorée.

La formulation de la gestion d'énergie avec le MPC a été la partie centrale de cette thèse et elle a représenté la contribution principale d'une perspective design. Pour la définition de la fonction coût, un critère énergétique a été proposée, exprimé comme un compromis entre la consommation carburant et électrochimique, plaÃğant le problème dans un cadre de MPC économique. Le modèle de SOC linéarisé autour du point de fonctionnement, ainsi que le modèle de consommation linéaire par morceaux définissent un problème LTV MPC, qui a été formulé sous une forme quadratique standard, permettant de cette manière une implémentation efficace. Il convient de mentionner que la formulation MPC peut également adresser le stop-start, mais en absence de l'introduction d'une variable d'optimisation discrète (moteur ON/OFF) ou d'un coût de démarrage moteur, ce qui représente un des avantages principaux de l'approche proposée, par rapport aux études actuellement présentes dans la littérature. L'arrêt moteur a été implémenté comme une décision *a-posteriori* issue de la séquence de commandes optimales fournie par le MPC.

La validation model-in-the-loop a montré la versatilité du design model-based et de l'implémentation basée-optimisation de la gestion d'énergie, qui utilise le plus souvent des techniques heuristiques. Concernant le gain en consommation, il a été montré que le bénéfice de la prédiction pour le MPC est presque exclusivement lié à la fonctionnalité S&S, pourvu que l'activation des contraintes hard soit évitée. Ce phénomène réside dans le fait que la fonction coût n'a pas été exprimée sous une forme classique, à savoir comme un compromis entre la réduction de l'erreur de suivie et de l'effort, mais comme un critère énergétique et que les contraintes sur l'état sont actives seulement pendant une relativement courte période de temps, à la fin du cycle de conduite. Si l'avantage principale du design MPC est la versatilité et la relative robustesse par rapport aux changements dans les scénarios, le désavantage est lié aux imprécisions dues à la linéarisation et à la prédiction de la demande du conducteur, les deux limitant l'horizon de prédiction du MPC à seulement quelques secondes. Un modèle de prédiction nonlinéaire pourrait représenter l'objet d'un travail future pour l'amélioration de la précision, mais dans ce cas le problème MPC nécessiterait un solveur plus compliqué. Concernant la demande conducteur, aujourd'hui il y a un signifiant potentiel d'amélioration dans le contexte des voitures connectées.

Le tuning du critère MPC représente un sujet à long terme dans le contrôle optimale à horizon fini et une partie importante de cette thèse lui est dédiée. Les futures vitesse et couple à la roue ont été exploités dans le calcul de la partie feedforward, sur un horizon plus large que celui employé pour l'algorithme MPC. Ceci a été justifié par sa définition comme une moyenne, ce qui permet de filtrer les imprécisions de la prédiction. Les résultats des simulations ont montré que la valeur optimale de l'horizon de prédiction utilisé pour le tuning dépend du cycle de conduite, ce qui a été expliqué à travers une analyse fréquentielle qui offre des informations sur le compromis tendance/agressivité. Dans des conditions de conduite réelle ce n'est pas possible d'avoir accès au profil de vitesse entier et cette contrainte limite

l'intervalle d'analyse et par conséquent, l'adaptation optimale de l'horizon de prédiction. Cependant, pour l'étude présente, c'était conclu que pour des cycles avec une caractéristique urbaine, un horizon de 10s est un choix approprié. L'avantage principale est donc l'inclusion d'un mécanisme d'auto-tuning, via l'exploitation automatique des données liées au cycle et au GMP.

Si l'hybridation ne peut assurer qu'un gain en consommation limité pour des profils routier et autoroutier, *coasting* (autrement connu sous le nom *free-wheeling* apparaît comme une solution potentielle pour la réduction de la consommation pour des scénarios extra-urbains, particulièrement en vue de la prochaine génération de conduite autonome. En plus par rapport à la distribution du couple et le stop-start, coasting a été un autre sujet adressé dans un cadre prédictif. Coasting s'est montré plus efficace pour la réduction carburant que la récupération d'énergie, ce résultat appuyant les travaux déjà existants pour les HEV. La nouveauté de la solution proposée a été d'adresser ce problème avec une approche basée sur optimisation i.e. évaluer une fonction coût et décider ensuite l'initiation et la durée du coasting, ainsi que l'acceptabilité du résultat, en termes de déviation de vitesse. Cette approche présente plusieurs avantages : adaptabilité par rapport aux paramètres véhicule, éviter des compensations importantes du régulateur de vitesse lors de l'appui pédale et application sur des sections de vitesse variante dans le temps. Le désavantage principal est sa forme avec une structure variable : la vitesse véhicule pendant le roulage libre peut seulement être évaluée pour une paire *coasting start - coasting stop*, des instants qui doivent être déterminés. En outre, la référence de vitesse n'a pas une expression paramétrisée, elle est fournie en tant que série de temps, conduisant à une évaluation à chaque point de la fonction coût, ce qui peut être complexe d'un point de vue calcul. Une perspective serait d'introduire une fonctionnalité qui gère des obstacles dépendants de la position.

Le suivi de vitesse a été supposé traité au niveau superviseur, par un conducteur virtuel. Une extension de ce travail pourrait être la co-optimisation de la vitesse et du partage du couple, dans un cadre d'éco-conduite prédictive. De plus, des informations sur le cycle ont été supposées connues à l'avance pour un certain intervalle, mais sans l'inclusion d'un mécanisme de prédiction de vitesse, comme la reconstruction à partir de la vitesse véhicule devant ou à partir des informations passées du conducteur. La fonction coût du MPC pourrait être modifiée afin de gérer les différents dégrées de confiances des données ou les scénarios multiples, renforçant de cette manière la robustesse de la stratégie. Une autre direction d'amélioration serait le modèle de prédiction, qui pourrait inclure le vieillissement de la batterie. Concernant la validation, un environnement MIL a été utilisé, mais une validation hardware-in-the-loop compléterait l'évaluation de la stratégie proposée.

Bibliography

[1] U.S. Departement of Energy. Alternative Fuels Data Center, 2017-05-21. https://www.afdc.energy.gov/vehicles/how-do-hybrid-electric-cars-work.

[2] University of Washington. Clean Energy Institute, 2017. http://www.cei.washington.edu/education/science-of-solar/battery-technology.

[3] L. Guzzella and A. Sciarretta. *Vehicle Propulsion Systems*. Springer, 2007.

[4] Z. Yang and A. Bandivadekar. Light-duty vehicle greenhouse gas and fuel economy standards. Technical report, The International Council on Clean Transportation, 2017.

[5] L. Zhou and Z. Dong. A performance optimisation-based e-CVT design method and analysis of representative HEV/PHEV powertrains. *Int. Journal Electric and Hybrid Vehicles*, 3(4): 318 - 339, 2011.

[6] Z. Liu, A. Ivanco, and Z. Filipi. Quantification of drive cycle's rapid speed fluctuations using Fourier analysis. *SAE International*, doi: 10.4271/2015-01-1213, 2015.

[7] E. Silvas, T. Hofman, N. Murgovski, P. Etman, and M. Steinbuch. Review of optimization strategies for system-level design in hybrid electric vehicles. *IEEE Trans. on Vehicular Technology*, 66(1): 57 - 70, 2017.

[8] M. Sh. Asfoor, S.W. Beyerlein, R. Lilley, and M. Santora. Discrete grid optimization of a rule-based energy management strategy for a formula hybrid electric vehicle. *SAE Technical Paper*, 2015-01-1212, doi:10.4271/2015-01-1212, 2015.

[9] H. Banvait, S. Anwar, and Y. Chen. A rule-based energy management strategy for plug-in hybrid electric vehicle (PHEV). *American Control Conf.*, 2009.

[10] D.F. Opila, D. Aswani, R. McGee, J.A. Cook, and J.W. Grizzle. Incorporating drivability metrics into optimal energy management strategies for hybrid vehicles. *47th IEEE Conf. on Decision and Control*, 2008.

[11] D. Kum, H. Peng, and N.K. Bucknor. Optimal energy and catalyst temperature management of plug-in hybrid electric vehicles for minimum fuel consumption and tail-pipe emissions. *IEEE Trans. on Control Systems Technology*, 21(1): 14 - 26, 2013.

[12] O. Grondin, L. Thibaut, P. Moulin, A. Chasse, and A. Sciarretta. Energy management strategy for Diesel hybrid electric vehicle. *IEEE Vehicle Power and Propulsion Conf.*, 2011.

[13] S. Ebbesen, P. Elbert, and L. Guzzella. Battery state-of-health perceptive energy management for hybrid electric vehicles. *IEEE Trans. on Vehicular Technology*, 61(7): 2893 - 2900, 2012.

[14] T. Miro-Padovani, M. Debert, G. Colin, and Y. Chamaillard. Optimal energy management strategy including battery health through thermal management for hybrid vehicles. *7th IFAC Symp. Advances in Automotive Control*, 2013.

[15] O. Sundstrom, L. Guzzella, and P. Soltic. Optimal hybridization in two parallel hybrid electric vehicles using dynamic programming. *Proc. of the 17th World Congress IFAC*, 2008.

[16] M. Back, M. Simons, F. Kirschaum, and V. Krebs. Predictive control of drivetrains. *15th IFAC World Congress*, 2002.

[17] T.S. Kim, C. Manzie, and H. Watson. Fuel economy benefits of look-ahead capability in a mild hybrid configuration. *Proc. of the 17th World Congress IFAC*, 2008.

[18] T.J Boehme, M. Schori, B. Frank, M. Schultalbers, and W. Drewelow. A predictive energy management for hybrid vehicles based on optimal control theory. *American Control Conf.*, 2013.

[19] M. Bassett, B. Brods, J. Hall, S. Borman, M. Grove, and S. Reader. GPS based energy management control for plug-in hybrid vehicles. *SAE Technical Paper*, 2015-01-1226, doi:10.4271/2015-01-1226, 2015.

[20] S. di Cairano, D. Yanakiev, A. Bemporad, I. Kolmanovsky, and D. Hrovat. Model predictive idle speed control: design, analysis and experimental evaluation. *IEEE Trans. on Control Systems Technology*, 20(1): 84 - 97, 2012.

[21] T. Besselmann, P. Rostalski, and M. Morari. Hybrid parameter-varying model predictive control for lateral vehicle stabilization. *Proc. European Control Conf.*, 2007.

[22] M. Vajedi and N.L. Azad. Ecological adaptive cruise controller for plug-in hybrid electric vehicles using nonlinear model predictive control. *IEEE Trans. on Intelligent Transportation Systems*, 17(1): 113 - 122, 2016.

[23] P. Falcone, F. Borelli, H. E. Tseng, J. Asgari, and D. Hrovat. A hierarchical model predictive control framework for autonomous ground vehicles. *American Control Conf.*, 2008.

[24] G. Paganelli, S. Delprat, T. M. Guerra, J. Rimaux, and J. J. Santin. Equivalent consumption minimization strategy for parallel hybrid powertrains. *IEEE 55th Vehicular Technology Conf. VTC Spring 2002*, 4: 2076 - 2081, 2002.

[25] A. Sciaretta, M. Back, and L. Guzzella. Optimal control of parallel hybrid electric vehicles. *IEEE Trans. on Control Systems Technology*, 12(3): 423 - 427, 2004.

[26] M. Debert. *Strategies optimales multi-criteres, predictives, temps reel de gestion des flux d'energies thermique et electrique dans un vehicule hybride*. PhD thesis, Universite d'Orleans, Laboratoire PRISME, 2011.

[27] G. Rizzoni, L. Guzzella, and B.M. Baumann. Unified modeling of hybrid electric vehicle drivetrains. *IEEE/ASME Trans. on Mechatronics*, 4(3): 246 - 257, 1999.

[28] K. Chen, A. Bouscayrol, A. Berthon, P. Delarue, D. Hissel, and R. Trigui. Global modeling of different vehicles. *IEEE Vehicular Technology Magazine*, 4(2): 80 - 89, 2009.

[29] S. Wang, S. Kodagoda, and R. Khushaba. Towards speed-independent road-type classification. *12th Int. Conf. on Control, Automation, Robotics & Vision*, 2012.

[30] T. Nuesch, P. Elbert, M. Flankl, C. Onder, and L. Guzzella. Convex optimization for the energy management of hybrid electric vehicles considering engine start and gearshift costs. *Energies*, 7, 2014.

[31] R. Beck, A. Bollig, and D. Abel. Comparison of two real-time predictive strategies for the optimal energy management of a hybrid electric vehicle. *E-COSM - Rencontres Scientifiques de l'IFP*, 2006.

[32] T.S. Kim, C. Manzie, and R. Sharma. Model predictive control of velocity and torque split in a parallel hybrid vehicle. *Proc. of the 2009 IEEE Int. Conf. Systems, Man and Cybernetics*, 2009.

[33] G. Heppeler, M. Sonntag, and O. Sawodny. Fuel efficiency analysis for simultaneous optimization of the velocity trajectory and the energy management in hybrid electric vehicles. *19th World Congress, IFAC*, 2014.

[34] Y. S. Wong, C. C. Chan, and S. Nazir. Encyclopedia of automotive engineering. chapter Hybrid and Electric Powertrains: Basic consideration. John Wiley & Sons, Ltd., 2014.

[35] M.A. Hannan, F.A. Azidin, and A. Mohamed. Hybrid electric vehicles and their challenges: A review. *Renewable and Sustainable Energy Reviews*, 29(2014): 135 - 150, 2014.

[36] E. Karden, S. Ploumen, B. Fricke, T. Miller, and K. Snyder. Energy storage devices for future hybrid electric vehicles. *Journal of Power sources*, 168: 2 - 21, 2007.

[37] F. Badin. *Les véhicules hybrides: des composants au système*. IFP Energies Nouvelles Publications, Editions TECHNIP, 2013.

[38] P. Miller. Automotive lithium-ion batteries: State of the art and future developments in lithium-ion battery packs for passenger car applications. *Johnson Matthey Technol. Rev.*, 59(1): 4 - 13, 2015.

[39] J. M. Miller. *Propulsion systems for hybrid vehicles*. Springer, 2010.

[40] U. Czarkowski. Modular battery management system for lithium ion batteries for plug-in hybrid vehicles. *Hybrid Vehicles and Energy Management, 5th Symposium*, pages 221 – 247, 2008.

[41] K. Young, C. Wang, L.Y. Wang, and K. Strunz. *Electrical vehicle integration into modern power networks; Chapter 2: Electric Vehicle Battery Technologies*. Springer, 2013.

[42] M. Nesbit, M. Fergusson, A. Colsa, J. Ohlendorf, C. Hayes, K. Paquel, and J.P. Schweitzer. Comparative study on the differences between the EU and US legislation on emissions in the automotive sector. Technical report, European Union, 2016.

[43] M. Andre, R. Joumard, R. Vidon, P. Tassel, and P. Perret. Real-world european driving cycles, for measuring pollutant emissions from high- and low- powered cars. *Atmospheric Environment*, 40: 5944 - 5953, 2006.

[44] R. Edwards, J-F. Larive, and J-C. Beziat. Well-to-wheels analysis of future automotive fuels and powertrains in the european context. Technical report, European Commission Joint Research Centre Institute for Energy and Transport, 2011.

[45] A. Elgowainy, J. Han, L. Poch, M. Wang, A. Vyas, M. Mahalik, and A. Rousseau. Well-to-wheels energy use and greenhouse gas emissions of plug-in hybrid electric vehicles. Technical report, Argonne National Laboratory, 2010.

[46] J. Lang, S. Cheng, Y. Zhou, B. Zhao, H. Wang, and S. Zhang. Energy and environmental implications of hybrid and electric vehicles in China. *Energies*, 6: 2663 - 2685, 2013.

[47] K. Yabe, Y. Shinoda, T. Seki, H. Tanaka, and A. Akisawa. Market penetration speed and effects on CO_2 reduction of electric vehicles and plug-in hybrid electric vehicles in Japan. *Energy Policy*, 45(2012): 529 - 540, 2012.

[48] L. Horrein, A. Bouscayrol, P. Delarue, J.N. Verhille, and C. Mayet. Forward and backward simulations of a power propulsion system. *IFAC Proc. Volumes, 8th Power Plant and Power System Control Symposium*, 45(21):441 – 446, 2012.

[49] J. Heywood. *Internal combustion engine fundamentals*. McGraw-Hill, 1988.

[50] M. El Lakkis, O. Sename, M. Corno, and D. B. Pietri. Combined battery soc/soh estimation using a nonlinear adaptive observer. *European Control Conf.*, 2015.

[51] E. Silvas, T. Hofman, A. Serebrenik, and M. Steinbuch. Functional and cost-based automatic generator for hybrid vehicles topologies. *IEEE/ASME Trans. on Mechatronics*, 20(4): 1561 - 1572, 2015.

[52] H. Liu and D. Kum. Comprehensive design methodology of input and output-split hybrid electric vehicles: In search of optimal configuration. *IEEE/ASME Trans. on Mechatronics*, 21(6): 2912 - 2923, 2016.

[53] H.K. Roy, A. McGordon, and P. A. Jennings. A generalized powertrain design optimization methodology to reduce fuel economy variability in hybrid electric vehicles. *IEEE Trans. on Vehicular Technology*, 63(3): 1055 - 1070, 2014.

[54] M. Pourabdollah, N. Murgovski, A. Grauers, and B. Egardt. Optimal sizing of a parallel PHEV powertrain. *IEEE Trans. on Vehicular Technology*, 62(6): 2469 - 2480, 2013.

[55] X. Zhang, H. Peng, and J. Sun. A near-optimal power management strategy for rapid component sizing of multimode power split hybrid vehicles. *IEEE Trans. on Control Systems Technology*, 23: 609 - 618, 2015.

[56] A. Sciarretta, L. Guzzella, and M. Back. A real-time optimal control strategy for parallel hybrid vehicles with on-board estimation of the control parameters. *Proc. IFAC Symp. Advances in Automotive Control*, 2004.

[57] X. Zeng and J. Wang. A parallel hybrid electric vehicle energy management strategy using stochastic model predictive control with road grade preview. *IEEE Trans. on Control Systems Technology*, 23(6): 2416 - 2423, 2015.

[58] T. O. Deppen, A. G. Alleyne, K. A. Stelson, and J. J. Meyer. Predictive energy management for parallel hydraulic hybrid passenger vehicle. *Proc. of the ASME 2010 Dynamic Systems and Control Conf.*, 2010.

[59] J.T.B.A Kessels, F. P. T. Willems, W. J. Schoot, and P. P. J. van den Bosch. Integrated energy & emission management for hybrid electric truck with SCR aftertreatment. *IEEE Vehicle Power and Propulsion Conf.*, 2010.

[60] D. Zhao, R. Stobart, G. Dong, and E. Winward. Real-time energy management for Diesel heavy duty hybrid electric vehicles. *IEEE Trans. on Control Systems Technology*, 23(3): 829 - 841, 2015.

[61] T.H Pham, J.T.B.A. Kessels, and P.P.J. van den Bosch ad R.G.M. Huisman. Analytical solution to energy management guaranteeing battery life for hybrid trucks. *IEEE Trans. on Vehicular Technology*, 65(10):7956 – 7971, 2015.

[62] A. Brahma, Y. Guezennec, and G. Rizzoni. Optimal energy management in series hybrid electric. *Proc. American Control Conf.*, 2000.

[63] S. Di Cairano, W. Liang, I.V. Kolmanosky, M.L. Kuang, and A.M. Phillips. Engine power smoothing energy management strategy for a series hybrid electric vehicle. *American Control Conf.*, 2011.

[64] M. Bichi, G. Ripaccioli, S.Di Cairano, D. Bernardini, A. Bemporad, and I.V Kolmanovsky. Stochastic MPC with driver behaviour for approach for improved powertrain control. *IEEE Conf. on Decision and Control*, 2010.

[65] C. Donitz, I. Vasile, C. Onder, and L. Guzzella. Dynamic programming for hybrid pneumatic vehicles. *American Control Conf.*, 2009.

[66] A. Ivanco, G. Colin, Y. Chamaillard, A. Charlet, and P. Higelin. Energy management strategies for a pneumatic-hybrid engine based on sliding window pattern recognition. *Oil & Gas Science and Technology - Rev. IFP*, 65(1): 179 - 190, 2010.

[67] L. Johannesson, S. Pettersson, and B. Egardt. Predictive energy management of a 4qt series-parallel hybrid electric bus. *Control Engineering Practice*, 17:1440 – 1453, 2009.

[68] R. Dudek, V. Smidl, and Z. Peroutka. Start - stop system for a city bus based on model predictive control. *Industrial Electronics Society, IECON*, 2014.

[69] P. Schrangl, D. Moser, P. Langthaler, and L. del Re. Quasi-optimal energy management of range extender buses in presence of changing traffic conditions. *IEEE Conf. on Control Applications*, 2016.

[70] C. Weng, X. Zhang, and J. Sun. Adaptive model predictive control for hybrid electric vehicles power management. *Proc. 32nd Chinese Control Conf.*, 2013.

[71] S. Dewenter, A. Binder, and M. Strauch. Simulation model for a serial hybrid bus and impact of energy management on fuel consumption. *IEEE Vehicle Power and Propulsion Conf.*, 2012.

[72] J. Liu and H. Peng. Modeling and control of a power-split hybrid vehicle. *IEEE Trans. Control Systems Technology*, 16(6): 1242 - 1251, 2008.

[73] H. Borhan, A.Vahidi, A. Phillips, M. Kuang, I. Kolmanovsky, and S. Di Cairano. MPC-based energy management of a power-split hybrid electric vehicle. *IEEE Trans. on Control Systems Technology*, 20(3): 593 - 603, 2012.

[74] W. Hongyu, Q. Yunqian, F. Yong, L. Zhimming, and Y. Zhiqiang. Study on engine start-stop control strategy for series-parallel hybrid vehicle. *Proc. of IEEE Int. Conf. on Mechatronics and Automation*, 2015.

[75] L. Feng, M. Cheng, and B. Chen. Predictive control of a power-split HEV with fuel consumption and SOC estimation. *SAE Technical Paper*, 2015-01-1161,doi: 10.4271/2015-01-1161, 2015.

[76] S. Kelouwani, N. Henao, K. Abbossou, Y. Dube, and L. Boulon. Two-layer energy management architecture for a fuel cell HEV using road trip information. *IEEE Trans. on Vehicular Technology*, 61(9): 3851 - 3864, 2012.

[77] R. Meyer, R. A. DeCarlo, P. H. Meckl, C. Doktorcik, and S. Pekarek. Hybrid model predictive power flow control of a fuel cell-battery vehicle. *American Control Conf.*, 2011.

[78] Z. Asus, D. Chrenko, E. Aglzim, A. Kebairi, A. Keromnes, and L. Le-Moyne. Model and control strategy simulation of a racing series hybrid car. *IEEE Vehicle Power and Propulsion Conf.*, 2014.

[79] F. L. Mapelli and D. Tarsitano. Energy control for plug-in HEV with ultracapacitors lithium-ion batteries storage system for FIA alternative energy cup race. *IEEE Vehicle Power and Propulsion Conf.*, 2015.

[80] M. Salazar, P. Elbert, S. Ebbessen, C. Bussi, and C. H. Onder. Time-optimal control policy for a hybrid electric race car. *IEEE Trans. on Control Systems Technology*, PP(99): 1 - 14, 2017.

[81] C. Zhang and A. Vahidi. Route preview in energy management of plug-in hybrid electric vehicles. *IEEE Trans. on Control Systems Technology*, 20(2): 546 - 553, 2012.

[82] H. Yu, M. Kuang, and R. McGee. Trip-oriented energy management control strategy for plug-in hybrid electric vehicles. *IEEE Trans. on Control Systems Technology*, 22(4): 1323 - 1336, 2014.

[83] V. Larsson, L. Johannesson Mardth, B. Egardt, and S. Karlsson. Commuter route optimized energy management of hybrid electric vehicles. *IEEE Trans. on Intelligent Transportation Systems*, 15(3): 1145 - 1154, 2014.

[84] V. Ngo, T. Hofman, M. Steinbuch, and A. Serrarens. Optimal control of the gearshift command for hybrid electric vehicles. *IEEE Trans. on Vehicular Technology*, 61(8): 3531 - 3543, 2012.

[85] E. Ozatay, U. Ozguner, J. Michelini, and D. Filev. Analytical solution to the minimum energy consumption based velocity profile optimization problem with variable road grade. *19th World Congress IFAC*, 2014.

[86] T. Miro-Padovani, G. Colin, A. Ketfi-Cherif, and Y. Chamaillard. Implementation of an energy management strategy for hybrid electric vehicles including drivability constraints. *IEEE Trans. on Vehicular Technology*, 65(8): 5918 - 5929, 2016.

[87] P. Pisu, K. Koprubasi, and G. Rizzoni. Energy management and drivability control problems for hybrid electric vehicles. *44th IEEE Conf. on Decision and Control*, 2005.

[88] P. Michel, A. Charlet, G. Colin, Y. Chamaillard, G. Bloch, and C. Nouillant. Catalytic converter modeling for optimal gasoline-HEV energy management. *19th IFAC World Congress*, 2014.

[89] L. Horrein, A. Bouscayrol, Y. Cheng, C. Dumand, G. Colin, and Y. Chamaillard. Influence of the heating system on the fuel consumption of a hybrid electric vehicle. *Energy Conversion and Management, Elsevier*, 129:250 – 261, 2016.

[90] E. Dincmen and B.A. Guvenc. A control strategy for parallel hybrid electric vehicles based on extremum seeking. *Vehicle System Dynamics*, 50(2): 199 - 227, 2012.

[91] O. Sundstrom, P. Soltic, and L. Guzzella. A transmission-actuated energy management strategy. *IEEE Trans. on Vehicular Technology*, 59(1): 84 - 92, 2010.

[92] M. H. Hajimiri and F. R. Salmasi. A fuzzy energy management strategy for series hybrid electric vehicle with predictive control and durability extension of the battery. *IEEE Conf. on Electric and Hybrid Vehicles*, 2006.

[93] S. G. Li, S. M. Sharkh, F. C. Walsh, and C. N. Zhang. Energy and battery management of a plug-in series hybrid electric vehicle using fuzzy logic. *IEEE Trans. on Vehicular Technology*, 60(8): 3571 - 3585, 2011.

[94] F. R. Salmasi. Control strategies for hybrid electric vehicles: evolution, classification, comparison and future trends. *IEEE Trans. on Vehicular Technology*, 56(5): 2393 - 2404, 2007.

[95] D. Goerke, M. Bargende, U. Keller, N. Ruzicka, and S. Schmiedler. Optimal control based calibration of rule-based energy management for parallel hybrid electric vehicles. *SAE Technical Paper*, 2015-01-1220,doi:10.4271/2015-01-1220, 2015.

[96] C. C. Lin, H. Peng, J.W. Grizzle, and J.M. Kang. Power management strategy for a parallel hybrid electric truck. *IEEE Trans. on Control Systems Technology*, 11(6): 839 - 849, 2003.

[97] A. A. Menezes and I. V. Kolmanovsky. Energy and power management in a series hybrid electric vehicle using selective evolutionary generation. *53rd Conf. on Decision and Control*, 2014.

[98] C. Dextreit and I. Kolmanovsky. Game theory controller for hybrid electric vehicles. *IEEE Trans. on Control Systems Technology*, 22(2): 652 - 663, 2014.

[99] O. Hegazy and J. Van Mierlo. Particle swarm optimization for optimal powertrain component sizing and design of fuel cell hybrid electric vehicle. *12th Int. Conf. on Optimization of Electrical and Electronic Equipment, OPTIM*, 2010.

[100] T. Nuesch, T. Ott, S. Ebbesen, and L. Guzzella. Cost and fuel-optimal selection of HEV topologies using particle swarm optimization and dynamic programming. *American Control Conf.*, 2012.

[101] G. Ripaccioli, D. Bernardini, S.Di Cairano, A. Bemporad, and I.V Kolmanovsky. A stochastic MPC approach for series hybrid electric vehicle power management. *American Control Conf.*, 2010.

[102] C. Sun, X. Hu, S. J. Moura, and F. Sun. Velocity predictors for predictive energy management in hybrid electric vehicles. *IEEE Trans. on Control Systems Technology*, 23(3): 1197 - 1204, 2015.

[103] X. Zeng and J. Wang. A parallel hybrid electric vehicle energy management strategy using stochastic model predictive control with road grade preview. *IEEE Trans. on Control Systems Technology*, 23(6): 2416 - 2423, 2015.

[104] J. Liu and H. Peng. Configuration, sizing and control of power-split hybrid vehicles. *AVEC Conf.*, 2007.

[105] M. Cipek, J. Deur, and J. Petric. Bond graph analysis of power flow in series-parallel hybrid electric vehicle transmissions. *UKACC Int. Conf. on Control*, 2010.

[106] W. Borutzky. Bond Graph Methodology: Development and Analysis of Multidisciplinary Dynamic System Models. chapter Bond Graph Based Physical Systems Modeling. Springer, 2010.

[107] M. Cipek, D. Pavkovic, and J. Petric. A control-oriented simulation model of a power-split hybrid electric vehicle. *Applied Energy*, 101: 121 - 133, 2012.

[108] X. Zhang, C.T. Li, D. Kum, and H. Peng. Prius$^+$ and Volt$^-$: Configuration analysis of power-split hybrid vehicles with a single planetary gear. *IEEE Trans. on Vehicular Technology*, 61(8): 3544 - 3552, 2012.

[109] X. Zhang. *Design of Power Split Hybrid Powertrains with Multiple Planetary Gears and Clutches*. PhD thesis, University of Michigan, 2015.

[110] W. Zhuang, X. Zhang, H. Peng, and L. Wang. Rapid configuration design of multiple-planetary-gear power-split hybrid powertrain via mode combination. *IEEE/ASME Trans. on Mechatronics*, 21(6): 2924 - 2934, 2016.

[111] M. Zhou, H. Jin, and W. Wang. A review of vehicle fuel consumption models to evaluate eco-driving and eco-routing. *Transportation Research Part D*, 49: 203 - 218, 2016.

[112] B. de Jager, T. van Keulen, and J. Kessels. *Optimal control of hybrid vehicles, Advances in industrial control*. Springer, 2013.

[113] T. van Keulen, B. de Jager, D. Foster, and M. Steinbuch. Velocity trajectory optimization in hybrid electric trucks. *Proc. American Control Conf.*, 2010.

[114] D. Ambuhl. *Energy management strategies for hybrid electric vehicles*. PhD thesis, ETH, 2009.

[115] C. Sun, S. J. Moura, X. Hu, J.K. Hedrick, and F. Sun. Analytical approach for the power management of blended-mode plug-in hybrid electric vehicles. *IEEE Trans. on Vehicular Technology*, vol. 61(4): 1554 - 1566, 2012.

[116] R. Mura, V. Utkin, and S. Onori. Recasting the HEV energy management problem into an infinite-time optimization problem including stability. *52nd IEEE Conf. on Decision and Control*, 2013.

[117] R. S. Vadamalu and C. Beidl. Online MPC based PHEV energy management using conic interior-point methods. *IEEE Intelligent Vehicles Symposium*, 2016.

[118] B. Passenberg, P. Kock, and P. Stursberg. Combined time and fuel optimal driving of trucks based on a hybrid model. *Proc. of the European Control Conf.*, 2009.

[119] K. Yu, M. Mukai, and T. Kawabe. Model predictive control of a power-split hybrid electric vehicle system with slope information. *SICE Annual Conf.*, September 2013.

[120] M.A.S Kamal, M. Mukai, J. Murata, and T. Kawabe. Ecological driver assistance system using model-based anticipation of vehicle-road-traffic information. *IET Intelligent Transport Systems*, 4(4): 244 - 251, 2010.

[121] M. Josevski and D. Abel. Energy management of a parallel hybrid electric vehicles based on stochastic model predictive control. *19th World Congress, IFAC*, 2014.

[122] S. Xu, S. E. Li, X. Zhang, B. Cheng, and H. Peng. Fuel-optimal cruising strategy for road vehicles with step-gear mechanical transmission. *IEEE Trans. on Intelligent Transportation Systems*, 16(6): 3496 - 3507, 2015.

[123] S. E. Li, H. Peng, K. Li, and J. Wang. Minimum fuel control strategy in automated car-following scenarios. *IEEE Trans. on Vehicular Technology*, 61(3): 998 - 1007, 2012.

[124] Z. Lu, J. Song, H. Yuan, and L. Shen. MPC - based torque distribution strategy for energy management of power-split hybrid electric vehicles. *Proc. of the 32nd Chinese Control Conf.*, July 2013.

[125] Q. Cheng, L. Nouveliere, and O. Orfila. A new eco-driving assistance system for a light vehicle: energy management and speed optimization. *IEEE Intelligent Vehicles Symposium*, 2013.

[126] B. Saerens, H. Rakhan, K. Ahn, and E. van den Bulck. Assessment of alternative polynomial fuel consumption models for use in its application. *Journal Intelligent Transportation Systems: Technol. Plan. Oper*, 17(4): 294 - 303, 2013.

[127] R. Bellman. The theory of dynamic programming. *Annual Summer Meeting of the American Mathematical Society*, 1954.

[128] M. Koot, J.T.B.A Kessels, B. de Jager, W.P.M.H. Heemels, P.P.J. van den Bosch, and M. Steinbuch. Energy management strategies for vehicular electric power systems. *IEEE Trans. on Vehicular Technology*, 54(3): 771 - 782, 2005.

[129] F. L. Lewis, , D. L. Vrabie, and V.L. Syrmos. *Optimal Control*. John Wiley & Sons, INC., third edition, 2012.

[130] O. Sundstrom and L. Guzzella. A generic dynamic programming Matlab function. *18th IEEE Int. Conf. on Control Applications, Part of IEEE Multi-conf. on Systems and Control*, 2009.

[131] L. Serrao. *A comparative analysis of energy management strategies for hybrid electric vehicles*. PhD thesis, The Ohio State Univ., 2009.

[132] E. Trelat. *Controle optimal: theorie et applications*. version electronique, 2013.

[133] Z. Yuan, L. Teng, S. Fengchun, and H. Peng. Comparative study of dynamic programming and Pontryagin's Minimum Principle on energy management for a parallel hybrid electric vehicles. *Energies*, 6: 2305 - 2318, 2013.

[134] L. Serrao, S. Onori, and G. Rizzoni. ECMS as a realization of Pontryagin's minimum principle for HEV control. *American Control Conf.*, 2009.

[135] T. Miro-Padovani, G. Colin, A. Ketfi-Cherif, and Y. Chamaillard. Optimal energy management strategy for a hybrid vehicle provided with a dual electric storage system. *Proc. IFAC Workshop on Engine and Powertrain Control, Simulation and Modeling (E-COSM'15)*, 2015.

[136] T. Van Keulen, B. de Jager, and M. Steinbuch. An adaptive sub-optimal energy management strategy for hybrid drivetrains. *Proc. of the 17th World Congress IFAC*, 2008.

[137] M. Sivertsson, C. Sundstrom, and L. Eriksson. Adaptive control of a hybrid powertrain with map-based ECMS. *IFAC World Congress*, 2011.

[138] C. Musardo, G. Rizzoni, Y. Guezennec, and B. Staccia. A-ECMS: An adaptive algorithm for hybrid electric vehicle energy management. *European Journal of Control*, 11:509 - 524, 2005.

[139] S. Kermani, S. Delprat, T. M. Guerra, R. Trigui, and B. Jeanneret. Predictive energy management for hybrid vehicle. *Control Engineering Practice*, 20(4): 408 - 420, 2012.

[140] T. Hofman, M. Steinbuch, R. van Druten, and A. Serrarens. Rule-based energy management strategies for hybrid vehicles. *Int. J. Electric and Hybrid Vehicles*, 1(1): 71 - 94, 2007.

[141] G. Rizzoni and S. Onori. Energy management of hybrid electric vehicles: 15 years of development at the ohio state university. *Oil and Gas Science and Technology - Rev. IFP Energies Nouvelles*, 70(1): 41 - 54, 2015.

[142] L. Serrao, A. Sciarretta, O. Grondin, A. Chasse, Y. Creff, D. di Domenico, P. Pognant-Gros, C. Querel, and L. Thibault. Open issues in supervisory control of hybrid electric vehicles: A unified approach using optimal control methods. *Oil & Gas Science and Technology, Rev. IFP Energies nouvelles*, 68(1): 23 - 33, 2013.

[143] R.S. Vadamalu and C. Beidl. Explicit MPC PHEV energy management using Markov chain based predictor: Development and validation at Engine-In-The-Loop testbed. *European Control Conf.*, 2016.

[144] P. Tulpule, V. Marano, and G. Rizzoni. Energy management for plug-in hybrid electric vehicles using equivalent consumption minimisation strategy. *Int. Journal of Electric and Hybrid Vehicles*, 2(4), 2010.

[145] V. Larsson, L. Johannesson, B. Egardt, and A. Lassson. Benefit of route recognition in energy management of plug-in hybrid electric vehicles. *American Control Conf.*, 2012.

[146] C. Sun, S. J. Moura, X. Hu, J.K. Hedrick, and F. Sun. Dynamic traffic feedback data enabled energy management in plug-in hybrid electric vehicles. *IEEE Trans. on Control Systems Technology*, 23(3): 1075 - 1086, 2015.

[147] J. Guanetti, S. Formentin, and S. M. Savaresi. Least costly energy management for electric vehicles with plug-in range extenders. *IEEE 54th Conf. on Decision and Control*, 2015.

[148] J. B. Rawlings, D. Angeli, and C.N. Bates. Fundamentals of economic model predictive control. *51st IEEE Conf. on Decision and Control*, 2012.

[149] P. Boucher and D. Dumur. *La commande prédictive*. Editions Technip, 1996.

[150] T. Albin, D. Ritter, D. Abel, N. Liberda, R. Quirynen, and M. Diehl. Nonlinear MPC for a two-stage turbocharged gasoline engine airpath. *54th Annual Conf. on Decision and Control*, 2015.

[151] A. Bemporad, S. Di Cairano, E. Henriksson, and K. H. Johansson. Hybrid model predictive control based on wireless sensor feedback: an experimental study. *46th IEEE Conf. on Decision and Control*, 2007.

[152] R. Findeisen, F. Allgower, and L. T. Biegler. *Assessment and future directions of nonlinear model predictive control*. Springer-Verlag Berlin Heidelberg, 2007.

[153] D. Q. Mayne, J. B. Rawlings, C. V. Rao, and P. O. M. Scokaert. Constrained model predictive control: stability and optimality. *Automatica*, 36: 789 - 814, 2000.

[154] J. Buerger and M. Cannon. Nonlinear MPC for supervisory control of hybrid electric vehicles. *European Control Conf.*, 2016.

[155] F. Yan, J. Wang, and K. Huang. Hybrid electric vehicle model predictive control torque-split strategy incorporating engine transient characteristics. *IEEE Trans. on Vehicular Technology*, 61(6): 2458 - 2467, 2012.

[156] K. Utchaichana, S. Bengea, R. DeCarlo, S. Pekarek, and M. Zefran. Hybrid model predictive control tracking of a sawtooth driving profile for an HEV. *American Control Conf.*, June 2008.

[157] G. E. Katasargyri, I. Kolmanovsky, J. Michelini, M. Kuang, A. Phillips, M. Rinehart, and M. Dahleh. Path dependent receding horizon control policies for hybrid electric vehicles. *18th IEEE Int. Conf. on Control Applications*, 2009.

[158] C.V. Rao and J.B. Rawlings. Linear programming and model predictive control. *Journal of Process Control*, 10(2000): 283 - 289, 2000.

[159] C. E. Garcia, D. M. Prett, and M. Morari. Model predictive control: theory and practice - a survey. *Automatica*, 25(3): 335 - 348, 1989.

[160] M. Alamir and G. Bornard. Stability of a truncated infinite constrained receding horizon scheme: the general discrete nonlinear case. *Automatica*, 31(9): 1353 - 1356, 1995.

[161] I. Sarac, A. Wagner, U. Fischer, and R. Schnurr. Predictive on-board diagnosis for hybrid electric vehicles with in-vehicle navigation unit. *SAE Technical Paper*, 2015-01-1224, doi:10.4271/2015-01-1224, 2015.

[162] S. Onori and L. Serrao. On Adaptive-ECMS strategies for hybrid electric vehicles. *Les Rencontres Scientifiques d'IFP Energies Nouvelles - RHEVE*, 2011.

[163] P. Stoica and R. Moses. *Spectral analysis of signals*. Prentice Hall, Upper Saddle River, New Jersey, 07458, 2005.

[164] N. Mueller, S. Strauss, S. Tumback, G.C. Goh, and A. Christ. Next generation engine start/stop systems: free-wheeling. *SAE International*, doi:10.4271/2011-01-0712, 2011.

[165] P. Willemsen, F. Ji, and M. Nalbach. Key items for future hybrid applications: Energy storage and power electronics for micro hybrids up to full hybrids and EVs. *Proc. of the FISITA 2012 World Automotive Congress, Lecture Notes in Electrical Engineering*, 191, 2012.

[166] M. Kremer. In-market application of start-stop systems in European market. Technical report, FEV Inc., 2011.

[167] D. J. McGeoch and P. Deutsch. Control of automated engine stop/start for vehicles with an automatic transmission. *UKACC Int. Conf. on Control*, 2010.

[168] N. Hollingsworth, J. Meyer, R. McGee, J. Doering, G. Konidaris, and L. Kaelbling. Optimizing a start-stop controller using policy search. *Proc. of 26th Annual Conf. on Innovative Applications of Artificial Intelligence*, 2014.

[169] L. Yang, H. He, F. Sun, S. Shi, Y. Li, and L. Liu. Research of fuzzy logic control strategy for engine start/stop in dual-clutch hybrid electric vehicle. *7th Int. Conf. on Fuzzy Systems and Knowledge Discovery*, 2010.

[170] S. Hahn, H. Waschl, G. Steinmaurer, and L. del Re. Extension of a linear optimal control strategy for HEV. *European Control Conf.*, 2015.

[171] H. Koch-Groeber and J. Wang. Criteria for coasting on highways for passenger cars. *SAE Technical Paper*, 2014-01-1157, 2014.

[172] J. Lee. *Vehicle Inertia Impact on Fuel Consumption of Conventional and Hybrid Electric Vehicles Using Acceleration and Coast Driving Strategy*. PhD thesis, Virginia Polytechnic Institute and State University, 2009.

[173] V.A. Petrushov. Coast down method in time-distance variables. *SAE Technical Paper Series*, 1997.

[174] M. Nagahara, D. E. Quevedo, and D. Nesic. Maximum hands-off control: A paradigm of control effort minimization. *IEEE Trans. on Automatic Control*, 61(3):735 - 747, 2016.

Nicoleta STROE

Contributions à la commande prédictive pour la gestion d'énergie d'un véhicule hybride électrique

Résumé : Pour un véhicule électrique hybride, un des challenges les plus compliqués d'une perspective orientée contrôle est la distribution de puissance entre le moteur thermique et les machines électriques, problème appelé gestion d'énergie. La question qui surgit est comment exploiter le degré de liberté supplémentaire - la voie électrique - afin que la performance véhicule, liée à la réduction de la consommation carburant, soit améliorée. Le besoin de robustesse des stratégies de contrôle encourage le choix de méthodes basées sur des modèles et dans le contexte actuel de possibilité d'acquisition des données télémétriques, la commande prédictive à base de modèle apparaît comme une option attractive, motivée aussi par sa capacité à gérer des contraintes. La plupart des stratégies courantes de gestion d'énergie sont orientées application et par conséquent, un modèle générique du GMP hybride offrirait plus de flexibilité. Cette thèse se construit sur deux axes principaux : la synthèse d'un modèle générique et d'une stratégie de contrôle basée sur la commande prédictive pour la gestion d'énergie, avec un mécanisme de calibration auto-adaptable. Si la distribution de couple est l'enjeu majeur du contrôle, d'autres fonctionnalités peuvent être introduites, comme l'arrêt/démarrage du moteur et le découplage du GMP des roues. Cette dernière est généralement traitée dans la littérature avec une stratégie basée sur cartographies, mais ici une approche analytique innovante a été proposée. Une validation sur un modèle haute-fidélité d'un véhicule hybride léger (mild) avec une transmission double-embrayage clôture les travaux et montre le potentiel de la stratégie proposée.
Mots clés : véhicule hybride, commande prédictive, gestion d'énergie

Contributions to model-based predictive energy management in hybrid electric vehicles

Abstract: For a hybrid electric vehicle, one of the most challenging aspects from a control perspective is the power split between the engine and the motors, problem referred to as energy management. The question that arises is how to exploit the additional degree of freedom - the electric path - such that the vehicle performance related to consumption is improved. The required robustness for the control strategies encourage the choice of model-based methods and in the present context of telemetry data acquisition, model predictive control emerges as an attractive option, motivated in addition by its ability to handle the constraints. Most of the current energy management strategies are application-oriented and therefore, a generic hybrid powertrain model would provide more flexibility. This thesis is developed on two main axes: the synthesis of a generic model and of a MPC-based control strategy for the energy management, with a self-tuning mechanism. If the torque split is the main control objective, other functionalities can be introduced, such as engine stop/start and coasting. The latter is usually handled in the literature with a map-based strategy, but here an analytical solution was proposed. A validation on a vehicle high-fidelity model for a mild hybrid with a dual-clutch transmission closes the work and shows the potential of the proposed strategy.
Keywords: hybrid electric vehicles, model predictive control, energy management

RENAULT

PRISME

CentraleSupélec